THE DEVELOPMENT OF A METHOD TO IMPROVE THE LIMIT DRAWING RATIO OF BLANKS USING PREFERENTIAL HEATING

A DOCTOR OF PHILOSOPHY THESIS

in

Modeling and Design of Engineering Systems (MODES)

(Main Field of Study : Manufacturing Engineering)

Atılım University

by

ERDEM KAYHAN

FEBRUARY 2015

GCRIS

THE DEVELOPMENT OF A METHOD TO IMPROVE THE LIMIT DRAWING RATIO OF BLANKS USING PREFERENTIAL HEATING

A THESIS SUBMITTED TO

THE GRADUATE SCHOOL OF NATURAL AND APPLIED SCIENCES

OF

ATILIM UNIVERSITY

BY

ERDEM KAYHAN

IN PARTIAL FULFILLMENT OF THE REQUIREMENTS FOR THE DEGREE OF

DOCTOR OF PHILOSOPHY

IN

MODELING AND DESIGN OF ENGINEERING SYTEMS (MODES)

(MAIN FIELD OF STUDY : MANUFACTURING ENGINEERING)

FEBRUARY 2015

GCRIS

Approval of the Graduate School of Natural and Applied Sciences, Atılım University.

_____

Prof. Dr. İbrahim AKMAN

Director

I certify that this thesis satisfies all the requirements as a thesis for the degree of Doctor of Philosophy.

_____

Prof. Dr. Abdülkadir ERDEN

Head of Department

This is to certify that we have read the thesis "The development of a method to improve the limit drawing ratio of blanks using preferential heating" submitted by "Erdem KAYHAN" and that in our opinion it is fully adequate, in scope and quality, as a thesis for the degree of Doctor of Philosophy.

_____	_____
Asst. Prof. Dr. Erkan KONCA	Prof. Dr. Bilgin KAFTANOĞLU
Co-Supervisor	Supervisor

Examining Committee Members

Prof. Dr Bilgin KAFTANOĞLU	_____
Prof. Dr. Birol KILKIŞ	_____
Asst. Prof. Dr. Erkan KONCA	_____
Asst. Prof. Dr. Celalettin KARADOĞAN	_____
Asst. Prof. Dr. Besim BARANOĞLU	_____

Date : 02/02/2015

GCRIS

I declare and guarantee that all data, knowledge and information in this document has been obtained, processed and presented in accordance with academic rules and ethical conduct. Based on these rules and conduct, I have fully cited and referenced all material and results that are not original to this work.

Name, Last name : Erdem KAYHAN

Signature :

GCRIS

ABSTRACT

THE DEVELOPMENT OF A METHOD TO IMPROVE THE LIMIT DRAWING RATIO OF BLANKS USING PREFERENTIAL HEATING

Kayhan, Erdem

PhD in Modelling and Design of Engineering Systems (MODES)

Supervisor: Prof. Dr. Bilgin KAFTANOĞLU

Co-Supervisor: Asst. Prof. Dr. Erkan KONCA

February 2015, 195 pages

The method developed in the current thesis can shortly be described as the application of nonisothermal local heating in the flange region of the blank to improve the formability of sheet metals in deep drawing. The use of elevated temperature gives the possibility of significantly increasing the ductility of the material and the associated forming capability. It also drastically reduces the yield point and hence the forming forces and required pressures. One of the advanced high strength sheet steels (AHSS), DP600, widely used in the automotive industry due to enabling the reduction in car weigth and increasing the crash safety is chosen as a work material in this reasearch. Using AHSS steels also reduce the material thickness and lower fuel consumption. The three different types of steels, two HSLA and one IF steels, are additionally examined to observe the validity of the developed method. As a result of the experiments conducted within the temperature limits 180ºC to 275ºC in flange region, the Limiting Drawing Ratio in deep drawing (LDR) is increased up to 25.58 %. Since the temperature range stays in the warm region, material properties are not influenced; but the strength remains the same while the required forming forces are reduced.

Keywords: Metal forming, Deep drawing, Non-isothermal forming

ÖZ

DERİN ÇEKME SINIR ORANIN, FLANŞ BÖLGESİNİN ISITILARAK ARTIRILMASI İÇİN YÖNTEM GELİŞTİRİLMESİ

Kayhan, Erdem
Doktora, Mühendislik Sistemlerinin Modellenmesi ve Tasarımı
Tez Yöneticisi: Prof. Dr. Bilgin KAFTANOĞLU
Ortak Tez Yöneticisi: Yrd. Doç. Dr. Erkan KONCA
Şubat 2015, 195 pages

Bu tez çalışmasında geliştirilen yöntem kısaca, sac metal malzemelerin şekillendirilme oranının flanş bölgesinin eş sıcaklık dağılımsız ısıtılarak artırılması olarak açıklanabilir. Sıcaklık artışı malzemenin sünekliğinde belirgin bir yükselmeye ve buna bağlı olarak şekillendirilme kapasitesinin artmasına neden olur. Sıcaklık artışı ayrıca malzemenin akma sınırının düşmesi ile birlikte, uygulama kuvvetlerinde ve basınçlarında azalma meydana gelir. Otomotiv endüstrisinde en yaygın kullanıma sahip olan Yüksek Mukavemet Sac Çelik (AHSS) malzeme DP600 olup, araç ağırlıklarının azalmasını ve çarpışma emniyet faktörünün artmasını sağlamasından dolayı bu tez çalışmasında araştırma malzemesi olarak seçilmiştir. Adı geçen çelik malzemelerin kullanımı malzeme kalınlıklarının ve yakıt sarfiyatının azalmasını sağlar. Yapılan araştırmada geliştirilen yöntemin geçerliliği üç farklı tip malzeme, bunlardan iki tanesi Düşük Alaşımlı Yüksek Mukavemet çeliği (HSLA), diğeri ise IF (Arayersiz Çelikler) çeliği kullanılarak, incelenmiştir. Flanş bölgesinin sıcaklığının 180^{o}C to 300^{o}C değerleri arasında oluşturulduğu deneylerde derin çekme sınır oranında %25.58 kadar artış sağlanmıştır. Kullanılan sıcaklık ılık işlem sıcaklığı seviyesinde olduğundan, şekillendirilme kuvvetlerinde azalma meydana gelmesine rağmen malzemenin özelliklerinde ve dayanımında bir değişim gerçekleşmemektedir.

Anahtar kelimeler: Malzeme şekillendirme, Derin çekme, Eş sıcaklık dağılımsız şekillendirme

To My Parents

GCRIS

ACKNOWLEDGMENTS

I express my sincere appreciation to my supervisor Prof. Dr. Bilgin KAFTANOĞLU for his guidance and insight throughout the research. Thanks also go to my co-supervisor Asst. Prof. Dr. Erkan KONCA and my friend Nuri ŞEN. I wish to thank to the members fo thesis committee: Prof. Dr. Birol KILKIŞ, Asst. Prof. Dr. Celalettin KARADOĞAN and Asst. Prof. Dr. Besim BARANOĞLU. Moreover, the technical assistance of Uğur ALTINSOY and Bülent AYDOĞAN is gratefully acknowledged.

To my wife, Handan, I offer sincere thanks for her continuous support and patience during this period.

GCRIS

TABLE OF CONTENTS

GCRIS

LIST OF TABLES

TABLE

CRIS

LIST OF FIGURES

FIGURES

GCRIS

LIST OF NOTATIONS

OPERATIONS

$f(*)$	function of $(*)$
$\Delta[*]$	increment of $[*]$
$\frac{d}{dx}[*]$	derivative of $[*]$ with respect to x
$(x)_{n+1}$	value of variable x at the increment of (n+1)
$(x)_n$	value of variable x at the increment of (n)

ABBREVIATIONS

FE	finite element
FEM	finite element method
IBVP	initial boundary value problem
LDR	limit or limiting drawing ratio
DR	drawing ratio
AHSS	advanced high strength steel
DP	dual phase steels
TRIP	transformation induced plasticity steel and
TWIP	twinning induced plasticity steels,
IF	interstitial free grade steels
HSLA	high strength low alloy steels
GHG	green house gas
LCA	life cycle assessment
BHF	blank holder force
FLD	forming limit diagram
FLC	forming limit curve
RVE	representative volume elements
GND	geometrically necessary dislocations
BHP	blank holder pressure

GCRIS

FEA	finite element analysis
PTFE	politetrafloroetilen
PL	programmable logic controller
BH	blank holder
Hera	a commercial software developed by Nell Electronic Company in Turkey
MFCE	Metal Forming Centre of Excellence in Atılım University
OM	optical microscope
SEM	scanning electron microscope
HV0.2	Vickers Hardness scales established on the dead weight having 1,961 N

SYMBOLS

F_R	radial tension forces
F_T	tangential compression forces
TS	ultimate tensile strength
YS	yield strength
F_f	friction force
F_N	normal force
F_B	blank holding force
F_d	drawing force
K	strength coefficient
F_b	bending force
M_b	bending moment
V	volume
w	weighted function
D_d	die diameter
D_p	punch diameter
P_{BH}	blank holder pressure
d_m	mean cup diameter
b	circumferential width at die shoulder

E	elastic modulus
α	bending angle
σ_{true}	true stress
ε_{true}	true strain
n	strain hardening coefficient
ε_0	initial strain
d_0	initial blank diameter
d_p	punch diameter
η_{def}	deformation efficiency
W_{id}	ideal deformation work
W_{tot}	actual needed deformation work
$e \approx 2{,}72$	natural logarithm e
ε_w	true strain in the width direction
ε_t	true strain in the thickness direction
w_0	initial width of the tensile specimen
r_0	initial radius of blank
r_p	punch radius ()
r_i	the average radius of punch radius (r_p) and die cavity radius (r_d)
w	intermediate width of the tensile specimen
t_0	initial thickness of the specimen
t	intermediate thickness of the specimen
σ_r, σ_θ and σ_Z	stresses in cylindirical coordinate system, in radial, angular and z directions, respectively
ε_r, ε_θ and ε_z	strains in cylindirical coordinate system, in radial, angular and z directions, respectively
σ_{true}	true stress
μ	coefficient of friction

ε_1, ε_2 and ε_3	principal strains
σ_1, σ_2 and σ_3	principal stresses
σ_r	stress in radial direction
$d\sigma_r$	differential form of stress in radial direction
r	radius variable
dr	differential form of variable radius in radial direction
θ	angular variable
$d\theta$	differential form of angular variable
dt	infinitesimal increment of thickness
σ_t	stress in tangential direction
ε_t	strain in tangential direction
σ_f	flow stress
$\sigma_{f,n}$	flow stress at certain location or section n
η	viscosity of the material
$\frac{d\varepsilon}{dt}$	time derivative of strain
$H_{Punch-PressTable}$	height between table and ram of the press
H_{Die}	thickness of die
H_{Free_Space}	height of free space reserved to set the blank into the die
H_{Stroke}	stroke of punch
H_{Blank_Holder}	thickness of blank holding plate
H_{Load_Cell}	height of load cell
H_{punch}	height of punch
σ_y	yield strength
σ_{yield}	yield strength
σ_{uts}	ultimate tensile strength
σ_{UTS}	ultimate tensile strength

η_F	efficiency of the operation
r_{cp}	punch corner radius
r_{cd}	die corner radius
d_b	blank diameter
d_p	punch diameter

GCRIS

CHAPTER 1

INTRODUCTION

This study is devoted to develop an application method of improving Limit Drawing Ratio by using preferential heating. Limit Drawing Ratio (LDR) is an important measure of formability in sheet metal manufacturing. The most common use area of sheet metal forming is the automobile manufacturing industry. For this reason, the automotive industry plays a key role in the development of new materials and processes because of the large amount of sheet metal parts used. The application of lightweight components, higher safety requirements and the ecological reasons are all crucial considerations which are taken into account in car design to fulfil customer's expectations. Automakers are still searching for new materials and engineering capabilities to meet requirements mentioned above.

The use of high strength and stiffness material provides lightweight construction of automobiles. As a result of the usage of AHSS, the fuel consumption and the rate of emission by automobiles are positively affected. Advanced High Strength Steels (AHSS), especially Dual-Phase (DP), Transformation Induced Plasticity (TRIP), and Twinning Induced Plasticity (TWIP) steels, exhibit promising results in terms of superior mechanical properties. Advanced high strength steels are the best candidates to produce light, safe and ecological cars, as long as their formability's are improved. For those reasons, one of the advanced high strength sheet steels, DP600, which is widely used in automotive industry is chosen as a work material for the improvement of limit drawing ratio. The application method developed in this study can be termed as "Non-Isothermal-Local Heating". Other steels like HSLA in two qualities described

as 7128 and 7140 grades, also, an interstitial-free grade (IF) steel (grade DC04) are additionally examined for the validity of the method developed.

The present thesis addresses the issues concerning properties of the materials used at room and elevated temperatures, parameters of deep drawing, explanation of the method which is developed and the results obtained.

1.1 MOTIVATION

In recent years, the automotive manufacturing industry has been showing remarkable developments, due to the improvement of new materials. According to the latest industry research, auto-manufacturers stress the important role that new grades of steel will play in the design of vehicles for next decades in vehicles of next decades. Those new types of high strength steels which are called as Advanced High Strength Steel (AHSS), were developed by the sheet steel suppliers as a result of the cooperation with the automakers and the design engineers.

AHSS is the one of the fast growing material in automotive applications. The high performance of such steels in the design and manufacturing industry provoked this growth. In addition to this, the other prominent advantages are low cost, mass reduction capabilities, reduced greenhouse gas emissions, safety attributes due to crash performance, and high recyclability.

The targeting limits for exhaust gas emissions to the atmosphere, vehicle safety and fuel consumption rate have already been defined in new global standard for auto manufacturing industry. So, in very near future, auto manufacturers will be obliged to produce the cars fulfilling the requirements in the standard. Otherwise, they may lose their places in auto market. The annual average value of CO_2 emissions per kilometre for countries are shown in Figure 1.1. There was a big differences in between 2000 – 2005, due to the regional regulations. It is expected to reach a possible lower limits about CO_2 emissions per kilometre in those countries by the year 2020. Some of the countries have already been approved the targeting limits for CO_2 emissions rate [1,3]. The fuel economy and exhaust gas emissions are positively impacted when the gauge thickness is reduced. In new designs of vehicles, the complex geometries are also preferred due to aesthetical reasons, but there are some difficulties in forming and joining operations of such parts. For these reasons; it is required to develop the manufacturing methods for the advanced high strength steels (AHSS). In the

development of new grades of steel, the increase in their strength and formability are comparatively considered, [1].

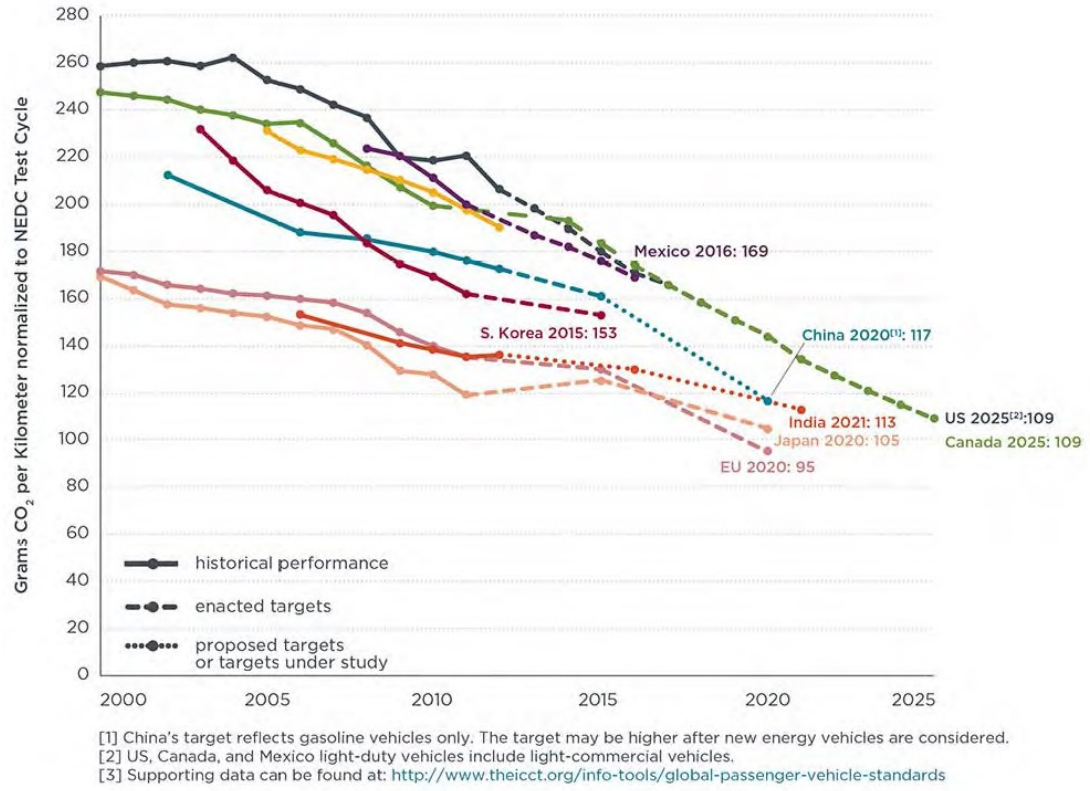

Figure 1.1 Global CO_2 emissions per kilometre for the years between 2000 and 2025, [3].

Steels with yield strength levels in excess of 550 MPa are generally referred to as AHSS. On the other hand, the steels having tensile strength exceeding 780 MPa are sometimes called “ultrahigh-strength steels”. Moreover, the definition “Giga Pascal steel” is often used for the Advanced High Strength Steels with tensile strength of at least 1000 MPa (1000 MPa = 1GPa).

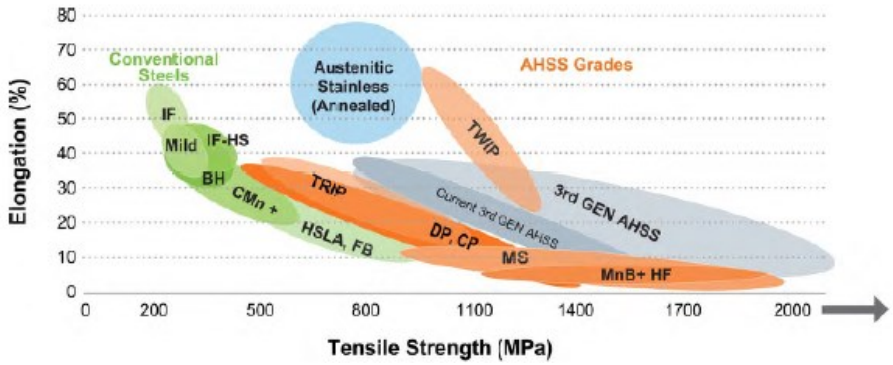

Figure 1.2 The formability diagram, for the today’s AHSS grades available in market, [1].

Because the nomenclature for steel differs all around the world, the general classification given as "XX aaa/bbb" can be used for indication of steel type, where:

XX = Type of steel (abbreviations expanded in Table 1.1 below)

aaa = Minimum yield strength (YS) in MPa

bbb = Minimum ultimate tensile strength (UTS) in MPa

These various steel product families are shown in Table 1.1, [2].

Table 1.1 Designations of steel types, [2]

XX	Type of Steel	XX	Type of Steel
Mild	Mild Steel	HSLA	High-Strength Low-Alloy
BH	Bake Hardenable	IF	Interstitial Free
CP	Complex Phase	MS	Martensitic (MART)
DP	Dual Phase	TRIP	Transformation Induced Plasticity
FB	Ferritic Bainitic	TWIP	Twinning-Induced Plasticity
HF	Hot Formed (and quenched)		

The auto manufacturers using AHSS materials in production line claimed that no additional cost required for the total production system and the investment. The grades of AHSS which are used widely in the production of cars are easily adopted into the existing production line. The use of such steels provide significant mass reduction in the car body while meeting crash worthiness due to their high strength material characteristic.

Independent marketing research reported that they are the fastest growing materials for future automotive applications as shown in Figure 1.3.

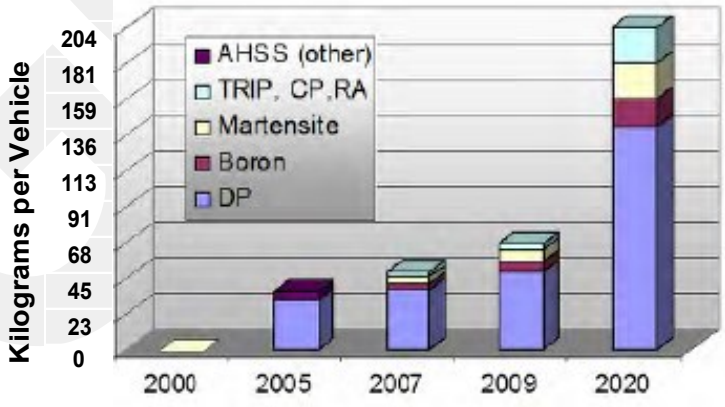

Figure 1.3 The usage of AHSS in automotive industry, [1].

Most steel companies are making new researches to produce AHSS materials having available properties for the production of safe and environmentally friendly vehicles.

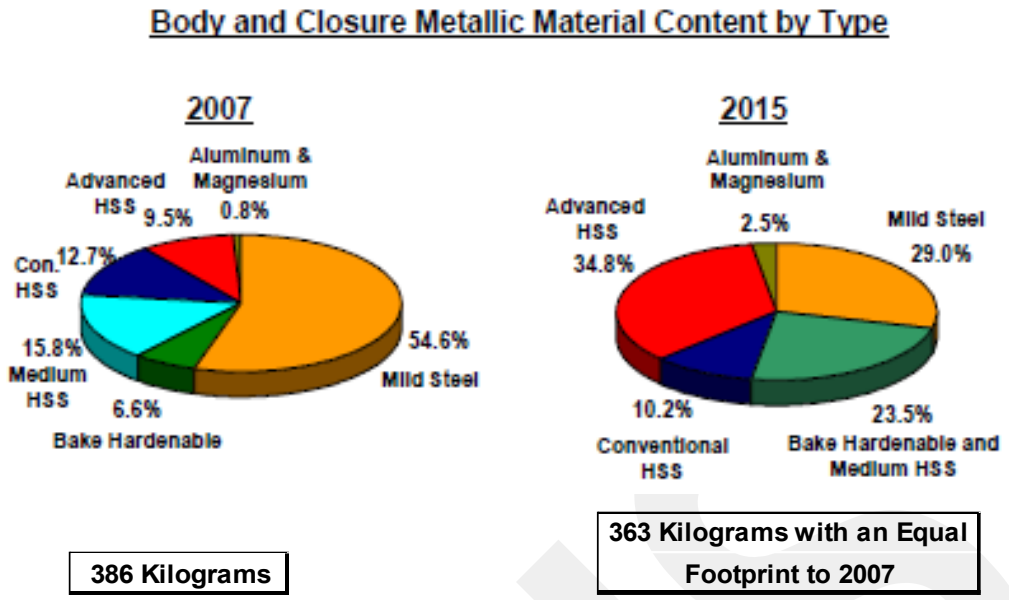

Figure 1.4 The use of high-strength steel (HSS) and AHSS grades are showing rapid increase in auto manufacturing sector in North America, [4].

The Green House Gas (GHG) emission standards are the main criteria's considered by the automobile industry in Europe, the U.S., and Canada, and while the fuel economy standards in Japan, China, and South Korea. As it is reported in Figure 1.5, when the alternative materials, Aluminium, Magnesium, Carbon FRP, are used instead of steel, the auto manufacturers produce 5 to 20 times more emissions than steel, [2].

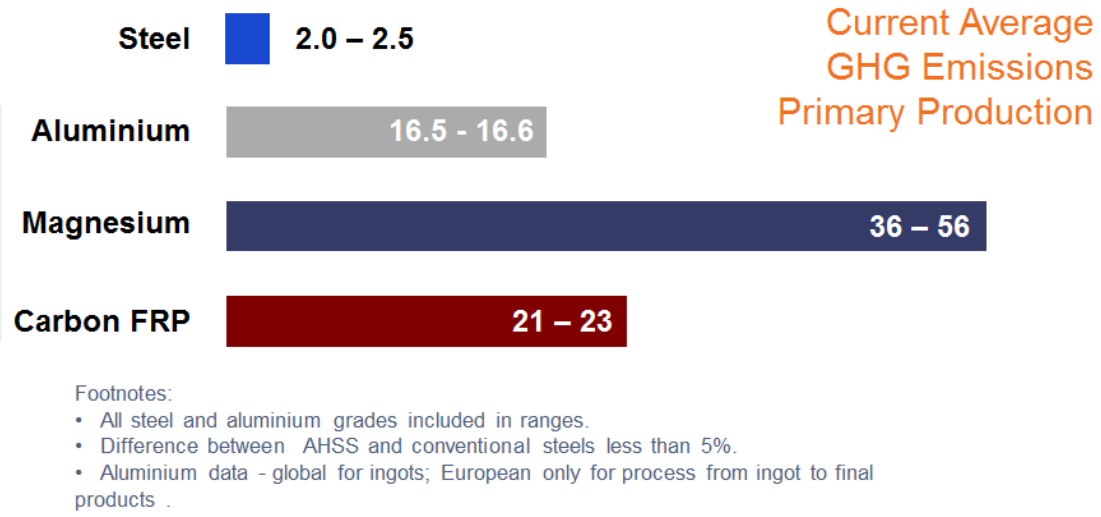

Figure 1.5 Material average GHG emissions in production, CO_2 emissions/kg material, [2, 5].

Steel is the most recycled material in the world. On the other hand, steel has 100% recyclability. Moreover, steel in all phases of the life cycle cause to produce lower CO_2 emissions. For this reason, Life Cycle Assessment (LCA) exposed the environmental

performance advantages of steel. According to the discussions held above, the use of steel in the automotive industry is another essential requirement fulfilled by considering the environmental reasons.

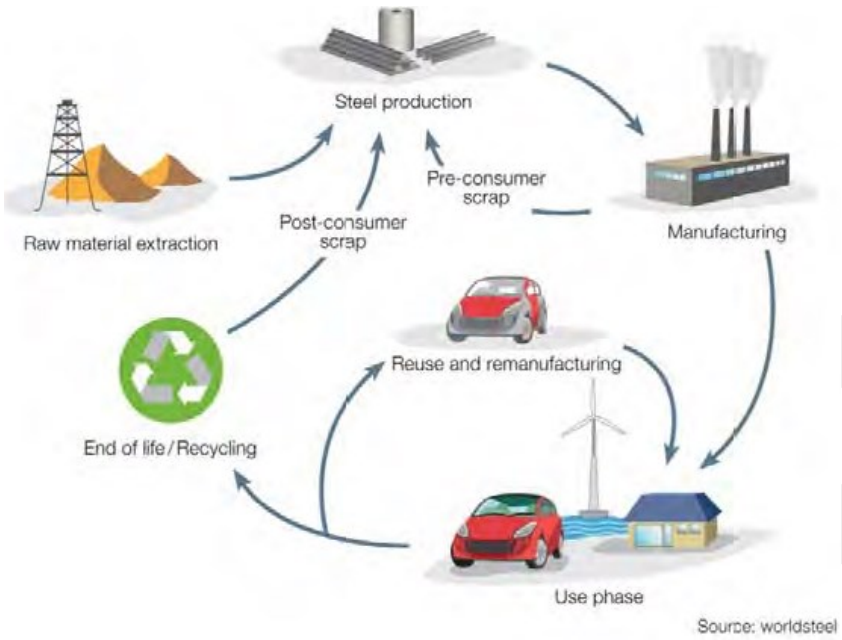

Figure 1.6 The total life cycle and the recycling material used in cars and vehicles [5].

For the conventional type of steels, there is an inverse relation between the mechanical properties of their strength and formability. The AHS steels are developed to address decreased formability with increased strength in conventional steels. When the sheet steels get increasingly stronger, they simultaneously become difficult to form. Some possible defects, early fracture, wrinkling, scratches, etc., can be met in the formed part. By adjusting the components in content and controlling the phase transformation in production the formability of AHS steels can be improved to manufacture the parts in complex geometries. On the other hand, AHSS offers high work hardening and bake hardening capabilities that allow increased formability.

Two car manufacturers, Honda and Volkswagen, quickly welcomed AHSS grades and started to manufacture some car parts by the use of AHS steels. Now, both of the companies have good experiences on designing and manufacturing AHSS car parts.

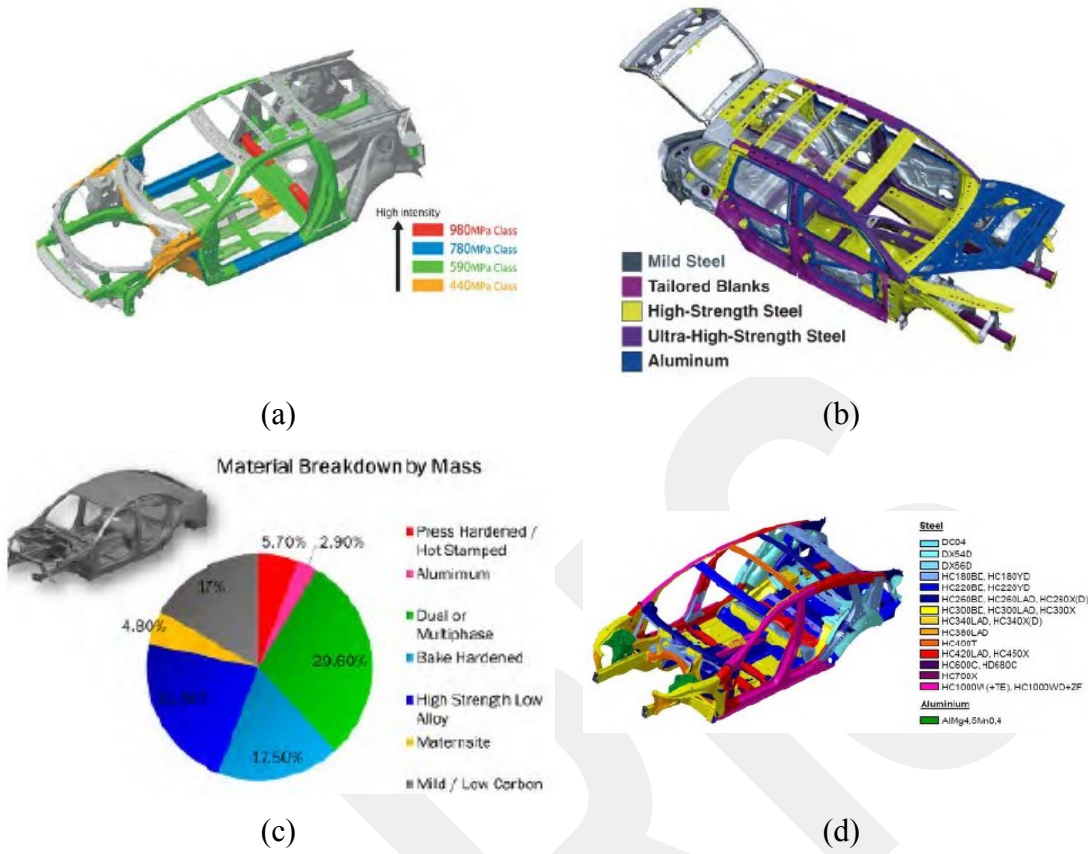

Figure 1.7 AHSS material usage for different cars, (a) AHSS in the 2011 Honda CR-Z, (b) Porsche Cayenne, in 2011, (c) Cadillac ATS produced in 2013 and reward as "Car Of The Year/2013" in North America (d) Mercedes E-Class, 2010, [1].

Steel is the most cost-competitive material for car bodies, due to their low prices.

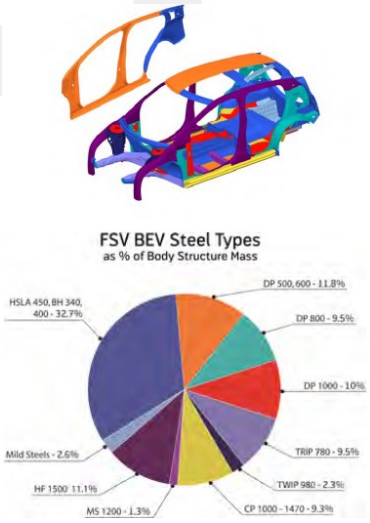

Figure 1.8 The material usage range for the future steel vehicle, [1].

Due to the appealing characteristics mentioned above AHSS is addressed as a current and future material which can be used in an increase percent for cars and vehicles by

auto makers. Some comments about AHSS are quoted by the people worked for auto industry

“The day of the mild steel part at the Ford Motor Company is dead,” said Ford’s chief safety engineer, Steve Kozak. “The majority of steels we’re using now are high strength or ultra-high strength.”[6]

“The real changes in technology have been the higher-strength materials we can still make into parts.” is said James G. Schroth, lab group manager in the Materials and Processes Lab of General Motors’ Research and Development Center.[6]

For steelmakers, that means continuing development of more advanced products that are stronger and yet remain formable. “It’s a systematic engineering process,” said Dr. Zuidema, of Arcelor Mittal. “We have a fairly comprehensive knowledge of how each of the potential phases in the iron-carbon system affects the mechanical properties.” So if they know what properties are desired, they can determine the structure needed, and thus the combination of alloying and processing to achieve that structure [6].

1.2 STATEMENT OF PROBLEM

By many authorities, the development of AHSS is defined as “Reinvention of Steel”, the present experimental study focused on the development of an application method to improve their formability which is the outmost important problem of AHSS encountered in auto industry.

Since the early 1900’s, the studies devoted to improve sheet forming method have been focused mainly on cold sheet forming. Most of the scientific research on hot sheet forming has been conducted during the recent years. This is due to the development of new materials like AHSS and the requirements for more precision parts. Recently, more research projects have started to explore the benefits of hot or warm drawing. However, very limited investigations are seen for preferential heating or non-isothermal heating of the flange region in the deep-drawing of sheet metal parts.

The cold formability of steels has limitations in terms of forming capability and forming characteristics. The cold forming of AHSS sheet materials need high blank holding forces which can be provided by high capacity presses. The design, manufacturing and operational costs of such a big capacity presses are very high. On the other hand, cold drawn parts have some serious problems. Those are dimensional instabilities due to spring back, not achieving the desired strength and strain values,

having high residual stresses. Sheet metal forming at elevated temperatures gives possibility to overcome those problems mentioned above.

The limiting drawing ratio (LDR) can be simply given as the maximum ratio of the initial radius of blank (r_0) to the average radius of punch radius and die cavity radius, it shows maximum drawability of sheet materials without any defects, for example, tearing, fracture, wrinkling, …etc. and can be formulated as,

$$LDR = \frac{r_0}{r_i} \tag{2.7}$$

where

r_0 is the initial radius of blank

r_i is the average of punch radius (r_p) and die cavity radius (r_d)

It is an important parameter which indicates the formability of sheet materials in deep drawing operation. Although the limiting drawing ratio is an important parameter, for the parts formed into complex shape in the deep draw operation, some more information is required to be obtained to predict possible modes of failure. Such information can be evaluated by executing uni-axial and bi-axial tests tensile tests, Nakazima and Marciniak for the evaluation of forming limit curves.

On the other hand, there are problems required to be solved in hot forming operation of AHSS sheet steels. Those are the determination of application technique for the preferential heating of blank and the oxidation problem of blank as a result of its contact with ambient air at high temperature.

1.3 AIM AND SCOPE

The increasing use of light metals and high strength steel in the automobile industry demands for new sheet metal forming processes that can be applied successfully. In this thesis the subject of warm sheet metal forming is studied. In warm sheet metal forming the temperature of the blank is elevated to a specified temperature range gradually in the flange region of the blank. A survey of existing knowledge on this subject shows that the formability can be improved remarkably.

When discussing forming at elevated temperature it is important to distinguish warm forming from hot forming. In warm forming the microstructure is basically stable, but in hot forming microstructural changes occur, including recrystallization and grain growth. Usually the temperature interval for warm forming starts at 0,3 times the

melting temperature and ends at 0,5 times the melting temperature. At higher temperatures the term hot forming is used.

As this review will show, warm sheet metal forming can be conducted either with a homogeneous heated blank or with a blank that is only heated partially. These two different concepts obtain the possible advantage of increased formability in different ways and this is further discussed in subsequent sections.

For the improvement of Limiting Drawing Ratio (LDR) of AHSS sheet materials, only the partial heating namely the flange region of blank will be heated up to a temperature which is below the recrystallization temperature. This new solution will be comparatively evaluated with industrial used heating of blanks in continuous ovens. The Induction Heating which is placed in a close position to test piece will be applied to the flange region of blank. Then, deep drawing tests will be executed. In further stages of this study, during warm forming operation, a cooling is applied to obtain the required temperature gradient in the blank.

With increase of yield strength and ultimate tensile strength, the formability of AHSS at room temperature is decreased. Therefore, the warm/ hot forming which drastically improves the material's formability, reduces punch/blank-holder forces and decrease the spring back become major issue of contemporary forming strategy where AHSS sheet metals are used.

Although many different temperature limits are examined, the effective temperature range improving LDR for the materials in the present study is stated in between 180ºC – 275ºC.

Four different type of steels having thicknesses between 0.8 mm -1.6 mm were intended to be used in this scientific research subjected on the improvement of LDR at elevated temperature, as given

1) DP600 (Dual Phase Steel),
2) Erdemir 7128 (HSLA / Grade: HC300LA / Standard: DIN EN 10268-2006),
3) Erdemir 7140 (HSLA / Grade: HC420LA / Standard: DIN EN 10268-2006),
4) Erdemir DC04

(IF/Interstitial-Free/ Steel Grade 7114/ Standard: DIN EN 10130-2006)

1.4 CONTENT

The first chapter aims to give the reader, an importance of improvement in the formability of AHSS. Second chapter is devoted to introduce the characteristics and

properties of DP steels and HSLA steels, and then deep drawing is described in details, the last section in this chapter is reserved for the previous studies done by primary contributors including their work scope. The third chapter gives the objective of the current dissertation. The theory of deep drawing and the possible mathematical solution methods are presented in Chapter 4. The setup designs, equipment and machine which are used, are introduced with their reasons. The experimental activities including calibration work and material characterization tests are given in Chapter 5. The result of experiments are represented in graphical form and the results are discussed in Chapter 6. Chapter 7 is devoted to conclusions and suggestions for the future work.

GCRIS

CHAPTER 2

LITERATURE SURVEY

2.1 MATERIAL

In this section, the characteristics and properties of Dual Phase (DP) steels and High Strength Low Alloy (HSLA) steels will be reviewed. The discussion of each steel will begin with a review of the microstructure, followed by a review of the mechanical properties and the high strain rate properties. This encompasses the material information which is necessary for carrying out this research.

2.1.1 Introduction

The term dual phase (DP) steels, refers to a class of high strength steels composed of two phases; normally a ferrite matrix and a dispersed second phase of martensite, retained esspecially austenite and/or bainite. In the 1970's, the development of DP steels was driven by the need for new high strength steels without reducing the formability or increasing costs. The automotive industry has demanded those steel grades with high tensile elongation to ensure formability, high tensile strength to establish fatigue and crash resistance, low alloy content to ensure weldability without influencing production cost [1]. The demand for DP steels is very high in auto steel market. These class of steels combine high strength and good formability in their material characteristic, thus reduce the weight of vehicles, onthe other hand give an environmental and economical advantages.

2.1.2 Microstructural and Mechanical Properties

2.1.2.1 Dual Phase (DP) Steels

DP steels can be described as the steels consist of a ferritic matrix containing a hard martensitic second phase in the form of islands. When the volume fraction of hard second phases is increased, it generally increases the strength.

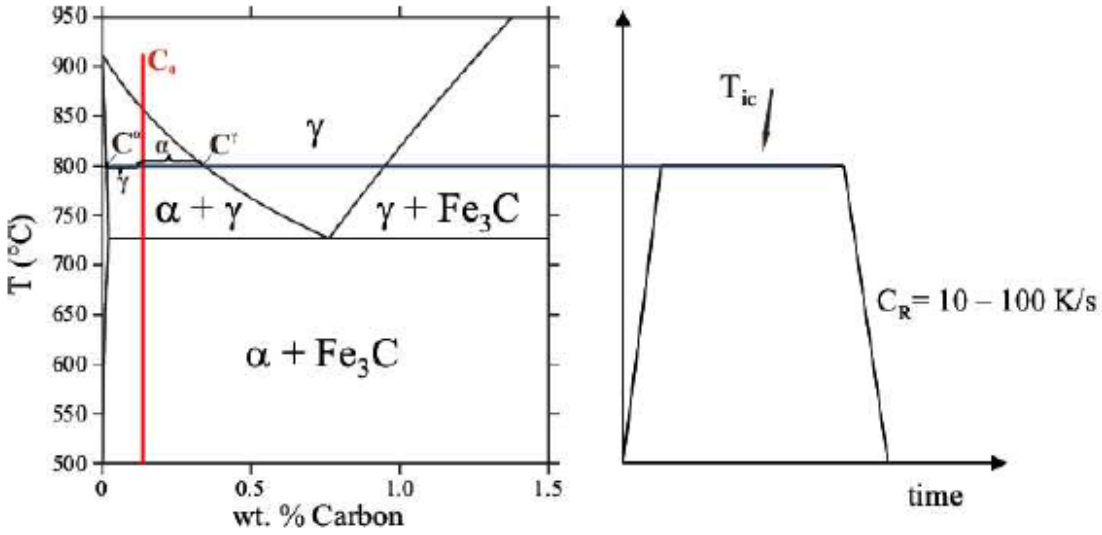

Figure 2.1 Production of Dual Phase (DP) steel, [1].

The dual phase steels are production of by intercritical annealing shown in Figure 2.1. the equilibrium fractions of austenite and ferrite as well as their carbon content at the annealing temperature can easily be estimated by applying the lever rule. DP (ferrite plus martensite) steels are produced by controlled cooling from the austenite phase or from the two-phase ferrite plus austenite phase to transform some austenite to ferrite before a rapid cooling transforms the remaining austenite to martensite.

Figure 2.2 shows a schematic microstructural view of DP steel, which contains ferrite plus islands of martensite. The soft ferrite phase generally gives these steels excellent ductility. When these steels are deformed, the strain is concentrated in the ferrite phase surrounding the islands of martensite, creating the unique high initial work-hardening rate (n-value) exhibited by these steels. Figure 2.3 is a real photomicrograph showing the ferrite and martensite constituents in its microstructure. The work hardening rate with excellent elongation creates DP steels with much higher ultimate tensile strengths than conventional steels of similar yield strength.

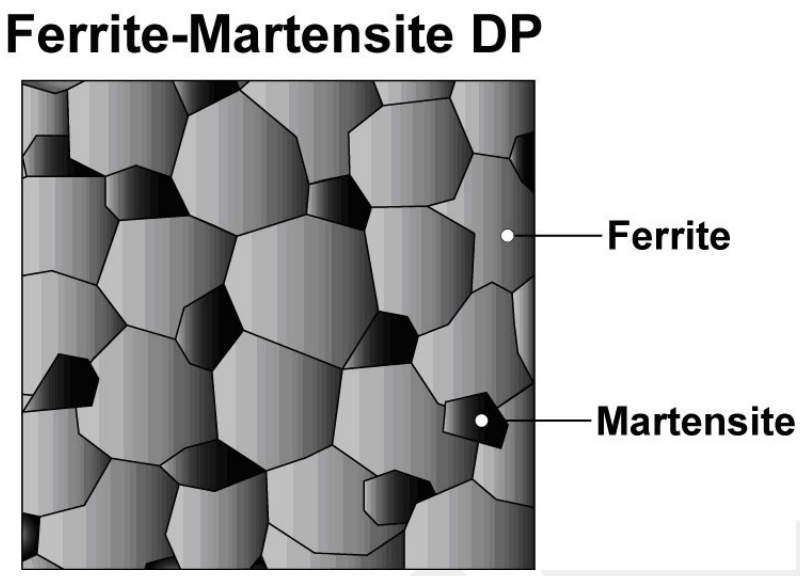

Figure 2.2 The islands of martensite in a matrix of ferrite is shown in schematic microstructural view, [1].

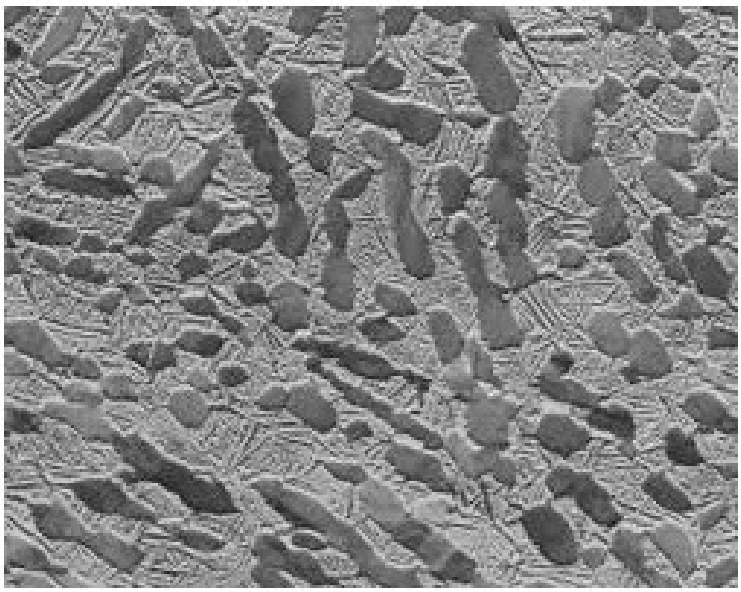

Figure 2.3 Photomicrograph of DP steel showing the ferrite and martensite constituents, [1].

In DP steels, carbon content enables the formation of martensite at suitable cooling rates by increasing the hardenability of the steel. The alloying elements, manganese, chromium, molybdenum, vanadium, and nickel, added individually or in combination, for improvement of hardenability. Carbon also strengthens the martensite as a ferrite solute strengthener. The other important considerations taken into account is the spot

welding capability, to maintain this, these additions are carefully balanced, not only to produce unique mechanical properties, [1].

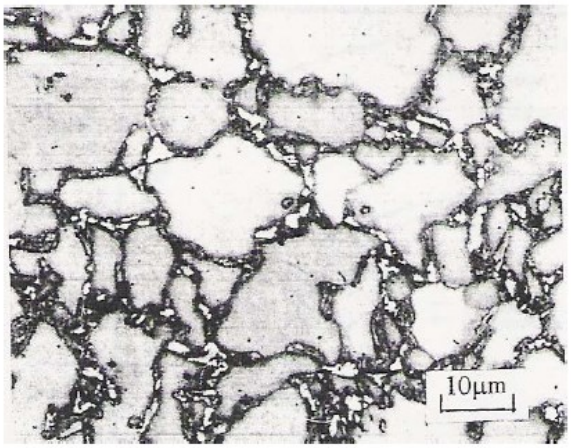

Figure 2.4 Microstructure of a dual phase steel, the regions colored as gray, black and white represents ferrite, martensite, and epitaxial ferrite, respectively [1].

Upon quenching a dual phase steel, residual stresses are created at the martensite-ferrite interfaces as a result of the volumetric expansion of the martensite. This creates an increased number of dislocations at the martensite-ferrite interfaces, these dislocations can be seen as black in Figure 2.5.

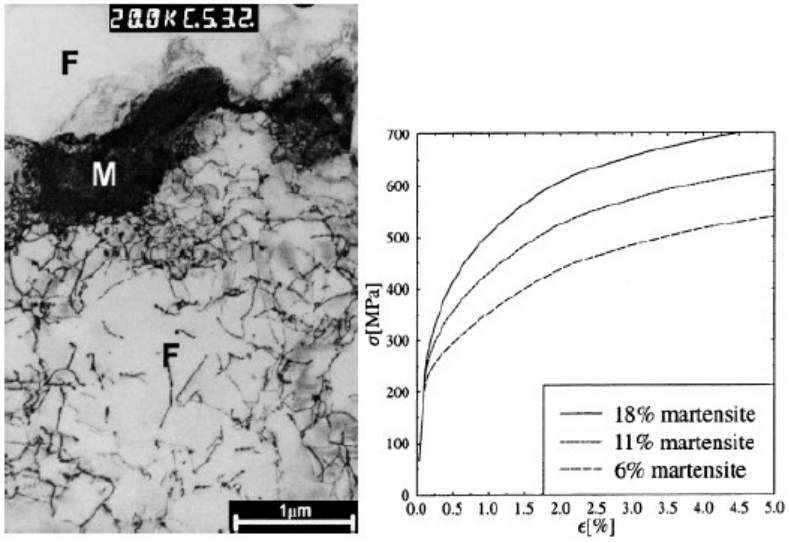

Figure 2.5 Transmission electron microscope image of the ferrite-martensite interface in a dual phase steel and the corresponding stress-strain curve which shows the effect of the volume percent of martensite, [1].

These type of steels have high fatigue strength and good energy absorption capacity, so these kind of properties make them suitable for use in structural parts and reinforcements in car production, giving superior crash performance.

2.1.2.2 High-Strength Low-Alloy Steel (HSLA)

High Strength Low Alloy Steels (HSLA) are another type of steel which show good performance in the weight reduction of automobiles. They also show good strength, formability and weldability, but their production cost is lower than equivalent heat-treated alloys because they achieve their desired characteristics directly from hot rolling. They have been using for automotive applications as well as warships, off-road trucks, offshore platforms, and equipment for oil-wells [1].

HSLA steels typically have a ferrite-pearlite microstructure. in the 1960' s, they were developed by adding niobium, vanadium, and titanium as alloying elements to improve mechanical properties. When these elements are added to the steel, Ti-N, Nb-N, and Nb-C are formed, the strength of the steel is increased, however these precipitates reduce their ductility and weldability.

The microstructure of HSLA generally comprises a fine grained ferrite matrix with pearlite and/or bainite islands, depending on the cooling rate, as seen in Figure 2.6. The microstructure on the right has a higher carbon content than the microstructure on the left.

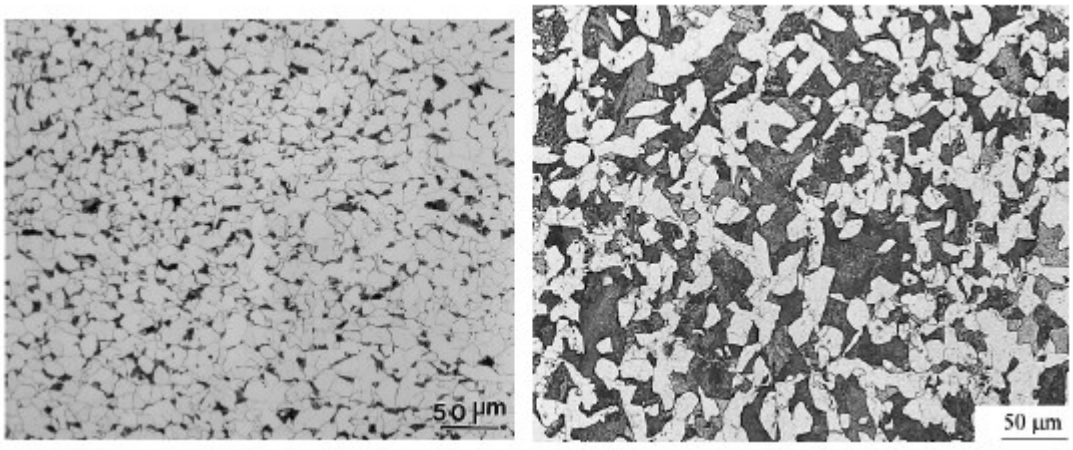

Figure 2.6 Two examples of HSLA microstructure, the one on the left contains higher carbon content. The white grains are ferrite, the light gray grains are pearlite, and the dark gray grains are bainite, [1].

The characteristic similiar to low-carbon steels can be observed in HSLA steels. The stress-strain relationship of HSLA is characterized by an upper and lower yield point, followed by discontinuous yielding and work-hardening. The mechanical properties of HSLA 65 at various temperatures are given in Figure 2.7 and 2.8

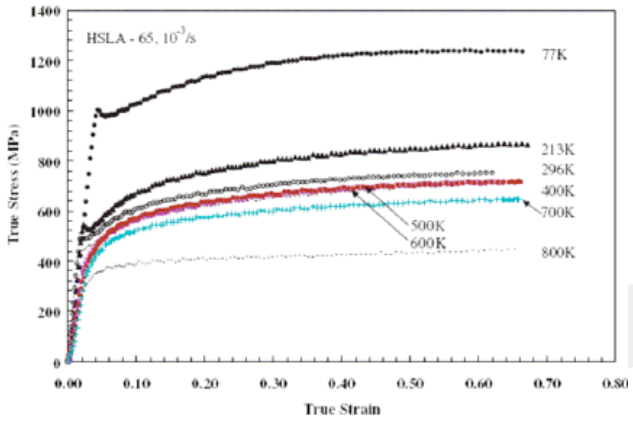

Figure 2.7 True stress-strain graphs of HSLA-65 at various temperatures, [7].

As with most annealed steels, accelerated cooling after heating substantially increases the strength, due to smaller grain size, as well as stronger constituents (i.e. bainite instead of pearlite).

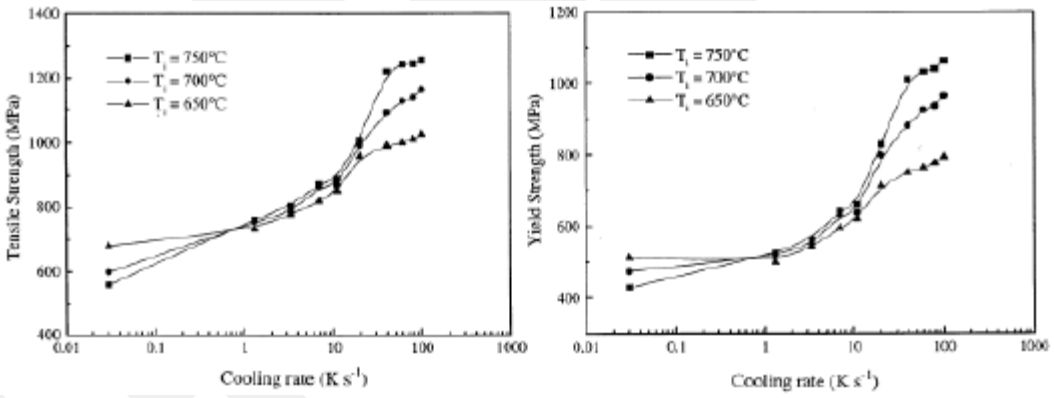

Figure 2.8 Yield and ultimate tensile strength of HSLA-65 having different cooling rates, [7].

2.1.3 Comparison of Advanced High Strength Steel and Conventional Type Steel

When DP steels are compared with other high strength low alloy (HSLA) steels, DP steels show superior properties (see Figure 2.9).

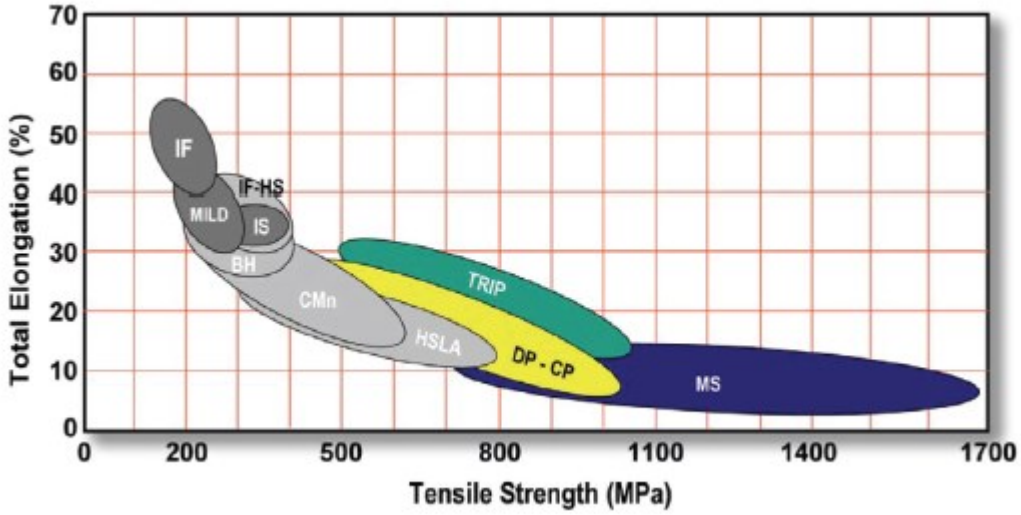

Figure 2.9 Schematic picture showing advanced high strength steels (shown in color) compared to low, strength steels (dark grey) and traditional HS steels (grey), [1].

DP and other AHSS also have a bake hardening effect that is an important benefit compared to conventional higher strength steels. The bake hardening effect is the increase in yield strength resulting from elevated temperature aging (created by the curing temperature of paint bake ovens) after pre-straining (generated by the work hardening due to deformation during stamping or other manufacturing process). The extent of the bake hardening effect in AHSS depends on an adequate amount of forming strain for the specific chemistry and thermal history of the steel.

Figure 2.10 compares the engineering stress-strain curve for HSLA steel to a DP steel curve of similar yield strength.

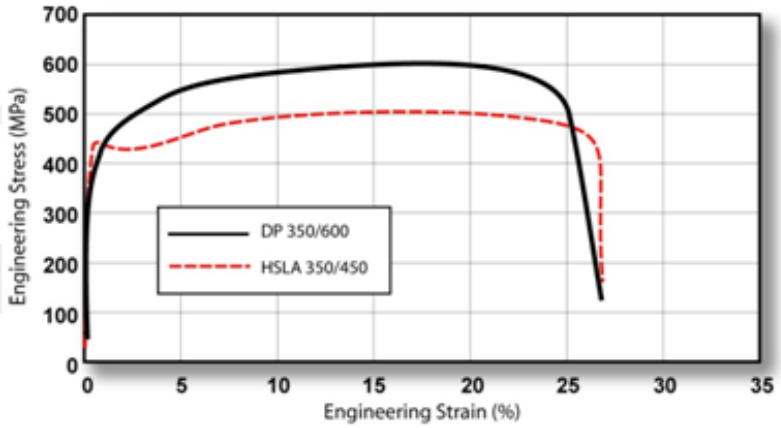

Figure 2.10 The DP 350/600 having close yield strength with higher ultimate tensile strength than the HSLA 350/450, [1].

AHSS addressed to a type of steel having poor formability with increased strength when they were compared with conventional steels. As steels became increasingly stronger, they simultaneously became increasingly difficult to form into automotive parts. AHSS, although much stronger than conventional low to high-strength steel, also offer high work hardening and bake hardening capabilities that allow increased formability and opportunities for optimization of part geometries.

The principal difference between conventional HSS and AHSS is their microstructure. Conventional HSS are single-phase ferritic steels with a potential for some pearlite in C-Mn steels. AHSS are primarily steels with a microstructure containing a phase other than ferrite, pearlite, or cementite for example martensite, bainite, austenite, and/or retained austenite in quantities sufficient to produce unique mechanical properties. Some types of AHSS have a higher strain hardening capacity resulting in a strength-ductility balance superior to conventional steels.

The work hardening rate plus excellent elongation creates DP steels with much higher ultimate tensile strengths than conventional steels of similar yield strength. Figure 2.10 shows HSLA and DP, both having the same yield strength on the same graph to demonstrate the differences in plastic flow behaviours. The DP steel exhibits higher initial work hardening rate, higher ultimate tensile strength, and higher TS/YS ratio than a similar yield strength HSLA. Additional engineering and true stress-strain curves for DP steel grades are located in Figure 2.11 and 2.12.

GORIS

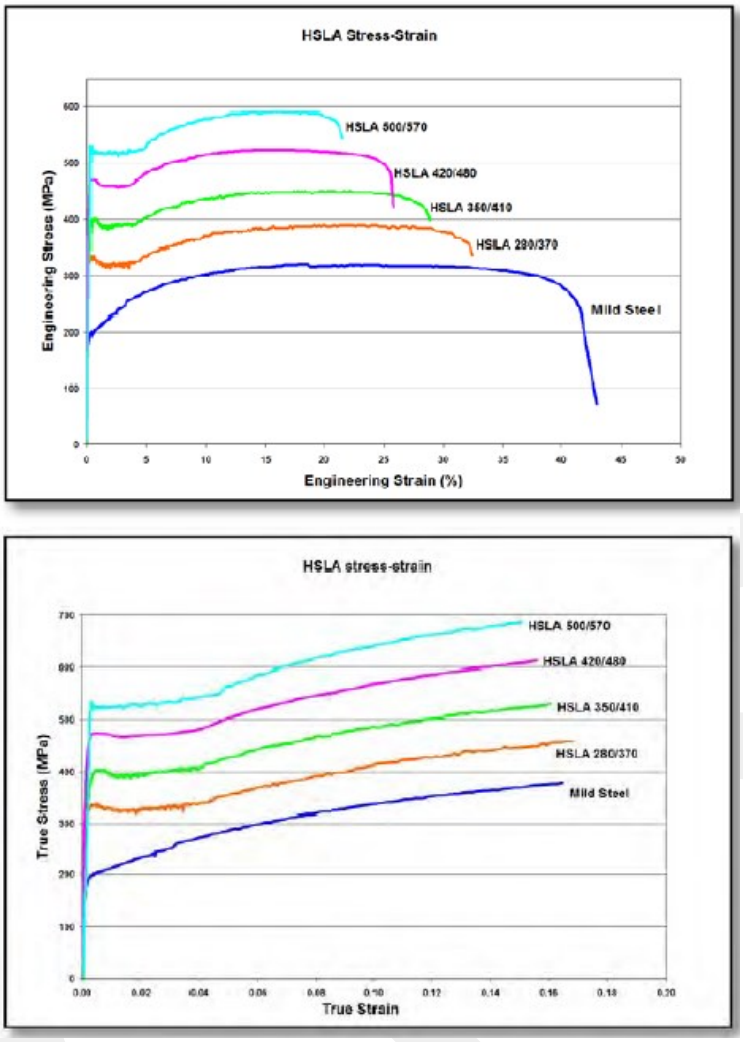

Figure 2.11 Engineering stress-strain (upper graphic) and true stress-strain (lower graphic) curves for different cold-rolled HSLA steel grades, [8,9].

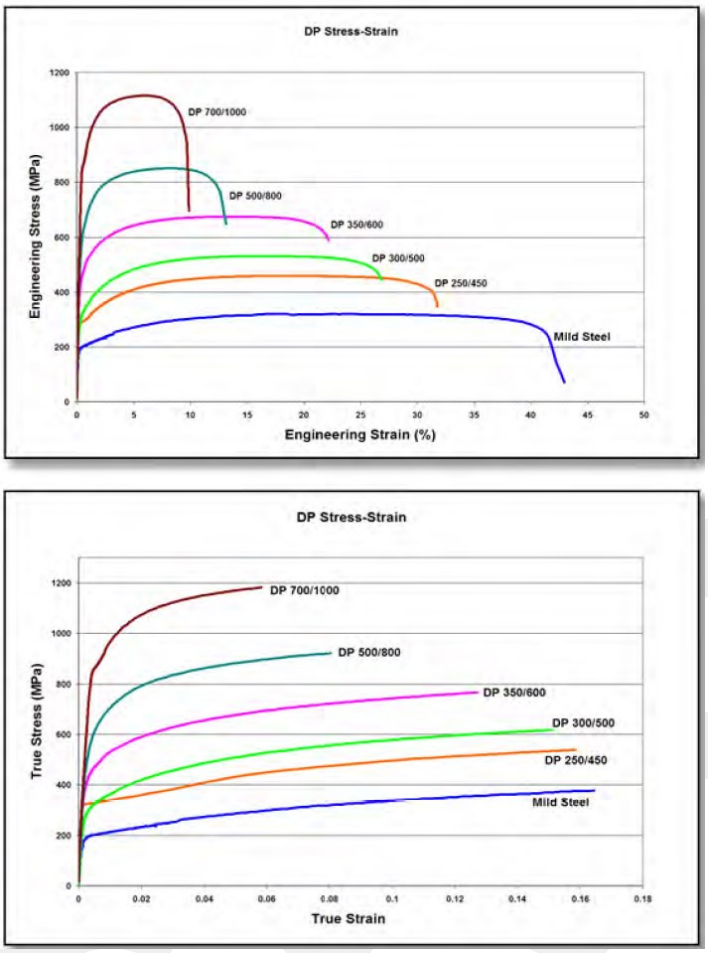

Figure 2.12 Engineering stress-strain (upper graphic) and true stress-strain (lower graphic) curves for different DP steel grades. The sheet thicknesses for DP250/450 and DP500/800 = 1.0mm. the thickness of other steels changes between 1.8-2.0mm, [8,9].

For the elaboration of the following sections on deep drawing, the reader may refer to A thesis by Arjan L. P. Coremans, June 1992, [48].

2.2 DEEP DRAWING

The deep drawing process includes series of deformation operations. In deep drawing a flat sheet metal is drawn into a die to form cylindrical or rectangular cups or irregular shapes, deep or shallow. Sometimes it is called as stamping in literature but in this dissertation, the term the deep drawing are always used.

2.2.1 Operation

In a deep drawing operation, a flat sheet metal is set between a die and a punch (Figure 2.13). As the punch moves into the die cavity, the metal blank is formed into the

desired shape. If the one wants to obtain a defect free deep drawn parts, those process parameters such as blank holder pressure, lubrication, ratio of the punch diameter to the blank diameter, and blank material, etc. should be chosen carefully.

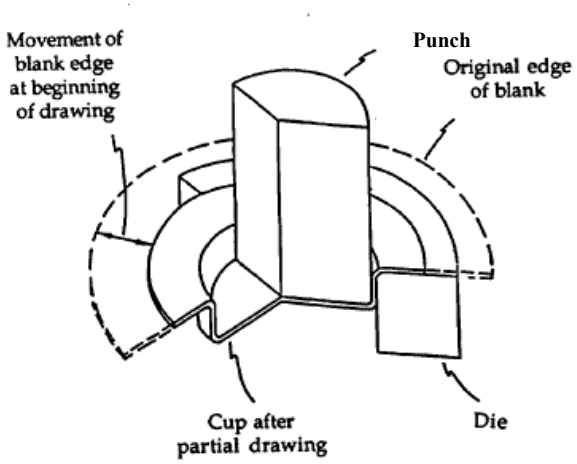

Figure 2.13 Deep drawing operation figured in 3D by sectioning.

During deep drawing of axisymmetric parts, the sheet metal blank is exposed to various types of deformation, radial drawing, bending, unbending, uni-axial streching, bi-axial streching, etc. As a result of those series of deformation processes, a sheet metal blank is gradually changed from a planar form to a deep drawn part. The one of the important process parameter is the Blank Holding Force. The blank holding force (BHF) required to be applied onto the flange of blank to prevent formation of wrinkles due to the circumferential compressive stresses.

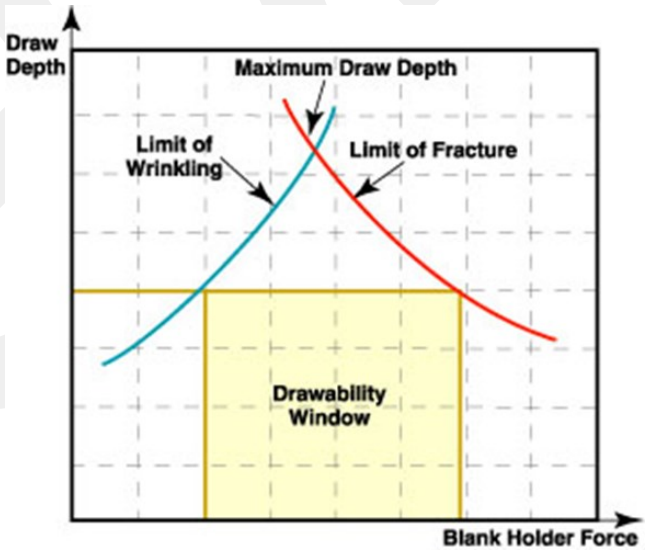

Figure 2.14 Schematic representation of the effect of blank holder force (BHF) upon achievable part depth, [41].

Figure 2.14 illustrates the effect of BHF on the failure of the sheet metal in deep drawing operation. If the BHF is very high so that the drawing operation into die is prevented, during the drawing operation, the side-wall of cup can only be stretched a small amount before it fractures; this is indicated as the tearing limit.

On the other hand, as the BHF is reduced, insufficient pressure may exist to prevent wrinkling in the flange region and the fracture during deep drawing process. The objective in a particular deep drawing operation is to apply available magnitude of blank holder force, as a result of this, the desired part depth (H), can be obtained. As the one can easily realize in Figure 2.14, there is a reasonable range of useful BHF. The theory as well as experimental evidence indicate that the varying blank holder force during deep drawing increases the limiting drawing ratio which can simply defined as the ratio of initial blank diameter to the average diameter of punch and die.

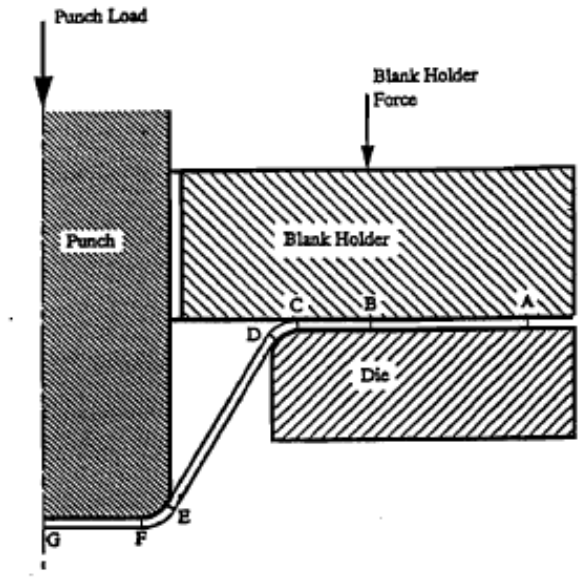

A-B: Radial drawing of the flange between die and the blankholder with friction resistance present at the interface.
B-C: Radial drawing of sheet not in contact with the blankholder.
C-D: Radial drawing and bending over the die corner radius.
D-E: Unbending and straightening to form the wall of the cup.
E-F: Bending, sliding, and stretching over the punch profile.
F-G: Bi-axial tensile stretching of sheet over the bottom surface of the punch.

Figure 2.15 Representation of deep drawing of a cylinder cup using blank holder, [42].

Some restraining is introduced for the flow of metal at the die corner radius. But this force is not individually enough to control the metal flow in deep drawing. An extra restraining force is obtained by means of frictional forces alone or/and by creating

geometric restrictions like draw beads before die. Frictional forces are developed by pressing the blankholder against the die. for this case, the restraining force is a function of lubrication and clamping pressure. As shown in Figure 2.15, the stages of deep drawing are well indicated by Ahmetoğlu, 1990, [42].

A theoretical and experimental evaluation of the effect of BHF variation on Limiting Drawing Ratio was carried out in different studies. These studies focused mainly on the establishment of the optimum BHF for different process parameters.

Schematic figures illustrating basic deep drawing process, and some examples of deep drawn products are shown in Figures 2.16 and 2.17 respectively.

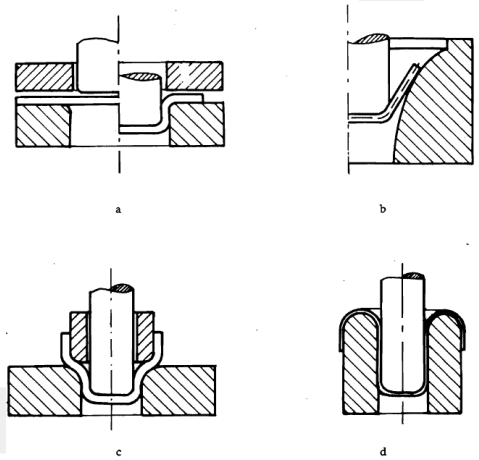

Figure 2.16 Schematic representations of some axisymmetric deep drawing processes, a) Deep drawing with a blankholder b) Deep drawing without a blankholder c) Direct redrawing d) Reverse redrawing, [42].

Figure 2.17 Examples to conventional deep drawing workpieces, [43].

In most industrial manufacturing systems, a certain deep drawn products require a number of drawing operations. The force necessary for a deep drawing process is applied to the blank by means of a punch. The force is then distributed as a stress in the sheet material formed over the punch corner radius. This causes high tensile stresses in the cup side wall. Usually the circumfrential area close to the bottom corner of the cup is the most critical area where fracture may occur.

The workpiece is subjected to radial tension forces F_R and tangential compression forces F_T (Fig. 2.18) in the flange region. As a result of this, the material is compressed in the tangential direction and stretched in the radial direction. As the deep drawing is progressing and stretch drawing depth is increased, the amount of deformation and the resistance to deformation are also increased. The sheet metal is most severely stretched on the corner of the draw punch. Failure generally occurs at this point (base fracturing). While it is drawing under the force applied by a blank holder, the press must also transfer the blankholding force onto the die.

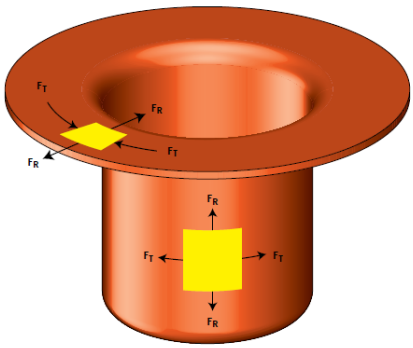

Figure 2.18 The representation of pressing forces in deep drawing of a round cup with a blank holder, [44].

2.2.2 Formability of Sheet Metals

In the following sections the main factors influencing on formability of sheet metal is explained in details. Methods used for the evaluation of sheet metal formability is shown Figure 2.19

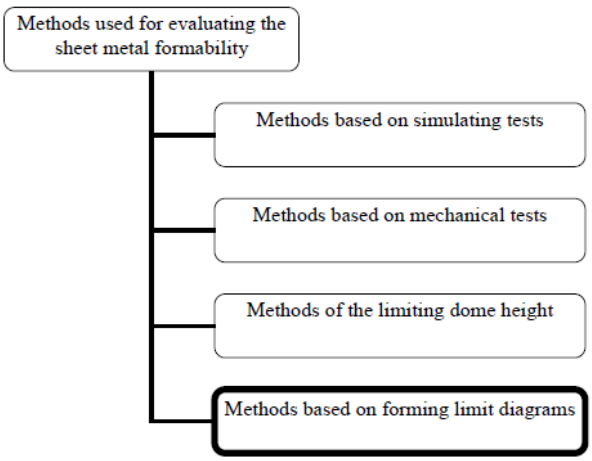

Figure 2.19 Methods for evaluating sheet metal formability, [47]

2.2.2.1 Material properties and their influences on its formability.

The behavior of materials under plastic flow conditions is generally described by a flow curve. The well known relation for the flow of material is the simple power law hardening relation expressed as

$$\sigma_{true} = K(\varepsilon_{true} + \varepsilon_0)^n \tag{2.1}$$

Where;

σ_{true} : true stress

K : strength coefficient

ε_{true} : true strain

n : strain hardening coefficient

ε_0 : initial strain

This law has been proposed by Swift but a special case with no initial strain is formulated is known as the Ludwik law. This law is quite simple to be used for the analysis in the plastic behavior of most metallic materials. Hence, the variables, K (strength coefficient) and n (strain hardening coefficient), represents material properties in Equation 2.1.

2.2.2.2 The influence of the n value on the deep drawability

The n value is determined by the dependence of the flow (yield) stress on the level of formed strain. For the materials having a high n value, the flow stress increases rapidly with strain . This tends to further distribution of strain to the regions of lower strain

and flow stress. This is particularly important in the post uniform elongation of the regions where necking and strain concentrations occurred. Hence high n values lead to good formability in stretching operation of sheet metals, but have little effect on drawability. In a drawing operation, the metal in the flange must be drawn without causing fracture in the side wall. Therefore, a high n value strengthens the wall, which is beneficial, but also strengthens the flange and make it harder to draw in, which is detrimental. In the beginning, however, the process is not exclusively deep drawing but a combination of drawing and stretching. As mentioned before, a high n value improves the formability in operations which involve stretching.

Zünkler has performed an analytical and experimental study on the influence of the n value on the deep drawability, [49]. He has found the following relationship;

$$Ln\left(\frac{d_0}{d_p}\right)=\left(\frac{\eta_{def}}{1.1}\right)^{\frac{1}{(n+1)}}(n+1) \qquad (2.2)$$

Where $\eta_{def}=\left(\frac{W_{id}}{W_{tot}}\right)$

d_0 : initial blank diameter

d_p : punch diameter

η_{def} : deformation efficiency

W_{id} : ideal deformation work

W_{tot} : actual needed deformation work

This equation clearly shows an influence of the strain hardening exponent (n) on the limiting draw ratio, [49].

2.2.2.3 The influence of the K value on the deep drawability.

The "K" value does not have much of an influence on the formability, due to the strength coefficient which is a material property. But it is a good sign of the material drawability. During a drawing operation, the metal in the flange must be drawn in easily without causing fracture in the wall. A high "K" value means a formation of strong wall, which is beneficial, but also a strong flange which makes it harder to draw in, due to compressive stresses formed in flange region. Therefore, to perform a

successful drawing operation the K value should not be too much small, to assure a reasonable strength of the product. On the other hand, it should not be too high to cause excessive punch force required to complete the draw.

2.2.2.4 The influence of the r value on the deep drawability.

Another parameter often used when deep drawing is analyzed is the r value. This value indicates the of a material, in other words it is the sign of material anisotropy. The anisotropy of a material is a kind of measure for the most preferred strain direction of a material.

The r value or anisotropy factor is defined as the ratio of the true thickness strain to the true width strain in a tensile test. Generally, its value depends on the elongation at which it is measured. Most commonly the r value is determined at 10, 15, or 20 percent of elongation.

The r value is calculated as shown below;

$$\varepsilon_w = \ln\left(\frac{w}{w_0}\right)$$

$$\varepsilon_t = \ln\left(\frac{t}{t_0}\right)$$

$$r = \frac{\varepsilon_w}{\varepsilon_t} = \frac{\ln\left[\frac{w}{w_0}\right]}{\ln\left[\frac{t}{t_0}\right]} \tag{2.3}$$

Where

ε_w : true width strain

ε_t : true thickness strain

w_0 : initial width of the tensile specimen

w : intermediate width of the tensile specimen

t_0 : initial thickness of the tensile specimen

t : intermediate thickness of the tensile specimen

The r value, however, is not constant in each directions of the sheet. During the manufacturing process (casting and rolling), every material has become more or less

anisotropic in sheet formation. The microstructural analysis of the sheet metal shows preferred directions. This results in the r value whose value differs in different directions on the sheet. The maxima are equally spaced with respect to the rolling direction of sheet. It is common to determine the r value in three directions which can be named as 0°,45°, and 90° according to rolling direction. From these values, two different parameters are calculated. These are;

a) the average r value, or average normal anisotropy;

$$r_m = \frac{\left(r_0 + r_{90} + 2r_{45}\right)}{4}$$

b) the planar anisotropy;

$$\Delta r = \frac{\left(r_0 + r_{90} - 2r_{45}\right)}{2}$$

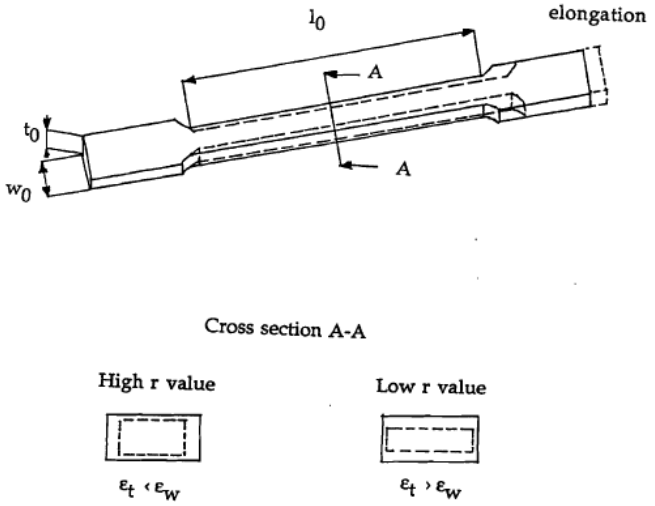

Figure 2.20 The influence of different r values in a tensile test. The thick lines refer to the original shape of the specimen, the dashed lines indicate the intermediate shape of the specimen, [40].

As can be seen from Equation 2.3, the r value is a measure of the ability of a material to resist thinning of sheet. The use of sheet metal with a large "r" value not only produces less wall thinning but also reduces the punch load used in the drawing operation. For a clear understanding of the influence of the "r" value, first of all a short theoretical explanation will be given. During a drawing operation, material in the flange is stretched radially, while it is compressed circumferentially. The resulting stress state can be seen in Figure 2.22. With the simplified assumption of isotropic

material ($r = 1$) which refers to a homogeneous stress state, this results in the following Von Mises yield criterion;

$$\sigma_{true} = \sqrt{\sigma_r + \sigma_\theta - 2\sigma_r\sigma_\theta} \tag{2.4}$$

Where $\sigma_r, \sigma_\theta, \sigma_Z$: stresses in cylindirical coordinate system

σ_{true} : yield stress

Hill has modified the Von Mises yield criterion for anisotropic materials, this criterion is later studied and simplified by Hosford et al. resulting in the following yield criterion [45]:

$$\sigma_{true} = \sqrt{\sigma_r + \sigma_\theta - 2\sigma_r\sigma_\theta \frac{2r}{r+1}} \tag{2.5}$$

This results in the flow surface plotted in a σ_r via σ_θ coordinate system as shown in Figure 2.24. The loci indicates the border limits between the plastic and elastic stress-strain state. As mentioned before, $\sigma_r > 0$ and $\sigma_\theta < 0$ in the flange region of a cup. This means that the stress state lies in the second quadrant in Figure 2.22. As can be seen from Figure 2.21, the higher the anisotropy is the lower the stresses need to be to reach the yielding point. Hence an increased anisotropy value will cause a decrease in the force necessary to pull in the flange area.

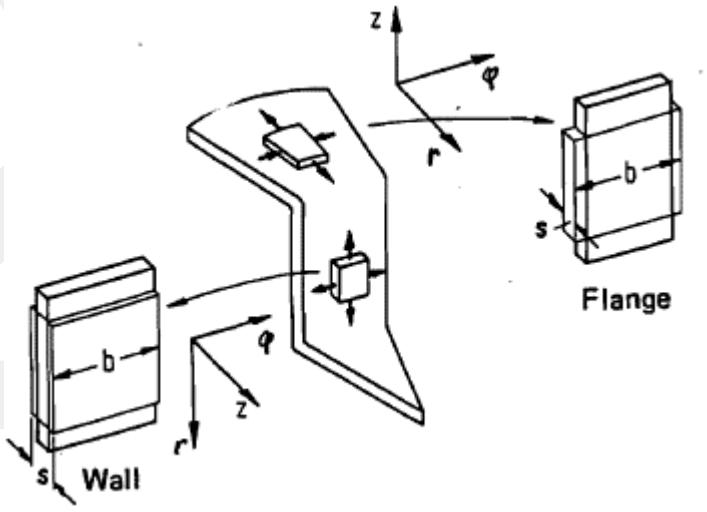

Figure 2.21 Schematic representation of the state of stress during deep drawing. Thin lines show the elements before deformation, thick lines indicate the element after deformation, [40].

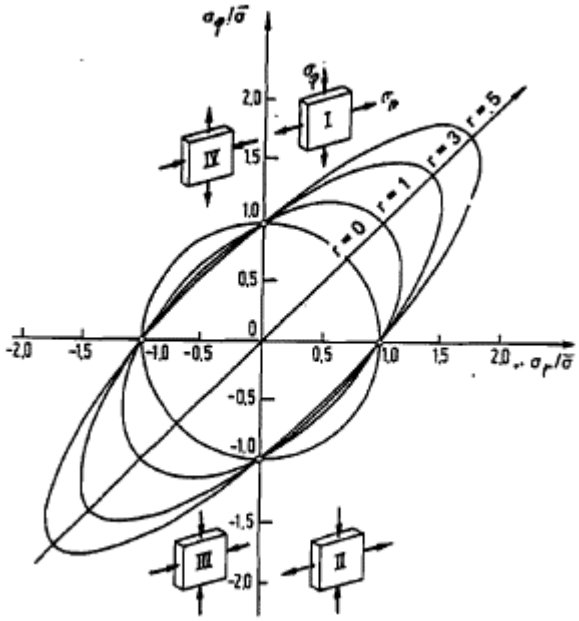

Figure 2.22 The yield surfaces for plane stress condition ($\sigma_Z = 0$), for 4 different anisotropy values, [40].

The stress state in the cup side wall is $\sigma_r > 0$ and $\sigma_\theta > 0$, as shown in Figure 2.22. It has to be noted that σ_r has substantially higher value than σ_θ. This means that the stresses are situated in the first quadrant. When yielding starts, the main deformation at this stage of drawing will be stretching of the cup wall. This will result in a decrease in its thickness. The higher r value, increases the stress necessary to start yielding. So a high r value will decrease the sensitivity for wall thinning. Since thinning will soon result in fracture, this is the criteria which determines the Limiting Drawing Ratio (LDR) which will be described deeply in the following section. The maximum draw ratio or LDR is the ratio between the initial diameter of the blank and the final diameter of the cup which can be formed without fracture. For cylindrical cups, the LDR is used as an important measure of the drawing operation [48].

As it is known that the earing is related to planar anisotropy. In the directions where the r value is highest, resistance against thickness changes is also highest. As the draw proceeds, material originally positioned at the outer circumference of the blank approaches to the die shoulder. Since the length in circumferential direction decreases considerably, material has to compensate for this decrease and the material in the flange region starts to thicken due to the volume constancy. The higher the r value the

more the material resists to compensate this circumferential reduction by means of an increase in the thickness of material.

The r_m value directly affects wall height. In non cylindrical axisymmetric cup drawing, it is advisable to position the sheet so that the directions with the largest strains coincide with the directions of the largest r values.

2.2.2.5 Friction and lubrication during sheet metal forming

Friction plays a major role in sheet metal forming. Friction is the result of internal deformation of the deformed material and controlled by the loads externally applied. In its different manifestations, friction results in complex wear mechanisms at the contact surfaces between the die / workpiece and blank holder / workpiece.

During forming operations, sliding friction conditions apply where lubrication is used. In describing friction in sheet metal forming, as a rule, the coefficient of friction μ is used and it is expressed as the friction force divided by the normal force, which can be formulated as given in Equation 2.6,

$$\mu = \frac{F_R}{F_N} \tag{2.6}$$

High local plastic deformations occur during friction in sheet forming. In the absence of sufficient lubrication, the boundary layers can break up locally and weld joints can develop. Coefficients of friction in the range of μ = 0,10 to 0,15 are indication of dry friction conditions. In sheet metal forming, the following parameters are of major importance:

– the material pair and the metallic surfaces which are in contact,

– the die geometry,

– the temperature-dependent properties of the lubricant as well as its volume and the location of lubricant application required to be considered

– the actual normal contact stress, which is a function of the load bearing surface portions of both surfaces should be taken in care

– the magnitude of the sliding velocity and the frictional path of the contacting surfaces in contact condition and

– the surface characteristics of the workpiece material as well as the changes of these characteristics that take place in

2.2.3 Limiting Drawing Ratio

The drawing ratio, generally speaking, can be defined as the ratio of optimum initial area of the blank to the cross-sectional area of punch. Maximum drawing ratio is an important numerical value to determine the required number of drawing steps. For cylindrical cup drawing process with circular cross-section, drawing ratio can be defined by the following equation:

$$LDR = \frac{r_0}{r_i} \tag{2.7}$$

where

r_0 is the initial radius of blank

r_i is the average of punch radius (r_p) and die cavity radius (r_d)

For non-circular cross-section, equivalent drawing ratio can be defined as the ratio of initial blank area and cross-sectional area of punch.

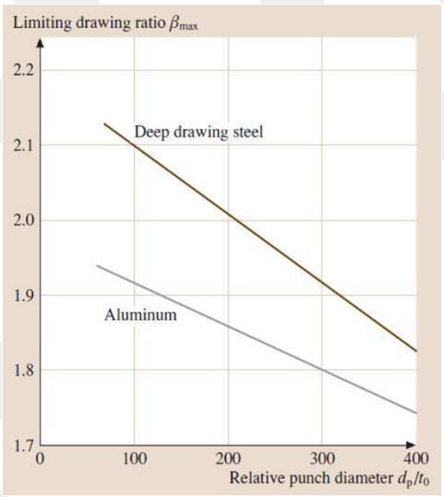

Figure 2.23 Effect of relative punch diameter on the limiting drawing ratio, for Aluminum and Steel, [35].

The drawing ratio is dependent on many factors like the tool geometry, lubrication conditions, and the amount of blank holding forces, sheet thickness, and material properties (especially R and n value). The limiting drawing ratio (LDR), which can be reached in a single drawing step, is theoretically calculated by membrane analysis. By membrane theory, the ideal limiting drawing ratio is $LDR \leq e \approx 2{,}72$.

2.2.4 Forming Limit Diagram (FLD)

Maximum values of principal strains ε_1 and ε_2 can be determined by measuring the strains at fracture on sheet components covered with grids of circles. During forming, the initial circles of the grid become ellipses. Keeler plotted the maximum principal strain against the minimum principal strain obtained from such ellipses at fracture of parts after biaxial stretching. By this way, a curve limiting the tolerable range is obtained.

Later Goodwin plotted the curve of tension/compression domain by using different mechanical tests. In this case, transverse compression allows obtaining high values of tensile strains like in rolling or wire drawing.

The diagrams of Keeler and Goodwin together give the values of ε_1 and ε_2 at fracture. Those strain values can be used to determine forming limit diagram (FLD) that is seen in Figure 2.24.

Keeler and Goodwin also suggested an empirical formula that was obtained from experimental trials on standard steel test specimens. This curve is only a function of work hardening exponent (n) and thickness (in mm), and it has been used for about twenty years and has yielded numerous successful results.

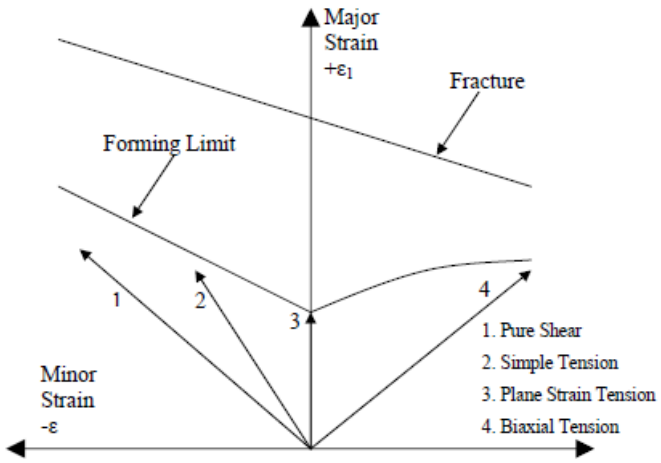

Figure 2.24 The forming limit diagram, loading types, [46].

2.2.5 Deep Drawing Parameters

Necking, tearing, wrinkling, bursting, or poor qualities in appearance are the factors that generally define a limit to the deformation in sheet metal forming (Figure 2.25). Figure 2.27 summarizes the parameters that have an effect on the formability of sheet

metals. Furthermore, the influence of various parameters on the formability in deep drawing is presented in Figure 2.26.

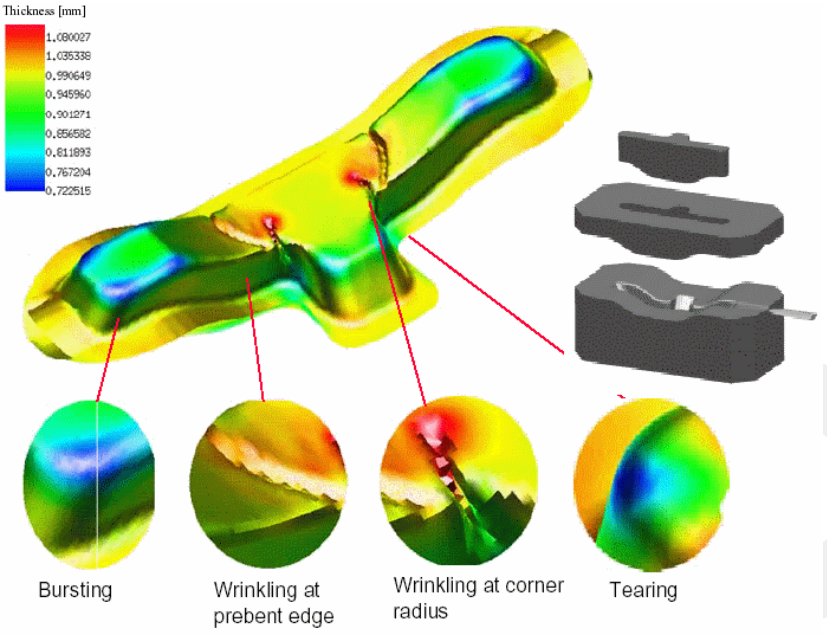

Figure 2.25 Possible failure (defects) modes in sheet metal products, [44].

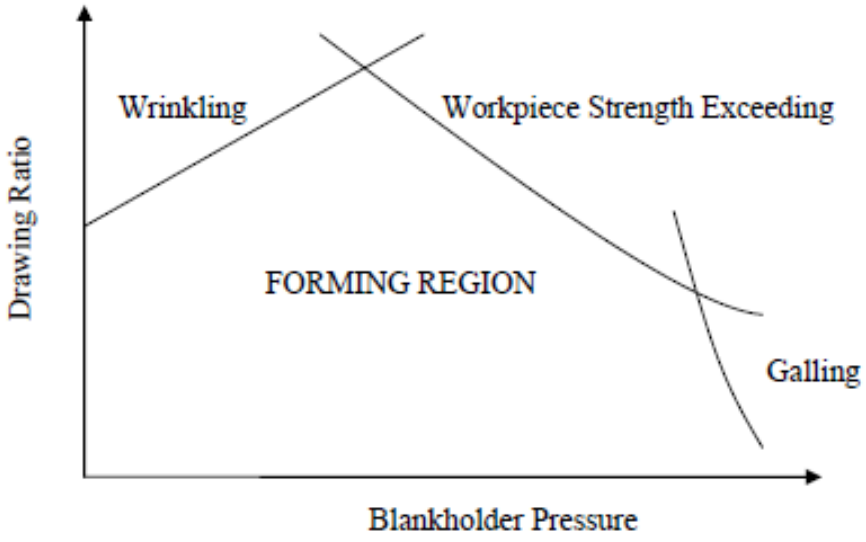

Figure 2.26 Influence of various parameters on formability in deep-drawing, [40].

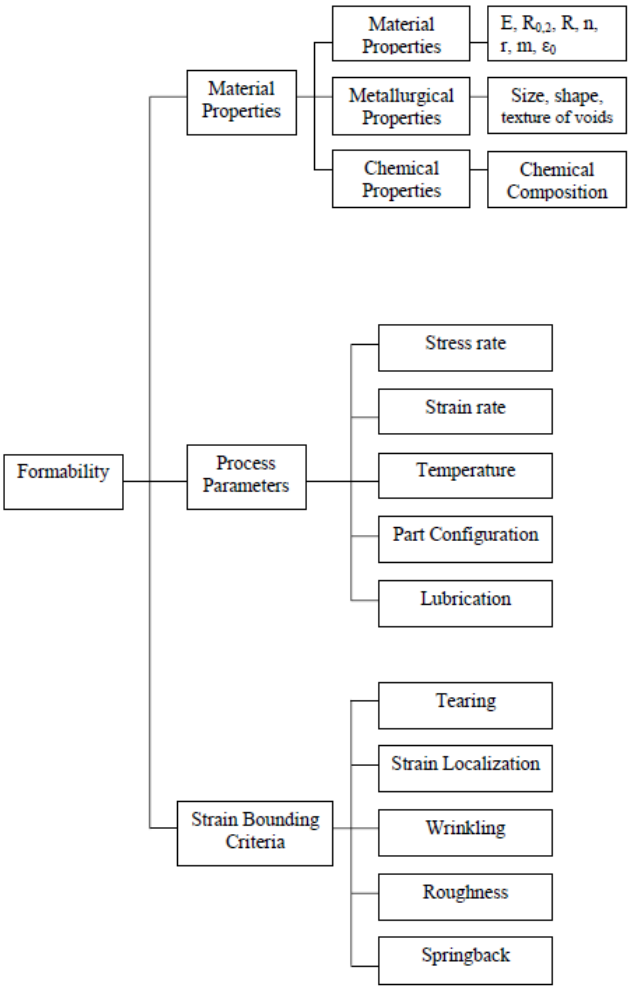

Figure 2.27 Parameters influencing sheet metal formability are given, [40].

2.3 PRIMARY CONTRIBUTORS AND THEIR WORK SCOPE

Literature is surveyed for the materials of AHSS including Aluminum/ Magnesium alloys, conventional steels HSLA and stainless steels in a large specs. Because the performance of the developed method was determined by comparing the results obtained in this present study with the findings from early studies. On the other hand another criteria considered in the selection of paper issued was the warm forming of sheet metal since there are many valuable experiences and findings which can used in the present research, i.e. choosing of lubricants for warm/ hot sheet metal forming, deciding on heating system, ..etc. Additionally most of the studies for warm deep drawing are based on the numerical solutions and the limited experimental studies performed, in such studies Aluminum/ Magnesium alloys are preferred as work material.

R. Neugebauer and et al. firmly stressed the importance of forming operations at elevated temperature for the improvement of formability in sheet metal applications. As it was mentioned in the study the metal forming at elevated temperatures not only on formability had other additional positive effects such as decrease in expenditures, costs for investment, maintenance, energy consumption due to use of high capacity press, labour, …etc. An overview about the research activities in the field of forming operations at elevated temperatures was also given. This paper convinced me to make research on the improvement of formability for AHS Sheet Steel at elevated temperature [10].

The paper titled as "Manufacturing of Lightweight Components by Metal Forming" was aimed to the current and future contributions of forming technology to manufacture lightweight components and structures by M. Kleiner et al. In this study, the local heat treatment was proposed as a promising solution method for further researches in sheet metal forming. It was noted that the development of a manufacturing method improving formability of AHSS should have a characteristic that can be applicable in sheet metal manufacturing industry, as well. This consideration was guided and figured out the design activities executed for the development of an application method in the present study [11].

As it was discussed in further sections, it was believed that in the experimental studies on sheet metal forming operations executing in warm and hot conditions it was vital to design heating system in die-tool configuration instead of furnace heating. The main reasons of this consideration are to prevent heat loss, oxidation, and distortion of work piece especially for the thin materials during the transfer of blank from furnace to die-tool assembly. K. Mori, S. Maki, Y. Tanaka [12] discovered the vital importance of heating system in die-tooling configuration in early dates of researches on the formability of High Strength Sheet Steels. As it is a well-known fact that the warm and hot stamping is attractive as a forming process of the ultra-high tensile strength steel sheets. The use of resistance heating represented could be applicable to real forming operations. Those findings are considered in the design of experimental set up used for the improvement LDR of DP600. It was claimed that the heating rate applied to the blank, 400ºC/s, by transferring heat from the heated die and blank holder to blank. Although how measurements for the temperature of blank taken was not defined, it was presented as the temperature of blank. However the part temperature was determined by calculating power input and compared with the temperature measured.

It was believed that at the interfaces of blank due to conductive heat transfer between die and blank holder, should have been taken into account, by considering that both, die and blank holder, of them existed at room temperature at the beginning of drawing operation. Although it was a nonisothermal sheet forming operation, it was presented as a drawing process at constant temperature. Another remarkable note on set-up was that the blank diameter was larger than the diameter of die, the similar positioning of die and blank happened unwillingly in this study as well not searched in details but it was observed that the positioning a blank on a die, whose outer diameter being smaller than diameter of blank, improved LDR of AHSS and HSLA sheet metals at room and warm conditions [12].

It was reported that the warm and hot stamping using resistance heating was an attractive way of forming process for the ultra-high tensile strength steel sheets. The springback, formability and hardness for the ultra-sheets are improved by the heating. The rapid electric resistance heating method prevented the decrease in temperature and the oxidation [13].

The modelling of hardening behaviour, yield criteria and description of the sheet metal formability limits were given systematically in the paper titled as "Testing and modelling of material behaviour and formability in sheet metal forming". Within this scope, the paper provided a critical review of the models available today for predicting the material behaviour at both industrial and scientific level, and the tests needed to identify the models' material parameters. The most recent advances in the field were also presented and discussed. By following the comments, criteria, theories given, the deep drawing process at elevated temperature which was applied in the experimental part of the present study was modelled and given in Chapter 4 [13].

An experimental study on nonisothermal deep drawing process using Aluminum and magnesium alloys was completed by Serhat Kaya, and et al. In this study, the work materials, Al 5754-O, Al 5052-H32, and Mg AZ31-O blanks having thickness values of 1,3 mm, 1,3 mm, and 1,2 mm, respectively, were used in the experiments. The die and the blank holder were heated with electrical cartridge heaters up to 310°C, while the punch was cooled approximately to room temperature 65°C with water circulation. K-Type thermocouples positioned to feedback to a temperature controller that keeps the temperature at constant value [14].

It was investigated that the very rapid heating was applied which was the right application for such materials not to let any metallurgical changes in the tests. But it

was thought that to attain the steady temperature, heating process should have been applied for a bit more, because for metals only the surface temperatures could be measured, it did not guaranteed that the inner part of the blank was at the same temperature. The sign of right temperature measurement for metals could be the observation of constant temperature referring steady state temperature range reached. Another sign of the right temperature measurement for sheet metals which is better was to read the same temperatures on both sides at certain position [14].

According to the results, it is reasonable for the materials studied, strain rate sensitive, it is claimed that it gave better results for the low velocities of punch, the process temperature was another important factor, by considering the graphs given, and a correlation between strain rate, BHF and drawing temperature are found to be the most important parameters in deep drawing operations. The similar correlation might exit for AHSS materials. This study advised that heating system should be designed in a close position to work piece to avoid heat lost and distortion due to residual stresses in the blank. Finally the choice of BHF is another very important item which should be taken in to the consideration, because it controls the plastic deformation in flange region to prevent wrinkling due to buckling. Moreover BHF also effects friction condition existing in flange of blank. For these reasons, it has been shown that a properly designed BHF profile can provide an increase in LDR of work material [14].

Shoichiro Yoshihara, and et al, studied on magnesium alloy for the enhancement of formability using a local heating and cooling technique. The objective of this study was to clarify how much the formability of a magnesium alloy sheet can be enhanced by using the technique proposed. But the applied method could only be used for circular cup deep drawing process, not applied in metal forming industry. All most all the known experienced, sophisticated methods, i.e. application of a cooling just after the die radius (to increase the plastification rate) while the cup had been drawing, application of variable BHF in a controlled manner, which improves the formability of sheet metals were used in their study. The findings are used in the comparison of the methods [15].

In deep drawing operation the high percent of deformation occurs in two regions of blank, flange and die corner. A.W. Hudgins, et al, studied instability for advanced high strength steels at die radii. They presented R/t value as a measure of formability for AHS Sheet steels including HSLA450, DP600, TRIP780, DP780, and DP980. It is

found that the critical R/t value is dependent primarily on tensile strength of the material, and to a lesser extent, material yield strength, strain hardening exponent (n value), and instability strain due to the complex transition instability from die corner to tensile condition [16].

A Deep Drawing Test for Determining the Punch Coefficient of Friction by S. Rajagopal, described a deep drawing test which could be used to obtain the coefficient of friction in the cylindrical region of contact between the punch and the inside of the cup in deep drawing. The tensile failure occurred at the punch radius transition, the dependence of the fracture load on the draw depth at fracture was used to compute an average coefficient of friction. The deep drawing is more complex metal forming process. This study was used to find out how the friction condition in deep drawing operations differs from conventional friction. The parameters effecting friction condition at different stages of deep draw process clearly indicated, and the results obtained in this search are similar to the results of earlier studies [17].

The influence of various lubrications on the friction condition at elevated temperature were searched by M. H. Pope, J. T. Berry. The bending and unbending stresses on the region at die radii had been shown to contribute a decreased percentage of the total stress at higher temperatures. Conversely, the stress due to die-profile friction had been shown to contribute a larger percentage of the total stress at higher temperatures. The other important factor which was emphasized was that the radial-drawing stress has been shown to be the largest contributor to the total punch load with the stress due to die profile friction, the bending stress and the unbending stress being progressively less important. Moreover, it is also shown that the ring-deformation test can be used to investigate blank holder friction [18].

Shrinidhi Chandrasekharan and et al examined various lubricants at room and a temperature, up to 100ºC. The parameters of friction were clearly given and their effects on formability of sheet metals were searched. This study gained valuable experiences in the selection of lubricants at elevated temperature [19].

Reliability of variable blank holder force control in sheet drawing under process uncertainties was investigated by Wenfeng Zhang, Rajiv Shivpuri. The practices had shown that a properly designed variable BHF profile, i.e., variation of BHF with punch stroke, could increase drawability of complex parts. In the variable BHF approach, BHF was varied according to the status of stress state in the sheet to ensure the desired

deformation state acceptable level of quality. The effects of variable BHF at elevated temperatures can be searched in a scientific project [20].

Thiruvarudchelvan et. al introduced a non-conventional friction-actuated blank-holders, in which an annular urethane pad is used to generate the BHF such that it is roughly proportional to the punch force throughout the process. They concluded that this method was effective in preventing early fracturing and wrinkling of the sheet. Those suggestions might be taken into account for the improvement of LDR at elevated temperatures. Because the results of the present thesis showed that the process temperature limits had to be in between 190ºC and 320ºC to improve LDR of AHSS (DP600) and HSLA (Erd 7128 and 7140) materials worked. Those temperature ranges are not high to design a variable BHF system and the coupling effect of both nonisothermal heating and variable BHF might be a good future work [21].

The formability of ultra-high strength steel sheets was tested for the dies coated with either titanium nitride (TiN) or vanadium carbide (VC) by Y. Abe, et al. The deep drawability is improved with coating of die. They claimed that VC-coated die gave comparatively better results in tests performed for deep drawing of ultra-high strength steel sheets [22].

In a sheet metal forming process, most material points experience complex loading modes, for example, abrupt strain path changes that may occur during bending and unbending over a die radius, or upon subsequent, discrete forming operations. Contrary to implementations intended for many formability simulations, plastic constitutive equations had to be known accurately in order to evaluate accurately the stress and moment before unloading and thus to predict springback. The Bauschinger effect (i.e. early reverse yielding) and the elastic–plastic response during non-coaxial loading paths should have been incorporated in constitutive equations. Almost all non-isotropic hardening models studied starting by Prager (1956), were examined carefully to carry out proportional and non-proportional hardening behaviours for DP steels. It is found that the Modified Chaboche model was able to capture the response following a path change much better than isotropic hardening models, but there was a fundamental difference between large-strain hardening after a path change that occurs between path reversals and changes of principal strain axis. The Chaboche model had an ability to reproduce either behaviours, but not both simultaneously [23].

The deformation taking place during the sheet metal forming at warm condition might change the characteristic of the material worked. For this reason it was necessary to

state the present characteristic condition of the formed parts. Because the plastic deformation processes in warm regime might cause alterations of the flow resistance of metal, such ductile fracture and bifurcation of plastic deformation. There are two ways to accomplish this issue. One way is to execute the lengthy and expensive material characterization tests and the other one is to make numerical analysis of the process applied and get the results in short time. The defects in warm forming conditions were analysed numerically by J.C. Gelin, A. Moisan who applied a thermo-viscoelastic model in their study. The reliability of results obtained by numerical analysis were determined by comparing with the experimental data. Moreover, this study showed the effectiveness of Thermo-Viscoplastic Modelling in forming operations [24].

Uni-axial quasi-static tests at strain rates 10^{-4}, 10^{-3}, and 10^{-2} s^{-1} and dynamic tensile tests at strain rates 500, 1100 and 1600 s^{-1} had been carried out to investigate the mechanical behaviour for the dual phase steel 600 by Haidong Yu, Yongjin Guo, Xinmin Lai. The initial yield stresses at high strain rates were approximately twice as those at low strain rates. It was indicated that the significant strain rate effected on the tensile deformation behaviour of DP600. The finite element models were also prepared and it was found that the numerical results at the six strain rates, were in excellent agreement with the experimental data, which illustrated that the new constitutive model could describe the mechanical behaviour for DP600 steel at low and high strain rates perfectly [25].

S. Curtze et al. searched the deformation behaviour of TRIP and DP steels. The mechanical properties of a DP600 and a TRIP 700 steel were characterized by tensile tests over a temperature range of $-100 \leq T \leq 235°C$ at strain rates ranging from 10^{-3} to 1250 s^{-1}. The results showed that the strain hardening behaviour of the TRIP steel depended strongly on the initial test temperature, to which the DP steel seemed to be relatively insensitive in the studied temperature interval. This was explained by the effects of deformation induced heating on the martensitic transformation based hardening of the TRIP steel, partially offsetting the direct effects of strain rate. The outputs on temperatures depending on strain rate were considered in the decision of processing temperature range in the present study [26].

Jeehyang Huh et al, examined the effect of strain rate on plastic anisotropy of advanced high strength steel sheets, TRIP590 and DP780 and a conventional cold-rolled steel

sheet, the strain rate had a distinct effect both on the shape and magnitude of the yield surface, and the plastic anisotropy tended to diminish at a higher strain rate [27].

One of the considerable trend for the researches is about the modelling of operations and the modelling of tests for characteristic analysis of materials by using the numerical solutions. Effects of microstructure on mechanical behaviour of the DP steels were studied in numerous investigations. A microstructure based Finite Element (FE) modelling is applied successfully by T. Sirinakorn, S. Wongwises, V. Uthaisangsuk. In Finite Element (FE) modelling, Representative Volume Elements (RVEs) for the effects of various microstructure constituents and characteristics, Geometrically Necessary Dislocations (GNDs) for the simulation of austenite–martensitic transformation due to quenching process were included in the model, moreover the flow behaviours of individual phases were defined on the basis of dislocation theory and partitioning of local chemical composition. The steps of modelling were shown and applied systematically by correlating with formulations based on theories. The numerical model showing the microstructural characteristic behaviour of DP was discussed, compared, correlated with experimental results. The results were quite positive and impressive. The procedures defined was tried out in finite element (FE) modelling of this present study [28].

HSLA-340, DP800, and TRIP800 advanced high strength steel sheets with thickness of 1,2, 1,5, and 1,5 mm respectively were studied by performing tensile tests at various strain rates by Ozturk, F. and et al. the results could be summarized as

- TRIP800 steel had large ductility, comparable with HSLA-340, and a large flow stress. Its yield stress was lower than that of DP800, but its ultimate tensile strength was higher. The pronounced and weakly strain-dependent strain hardening rate of TRIP was due to the deformation-induced phase transformation.
- All these materials have positive strain rate sensitivity, and the rate sensitivity of TRIP800 increases significantly during deformation, while that of the other two alloys remained constant.
- HSLA-340 had the maximum post-uniform extension (neck extension), followed by the TRIP and the DP steels [29].

Al–Mg–Si alloys (EN AW-6016 and EN AW-6061) were deep-drawn at room temperature and 250°C both die and blank holder heated by the use of electrical

resistances as a result of this the flange area is heated. The recorded temperatures for the process are the temperatures of die and blank holder. On the other hand, there is no information about temperature vs time. M. Ghosh, et al, reported that with increasing temperature, the amplitude of earing decreased while the number of ears remained the same, indicating that there is no change in anisotropy with temperature. It could be concluded that temperature did not change the anisotropy of EN AW-6016 and EN AW-6061 [30].

A.K. Gupta, et al, reported that ASS 304 was deep-drawn at room temperature and 250 °C heating die and blank holder heated by the use of inductance heater. The recorded temperatures in process are the temperatures of die and blank holder. However, the experimental setup was not even viewed schematically, no information given for the temperature vs time. Although there were some deficiencies as mentioned above. The improvement in formability was taken place at 150°C for ASS 304 and 300°C – 350°C for Aluminum alloys. These results were more or less similar to the findings obtained in this study [31].

The results revealed by A. Alaie et al., important deformational characteristics of the microstructure at the microscopic level. It was observed that despite the formation of slip bands inside the large grains during the early stages of deformation, the large ferrite grains did not contribute to the formation of high-strain bands until the final stages of severe necking. It was observed that in the final stages of deformation, the defects or voids outside the deformation bands do not contribute to the final failure mechanisms and could be considered to be of minor importance. Thanks for those valuable findings, it was believed that the results could have also been examined additionally within the scope of dislocation theory [32].

Kim et al. developed an analytical model to investigate the effects of material, process, and geometric parameters in the warm forming of aluminum alloys under simple cylindrical deep drawing conditions. The effects of the main process parameters (i.e., temperature, forming rate, blank holder pressure (BHP), and friction between a blank and a tooling element) on formability were studied under a variety of warm forming conditions. The results of their study for the analytical design of warm forming process by predicting the deformation mechanism of the material and the relationships between limiting drawing ratio (LDR) and process parameters in isothermal and non-isothermal heating conditions. The background knowledge proposed in this paper helped to constitute the required mathematical formulations and the criteria needed to be taken

in to consideration for FEA of the nonisothermal warm deep drawing process for DP600 [33].

Although it is a FEA study, the method offered by R.A. Lingbeek, T. Meinders and S. Ohnimus for the measurement of springback is quite reasonable to be applied especially on DP600 at room and elevated temperatures. But the code developed in this study required to be improved for nonisothermal heating of flange region of blank [34].

GCRIS

CHAPTER 3

OBJECTIVE OF THE CURRENT DISSERTATION

The present dissertation is focused on the development of a method to improve the limiting drawing ratio of blanks using preferential heating. The method can be described as an application of nonisothermal local heating in the flange region of the blank to improve formability of sheet metals. The use of temperature gives the possibility of significantly increasing the ductility of the material and the associated forming capability. On the other hand, it also drastically reduces the yield point and hence the forming forces and required pressures.

It is an experimental study and the criteria considered through this study is to find an applicable manufacturing method in sheet metal forming industry. For this reason, one of the important criteria taken into consideration through the activities executed in the improvement of LDR is to develop an application method which can easily be integrated into the existing production line by preventing a substantial increase in investment, labour costs and expenditures.

One of the advanced high strength sheet steels (AHSS), DP600 is chosen as a work material in this research, due to its wide use in automotive industry. The use of AHSS materials can provide reduction in car weigth and increase in crash safety, in addition to these; lower the fuel ccomsumption. The important problem reported in literature related to the property of these high strength steels is their low formability. This dissertation is mainly devoted to improve the formability of DP600. After the developed method is approved as a successful and applicable method which improves the formability of DP600. The three different types of steels, two HSLA and one IF steels, are additionally examined to observe the validity of the developed method.

On the other hand, high strength materials requires high capacity press. In the literature, there are many studies mainly focusing on the improvements of their formability in the production line by changing its chemical content with the inclusion of different alloying elements, or changing percentages of compounds, or applying various quenching procedures. Although those newly produced AHSS materials are more formable than the early AHSS materials, but they still require high capacity press for forming operation. For this reason it is believed that the metallurgical efforts contributed in the development of formability for AHSS is limited. For the solution of problem, the development of an application method improving formability of AHSS is vitally required. In other words, the development of an application method makes high percent contribution to the improvement of formability addressing to an increase in LDR of sheet metals. The main objective about the improvement of sheet metal formability is to attain the production of parts in complex shape with desired depth keeping high strength properties by preventing phase changes in their micro-structures and defects-free products.

For the solution of the problem; nonisothermal local heating is considered. Because, the use of temperature opens up the possibility of significantly increasing the ductility of the material and the associated forming capability. On the other hand, it also offers the possibility of significantly reducing the yield point and hence the forming forces and pressures required.

In order to be able to fully exploit the potential of temperature-supported forming processes and guarantee economic production of complex component geometries, the related challenges must be faced. Some of these include:

- Identification of suitable temperatures or temperature distributions,
- Integration of the temperature-supported forming process within the overall process chain,
- Regulation of the temperature distributions within a satisfactory time limit,

The deep drawing is the combination of various formation operations, such as bending and unbending at the die shoulder and cup corner, wrinkling as a result of buckling in flange region, tensile deformations in the side wall and the bottom of cup. On the other hand, there are many process variables controlling the formations in deep drawing. For these reasons, in subsequent paragraphs, the objective of each activities executed for the improvement of LDR is going to be given individually in details with including the reasons.

The Induction Heating, one of the rapid heat application method, is selected due to preventing grain growth and phase changes, it provides local heating of work pieces. The other issue about temperature is the application temperature ranges. By considering the discussions above the temperature limits should certainly be below the recrystallization which addresses to warm forming condition. The exact temperature limits is determined, as a result of the experiments executed at elevated temperature. Since the temperature range stays in the warm region, material properties are not influenced but the strength remains the same while forming forces are reduced.

The heating configuration is designed in such a way that the copper coil of inductance heater is inserted in die by insulating it electrically due to preventing heat loss and distortion of work pieces. The blank heated at the outside of die should be relocated on die. Transferring and placing warm blank on die causes heat losses in blank within a certain time period. The application of heat at outside of die would cause fluctuation in temperature of blank which is undesired because in transferring stage, the heat would be lost by convection to ambient air and in replacement of blank on die, the heat is lost again by contacting of blank with blank holder and die due to the conduction. On the other hand, it is difficult to control the blank's temperature in this case. By taking into account of those heat losses, the blank would be preferred to be heated up to higher temperature and this may cause microstructural changes in material. The Induction Heating system designed by inserting inductance coil in die is the new application form of Induction Heating system in deep draw operations.

The local heating system is chosen to increase the ductility of material within a specified region of the blank which will be formed. The mentioned region refers to the flange part of work material. For axisymmetric warm deep drawing operation, while the flange area of the blank is heated, the mid-region of blank which corresponds to the projected area of punch bottom is preferred to be at lower temperature which can be termed as nonisothermal heating

The application of the local heating provides to save the process energy which is consumed through the deep drawing operation. It is important to note that the process energy in this study expresses the forming energy supplied by the press.

After the heat applied to edge of circular blank by inductance coil, the temperature of circular blank increases gradually in radial direction of the flange region. As the punch is progressed into the die, the ductility of material in flange region required to be improved progressively due to accumulation of more and more draw material in flange

region. This required condition is provided by gradually improving the flange temperature of blank in radial direction. This is the reason why the highest temperature constituted at edge of blank.

The required temperature distribution in the flange region of blank is obtained by the application of heating and cooling simultaneously. The cooling operation can be expressed in such a way that in the punch, there exists a hole drilled letting air get in to prevent vacuum formed at the end of deep drawing operation; this hole is additionally used for the cooling of blank. The water through this hole is dropped onto the centre of the blank while it is heating, to constitute the required temperature distribution in the result of heating and cooling operation. These heating and cooling operations are all controlled manually until the demanded temperature gradient is formed. As one can realize that the measured temperatures are the surface temperature of blank. When there is no change in the readings of temperature sensors, it refers to the steady state condition reached as a result of heat conduction through the thickness direction. In other words, the required temperature distribution is obtained in the thickness direction of blank, as well. It is important to note that when the documents and literature related with forming of sheet metals in warm or hot condition are searched, it is noticed that the temperature measurement system is not successfully explained and in addition to this, the temperature claimed as the measured temperature does not refer to the blank's temperature or even the process temperature in those documents. For these reasons the measurement of temperature is taken as a serious issue required to be accomplished and expressed in detail.

Other important issue concerning with warm deep drawing operation is about the measurement of the blank temperature and control of it. When the blank is placed on die and pressed by blank holder plate, the upper and lower surfaces of blank becomes closed and no gap left to measure the blank's temperature. To overcome this issue, a hole in die is opened which targets to the edge of blank and an infrared temperature sensor focusing blank through this hole is located on the bottom of die. In addition to this, another infrared temperature sensor directed to a point on the inner circle of blank flange is also placed on the bottom of die. So the developed temperature measurement system provides the record of the temperatures at the start and end of flange region.

The application of blank holder force also influences the formability of sheet metals but it doesn't primarily effect on the development of a method which improves LDR in warm deep drawing operations. Because this study is devoted to investigate the

benefits of nonisothermal local heating on the formability of DP600. It is believed the available range for BHF can easily be determined by observing the shape of drawn parts at elevated temperatures. So the constant blank holder is planned to be applied and the various application of BHF can be searched in future work.

According to the results of the tensile tests for DP600 executed at different strain rates, $1,0 \times 10^{-1}\ s^{-1}$ and $2,08 \times 10^{-3}\ s^{-1}$, there is no significant differences observed between the resultant graphs. So it is assumed that DP600 studied in this research is characterized as a strain independent sheet steel. The determination of strain independency for DP600 in this dissertation made possible to use an eccentric press in the deep drawing experiments. Because the punch force actuated by eccentric loading is not constant, in an eccentric press, the punch exerts force in quadratic form. But the various application of punch force can be studied as a new research subject in future for the warm deep drawing operation.

The formability of sheet steels is highly influenced by the lubrication used in deep drawing processes. The number of lubricants which can be used in warm and hot forming operations of sheet metals is very limited. Many of them are based on boron and graphite, additionally PTFE. In the experiments the benefits of mixed type of lubrication system, PTFE + Graphite, is investigated.

As the one may realize in this chapter the main objectives of the current dissertation is given and in subsequent chapters the more detailed information will be presented.

CHAPTER 4

THEORY

4.1 BASIC DEFINITIONS AND FORMULATIONS

This chapter adresses the derivation of the basic analytical formulations about the deep drawing theory and additionally the discussions of numerical methods used in the analysis of metal forming.

In the following, the deep drawing operation is divided into 3 particular stages and particular assumptions are made to bring the important parameters in front in the deep drawing operations. An infinitesimal element is used to derive stress and strain relationships for the different stages of deep drawing operation. In numerical analysis, the vital assumptions are taken into consideration and they are converted into mathematical expressions and included in constitutive equations.

For the elaboration of the following sections on theoretical framework, the reader may refer to Handbook of Metal Forming, 1985 by K. LANGE, [40].

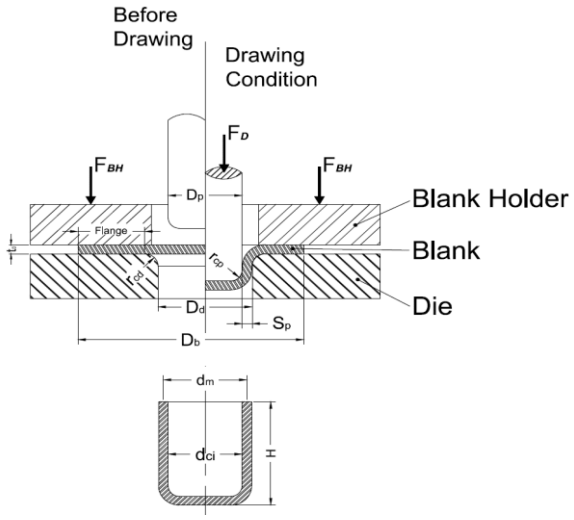

Figure 4.1 Schematic Representation of Deep Drawing Operation.

In deep drawing, the annulus between the diameters of blank and die is deformed into the cylindrical wall of cup by the punch. Figure 4.1 shows the schematic representation of deep drawing operation in single stroke. In early stage of the process, the central portion of blank is slightly strained, as shown in Figure 4.2.

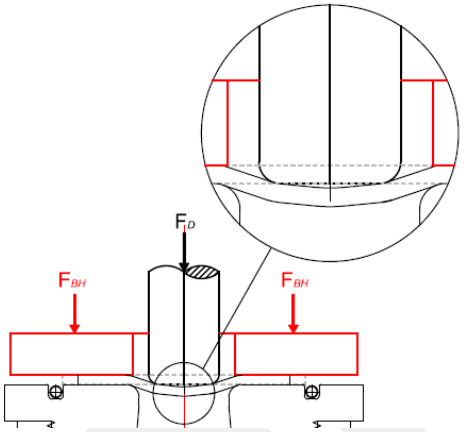

Figure 4.2 Early stage of deep drawing operation.

It is assumed that the thickness of material is constant during the deformation. By the use of volume constancy. The height of the drawn cylinder can be evaluated as;

$$H = \left(1 + \frac{D_b}{d_{ci}}\right)\left(\frac{D_b - d_{ci}}{4}\right) \tag{4.1}$$

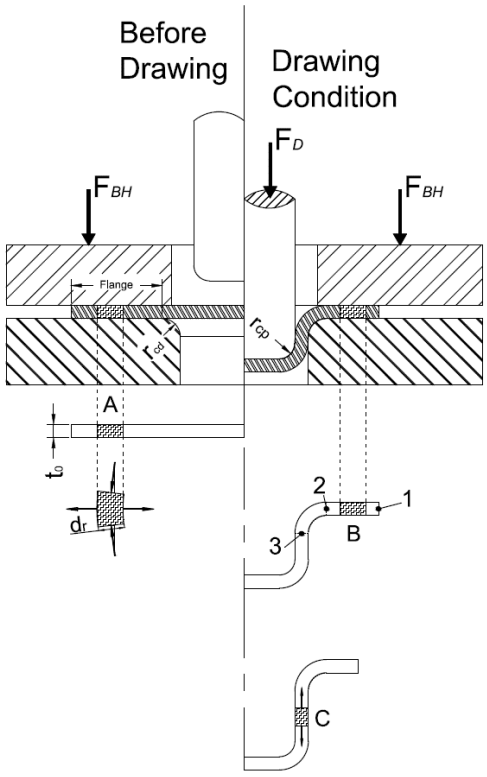

Figure 4.3 Stages of Drawing Operation.

An infinitesimal volume element is taken into consideration to analyse the deep drawing operation. At the beginning drawing operation, it is assumed that this infinitesimal element is located at position A in the flange region of blank. As the punch goes downward, it moves to B in flange region, after it is bent and unbent on die shoulder finally it reaches to the position C in the wall of cup. The condition where the infinitesimal volume element on the die shoulder is examined in the following sections.

During the travel of the infinitesimal element from A to B, the element radially stretched and tangentially compressed, correspondingly, which means that it is exposed to tensile stresses in radial direction and compressive stresses in the circumferential direction (see Figure 4.3). The full equilibrium equation in radial direction can be written as;

$$\left(\sigma_r + d\sigma_r\right)\cdot\left(r+dr\right)\cdot d\theta\cdot\left(t+dt\right)-\sigma_r\cdot r\cdot d\theta\cdot t+$$
$$2\cdot\sigma_t\cdot\left(\frac{t+\left(t+dt\right)}{2}\right)\cdot dr\cdot\sin\left(\frac{d\theta}{2}\right)+2\mu\sigma_z dr\left(\frac{rd\theta+\left(r+dr\right)d\theta}{2}\right)=0 \qquad (4.2)$$

In Equation 4.2

The frictional terms are

$$F_f = 2\mu\sigma_z dr\left(\frac{rd\theta+\left(r+dr\right)d\theta}{2}\right) \qquad (4.3)$$

by assuming no change in thickness $\left(t+dt\right)\rightarrow t_0$ at $\left(r+dr\right)$ and $t=t_0$ at r

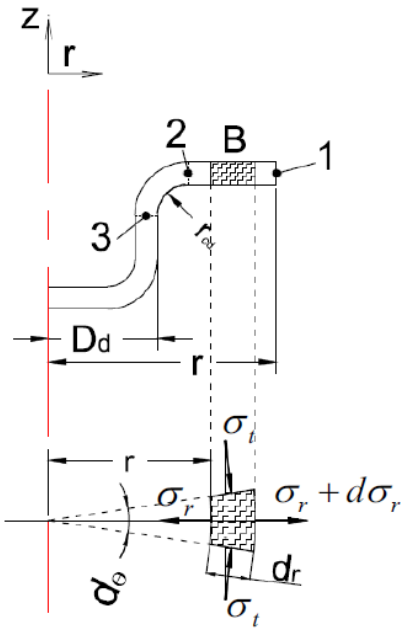

Figure 4.4 Stresses in Flange region for the movement from A to B.

By neglecting the frictional terms and assuming that the thickness is constant, the equilibrium condition in the radial direction becomes;

$$\left(\sigma_r + d\sigma_r\right)\cdot\left(r + dr\right)\cdot d\theta\cdot t_0 - \sigma_r\cdot r\cdot d\theta\cdot t_0 + 2\cdot\sigma_t\cdot t_0\cdot dr\cdot\sin\left(\frac{d\theta}{2}\right) = 0 \tag{4.4}$$

Note that: The frictional terms will be included in Equation 4.4 later and discussed in detail.

Approximating the term, $\sin\left(\frac{d\theta}{2}\right)$ to $\frac{d\theta}{2}$ and omitting the products of differential terms, Equation 4.4 is simplified to

$$d\sigma_r = -\left(\sigma_r + \left|\sigma_t\right|\right)\frac{dr}{r} \tag{4.5}$$

Tresca yield criterion by considering plastic flow stress states that

$$\sigma_1 - \sigma_3 = \sigma_f \tag{4.6}$$

By substituting $\sigma_1 = \sigma_r$ and $\sigma_3 = -\sigma_t$ due to sign convention arising compressive stress σ_t and Equation 4.6 becomes

$$\sigma_r + \left|\sigma_t\right| = \sigma_f \tag{4.7}$$

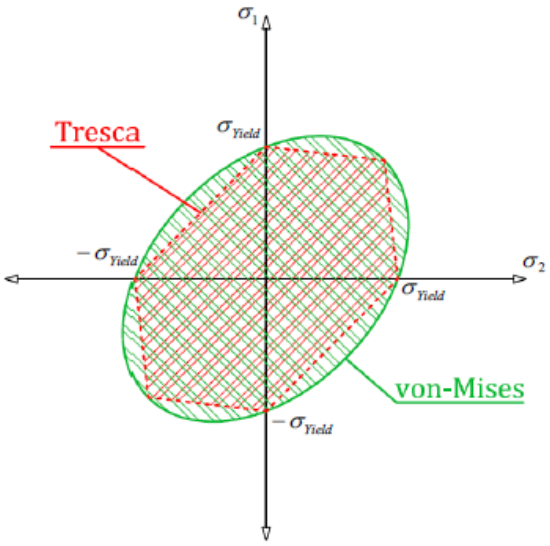

Figure 4.5 Tresca and Von Mises.

Frequently, the Von Misses yield criterion is used instead of the Tresca yield criterion. The reason is that Von Mises yield criteria gives more reliable results because it covers Tresca yield condition as shown in Figure 4.5. In other words, the former is more accurate and predicts higher shear stresses than are determined using the maximum shear stress theory [40].

During deep drawing both criteria agree only at one location, which is the point where the mean normal stress σ_m is equal to the median principle stress σ_2. At all other points the Tresca criteria predicts which is on the average are about 10% smaller. In order to use the simpler Tresca equation, a correction factor is introduced to make use of it practically [40],

$$\sigma_r + |\sigma_t| = 1{,}1\sigma_f \tag{4.8}$$

By the use of Equation 4.5 and 4.8, the equality can easily be obtained

$$d\sigma_r = -1{,}1\sigma_f \frac{dr}{r} \tag{4.9}$$

Integrating Equation 4.9 for from the outter diameter (at $r = R$, $\sigma_r = 0$) to inner diameter (at r; σ_r) of the flange region, where R is the current radius in drawing operation and

$$r \le R \le \frac{D_d}{2} \tag{4.10}$$

The stress in radial direction can be found as

$$\int_{\sigma_r=0}^{\sigma_r} d\sigma_r = -1{,}1 \int_{r=R}^{r} \sigma_f \frac{dr}{r} \tag{4.11}$$

Finally, the equality for the evaluation of the stresses in radial direction is

$$\sigma_r(r) = 1{,}1\sigma_{f,1\cdot\to 2\cdot} \ln\left(\frac{R}{r}\right) \tag{4.12}$$

The mean flow stress in the flange zone is designated with term $\sigma_{f,1\cdot\to 2\cdot}$ describes the radial stresses between points 1 and 2. Geleji (1967) claimed that the error is less than

3% if the arithmetic mean of the values of σ_f at points A and B in Figure 4.3 is used for $\sigma_{f,1\cdot\to 2\cdot}$

$$\sigma_{f,1\cdot\to 2\cdot} = \frac{\sigma_{f,1\cdot} + \sigma_{f,2\cdot}}{2} \tag{4.13}$$

It is important to that a more accurate value of mean flow stress can be obtained from

$$\sigma_{f,1\cdot\to 2\cdot} = \frac{1}{\varepsilon_{f,2\cdot} - \varepsilon_{f,1\cdot}} \int_{\varepsilon_{f,1\cdot}}^{\varepsilon_{f,2\cdot}} \sigma_f .d\varepsilon \tag{4.14}$$

Where $\varepsilon_{f,1\cdot}$ and $\varepsilon_{f,2\cdot}$ are the tangential strains at points 1 and 2 respectively.

In order to prevent wrinkle formation in flange area, a blank holder exerting force is commonly used (Figure 4.2 and 4.3). In this case the principal stress in z direction is in the form of compressive stress.

$$\sigma_z < 0 \tag{4.15}$$

If a blankholder force is not applied,

$$\sigma_z = 0 \tag{4.16}$$

In the above discussion, friction in between die-flange of blank and blank holder-flange of blank been ignored. If friction is included in the analysis and necessary integrations then Equation 4.3 becomes

$$\sigma_r(r) = 1{,}1\sigma_{f,m,A} \ln\left(\frac{R}{r}\right) + 2\mu(R-r)\frac{P_{BH}}{s} \tag{4.17}$$

Where

μ is the coefficient of friction and P_{BH} is blank holder pressure

Since friction is included, the radial stress is increased. The friction in flange is inversely proportional to the work piece thickness.

On the die corner, the stress components due to friction and bending increase the axial stress in the cup wall significantly.

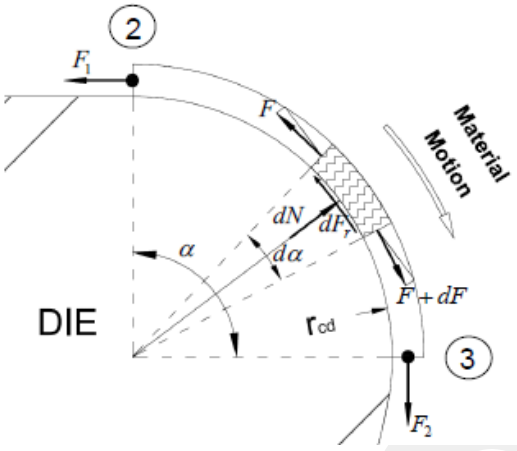

Figure 4.6 Friction conditions at the die radius.

Assuming that no forces due to frictional and bending at the die corner, the radial stress (σ_r) in flange will be equal to the axial stress (σ_z) in the wall of cup.

To analyse the friction condition at the die corner, the equilibrium in radial direction for the volume element indicated in Figure 4.6 can be written simply as

$$dN - F\sin\left(\frac{d\alpha}{2}\right) - (F + dF)\sin\left(\frac{d\alpha}{2}\right) = 0 \tag{4.18}$$

Where N represents the normal force between blank and die, in additon to this, F is the radial tension force. Equation 4.18 states the equilibrium condition for the element travelling from point 2 to point 3.

By making approximation that $\sin\left(\frac{d\alpha}{2}\right) \rightarrow \left(\frac{d\alpha}{2}\right)$ and omitting Equation 4.18 reduces to

$$dN - Fd\alpha = 0 \tag{4.19}$$

On the other hand, the equilibrium condition simplified in tangential direction is

$$dF = dF_r = \mu dN \tag{4.20}$$

Note that: $dF_r = \mu dN$

By replacing Equation 4.19 into 4.20

$$\frac{dF}{F} = \mu d\alpha \tag{4.21}$$

Taking the integral of both sides,

$$\int_{F_1}^{F_2} \frac{dF}{F} = \int_0^{\alpha} \mu d\alpha \tag{4.22}$$

One can easily find the following equality

$$\ln\left(\frac{F_2}{F_1}\right) = \mu\alpha$$

Or

$$F_2 = F_1 e^{\mu\alpha} \tag{4.23}$$

The corresponding cross sectional areas are

For F_1 at Point 2 $\quad A_2 = s(D_d + 2r_{cd})\pi$

For F_2 at Point 3 $\quad A_3 = s(D_d)\pi$

$D_d >> 2r_{cd}$ so; it can be estimated as $A_2 = A_3$

In other words; Since the die radius r_{cd} is very small compared with the diameter of the cup, the stress components due to for $\alpha = 90^0$ can be calculated from

$$\sigma_z = \sigma_r e^{\mu\frac{\pi}{2}} \tag{4.24}$$

Where σ_z is the radial stress in the flange at the die entrance and σ_r is the axial stress at the die exit. However, it is important to note that the stress due to bending is not included into Equation 4.22

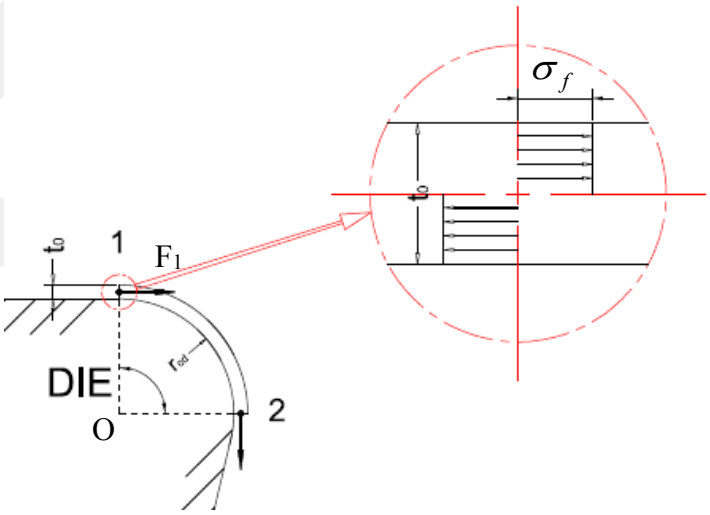

Figure 4.7 Stress distribution at the entrance of die shoulder.

In the region of the die radius the sheet metal undergoes twofold bending. The central fiber is bent to a radius $\left(r_{cd}+\frac{t_0}{2}\right)$ at the die entrance and is unbent again at the exit. Geleji calculates the required force for bending as follows. At the entrance of the die (Section 1 in Figure 4.7) an element of thickness s and width b is bent over the die radius r_{cd}. The required work W equals to the product of the bending moment M_b times the angle of bending α:

$$W = M_b\alpha = F_1 r_{cd}\alpha \tag{4.25}$$

or,

$$F_1 = \frac{M_b}{r_{cd}} \tag{4.26}$$

The flow stress, σ_f, acts as shown in Figure 4.7 at the section 1

During bending fibre stretched / compressed until the internal moment in the cross section is equal to the externally applied bending moment. The internal moment can be calculated based on the assumption that the material is deformed plastically and the magnitude of bending stress equals to the flow stress, σ_f. If the moment is taken according to the centre of the die shoulder radius to evaluate M_b;

$$\left(\sigma_f bt_0\right)\left(r_{cd}+\frac{t_0}{2}+\frac{t_0}{4}\right)-\left(\sigma_f bt_0\right)\left(r_{cd}+\frac{t_0}{2}\right)-M_b=0 \tag{4.27}$$

Then, the internal moment, M_b, is equal to

$$M_b = \frac{\sigma_f bt_0{}^2}{4} \tag{4.28}$$

Combining Equations 4.26 and 4.28 yields

$$M_b = \frac{\sigma_f bt_0{}^2}{4r_{cd}} \tag{4.29}$$

At the exit of the die (Section 2 in Figure 4.7) the sheet is straightened in other way around again. Since this restores the original state, the same amount of work is neccesary as in Section 1, assuming that the material does not work harden. The total force required for bending, which must be transmitted in Section 2 in Figure 4.7 is therefore

$$F_b = 2F_1 = \frac{\sigma_f b t_0^{\,2}}{2r_{cd}} \tag{4.30}$$

For circular deep drawing tools the width b is given by

$$b = \pi d_m \tag{4.31}$$

Where d_m is the mean diameter of the cup wall, and the bending force in Section 2 in Figure 4.7 is given by

$$F_b = 2F_1 = \frac{\pi \sigma_f d_m b t_0^{\,2}}{2r_{cd}} \tag{4.32}$$

Strains are evaluated without considering bending over the radius. The directions of the principal stresses coincide with the strains in the radial, circumferential, and directions. The finished cup shows the following strains, where s is the instantaneous wall thickness and D_b is the original diameter of the ring element under consideration:

$$\varepsilon_t = \ln\left(\frac{d}{D_b}\right)$$

$$\varepsilon_z = \ln\left(\frac{t}{t_0}\right) \tag{4.33}$$

$$\varepsilon_r = \ln\left(\frac{t_0 D_b}{td}\right)$$

From the volume constancy condition the following equality can be written

$$\varepsilon_t + \varepsilon_z + \varepsilon_r = 0 \tag{4.34}$$

The magnitude of the deformation of a deep drawn part is usually characterized by the drawing ratio of the initial blank diameter d_0 to the punch diameter.

$$DR = \frac{D_b}{D_p} \tag{4.35}$$

The derivation of analytical formulas corresponding to deep drawing operation are not kept further because in this present study, the finite element method is chosen to be the solution method. After the various solution methods are reviewed, the modelling of deep drawing operation at elevated temperature for finite element method will be given in conjunction with the implementation of the model into ABAQUS will be given.

4.2 SOLUTION METHODS

Analysis methods in simulation of metal forming is used to predict one or more of the process parameters of a real physical process, approximately. The approximate methods of analysis are employed on the basis of idealized models. In solving metal forming problems, both analytical and numerical methods can be used. The analysis methods in metal forming are summarized in Figure 4.8.

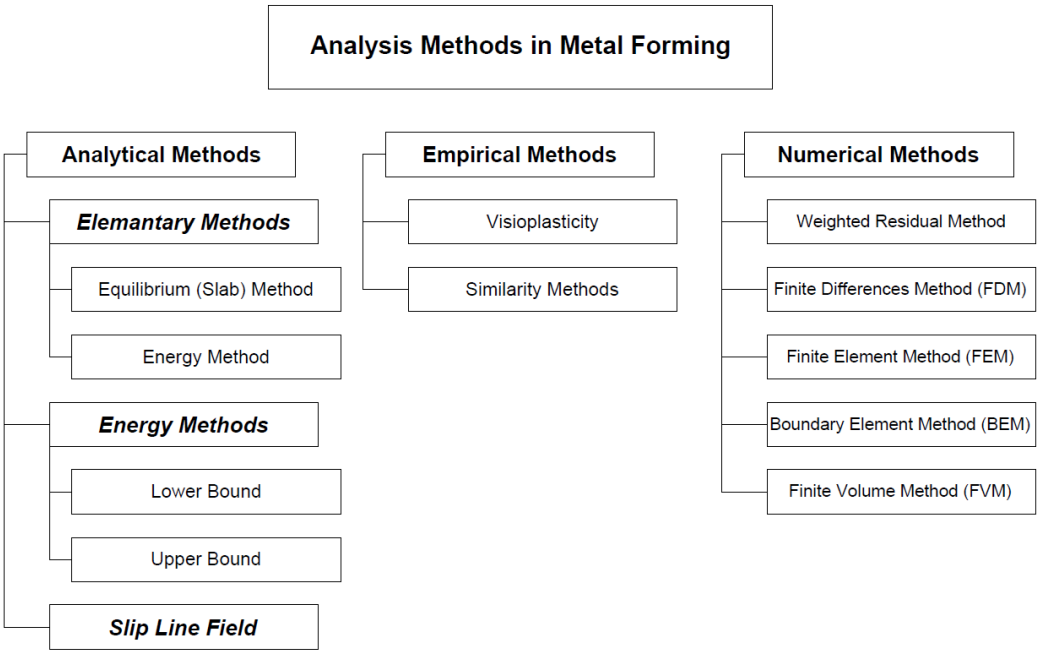

Figure 4.8 Some analysis methods in metal forming, [39].

4.2.1 Analytical Methods in Metal Forming

In this chapter some of the important analytic methods, are introduced and described. The analysis methods used in metal forming can be classified into three categories such that Analytical, Empirical and Numerical Methods.

4.2.1.1 Slab Equilibrium

In the slab equilibrium technique, a small element (or slab) is extracted from the deforming workpiece as seen in Figure 4.9. A force balance is performed on this small slab taken in consideration. This balance of forces leads to a differential equation, which relates the stresses in the work piece to geometrical variables of the process applied. With the use of a yield criterion, an assumption of the principal stress directions, and some knowledge of the boundary conditions, a solution to the

differential equation can be obtained by numerical methods. For simple geometrical shapes, an analytical solution can easily be achieved. For more complex shapes, the solution can only be obtained by numerical solutions of the differential equation [36].

,

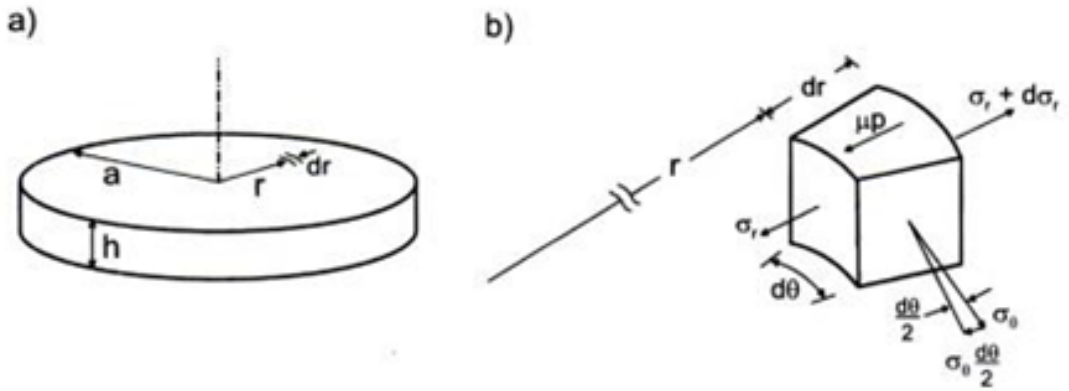

Figure 4.9 Schematic of slab equilibrium analysis for disc forging : (a) general geometry; and (b) slab element used for analysis, [36].

4.2.1.2 Uniform Energy Method

The uniform energy (or work) method or sometimes named also as uniform plastic deformation energy method was originally proposed by Siebel. This method is especially used for the solution of steady-state problems such as extrusion and drawing, although it can be applied also to non-steady-state problems.

The method is based on the following basic assumptions:

(1) straining or plastic deformation occurs only under principal stresses or maximum shearing stresses;

(2) surface frictional effects are superimposed on the system and are assumed not to affect the stress distribution.

In this method the infinitesimal external work is put equal to the infinitesimal internal work [37].

4.2.1.3 Energy Methods

4.2.1.3.a Lower-Bound Method

The upper and lower bound methods were developed on the basis of the limit theorems invested by Prager and Hodge and Hill. The lower bound analysis provides an underestimate for exact load from a statically admissible stress field equation, which satisfies the equilibrium of force and the boundary condition of traction and does not violate the yield condition. Since it is extremely difficult to find a statically admissible stress field, generally the lower bound method is not used for practical purposes.

4.2.1.3.b Upper-Bound Method

The upper-bound technique is an energy method where the energy per unit time needed by the workpiece to undergo deformation is similiarly set equal to the externally supplied energy per unit time. The primary power terms that must be calculated for the work piece and the internal power of deformation, the power to overcome friction, and the shear power are required to be included. The internal power is determined from the assumed velocity field and is calculated from the strain rate field. The frictional power term is the power needed to overcome any tool-work piece frictional interaction. The constant friction factor model is generally assumed for this type of analysis. The shear power is determined by calculating the energy per unit time associated with the internal shear that occurs over any assumed internal surfaces of velocity discontinuity.

In the upper bound analysis, an overestimate for the exact load is obtained from a kinematically admissible velocity field which satisfies the condition of incompressibility and the boundary condition of velocity. The upper bound technique has been widely applied in the analysis of cold forging processes because kinematically admissible velocity fields could be obtained by combining simple flow modes.

4.2.1.4 Slip line Method

The slip line method is a classical approach to the analysis of deforming bodies. In mechanics, the slip line method probabl should be called “maximum shear stress plane” technique.

In slip line method, a network of maximum shear stress planes is superimposed onto the deforming body. There are a variety of restrictions on the generation of such a network. The network must adhere to specific shape requirements and boundary

conditions, and provide a realistic flow for the deforming material. The method is valid for plane-strain conditions.

4.2.2 Emprical Methods

4.2.2.1 Visioplasticity

Viscoelastic materials, such as amorphous polymers, semicrystalline polymers, and biopolymers, can be modeled in order to determine their stress or strain interactions as well as their temporal dependencies, respectively. These models, which include the Maxwell, the Kelvin–Voigt, and the standard linear solid models, are used to predict a material's response under different loading conditions. Viscoelastic behavior has elastic and viscous components; they are modeled as linear combinations of springs and dashpots, respectively. Each model differs in the arrangement of these elements, and all of these viscoelastic models can be equivalently modeled as electrical circuit configuration. In an equivalent electrical circuits, stress is introduced by current, and strain rate by voltage. The elastic modulus of a spring is analogous to a circuit's capacitance (energy storage) and the viscosity of a dashpot to a circuit's resistance (it dissipates energy).

The elastic components, as previously mentioned, can be modeled as springs of elastic constant E, given by the formula:

$$\sigma = E\varepsilon \tag{4.36}$$

where σ is the stress, E is the elastic modulus of the material in model, and ε is the strain that occurs under the given stress, similar to Hooke's Law.

The viscous components can be modeled as dashpots such that the stress–strain rate relationship can be given as,

$$\sigma = \eta \frac{d\varepsilon}{dt} \tag{4.37}$$

where σ is the stress, η is the viscosity of the material, and $\frac{d\varepsilon}{dt}$ is the time derivative of strain.

The relationship between stress and strain can be simplified for specific stress rates. For high stress states/short time periods, the time derivative components of the stress–strain relationship dominate in calculation. A dashpot resists changes in length, and in a high stress state it can be approximated as a rigid rod within the error range estimated.

Since a rigid rod cannot be stretched past its original length, no strain is added to the system [38].

4.2.3 Numerical Metods

4.2.3.1 Weighted Residuals

The method of weighted residuals, used to obtain approximate solutions to linear and non-linear differential equations in continuum problems, does not require a knowledge of the functional value. The statement of the problem can be formulated as:

$$F(\phi) = G(\phi) \text{ in a volume V} \tag{4.38}$$

Subject to a set of boundary conditions on the surface S. The field variable itself is again approximated, as given in Equation 4.39 below

$$\phi(x) = \sum_{i=1}^{n} c_i g_i(x) \tag{4.39}$$

Where $g_i(x)$ are known functions defined over the volume and its surface. The parameters c_i have to be determined, to satisfy the condition:

$$\frac{\partial I(\phi)}{\partial c_i} = 0 \text{ for i = 1, n} \tag{4.40}$$

Which leads to n number of simultaneous equations with n number of unknowns for the proper solution. The g_i accuracy of the solution depends on the choice of the trial function, these must be part of a set that produces a convergence to the correct solution, and they must be continuous up (continuity rule required to be satisfied) to the necessary degree of differentiation in the functional, etc. Usually these functions are in the form of a polynomial or a trigonometric expression.

The next step is to define a residual or error functional R, such that:

$$R(\phi) = G(\phi) - F(\phi) \tag{4.41}$$

and R has to be minimised for the best solution.

A weighted function of this residual, $w.p(R)$, is assumed to satisfy the acceptable residual condition for the solution of the problem. If the function is chosen so that p(R) = 0; when R = 0, then the corresponding function, ϕ(x) , will be equal to the exact function, the one can easily be realized.

The trial function, ϕ(x), is chosen to satisfy the boundary conditions introduced and the acceptably small residual is given by the integration over the whole volume:

$$\int w \cdot p(R) dV = 0 \tag{4.42}$$

4.2.3.2 The Finite Difference Method

The basis of this method is to approximate a first derivative by a small enough finite step. For example if the quantity T, which might be temperature, varies with time:

$$\frac{dT}{dt} \cong \frac{T^1 - T^0}{\Delta t} \tag{4.43}$$

Where

$$T^1 = T(t + (\tfrac{1}{2})\Delta t) \text{ and } T^0 = T(t - (\tfrac{1}{2})\Delta t) \tag{4.44}$$

And Δt is a small time interval

Finite-Difference methods have proved to be useful in solving thermal problems and have some proponents for structural analysis [39].

4.2.3.3 Boundary Element Method

The boundary element method (BEM) is a numerical computational method of solving linear partial differential equations which have been formulated as integral form of equations. It can be applied in many different fields of engineering and science including fluid mechanics, acoustics, electromagnetics, and fracture mechanics.

The integral equation may be regarded as an exact solution of the governing partial differential equation. The boundary element method attempts to use the given boundary conditions which has already been defined at the begining to fit boundary values into the integral equation, rather than values throughout the space defined by a partial differential equation. Once this is done, in the post-processing stage of solution, the integral equation can then be used again to calculate numerically the solution directly at any desired point in the interior of the solution domain.

BEM is applicable method solving problems for which Green's functions can be calculated. These usually involve fields in linear homogeneous media. This puts considerable restrictions on the range and generality of problems to which boundary elements can usefully be applied. Nonlinearities can be included in the formulation, although they will generally introduce volume integrals which then require the volume to be discretised into finite mesh parts before solution can be attempted, removing one of the most often cited advantages of BEM. A useful technique for treating the volume integral without discretising the volume is the dual-reciprocity method which is an

effective solution method. The technique approximates part of the integrand using radial basis functions (local interpolating functions) and converts the volume integral into boundary integral after collocating at selected points distributed throughout the volume domain (which includes the boundary points). In the dual-reciprocity BEM, although there is no need to discretize the volume in consideration into meshes, unknowns at chosen points inside the solution domain are involved in the linear algebraic equations approximating the problem being considered.

4.2.3.4 Finite Volume Method

The finite-volume method (FVM) is a method for representing and evaluating partial differential equations in the form of algebraic equations [LeVeque, 2002; Toro, 1999]. Similar to the finite difference method or finite element method, values are calculated at discrete places on a meshed geometry. "Finite volume" refers to the small volume surrounding each node point on a mesh. In the finite volume method, volume integrals in a partial differential equation that contain a divergence term are converted to surface integrals, using the divergence theorem. These terms are then evaluated as fluxes at the surfaces of each finite volume. Because the flux entering a given volume is identical to that leaving the adjacent volume, these methods are conservative. Another advantage of the finite volume method is that it is easily formulated to allow for unstructured meshes. The method is used in many computational fluid dynamics packages.

4.3 FINITE ELEMENT ANALYSIS ON WARM DEEP DRAWING

In metal forming technology, proper design and control requires, among other things, the determination of deformation mechanics involved for the processes applied. Without the knowledge of variables influencing such as material properties, workpiece geometry, friction and contact conditions on the process mechanics, it would not be possible to design the dies and equipments adequately, or to predict or in some how prevent the occurrence of defects in the components produced. Thus, recently the process modelling for computer simulation has been a major concern in modern metal forming technology.

There are many commercially available software packages for finite element method such as NUMISHEET’93, DEFORM, AUTOFORM, DD3IMP, LS-DYNA, MSC.MARC, PAM-STAMP, ANSYS and ABAQUS, ... etc. 2-Dimensional (2D) and

3-dimensional (3D) simulation for finite element analysis is possible in these software packages. Nowadays, Mark Colgan and John Monaghan (2003) have combined experimental and finite element analysis using the program AUTOFORM and in addition to this Padmanabhan et al (2007) have performed the finite element method combined with Taguchi technique using deep drawing 3 dimensional implicit codes (DD3IMP) to analyze the deep drawing operation.

4.3.1 ABAQUS Software Package

The ABAQUS software is a product of Dassault systèmes simulia corporation, USA. ABAQUS/CAE is a complete ABAQUS environment that provides a simple, consistent interface for creating, submitting, monitoring and evaluating results from two fundamental solution methods or frames, ABAQUS/Standard or ABAQUS/Explicit. Different types of modules are available in ABAQUS/CAE such as defining the geometry, defining the material and generating the mesh etc., and each module defines a logical aspect of modeling process. First step in analysis all or required modules are defined, a model is built from which the ABAQUS/CAE generates an input file which is then submitted to ABAQUS/Standard or ABAQUS/ Explicit for analysis. Analysis is performed and the information is sent to the ABAQUS/CAE so that the user can know the progress of the job and any error indicated can be rectified, after the problem is solved by the user it is uploaded again. Once the input is accepted successfully, the job is analyzed and the result database is generated. Finally the visualization module helps to read the wide output database and to view the results of the analysis.

The meshing of parts of the model is very important in finite element analysis. In ABAQUS, there are many different types of elements that are available for meshing. To name a few, the widely used softwares are: CAX4R- 4 node, reduced integration, axisymmetric quadrilateral element, SAX1- first order, axisymmetric shell element, S4R- first order, finite strain quadrilateral shell element, MAX1 first order, axisymmetric membrane element etc (ABAQUS user's manual 2009).

CHAPTER 5

EXPERIMENTAL STUDIES

5.1 EXPERIMENTAL SETUP

The experimental setup is designed to execute the deep drawing operations at elevated temperatures. The main points considered can be given as;

1) Design activities should be carried out by considering material properties, the requirements for deep drawing in warm condition and geometrical constrains, etc.
2) The flange region of test specimen should be heated up to a temperature in specified range and to provide the required temperature distribution at the rim of blank, when necessary, the cooling can be applied in heating stage before deep drawing.
3) The temperature should be within the range of warm condition which is below recrystallization temperature, not to allow microstructural changes.
4) The time period for heating should be within the certain limits, not to have grain growth in microstructure.
5) A mechanism exerting a force on the flange area of the test specimen should be developed to avoid wrinkling defect for drawn part due to circumferential compressive stresses.
6) The required devices for the measurements in deep drawing operation should be selected carefully. They should be placed in right positions in experimental setup to control the process and record data obtained through the deep drawing.
7) The measurement devices should be adjusted and calibrated.
8) The experiments on selection of lubricant should be executed and effect of lubricant should be discovered for the deep drawing in warm condition.

The considerations mentioned above are taken into account in design activities. The experimental setup can be described briefly as follows:

A mechanical press, whose capacity is 80 tons, is developed by adding a heating system and a blank holding mechanism to conduct deep drawing experiments at elevated temperatures. For heating system, an inductance heater is chosen to be used in this study, due to crucial advantages which will be given in further sections of this chapter. On the other hand, it is required to apply available pressure on blank during the deep drawing operation to prevent wrinkling of drawn part. A blank holding mechanism is designed, projected, and finally manufactured by the use of the facilities in the machine shop of Manufacturing EngineeringDepartment / Atılım University (İncek/Ankara).

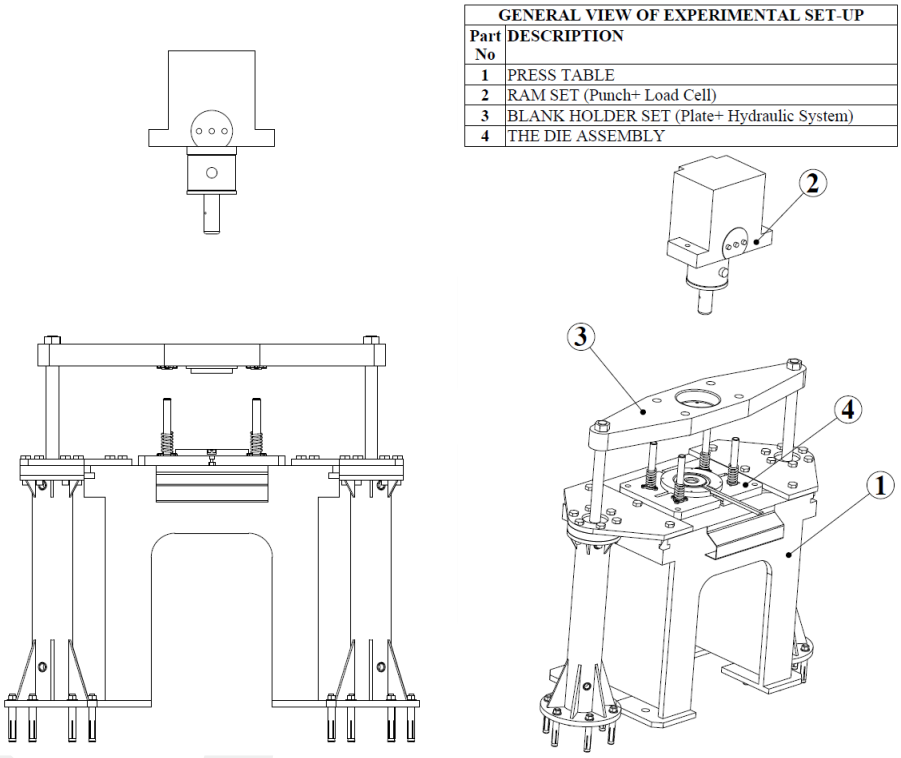

Figure 5.1 General view of experimental set-up.

5.1.1 Eccentric press (C-Type)

The capacity of the eccentric (C-Type) press is 80 tons whose stroke length is 110 mm.

Figure 5.2 Eccentric press (C-Type).

Technical and geometrical specifications of mechanical press, i.e. stroke, capacity and space for die, blank holder and punch, determined important limitations in part design and in selection of equipment's and devices used in experimental setup.

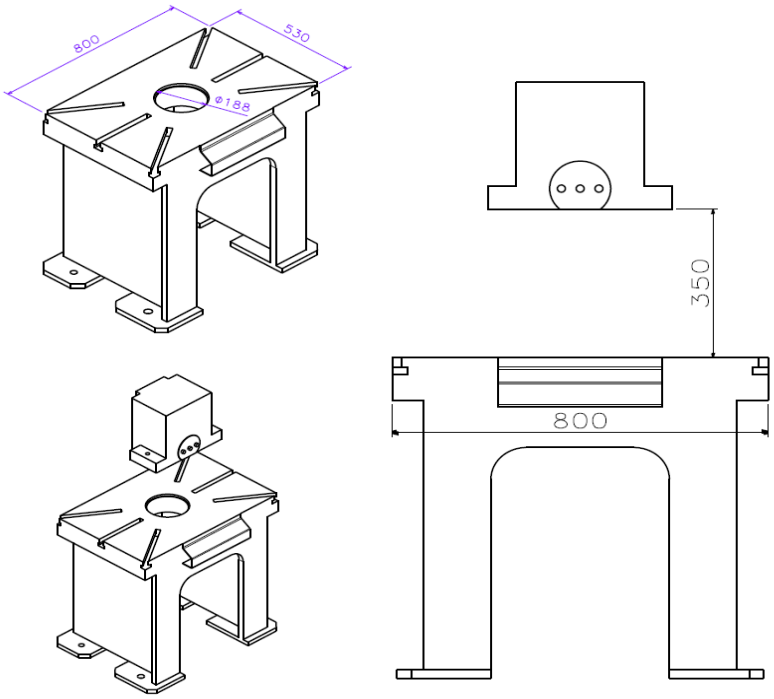

Figure 5.3 Outer Dimensions of eccentric press.

To clarify the effect of dimensions of press in the design of parts, the following formulation is driven and some simple calculations are made;

$$H_{Punch-PressTable} = H_{Die} + H_{Free\_Space} + H_{Stroke} + H_{Blank\_Holder} + H_{Load\_Cell} + H_{Load\_Cell} + H_{punch} = 350 \text{ mm} \quad (5.1))$$

Where,

$H_{Punch-PressTable}$: Height between table and ram of the pres

H_{Die} : Thickness of die

H_{Free_Space} : The height of the free space reserved to set the blank into the die (>20 mm)

H_{Stroke} : The punch stroke height (0 – 110 mm)

H_{Blank_Holder} : Thickness of blank holding base plate (Part No 3.1.1 in Figure 5.4)

H_{Load_Cell} : Load Cell Height (113 mm)

H_{punch} : Punch Length (>120 mm)

When the known values are substituted into Equation 5.1, the given formula becomes

$$H_{Die} + H_{Blank\_Holder} + H_{punch} = 107mm \quad (5.2)$$

As it is seen in Equation 5.2, the height between press table and ram of the press (107 mm) is so limited that it should always be considered in each part design. Because die, blankholder and punch should be placed in the height of 107 mm.

5.1.2 Blank holder mechanism

Two identical hydraulic cylinders operating simultaneously are connected to base plate (Part No: 3.1.1 in Figure 5.4) in the blank holder configuration. Simultaneous motion of hydraulic cylinders is provided by the use of hydraulic flow divider as shown in Figure 5.5. The blank holder set is powered by the hydraulic power control (PLC, Programmable Logic Controller) unit. The two hydraulic cylinders having double stroke, compression – tension, are used.

THE BLANK HOLDER SET (Part No : 3)	
Part No	DESCRIPTION
3.1	THE BLANK HOLDER CONFIGURATION
3.2	THE HYDRAULIC CYLINDER SET
3.3	THE CONNECTOR PLATE (FIXING CYLINDERS TO TABLE OF PRESS)

THE BLANK HOLDER CONFIGURATION (Part No : 3.1)	
Part No	DESCRIPTION
3.1.1	THE BASE PLATE OF BLANK HOLDER
3.1.2	The BLANK HOLDER PLATE

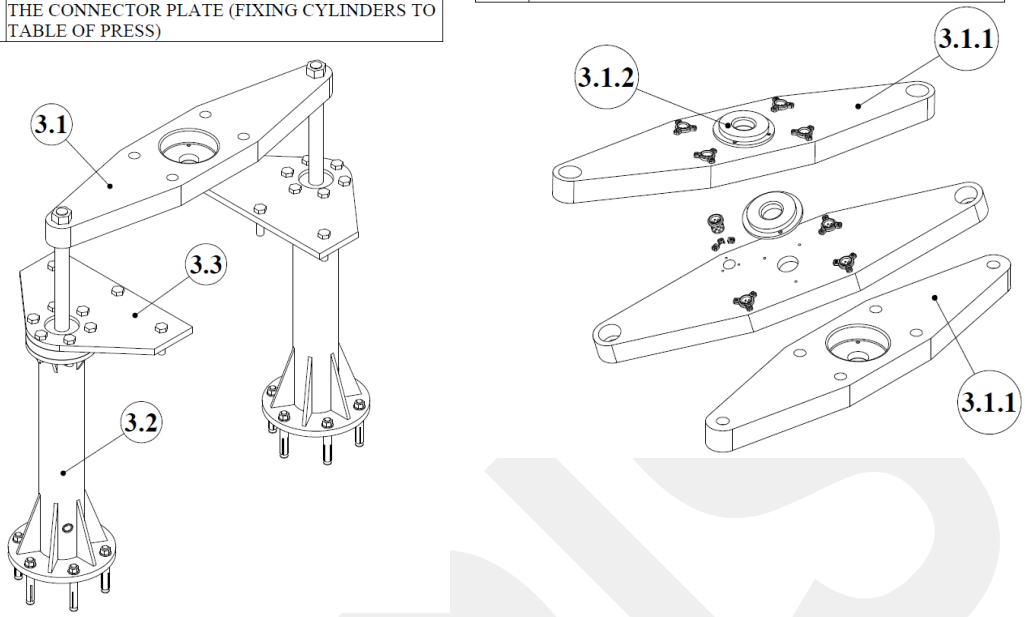

(a) (b)

Figure 5.4 Design drawings of Blank Holding System (BHS);
(a) general view (b) BH configuration.

The blank holder (BH) configuration is shown in Figure 5.4 (b). The four number of columns guide blank holding plate (as shown Figure 5.1) to work within the axis of die. Four holes (Part No: 3.1.2, Figure 5.4) on base plate of blank holder equipped with bushings are prepared to provide the sliding of blank holder plate in the correct position. When the force is exerted by the blank holder, only the surface of BH plate contacts with the surface of blank (Part No: 3.1.2 in Figure 5.4).

The cylindrical volume at the middle of blank holder base plate is removed to place (see part No 3.1.1 at the bottom drawing in Figure 5.4 (b)) some part of load cell in the motion of punch.

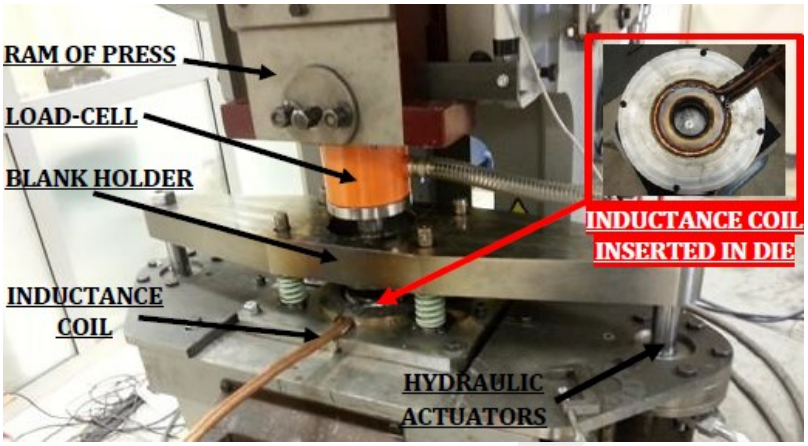

(a)

(c) (b)

Figure 5.5 Experimental setup and hydraulics (a) general (b) hydraulic cylinder (c) hydraulic power unit & hydraulic flow divider.

5.1.3 Heating system

Induction heating has many advantages compared with other methods of heating. In theory, an inductance heater uses the same working principle as an electric transformer does. The work piece is the secondary coil while copper pipe is the primary coil. Passing high frequency current through primary coil induces the job (secondary coil) and a high frequency current formed in the job (Eddy current) causes an increase in its temperature. The induced Eddy current circulates circumferentially, therefore, the heating is concentrated in thin outer layer of the work piece.

The reasons to choose induction heating are given below

- In induction heating, the heat generation rate is very high due to the use of high power densities (0,01 to 2 kW/cm^2).
- Quick heating eliminates oxidation of the work piece.
- There is excellent control on the power input and time, hence, the heat rate and the depth of heating can be controlled.

- It is possible to restrict heating only on the desired location

In contrast to the advantages mentioned above, there exists some disadvantages. The most distinctive disadvantage is that this method of heating is not economical as furnace heating and the efficiency of induction heating is very low.

Induction Heating having 50W power capacity with frequency ranging from1,7 kHz to 12 kHz is used to heat the flange zone of blank, in this study.

Figure 5.6 Induction heating machine.

5.1.4 Punch and load cell

A load cell (Part No: 2.2 in Figure 5.7) is placed between the ram and the punch to monitor and record the force exerted by press during deep drawing operation. The capacity of load cell is 100 tons.

A hole is drilled at the centre of punch, to let the air go inside when the formed part is removed from the punch. Another important function of this hole in experimental part of this research is to inject water through this hole to cool the punch and the central region of blank. The process mentioned above is applied to obtain desired temperature gradient in flange region.

THE RAM SET (Part No: 2)	
Part No	DESCRIPTION
2.1	THE RAM
2.2	THE LOAD CELL
2.3	THE PUNCH

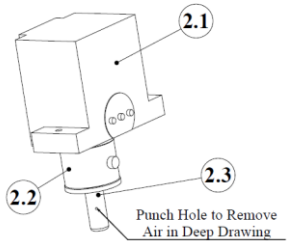

Figure 5.7 Ram set.

5.1.5 Die components

The die assembly consists of two sets which are the die base plate set and the die-heater configuration.

THE DIE ASSEMBLY (Part No : 4)	
Part No	**DESCRIPTION**
4.1	THE DIE BASE PLATE SET
4.2	THE DIE-HEATER CONFIGURATION

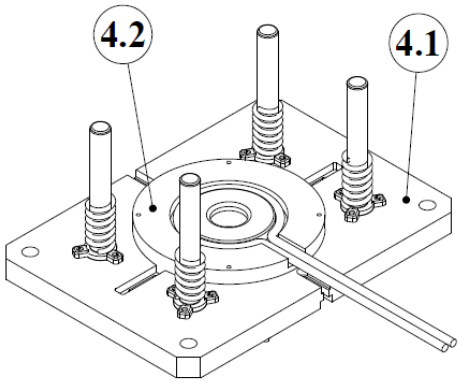

Figure 5.8 General view of die assembly.

For the proper deep drawing operations, the centrelines of punch, die and blank holder plate should be coincided to work properly. In order to ensure this, the guide columns placed on die base plate are used.

THE DIE-BASE PLATE SET (Part No : 4.1)	
Part No	**DESCRIPTION**
4.1.1	THE DIE BASE PLATE
4.1.2	THE COLUMNS
4.1.3	THE SPRINGS
4.1.4	THE FIXTURE for COLUMNS

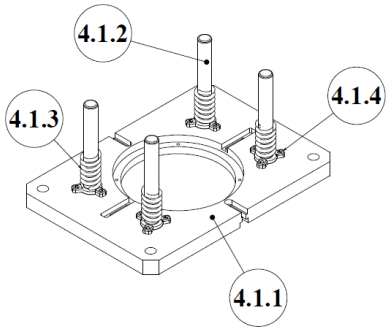

Figure 5.9 Die base plate set.

As it is mentioned above, the blank holder is actuated by the hydraulic power unit. By the use of this hydraulic power unit, the minimum force can be applied onto the blank is nearly 1 metric ton In some of deep drawing tests, that much of force exceeds the required magnitude. In order to lower the blank holding force, four number of pressure

springs formed in helical are set through the guide columns to apply force against to blank holding plate in the direction of motion. The use of those springs reduce the force applied by the blank holder.

5.1.6 Die and heater configuration

THE DIE-HEATER CONFIGURATION (Part No : 4.2)	
Part No	DESCRIPTION
4.2.1	THE DIE RING
4.2.2	THE COPPER PIPE (FOR THE INDUCTANCE HEATER)
4.2.3	THE DIE BASE CONFIGURATION

THE DIE BASE CONFIGURATION (Part No : 4.2.3)	
Part No	DESCRIPTION
4.2.3.a	THE DIE BASE PLATE
4.2.3.b	THE FIXER FOR THE SENSOR IN VERTICAL POSITION
4.2.3.c	THE FIXER FOR THE SENSOR INCLINED
4.2.3.d	THE TEMPERATURE SENSORS

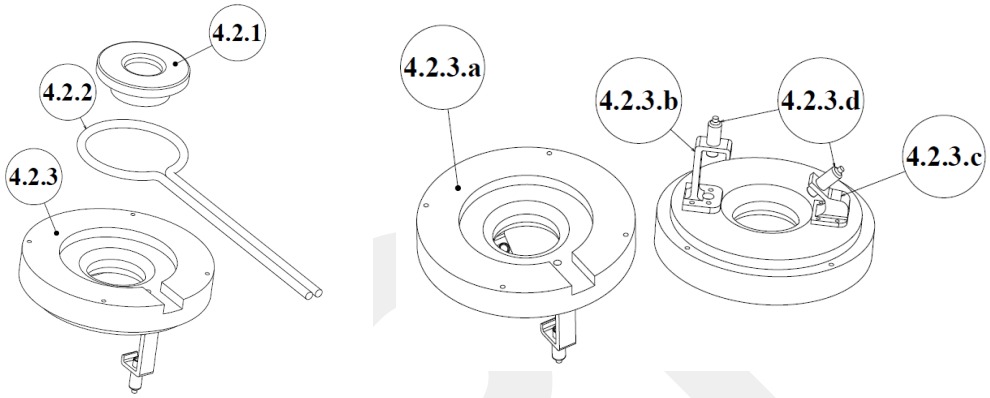

Figure 5.10 Die and heater general view.

The Induction Heating system is selected to heat the flange region of test specimen. Copper coil which is the part of heating system is fixed in die. The copper pipe, primary coil, (Part No: 4.2.2 in Figure 5.10) is wrapped around the die ring (Part No: 4.2.1 in Figure 5.10) in die. The copper pipe is insulated to prevent electrical short cut by covering it with soft mica sheet.

Figure 5.11 Insertion of copper coil into die.

The insertion of heater coil in die serves to avoid heat loss of blank. On the other hand, it is observed that thin blanks (t < 1 mm) distorted due to increase in its temperature (see Figure 5.12). Because of the distortion, test sample changes its position on die and so this misaligns blank at the beginning of deep drawing test. Heating in die also provides to develop an application method preventing distortion of blank. It can be described in such a way that during heating process, the blank holding force is applied onto the blank, not to allow blank to be distorted.

In this research, the method, heating blank under blank holding force is applied in every deep drawing experiments at elevated temperature.

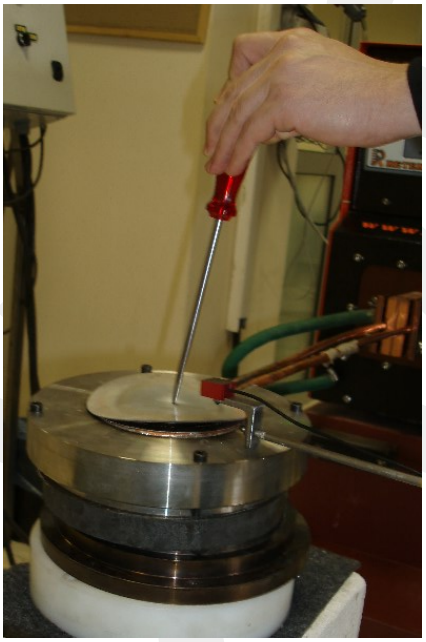

Figure 5.12 Distortion of the blank at warm temperature (t<1 mm).

The two infrared temperature sensors are located on other side of the die base plate (Part No: 4.2.3 d in Figure 5.10) to monitor and record local temperature increases of blank.

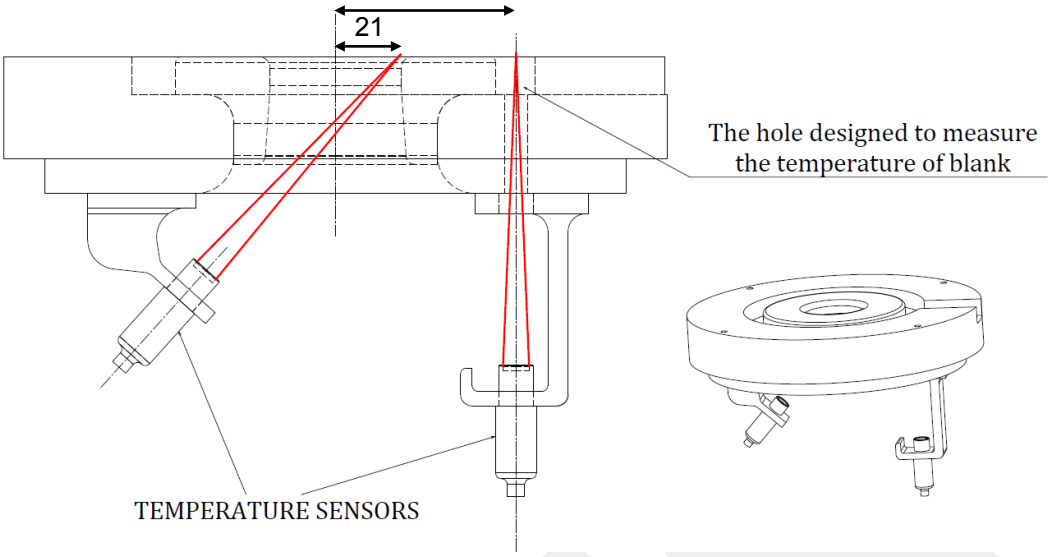

Figure 5.13 Locations of temperature sensors.

The blank flange is a region which is virtually bounded by inner and outer circles (Figure 5.14 a). Outer circle always equals to blank's diameter.

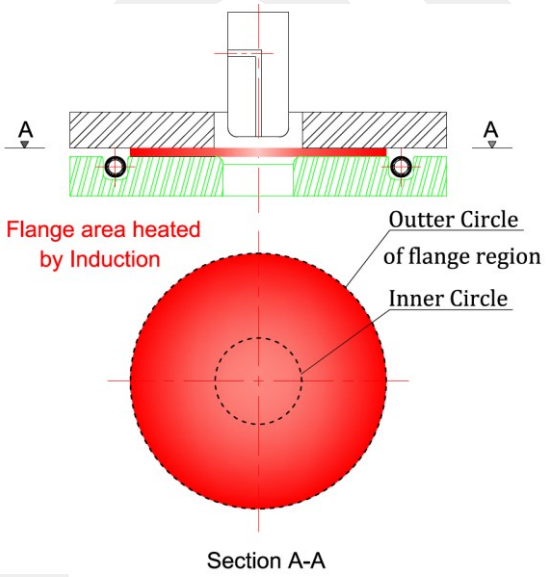

Figure 5.14 Schematic representation of flange heating.

The two infrared temperature sensors are located in fix positions on bottom surface of die. As it is seen in Figure 5.13, one of the temperature sensor is located in an inclined position, while the other is placed in vertically upward. An inclined and vertical temperature sensors focus on two different points on flange region, the locations of those points, whose distances are 42 mm and 56 mm to the die axis, are shown in Figure 5.13. Both of the sensors read average surface temperature. Vertical temperature sensor makes temperature measurements through a hole drilled through die base plate. Diameter of this hole is 8 mm as shown in Figure 5.13. Locations of

those sensors and diameter of this hole are determined by considering cone focus of infrared temperature sensors.

Functions of those sensors can be described in such a way that for the experiments at elevated temperatures, first blank is placed on die, and then, after blank holding force applied on it, heating starts. During heating of blank, temperature readings by those sensors are observed carefully; when the desired temperature ranges are attained, the deep drawing operation starts with the movement of punch towards to blank for experiments in warm condition. The readings on force via displacement taken through process are recorded and saved in a file.

5.2 PART DESIGN

Die, punch and auxiliary tools were designed to conduct axisymmetric deep drawing experiments and then manufactured by the use of the facilities in the machine shop of Manufacturing Engineering Department / Atılım University (İncek/Ankara).

Four different type of steels having thicknesses between 0,8 mm -1,6 mm were intended to be used in this scientific research subjected on the improvement of LDR at elevated temperature. These steels are

1) DP600 (Dual Phase Steel),
2) Erdemir 7128 (HSLA / Grade: HC300LA / Standard: DIN EN 10268-2006),
3) Erdemir 7140 (HSLA / Grade: HC420LA / Standard: DIN EN 10268-2006),
4) Erdemir DC04

(IF/Interstitial-Free/ Steel Grade 7114/ Standard: DIN EN 10130-2006)

Among these materials, DP600 has highest yield and ultimate tensile strength values. For this reason, die, punch and other tools are designed to draw DP600, whose thickness is 1,6 mm, at ambient temperature. At the beginning of design, two important assumptions are made, the first one is that design parameters investigated for DP600 with t = 1,6 mm covers safely the force requirements, punch and blank holding force, and the selection of tool and die material. On the other hand, when work material and its thickness are changed, this varies the geometry of die and toolings which will be used. The other assumption made is that the maximum process temperature for warm tests is expected to be lower than 400ºC. The forces determined for room condition are also acceptable for the temperatures ranging from room temperature to 400ºC.

The design activities outlined in the following sections can be used as guideline to design tools, die and punch for axisymmetric forming operations.

Selection of Geometrical Design Parameters

Yield and tensile strength of DP600 are

$$\sigma_{yield} = 470 \text{ MPa}, \ \sigma_{uts} = 670 \text{ MPa}$$

5.2.1 The thickness of blank (t);

In this study, the maximum thickness of sheet for DP600 is 1,6 mm (t)

Average thickness of a cup drawn is assumed to be 1,55 mm (t_{avg})

$t = 1,6$ mm and $t_{avg} = 1,55$ mm

5.2.2 Punch diameter (d_p);

As a result of design calculations made by considering force required to form a axisymmetric cup in deep draw operation and height between press table and ram, punch diameter is 40,9 mm (d_p).

$d_p = 40,89$ mm and $r_p = d_p/2 = 20,45$ mm

5.2.3 Corner radii of punch (r_{cp}), and die (r_{cd});

The selection of maximum possible value for punch and die corner's radii reduces punch force, significantly. If those corner radii are chosen to be smaller than the required value, because of the localized strain hardening, it is torn on a region closer to base corner (r_b) before it is drawn completely. In contrast to this, when the punch and die having larger radii than maximum values are designed, the formed part is distorted.

The recommended values for r_{cp} & r_{cd} are

$r_{cp} = 5*t$ ASM, 1988 For Stainless Steel $r_{cp} = 8$ mm ($t = 1,6$ mm)

$r_{cd} = 10*t$ ASM, 1988 For Stainless Steel $r_{cd} = 16$ mm ($t = 1,6$ mm)

as a result of literature survey on this, the following values for corner's radii are decided to be taken in design;

$r_{cp} = r_{cd} = 8,13$ mm

5.2.4 Clearance between punch and die (C);

The clearance is another important issue on the design of die and punch. Small values may lead to ironing, which is simply explained as the intentional thinning of the blank

at the die cavity. To avoid ironing, the clearance amount must be larger than the initial blank thickness.

$C = r_d - r_p = 1{,}25*t$ (Usually %25 percent larger than the thickness of blank)

The following criteria's in the selection of clearance can also be given,

$$C = r_d - r_p = 1{,}2t \quad \text{.....(100)} \tag{5.3}$$

For Sheet Steels;

$$C = r_d - r_p = t + 0{,}07\sqrt{10t} \quad \text{.....(101)} \tag{5.4}$$

t = 1,6 mm için ,

1,88 mm > C > 2,00 mm

5.2.5 Determination of blank diameters (d_b);

Unless otherwise is specified, the Draw Ratio (DR) is defined as the ratio of initial blank radius (r_b) to punch (r_p) radius in this study.

$$DR = \frac{r_b}{r_p} \tag{5.5}$$

The diameter of drawn cup is assumed to be

$$d_c = d_p + 2t = 44{,}1 \text{ mm} \tag{5.5}$$

Upper and lower limits for Draw Ratio (DR) is expected to be roughly between two (2) to three (3). So, the diameters for specimen become,

$$125mm \geq d_b \geq 82mm \tag{5.6}$$

5.2.6 Calculation of the cup height (H);

Since the initial blank diameter (d_b), punch profile (r_{cp}) and estimated diameter of cup (d_c) are known, the final height of the cup can be calculated (K. Lange, 1985) [40] to make comparison with stroke of the press used;

$$d_b = \sqrt{d_c^{\,2} + 4d_c\left(H + 0{,}57r_{cp}\right) - 0{,}56r_{cp}^2} \tag{5.7}$$

By the use of Equation (5.7), the upper and lower values determined for the cup height are

H_{min} = 22,68 mm and H_{max} = 73,15 mm < 110 mm

Since both values are less than the stroke of punch, the designed geometry for punch and die is approved to be reasonable.

5.2.7 Punch load and blank holder force;

Punch load :

DP600 has the highest strength among the materials used. For this reason, punch and blank holding forces should be evaluated by the use of DP600 in a single stroke deep drawing operation. For the calculation of load requirements, there are many analytical formulas, graphs and tables. These scientific materials are prepared for known Limiting Drawing Ratio (LDR) via required drawing ratio (DR). They are generally used by the sheet metal manufacturers. But this study is subjected to the development of Limiting Drawing Ratio (LDR). In other words, LDR is unknown and will be searched. As a result of literature search, two useful formulas which do not depend on LDR were found to evaluate punch load, those formulas are developed by

a. K. Lange, 1985, Hand Book of metal forming, university of Stuttgart, [40];

$$F_d = \pi d_m t \left[1{,}1 \frac{\sigma_{Flow}}{\eta_F} \left(\ln \frac{d_b}{d_p} - 0{,}25 \right) \right] \tag{5.8}$$

a. Kalpakjian, Schmid (c) 2008, Manufacturing Processes for Engineering Materials, 5th ed. Pearson Education ISBN No. 0-13-227271-7

$$F_d = \pi d_p t \sigma_{uts} \left(\frac{d_b}{d_p} - 0{,}7 \right) \tag{5.9}$$

The notations used in Equations 5.8, and 5.9 and the numerical values taken in the calculations are shown below;

F_d = drawing force

t = original blank thickness = 1,6 mm

σ_{UTS} = ultimate tensile stress = 670 MPa (For DP600)

σ_Y = yield stress = 470 MPa (For DP600)

σ_{Flow} = flow stress, $\sigma_{Flow} = 1{,}3 \cdot \sigma_{UTS}$ = 871 MPa (calculated)

d_b = blank diameter = 125 mm (Maximum)

d_p = punch diameter = 40,89 mm

d_m = mean cup diameter = 42,49 mm

η_F = efficiency of the operation, (0,5 – 0,7) = 0,5 (to maximize F_d in Equation 5.8)

Results of calculation for punch force are summarized in Table 5.1.

Table 5.1 Resultant punch force table.

Blank diameter	Drawing Force (F_d) By the use of Equation	
	(5.8)	(5.9)
125 mm	355 kN	324,6 kN

Blank Holding Force:

The magnitude of blank holder force is an important factor controlling the straining of material in the flange region of blank. In addition to this, the compressive stress taking place in flange region during the deep drawing operation should be balanced by applying pressure on blank region to avoid wrinkling of the material. The magnitude of the blank holding pressure required to be applied depends mainly on the material, thickness, blank diameter, punch diameter and also the lubricant used. It is thought that the study in flange region and blank holding force are important issues which can be searched on the improvement of the Limiting Drawing Ratio (LDR) in further researches.

For drawing round parts in a single drawing, the required blank holding force can be estimated by the formula [44] given as;

$$F_B = P \cdot \frac{\pi}{4} \cdot \left({d_b}^2 - \left(d_d + r_{cd} \right)^2 \right) \qquad \text{Where } P = 2{,}5\,\text{N/mm}^2\text{, for steel} \qquad (5.10)$$

After the numerical values inserted into Equation 5.10; blank holding force is;

$$F_B = 2645 \text{ kg} < 10 \text{ tons}$$

Which is a reasonable result by considering total capacity of hydraulic power unit which is 10 tons.

5.2.8 Design summary & selection of tool and die material

Based on the parameters selected, a set of toolings designed can be manufactured to perform the required deep drawing operations at elevated temperature for AHSS. The final specifications for the geometry of tool and die are summarized in Table 5.2;

Table 5.2 Summary table for the geometry of punch and die.

Thickness	d_{Punch}	d_{Die}	$r_{Die\ Corner}=r_{Punch\ Corner}$
0,8 mm	43,00	44,96	4,00
1,2 mm	45,60	48,50	6,15
1,6 mm	40,89	44,63	8,13

Some of the parts manufactured are shown in Figure 5.14

Figure 5.15 Various manufactured parts, (die plate, die ring, punch, etc.).

Sleipner produced by Uddeholm is selected as punch and die material due to mechanical and thermal properties specified in its data sheet. It is a chromium-molybdenum-vanadium alloyed tool steel. Uddeholm Sleipner is a general purpose steel for cold and warm work tool and die material. It is recommended for medium run applications where a resistance to abrasive wear is required.

Technical Specifications for Uddeholm Sleipner is given in Figure 5.15

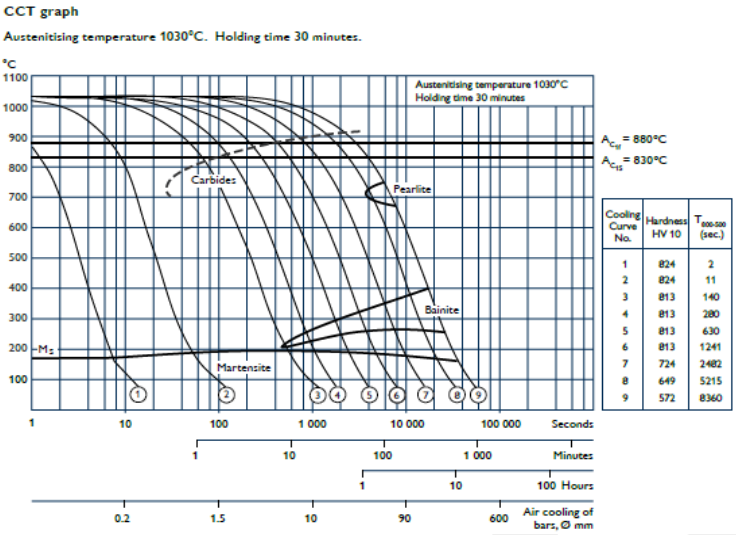

(a)

Typical analysis %	C 0.9	Si 0.9	Mn 0.5	Cr 7.8	Mo 2.5	V 0.5
Standard spec.	None					

COMPRESSIVE STRENGTH

Approximate compressive strength at room temperature.

Hardness HRC	Compressive yield strength $R_{c0.2}$ (MPa)
50	1 700
55	2 050
60	2 350
62	2 500
64	2 650

Properties

PHYSICAL DATA

Hardened and tempered to 62 HRC.

Temperature	20°C	200°C	400°C
Density kg/m³	7 730	7 680	7 620
Modulus of elasticity MPa	205 000	190 000	180 000
Coefficient of thermal expansion - low tempered* per °C from 20°C	-	12.7×10^{-6}	-
- high tempered* per °C from 20°C	-	11.6×10^{-6}	12.4×10^{-6}
Thermal conductivity W/m °C	-	20	25
Specific heat J/kg °C	460	-	-

* Low tempered ~200°C, high tempered ~550°C

(b)

Figure 5.16 Technical specifications of Uddeholm Sleipner, (a) continous cooling transformation diagram, (b) chemical composition, mechanical and physical properties

5.3 MEASUREMENT DEVICES

The experimental setup is equipped with various transducers and sensors that measure position, pressure, temperature and force. In the following sections, the detailed information about their functions, usages and criteria's considered in selection, etc. will be discussed in details.

5.3.1 Hydraulic Pressure Transducer

The hydraulic pressure transducer is mounted on one of the cylinders (see Figure 5.17) used in the hydraulic power set to control the pressure of blank holding plate. It senses

the pressure in the cylinder and give signal to (feedback control) hydraulic power control unit to keep the blank holding pressure at a constant value.

Figure 5.17 Pressure transducer attached on hydraulic cylinder

In hydraulic system, there is also a pressure gauge, which can be controlled manually to adjust blank holding pressure that will be applied

5.3.2 Displacement Transducer

The displacement transducer attached to the press ram monitors the position of the punch in motion (Figure 5.4 a). It is connected to the data acquisition system to record displacement data during the deep drawing operation in a file.

Precision Potentiometric Output
Ranges: 0-3 to 0-30 inches [0-75 to 0-750 mm]
3K – 10K ohms • IP65

CE

Specification Summary:

GENERAL

Full Stroke Ranges	0-3 to 0-30 in. (0-75 to 0-750 mm)
Output Signal	voltage divider (potentiometer)
Linearity	± 0.04 to 0.1% full stroke, see ordercode
Repeatability	< 0.01 mm
Resolution	essentially infinite
Life Expectancy	50 million cycles
Enclosure Material	aluminum
Sensor	conductive plastic linear potentiometer
Operating Speed	200 inches (5 M) per second, max.

ELECTRICAL

Input Resistance	5K to 10K ohms (±20%), see ordercode
Recommended Maximum Input Voltage	25-30 V(AC or DC)
Recommended Operating Wiper Current	≤ 1 µA

ENVIRONMENTAL

Enclosure Design	IP65
Operating Temperature	-22º to 212ºF
Vibration	up to 10 G's to 2000 Hz maximum

CLWG

Developed specifically for a wide range of demanding applications, Celesco's CL series position transducers offer unrivalled performance in terms of accuracy, repeatability, life expectancy and ease of mounting. Such applications include industrial automation, automotive and robotics.

The CLWG uses a twin-bearing actuating rod, backlash-free pivot heads and a superior wiper system to provide outstanding linearity and performance.

(a) (b)

Figure 5.18 (a) Displacement transducer mounted on press (b) specifications of displacement transducer, 0 – 200 mm, [53]

It is vitally important to record readings for the position of punch via punch load, simultaneously in a precise manner. The specifications of potentiometer can be seen in Figure 5.18 (b) and by considering the length of stroke (110 mm), the displacement potentiometer, whose travel length is 0 – 200 mm, is chosen.

5.3.3 Load cell

As it is mentioned above, the punch load applied on test specimen during the drawing operation should also be measured and recorded. The centre-hole type compression load cell was chosen and used in experiments. By considering the capacity of the eccentric press (80 tons) in setup; the load cell, whose capacity is 100 tons, is preferred. As it is seen in Figure 5.19, the meaning of centre-hole type is that there is an empty cylindrical volume at its centre. This type load cell can deliver stable measurement performance under somewhat eccentric load. In addition to this, it can make precise measurements in warm condition (-10 – 80º C), as well.

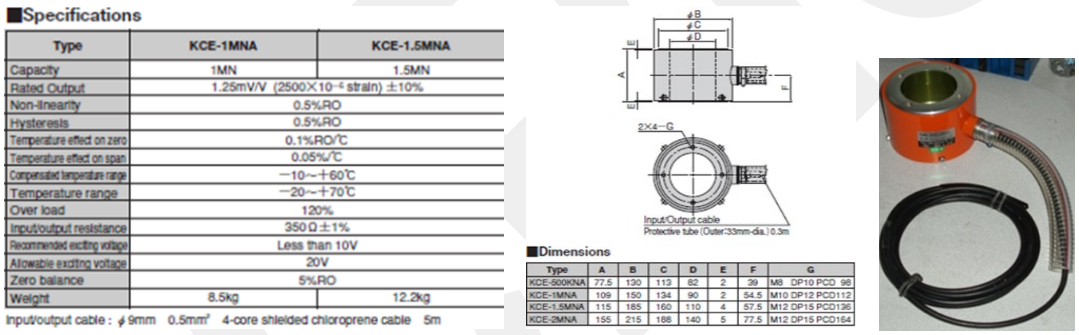

■Specifications

Type	KCE-1MNA	KCE-1.5MNA
Capacity	1MN	1.5MN
Rated Output	1.25mV/V (2500×10⁻⁶ strain) ±10%	
Non-linearity	0.5%RO	
Hysteresis	0.5%RO	
Temperature effect on zero	0.1%RO/℃	
Temperature effect on span	0.05%/℃	
Compensated temperature range	−10～+60℃	
Temperature range	−20～+70℃	
Over load	120%	
Input/output resistance	350Ω±1%	
Recommended exciting voltage	Less than 10V	
Allowable exciting voltage	20V	
Zero balance	5%RO	
Weight	8.5kg	12.2kg

Input/output cable : φ9mm 0.5mm² 4-core shielded chloroprene cable 5m

■Dimensions

Type	A	B	C	D	E	F	G
KCE-500KNA	77.5	130	113	82	2	39	M8 DP10 PCD 98
KCE-1MNA	109	150	134	90	2	54.5	M10 DP12 PCD112
KCE-1.5MNA	115	185	160	110	4	57.5	M12 DP15 PCD136
KCE-2MNA	155	215	188	140	5	77.5	M12 DP15 PCD164

(a) (b) (c)

Figure 5.19 Load cell, TML centre-hole type compression load cell, KCE - 1MNA (100 Tons), [54].

5.3.4 Infrared temperature sensors (Pyrometers)

The temperature measurement method used in this study is supposed to be an innovative method in warm deep draw operation. As it is known that upper and lower surfaces of blank flange region contact to die and blank holding plate, the flange region is fully closed during the deep drawing process. It is believed that; a non-contact type, temperature sensors, is a good solution to measure temperature of blank in heating operation. The two infrared temperature sensors used, one directed to a point at start of flange region, while other one focused, through a hole opened in die plate, to another point close to the end of flange region. So, a temperature measurement method is

developed to read local temperatures at the start and end of flange region. These temperature readings consist of some percent of error due to the positions focused, this will be discussed in further sections.

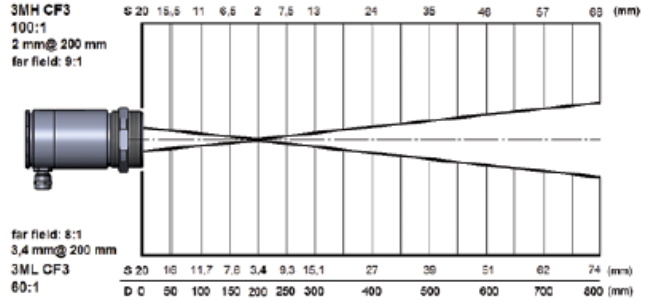

Technical Specifications

OPTRIS CT Laser (OPTCT3MH1CF3) infrared type thermometer

Non-contact temperature measurement with precise aiming from 50°C to 1800°C

Accurate temperature measurements of metals, secondary metal processing and ceramic materials. Double laser aiming marks real spot location at any distance Optical resolution up to 100:1 with selectable focus Temperature ranges from 50°C to 1800°C, measuring spots up from 0.7 mm and response times up from 1 ms Usable up to 85°C ambient temperature without cooling Short measuring wave length of 2.3 µm reduces error of temperature readings on surfaces with low or unknown emissivity.

Figure 5.20 OPTRIS CT Laser (OPTCT3MH1CF3), infrared type thermometer, [55].

By considering the technical specifications given in Figure 5.20 such as focus length, work temperature range, error for the readings on surfaces with low or unknown emissivity and response time, etc. in addition to those, various sensors are examined, OPTRIS CT Laser (OPTCT3MH1CF3), and finally the infrared type temperature sensor, is chosen to be used in the experimental setup.

5.3.5 Data acquisition system

The data acquisition system developed and produced by National Instrument (NI USB – 6259 M Series) are used to collect signals sent by the load cell connected to punch, the displacement transducer and two infrared temperature sensors placed on bottom of die. It has 16 differential or 32 single ended analog input channels, total 48 digital I/O channels, and a counter/timer. The signals are amplified and fed through an A/D converter. For data transfers, it is equipped with USB signal stream, programmed I/O. The other specifications of this board can be seen in Figure 5.21.

All measurement devices including data acquisition unit used in setup are powered by DC Batteries to reduce noise level in the measurements. So the quality of data/signal

streaming is significantly increased. In experiments, full charged batteries are always used.

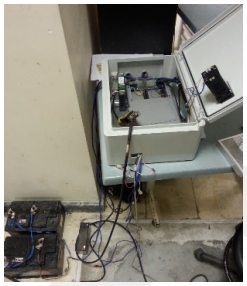

Typical Performance Graphs

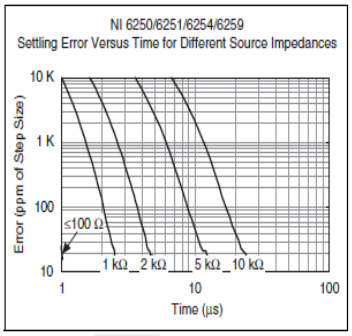

Settling Time for Multichannel Measurements

NI 6250/6251/6254/6259

Range	±60 ppm of Step (±4 LSB for Full Scale Step)	±15 ppm of Step (±1 LSB for Full Scale Step)
±10 V, ±5 V, ±2 V, ±1 V	1 µs	1.5 µs
±0.5 V	1.5 µs	2 µs
±0.2 V, ±0.1 V	2 µs	8 µs

(a)

Analog Input

Number of channels
- NI 6250/6251 ..... 8 differential or 16 single ended
- NI 6254/6259 ..... 16 differential or 32 single ended
- NI 6255 ..... 40 differential or 80 single ended

ADC resolution ..... 16 bits

DNL ..... No missing codes guaranteed

INL ..... Refer to the *AI Absolute Accuracy Table*

Sampling rate
- Maximum
  - NI 6250/6251/6254/6259 ..... 1.25 MS/s single channel, 1.00 MS/s multi-channel (aggregate)
  - NI 6255 ..... 1.25 MS/s single channel 750 kS/s multi-channel (aggregate)
- Minimum ..... No minimum
- Timing accuracy ..... 50 ppm of sample rate
- Timing resolution ..... 50 ns

Input coupling ..... DC

Input range ..... ±10 V, ±5 V, ±2 V, ±1 V, ±0.5 V, ±0.2 V, ±0.1 V

Maximum working voltage for analog inputs (signal + common mode) ..... ±11 V of AI GND

CMRR (DC to 60 Hz) ..... 100 dB

Input impedance
- Device on
  - AI+ to AI GND ..... >10 GΩ in parallel with 100 pF
  - AI– to AI GND ..... >10 GΩ in parallel with 100 pF
- Device off
  - AI+ to AI GND ..... 820 Ω
  - AI– to AI GND ..... 820 Ω

Input bias current ..... ±100 pA

Crosstalk (at 100 kHz)
- Adjacent channels ..... –75 dB
- Non-adjacent channels ..... –95 dB[1]

Small signal bandwidth (–3 dB) ..... 1.7 MHz

Input FIFO size ..... 4,095 samples

Scan list memory ..... 4,095 entries

Data transfers
- PCI/PCIe/PXI/PXIe devices ..... DMA (scatter-gather), interrupts, programmed I/O
- USB devices ..... USB Signal Stream, programmed I/O

(b)

Figure 5.21 National Instrument NI USB – 6259 M Series DAQ Device; BNC data logger.

5.3.6 Commercial data processing software package (Hera)

Hera is the name of a commercial software developed by Nell Electronic Company in Turkey. It receives, records, monitors, processes data sent from data logger. It is an object oriented programming package, the proceeded data can be displayed in different modes of graphical form or tabulated form. The collected log files are compatible both with word processing and spreadsheet programs, making it easier to utilize and analyse data. An example of a workbench data collection screen can be seen in Figure 5.22.

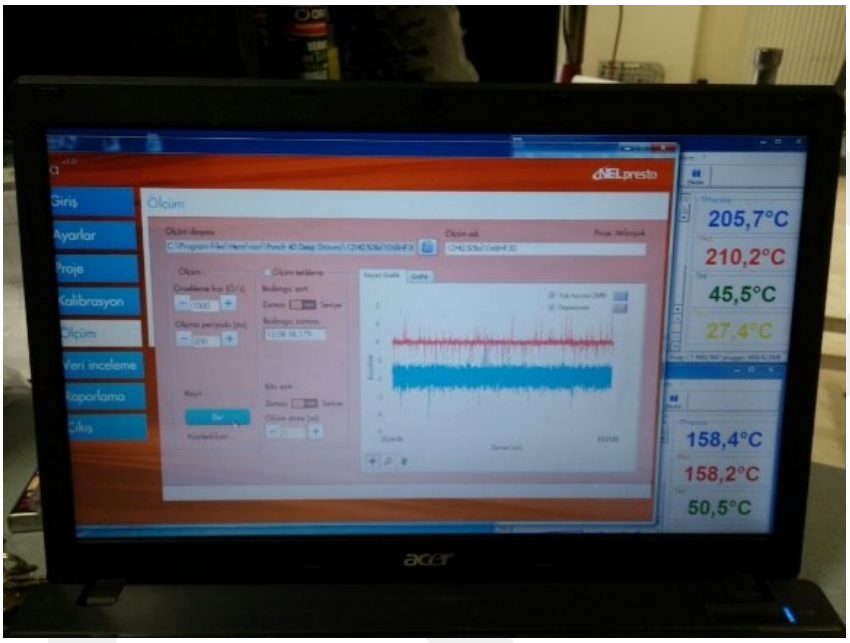

Figure 5.22 Hera, Software Package used for processing data.

5.4 CALIBRATION ACTIVITIES

In this experimental study, the calibrated measurement devices and systems were used. Although the measurement devices have already been calibrated by their manufacturers, they were tested by the use of facilities in the measurement laboratory and also Metal Forming Centre of Excellence (MFCE) in Atılım University. To check their calibrations; the simple test methods were performed and the results were compared with known values such as, the known load, measured length, etc. to see the difference in between. If the difference is within acceptable range, then that device is approved to be calibrated and it is accepted to be used in experiments.

5.4.1 Accuracy of TML load cell (1 MN)

Calibration of Zwick Roell Z300, tensile and compression testing machine, is made in regular periods, in the facilities of Metal Forming Centre of Excellence, Atılım

University/ Ankara. To check calibration of TML load cell used in deep draw tests; it is placed in Zwick and then constant known compression loads are applied on it. The resultant graphs shown in Figure 5.23 are obtained. The results of this test are quite reasonable and guarantees the accuracy of readings by TML load cell.

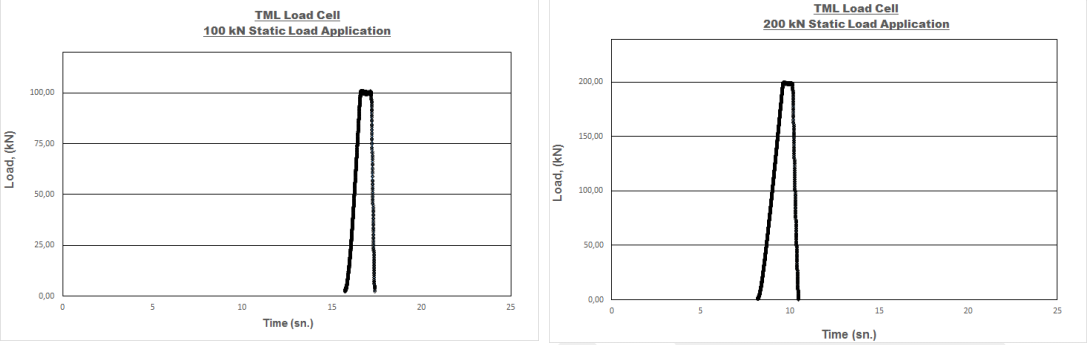

(a) Exposed to 100 kN Static Load (b) Exposed to 200 kN Static Load

Figure 5.23 Resultant graphs of TML load cell tested under loads 100 & 200 kN.

5.4.2 Blank holding system

The blank holding system actuated by the hydraulic power unit is tested and calibrated by the use of TML load cell. The load cell is placed between the press table and blank holder plate. Then the blank holder is actuated to apply a force onto the load cell. The readings obtained by load cell are compared with the values by hydraulic pressure applied and then displayed on screen. The calibration activities for blank holder are continued until the differences between two readings are reduced in an acceptable range. After the required range for calibration is attained, the blank holder is started to be used in the deep drawing tests.

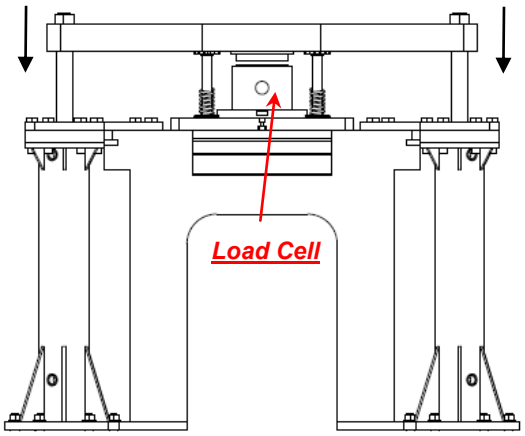

Figure 5.24 Calibration of Blank Holder by the use of load cell having been calibrated.

5.4.3 Temperature sensors

The two important factors which affect temperature measurements should clearly be stated. While the blank is heating, the temperatures of die and the blank holding plate is also increased by the inductance heater. As explained before, the temperature sensors are located on the bottom surface of die. Both of them work in warm condition due to heating of die. One of the infrared temperature sensor positioned perpendicular to the die surface and it makes measurements through a hole opened in the die. The temperature of die is elevated by the inductance heater. Although the temperature sensors have already been calibrated by the manufacturer, those sensors required to be adjusted and recalibrated for the working conditions mentioned above. An experienced technician working in OPTRIS made those all necessary calibrations and the readings checked with the measurements taken by the calibrated sensor.

5.5 OTHER ACTIVITIES

5.5.1 Preparation of Test Specimens

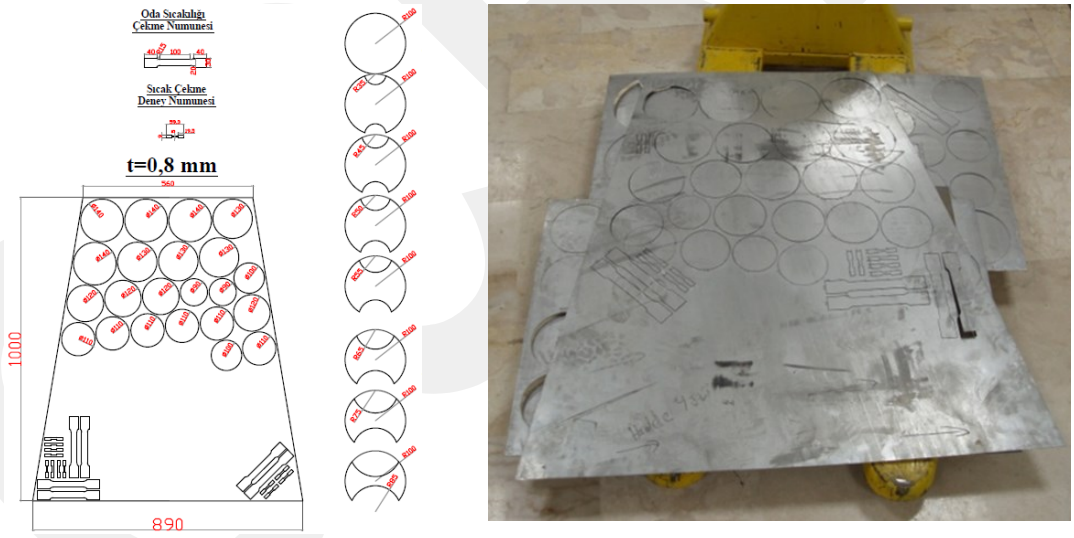

Figure 5.25 Test specimen prepared by the use of water-jet cutting.

Water jet cutting is used in the preparation of test samples. Water jet is a cold cutting operation for sheet metals. An important benefit of the water jet cutter is the ability to cut material without interfering with the material's inherent structure as there is no heat-affected zone. Moreover, Water jet cutting places no mechanical stresses into the work-piece. No side pressures are created because water jet pressure is forced downward, forcing the material onto the table, therefore clamping and fixturing is very minimal and could practically be non-existent.

Nesting plan is prepared for the cutting of test specimen (See Figure 5.25).

5.5.2 Lubrication

When forming steel sheet, a lubricant is used to enable work piece to slide over die and tool surface under reduced frictions. Friction and lubrication in sheet metal forming are influenced by such parameters as material properties, surface finish, temperature, sliding velocity, contact pressure, and lubricant characteristics. Depending on these parameters, the performance of a lubricant and the coefficient of friction varies.

Material flow in the die cavity is influenced by frictional conditions at the die/work piece interface. Therefore, a good understanding of the parameters that effect friction is essential for selecting lubricants and producing good-quality sheet metal parts with high LDR.

In deep drawing, the most severe friction usually takes place at die shoulder. The lubrication condition in these areas influences the thinning or possible failure of the sidewall in the drawn cup. Therefore, lubricants can be evaluated in deep drawing by determining the maximum applicable BHF without fracture in the cup wall. The basic knowledge mentioned above used for the selection and application of available lubricant.

For deep drawing experiments at elevated temperatures, solid lubricants give good solutions. Graphite and molybdenum disulphide (MoS_2) are the predominant materials used as solid lubricant. In the form of dry powder these materials are effective lubricant additives.

Forming of high strength steels requires higher forces than conventional steels and as a result this, higher contact pressure requires to be applied.

In tests executed to determine type of lubricant, Gaphene702 produced by ORAPI / France, showed high performance in deep drawing operation at elevated temperature. It is a graphite-based dry lubricant in aerosol form for easy application.

In this study, a mixed lubrication system, sheet PTFE and Gaphene702 are applied together, is also used. The results of deep drawing tests in warm condition showed that a mixed lubrication system introduced better performance than a single lubricant on the improvement of LDR for AHSS material.

5.6 MATERIAL CHARACTERIZATION TESTS AND DEVICES

Material characterization tests done are summarized in Table 5.3;

Table 5.3 Summary table for material characterization tests.

Material Characterisation Tests		Materials studied			
		DP 600 (DP)	Erd 7128 (HSLA I)	Erd 7140 (HSLA II)	Erd 7114 (IF)
Chemical Analysis		√	√	√	√
Tensile	in ambient condition	√	√	√	√
	in warm condition	√	√	√	√
Nakazima (FLC) at Room Temperature		√	√	-	-
Hardness		√	√	-	-
Searchings in SEM (Scanning Electron Microscope)		√	-	-	-

Results of these tests will be used to investigate the mechanical characteristic and formability of each material, and also in the numerical analysis.

5.6.1 Testing Machines and Devices

Tension test is a fundamental materials science test in which a sample is subjected to a controlled tension until failure, data during tensile test are recorded and then are displayed in graphical form. The results from the test are commonly used to predict characteristic reaction of material by application of various forces.

GCRIS

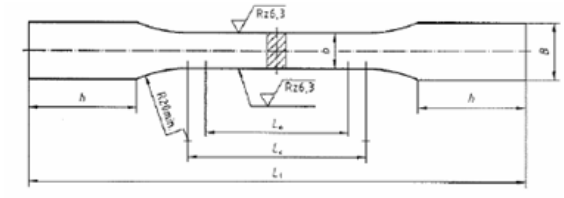

(a)

a: Specimen thickness b: Specimen width

B: Grip width h: Grip length

L_0: Gage length L_c: Test length

L_1: Total length

Figure 5.26 Zwick Roell Z300, uniaxial testing machine, [52].

Properties that are directly measured via a tensile test are ultimate tensile strength, maximum elongation and reduction in area. From these measurements the following properties can also be determined: Young's modulus, Poisson's ratio, yield strength, and strain-hardening characteristics. Tensile testing is the most commonly used for obtaining the mechanical characteristics of isotropic materials.

Uniaxial tensile tests are executed by Zwick Roell Z300 in the facilities of Metal Forming Center of Excellence, Atılım University – Ankara

Tensile test specimen are prepared by following the rules and claims given in ISO 6892-1: "Metallic materials. Tensile testing. Method of test at ambient temperature" (2009). In addition to this the recommendations done by Manufacturer, Zwick are also considered.

5.6.2 Test for Forming Limit Curve (FLC)

A forming limit curve, is used in sheet metal forming to predict forming behaviour of sheet metal. The Forming Limit Curve (FLC) is a very common tool used as a failure criterion in sheet metal forming. Good sheet metal formability is essential in the production of quality stamped products.

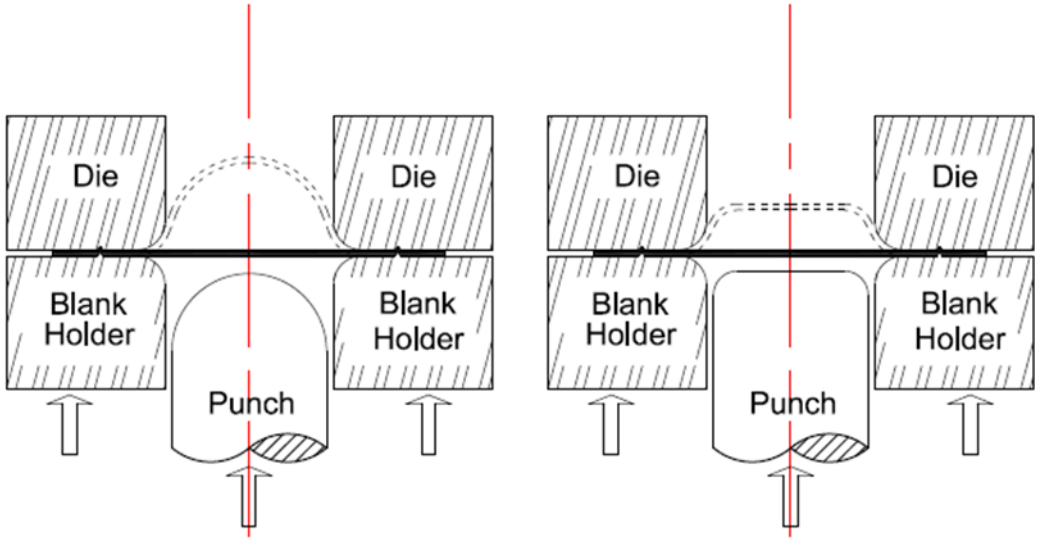

(a) (b)

Figure 5.27 Schematic representation of Nakazima (a) and Marciniak (b) Tests, [48].

The FLC is usually determined experimentally by using one of the following two types of test methods: Nakazima out-of-plane test (see in Figure 5.27 (a)), which uses a hemispherical punch, and Marciniak in-plane test (see in Figure 5.27 (b)), where a sheet metal sample is strained by a flat-bottomed cylindrical punch.

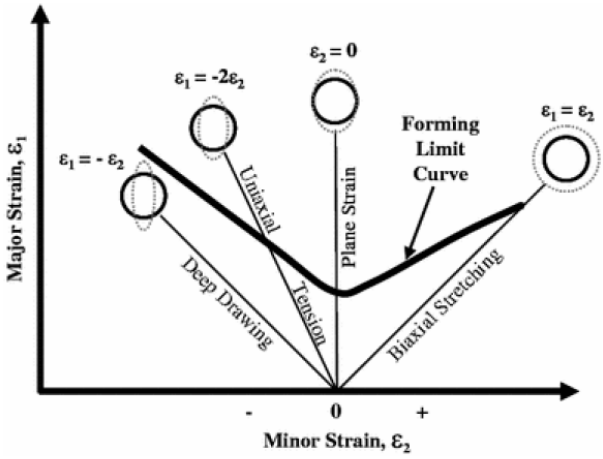

Figure 5.28 Forming Limit Curve (FLC), [41].

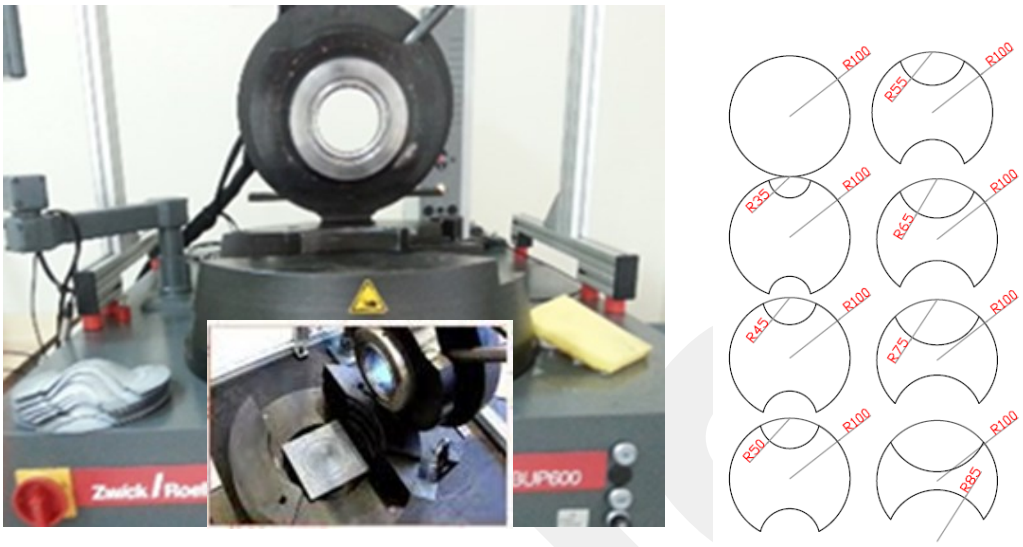

Figure 5.29 Zwick Roell BUP600 for FLC tests, [50].

In this study, Zwick Roell BUP600, in facilities of MFCE, Atılım University, is used to make Nakazima tests for FLC. Test specimen are prepared by the use of in water-jet cutting as shown in Figure 5.29.

5.6.3 Tension tests at warm temperature

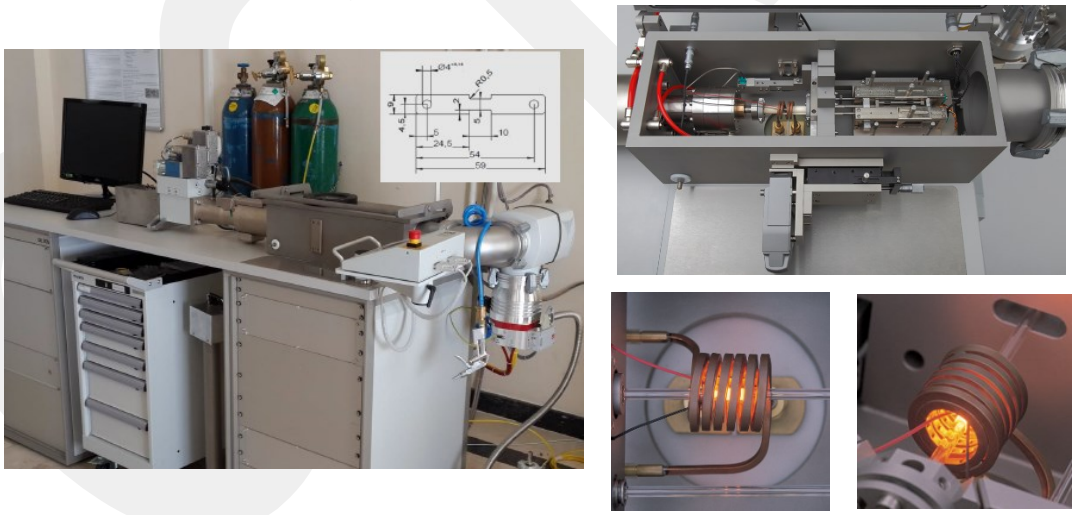

Figure 5.30 Dilatometer, Bähr DIL805 AD, [51]

Dilatometer, Bähr DIL805 AD, is used to make uniaxial tensile tests to investigate material characterisation at elevated temperature. Test sample is heated by Induction in ambient condition.

The technical specifications of Dilatometer, Bähr DIL805 AD is given in Figure 5.31

	DIL 805L	DIL 805A	DIL 805D
Temperature Range (dependent on sample material)	20 °C to1500 °C -150 °C to 1300 °C	20 °C to 1500 °C -150 °C to 1300 °C	20 °C to 1500 °C
Heating Principle	Inductive	Inductive	Inductive
Heating Rate	≤ 2000 K/s	≤ 4000 K/s	100 K/s
Cooling Rate	≤ 2500 K/s	≤ 2500 K/s	≤ 100 K/s
Sample Material and Geometry	electro-conductive solid or hollow samples OD=4 mm, L=10 mm		electro-conductive solid samples OD=5 mm, L=10 mm
Atmosphere	air, vacuum, inert gas		air, vacuum, inert gas
Resolution (ΔL/°C)	0.05 µm / 0.05 °C		0.05 µm / 0.05 °C
Deformation Force			≤ 20 kN
Deformation Rate			0.01 mm/s to 200 mm/s
Strain Rate $\dot{\varphi}$			0.001 to 20.0 s^{-1}
True Strain φ			0.05 - 1.2
Deformation			max. 7 mm
Number of deformation steps			Unlimited
Min. pause between deformation steps			40 ms

Figure 5.31 Technical specification of Dilatometer, Bähr DIL805 AD, [51]

5.6.4 Operation sequence in deep drawing experiments

The operation sequence of experimental setup is shown in Figure 5.32.

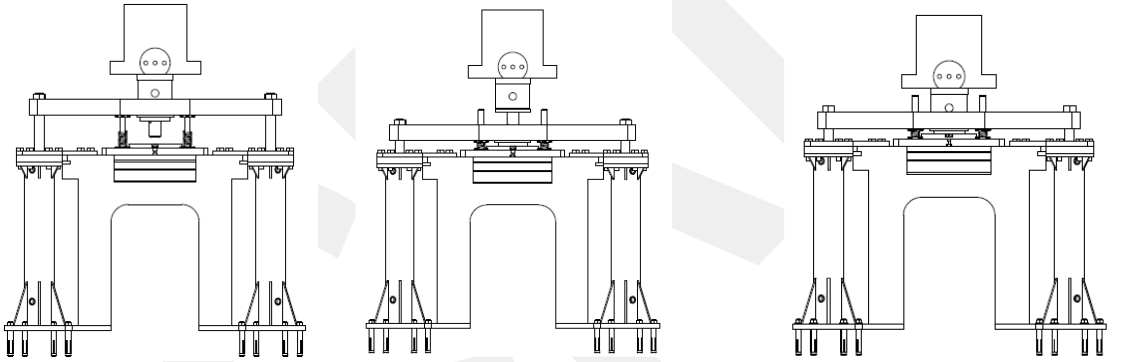

(a) Start Position. (b) Exerting BHF and heating is on. (c) Punch draws the blank

Figure 5.32 Schematic representation of operation sequence.

The operation sequence for deep operation at elevated temperature is simply explained in this part of the thesis report.

At the beginning of deep drawing operation, the sheet metal blank is placed on top of the die ring by considering its axis coincide with the axis of punch (Figure 5.32 a). The blank holding plate starts to exert available constant pressure onto the blank, and then the heater is turned on, to warm the flange region of the blank up to certain temperature range (Figure 5.32 b).

Table 5.4 Temperature ranges for the preheating of the blank.

Material	Thickness	**Inclined** Temperature Sensor focused to a point at the distance ***21 mm*** to die axis ***desired Temperature Range***	**Vertical** Temperature Sensor focused to a point at the distance ***56 mm*** to die axis ***desired Temperature Range***
DP600	0,80	170 - 207	230 - 310
	1,20	165 - 195	245 - 295
	1,60	180 - 225	220 - 300
ERD 7128	1,20	170 - 200	245 - 290
	1,50	175 - 210	235 - 295
ERD 7128	1,20	170 - 190	250 - 295
	1,50	165 - 190	220 - 275
DC04 (IF Steel)	0,80	165 - 195	215 - 305
	1,20	170 - 195	250 - 290
	1,57	160 - 195	235 - 278

Finally the circular sheet blank at elevated temperature, while the constant holding pressure acting on it, is drawn into the die to form an axisymmetric cup (Figure 5.32 c).

It is important to note that during the heating of the blank, the temperatures at the outer and inner circle of flange region are observed to assure the specified ranges reached. All temperature data along with the heating of blank measured by the infrared sensors are recorded into a file and summarized in Table 5.4.

Similarly, during the downward motion of the press ram, the punch displacement and the punch force are also recorded simultaneously by the data taker. The data taker collects the signals from the displacement transducer and load cell, then turn them into the data.

CHAPTER 6

RESULTS AND DISCUSSION

6.1 RESULT OF EXPERIMENTS

6.1.1 Investigation of material characteristics

The main material which is of interest in this investigation is DP600. For this reason, the experimental results including material characterization of DP600 are given in this chapter. The similar results for the additional materials used in this study, like HSLA in two qualities described as 7128 and 7140 grades, an interstitial-free grade (IF) and steel (grade DC04) are given in Appendices.

All the materials are tested in tension at room temperature by a universal tensile testing machine (300 kN Zwick). At elevated temperatures between 150ºC – 300ºC, which corresponds to the warm region for these materials, tensile testing is also carried out. Flow stress curves are obtained at room temperature and in the warm region (150 º - 300ºC) for all thicknesses. Tests at room temperature are also conducted along the rolling, transverse and 45º directions to determine the anisotropy. Strain rate dependency is also checked by conducting tests at $1{,}0 \times 10^{-1}$ s^{-1} and $2{,}08 \times 10^{-3}$ s^{-1} strain rates. Microstructure of the DP600 material is also investigated before and after forming together with its hardness.

Table 6.1 shows the chemical compositions (by weight %) of the DP600 steel used in this study. The nominal thicknesses used in the experiments are 0,8, 1,2 and 1,6 mm.

Table 6.1 The chemical compositions (by weight %) of the DP600 steel used in this study.

C	0,0833	Ni	0,0477	Pb	<0,002	Se	<0,0015
Mn	1,47	Co	0,0123	Sn	0,004	La	<0,0005
Si	0,366	Fe	97	Mg	<0,001	Sb	0,0032
P	0,027	Mo	<0,001	As	<0,0015	Ta	0,02
S	<0,0005	Ti	<0,001	Zr	<,0015	N	0,0197
Cr	0,808	V	0,0096	Bi	<0,002	B	0,0004
Al	0,0468	Nb	<0,004	Ca	0,0032	Zn	0,0029
Cu	0,0291	W	<0,007	Ce	<0,0015	Te	0,0025

At the start of experiments, to investigate the percentages of phases, martensitic and ferrite contained in the microstructure of DP600, the blank having thickness, 1.6 mm are examined by the use of Optical Microscope (OM) and Scanning Electron Microscope (SEM) is also used for the detailed survey. The micrographs as a result of microstructural examinations of the original material are saved to follow the changes in microstructure of DP600 when it is drawn into a cup.

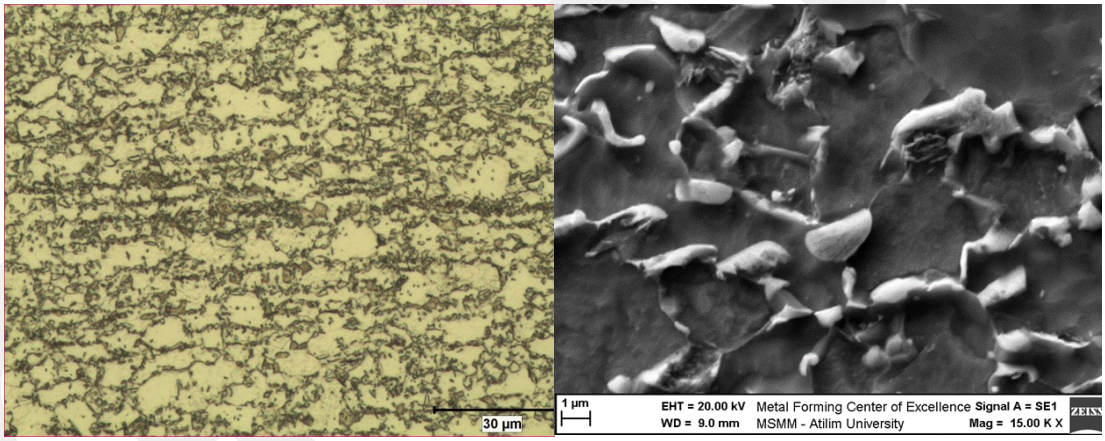

(a) Blank – OM 500x (b) Blank – SEM 15000x

Figure 6.1 Microstructure of DP600 at original state as blank.

The bright areas in Figure 6.1 (b) pictured by SEM 15000x indicate the martensite phases, where the dark zones referring to the ferrite regions constituted in the microstructure of DP600. In OM 500x, the dark areas show martensitic, where the bright regions indicate the ferrite phases. The volume contributions of phases martensite and ferrite phases are evaluated as given in Table 6.2.

Table 6.2 Volume percentages of the martensite and ferrite phases in the steel, DP600 studied.

Material	Martensite (%)	Ferrite (%)
DP600 (Blank)	26,2±1,2	73,3±0,8

The hardness of DP600 blank is measured as 196 (HV0.2).

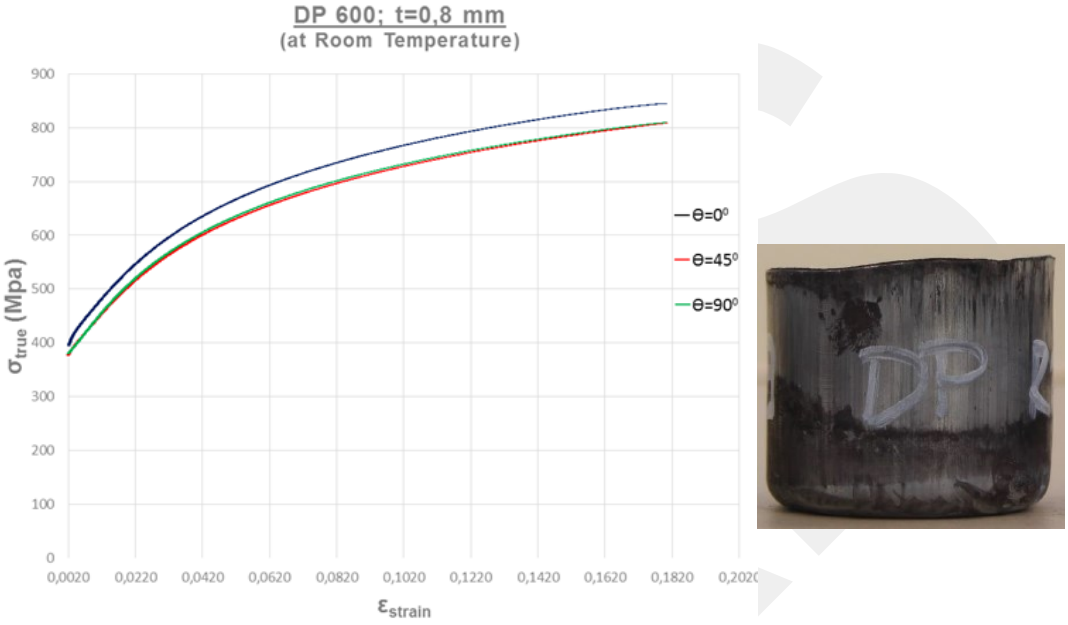

Figure 6.2 The resultant graph of tensile tests executed for the investigation of anisotropy, DP600; t = 0,8 mm at room condition and strain rate; $2{,}08 \times 10^{-3}$ s^{-1}.

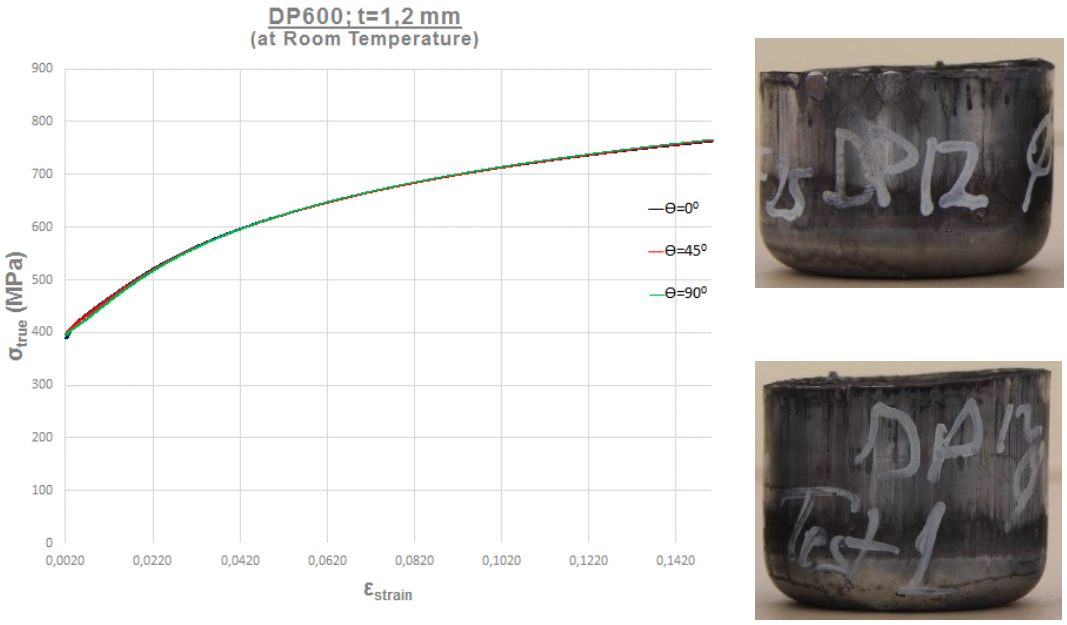

Figure 6.3 The resultant graph of tensile tests executed for the investigation of anisotropy, DP600; t = 1,2 mm at room condition and strain rate; $2{,}08 \times 10^{-3}$ s^{-1}.

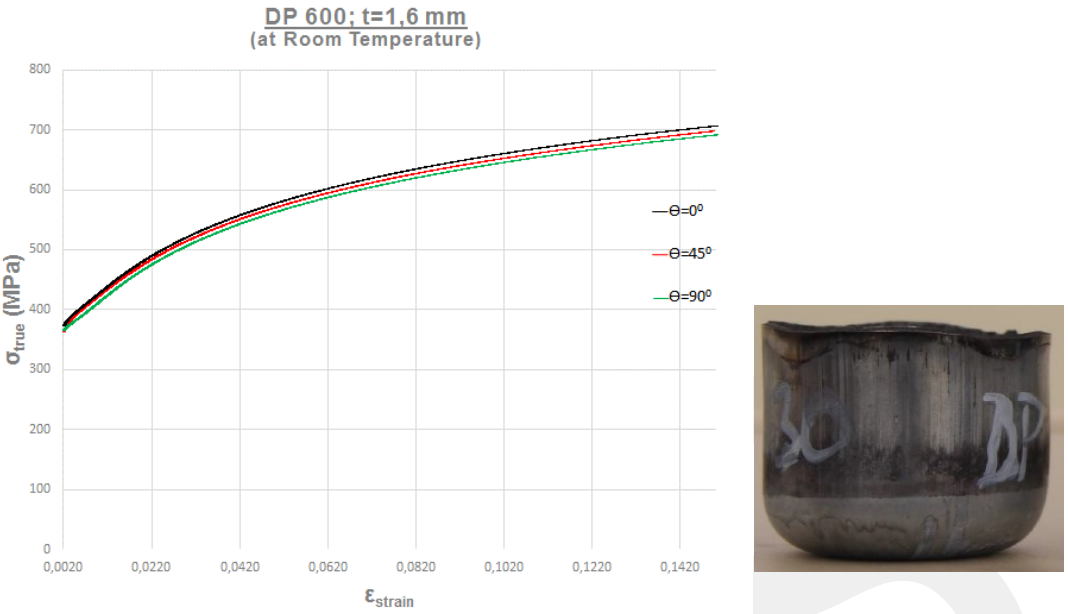

Figure 6.4 The resultant graph of tensile tests executed for the investigation of anisotropy, DP600; t = 1,6 mm at room condition and strain rate; $2{,}08 \times 10^{-3}$ s^{-1}.

Table 6.3 Summary table of Figures 6.2 to 6.4

DP 600, at strain rate = $2{,}08 \times 10^{-3}$ s^{-1}				
t (mm)	**Stresses**	**0°**	**45°**	**90°**
		(Mpa)		
0,8	**σ_{Yield}**	395	380	380
	σ_{UTS}	845	810	810
1,2	**σ_{Yield}**	397	397	380
	σ_{UTS}	767	765	763
1,6	**σ_{Yield}**	374	366	364
	σ_{UTS}	708	698	692

The sign of anisotropy in deep drawing is the forming of ears in the drawn cup. The pictures of cup are given together with the resultant graphs. It can be concluded that no obvious anisotropy is detected for all thickness of DP600 surveyed in this study. In some of the researches, DP600 is defined as strain rate dependent material. For this reason, DP600 is tested at different strain rates.

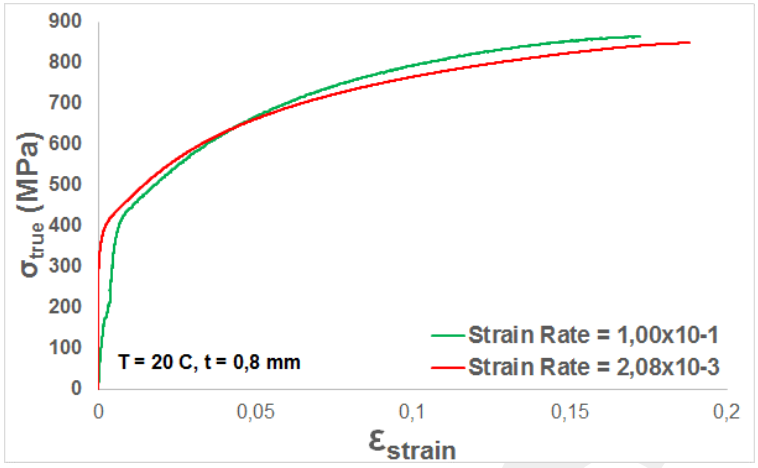

Figure 6.5 The flow behaviour of DP600 at different strain rates, t = 0,8 mm and at 20ºC

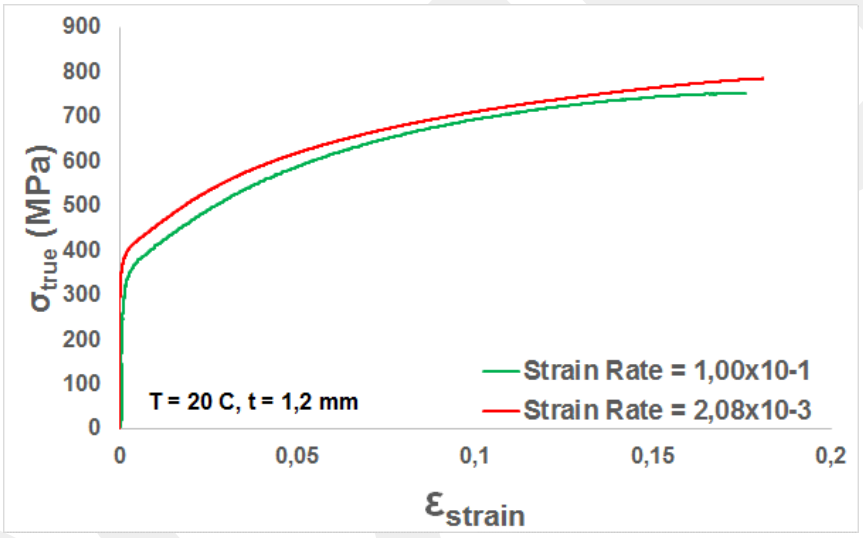

Figure 6.6 The flow behaviour of DP600 at different strain rates, t = 1,2 mm and at 20ºC

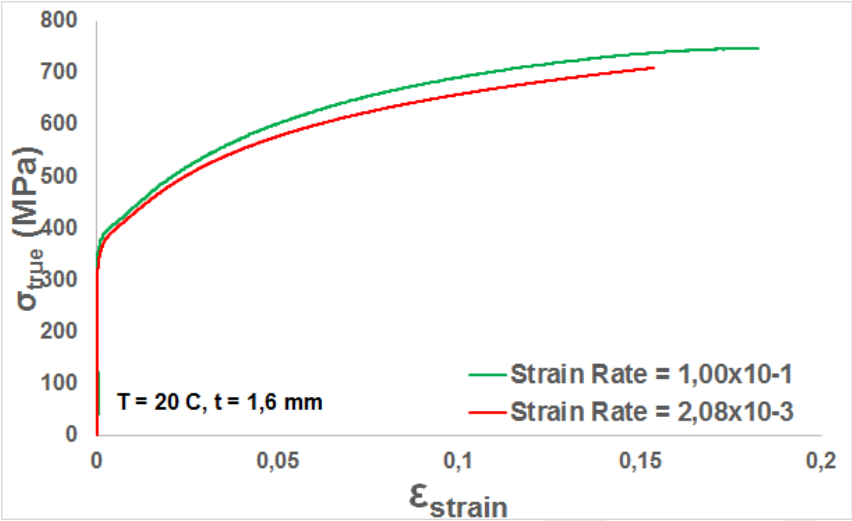

Figure 6.7 The flow behaviour of DP600 at different strain rates, t = 1,6 mm and at 20ºC.

The strain rate dependency of DP600 is determined by comparing the flow graphs at different strain rates for constant temperature. It is seen in Figures 6.5 to 6.7, the strain rate dependency is minimum and it can be neglected as an influencing parameter. However, the strain rate in deep drawing varies from point to point and changes as a function of time and its average is closer to 1,0 x $10^{-1}s^{-1}$. For varying thicknesses, the flow stress behaviour of DP600 at constant temperature and constant strain rate, are shown in Figures from 6.8 to 6.10.

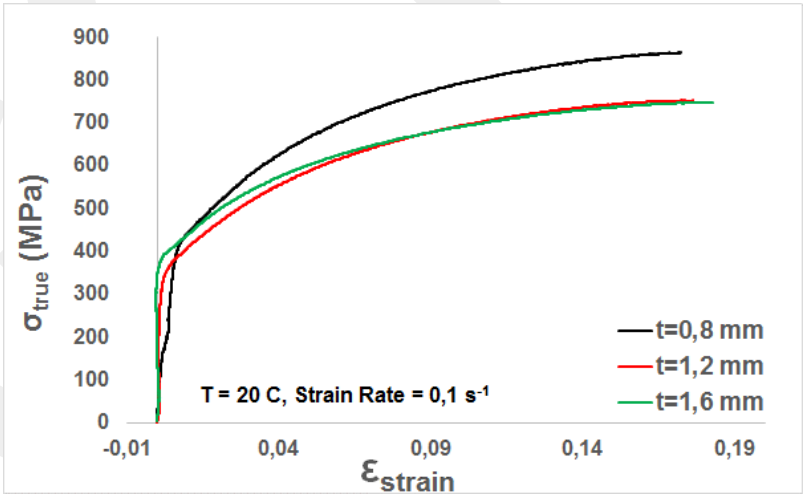

Figure 6.8 Flow stress curves for DP600 steel sheet for different thicknesses at 20ºC.

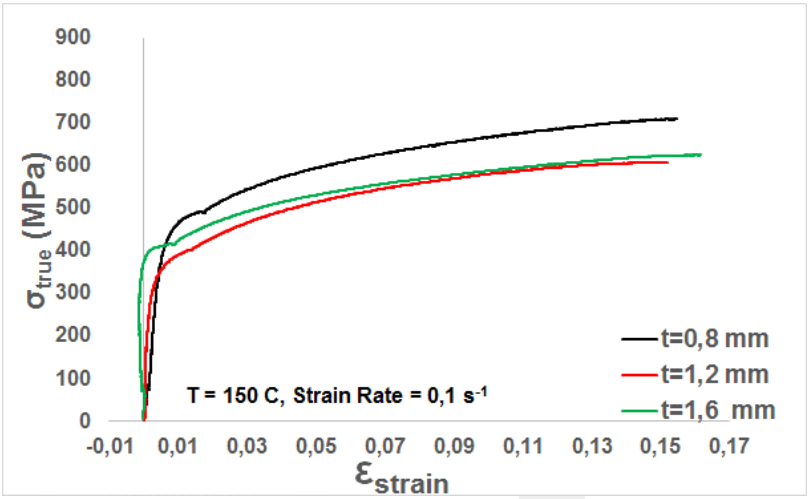

Figure 6.9 Flow stress curves for DP600 steel sheet for different thicknesses at 150ºC.

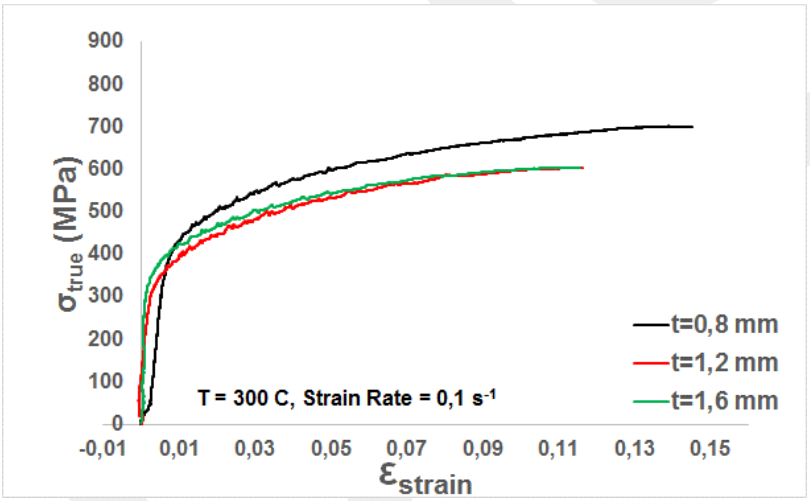

Figure 6.10 Flow stress curves for DP600 steel sheet for different thicknesses at 300ºC.

By considering the above graphs, the flow stress curves for 1,2 and 1,6 mm thicknesses are showing almost the same behaviour, while the other having 0,8 mm in thickness is higher as expected.

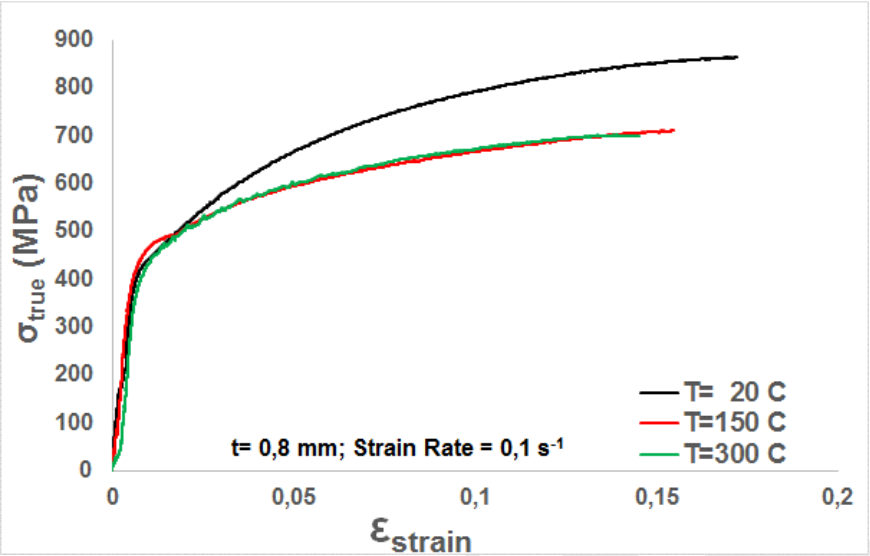

Figure 6.11 Temperature dependency of flow stress for DP600 steel sheet, t = 0,8 mm and strain rate = 0,1 s^{-1}.

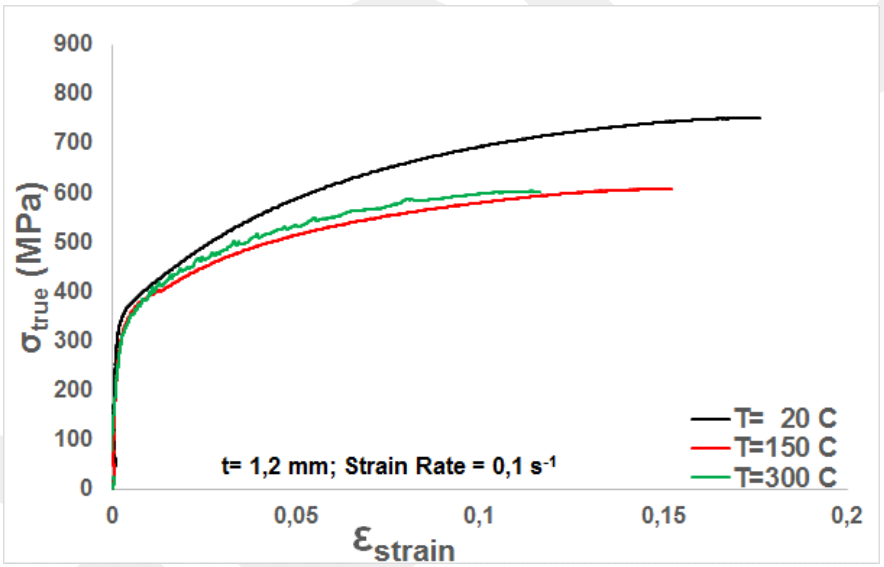

Figure 6.12 Temperature dependency of flow stress for DP600 steel sheet, t = 1,2 mm and strain rate = 0,1 s^{-1}.

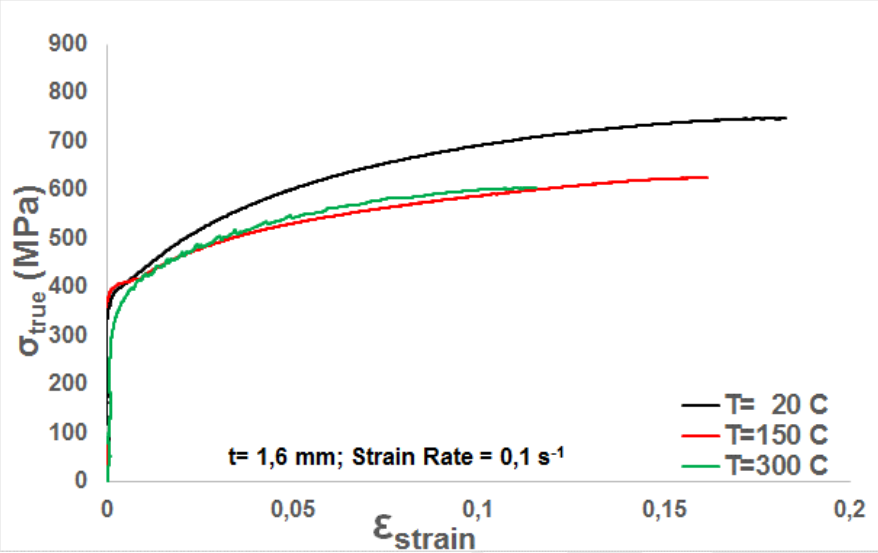

Figure 6.13 Temperature dependency of flow stress for DP600 steel sheet, t = 1,6 mm and strain rate = 0,1 s^{-1}.

Table 6.5 Summary table for Figures 6.5 to 6.13

DP 600, at strain rate = 0,1 s^{-1}

t (mm)	Stresses	20°C	150°C	300°C
		(Mpa)		
0,8	σ_{Yield}	420	475	420
	σ_{UTS}	864	711	700
1,2	σ_{Yield}	385	390	365
	σ_{UTS}	750	625	605
1,6	σ_{Yield}	390	375	370
	σ_{UTS}	752	608	604

DP 600, at 20°C

t (mm)	Stresses	Strain Rates	
		$1{,}00x10^{-1}$	$2{,}08x10^{-1}$
0,8	σ_{Yield}	420	395
	σ_{UTS}	864	845
1,2	σ_{Yield}	385	397
	σ_{UTS}	750	767
1,6	σ_{Yield}	390	374
	σ_{UTS}	752	708

Figure 6.11 shows the temperature dependency for DP600 steel sheet with 0.8 mm thickness for room temperature and 150°C - 300°C in the warm region. Similar behaviour is also found for DP600 steel sheets having 1,2 mm and 1,6 mm thicknesses for room temperature and the warm region as seen in Figures 6.12 and 6.13. For all thicknesses studied, the flow stresses at 150°C and 300°C temperatures are nearly the same. This shows that the flow stress in this region is lower than that of at room temperature but does not show a significant variation with temperature in the warm region.

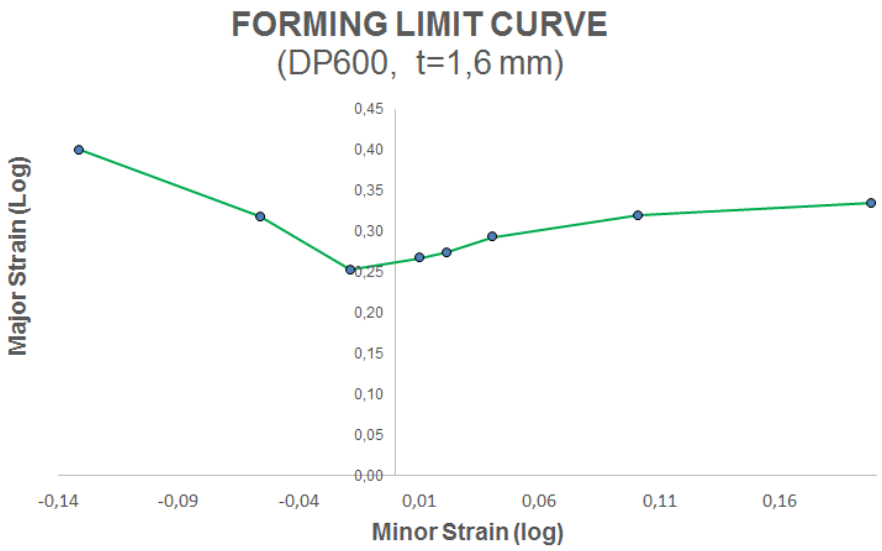

Figure 6.14 The forming limit curve of DP600, t = 1,6 mm at room temperature, at strain rate 0,01 s^{-1}.

Nakazima test is generally done to predict forming behaviour of sheet material. As it is known that the Forming Limit Curve (FLC) is a very common tool used in formability of sheet materials and it is a biaxial test. There exits additionally two extra methods forming FLC which characterizes the formability of sheet materials, one is by etching equal circulates on the surface of blank for the evaluation of the major and minor strains on the drawn cup. The other applicable method can be explained in such a way that; the results by Nakazima bulge test are proceeded with the simulation data on the same graph for the determination of the safe, marginal and fail zones. In the current dissertation, the method proceeding the simulation data is preferred but unfortunately, the modelling of deep drawing test is not completed in ABAQUS. For this reason, it is excluded in the current study. It is planned to use the data by Nakazima in a paper which will be prepared for numerical analysis of the deep drawing tests executed in the specified condition and the comparison of the experimental results and the data obtained by ABAQUS will be included in this paper.

6.1.2 Determination of temperature limits for experiments

The temperature is the main parameter which is searched in the current dissertation. The system for the measurement of temperature is described in early sections of this study.

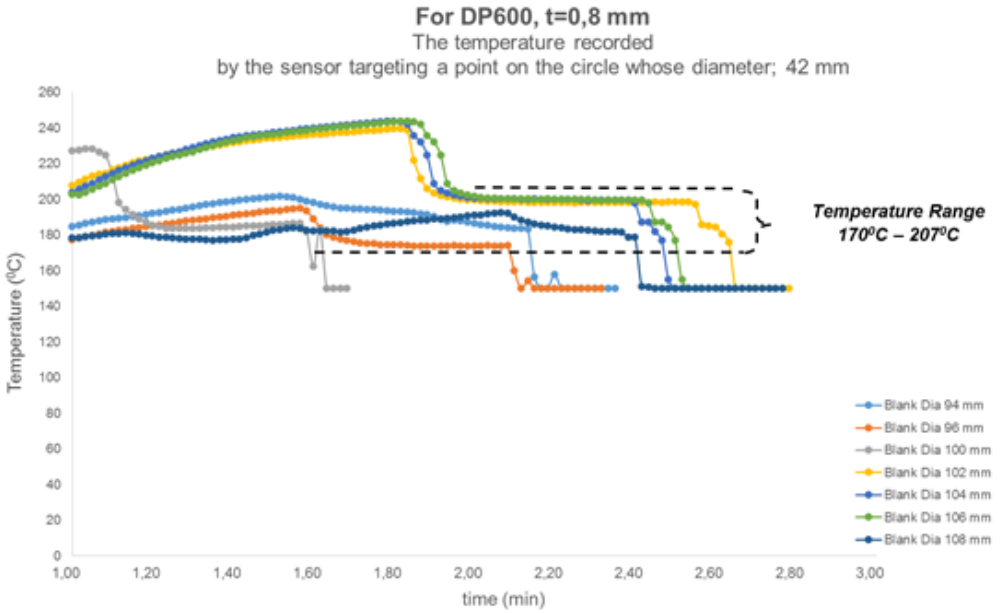

Figure 6.15 For DP600 (Dual Phase), t = 0,8 mm, the temperature recorded by the sensor targeting a point on the circle whose (blank) diameter; 42 mm.

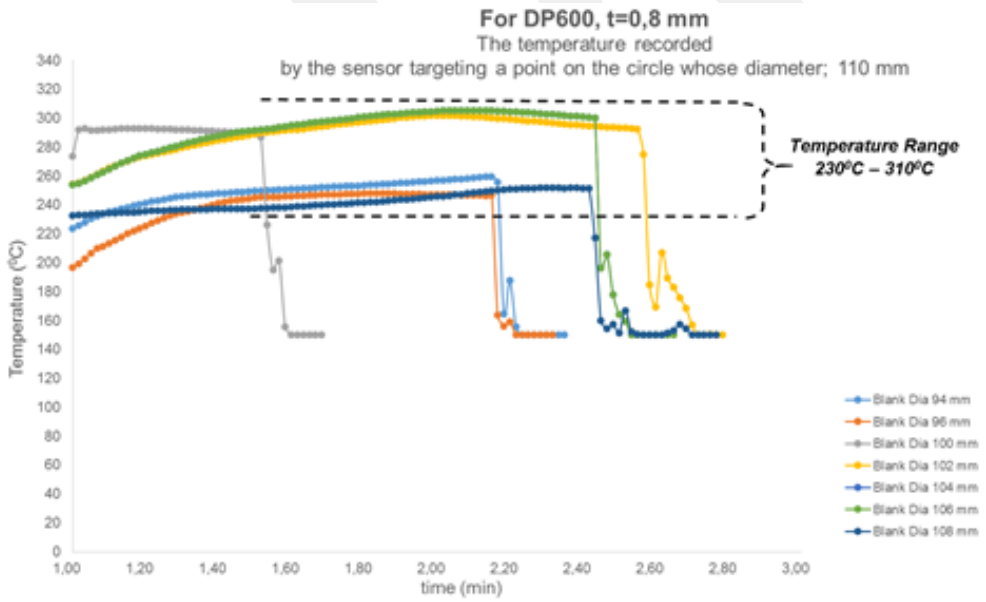

Figure 6.16 For DP600 (Dual Phase), t = 0,8 mm, the temperature recorded by the sensor targeting a point on the circle whose (blank) diameter; 110 mm.

The temperature versus time graphs represents the temperature of the blank placed between die and blank holder. As a result of heat application, the recorded temperatures by the sensor which targets a point on smaller circle of flange region of blank and by the sensor focusing a point on blank holder plate referencing the circle at radius 55 mm are shown in Figures 6.15 and 6.16, respectively. On these graphs, the

sharp decrease in measurements refers to the application cooling by dropping water through the hole in punch to constitute the required temperature gradient at the rim of blank. After graphing the applied temperatures of blanks at various diameters on a common graph, the required temperature ranges are evaluated at the start and at the end of flange area, respectively. The summary table for these resultant temperature ranges are presented in Table 6.5,

Table 6.5 The resultant temperature ranges obtained as a result of the application preheating to the rim of blank.

Material	Thickness	**Inclined** Temperature Sensor focused to a point at the distance ***21 mm*** to die axis ***desired Temperature Range***	**Vertical** Temperature Sensor focused to a point at the distance ***55 mm*** to die axis ***desired Temperature Range***
DP600	0,80	170 - 207	230 - 310
	1,20	165 - 195	245 - 295
	1,60	180 - 225	220 - 300
ERD 7128	1,20	170 - 200	245 - 290
	1,50	175 - 210	235 - 295
ERD 7128	1,20	170 - 190	250 - 295
	1,50	165 - 190	220 - 275
DC04 (IF Steel)	0,80	165 - 195	215 - 305
	1,20	170 - 195	250 - 290
	1,57	160 - 195	235 - 278

All temperature measurements taken during the experiments are given in Part B of Appendices. At the end of the deep drawing experiments it can be concluded that the highest development in LDR is obtained for the temperature ranges, 170-190ºC on a circle whose radius is 21 mm and 230ºC - 290ºC on a circle at the radius, 55 mm. This is totally an experimental result obtained by the deep drawing experiments. The trial and error method is applied the development of these temperature ranges.

6.1.3 The graphs obtained as a result of deep drawing tests

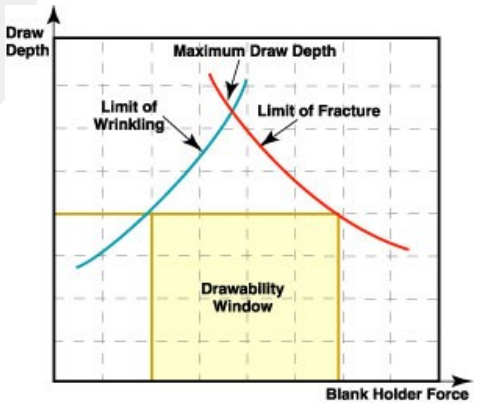

Figure 6.17 The intersection of the lines plotting the BHF and the draw depth of a cup reveal the maximum possible draw depth for a given cup.

In Figure 6.17, the maximum draw depth is defined by the point at the intersection of wrinkling and fracture limit curves, which refers to the optimum value for BHF maximizing the limiting drawing ratio. The optimum blank holder force (BHF) corresponding to a value between the curves of wrinkling and fracture is required to be evaluated. When the improvement of LDR is considered, the available value for BHF lies in a very narrow area as it can be seen in Figure 6.16; which means that the selection of the value for BHF becomes vitally critical issue for the improvement of Limiting Drawing Ratio (LDR).

On the other hand, as it was mentioned before BHF system used in this study was actuated by hydraulic power control unit which was not very sensitive to pressure changes and the fluctuations, ±2 bars, in the pressure readings were observed. The blank holding system used in experiments of this study required to be equipped with the rational power control unit which is highly sensitive to the changes in pressure.

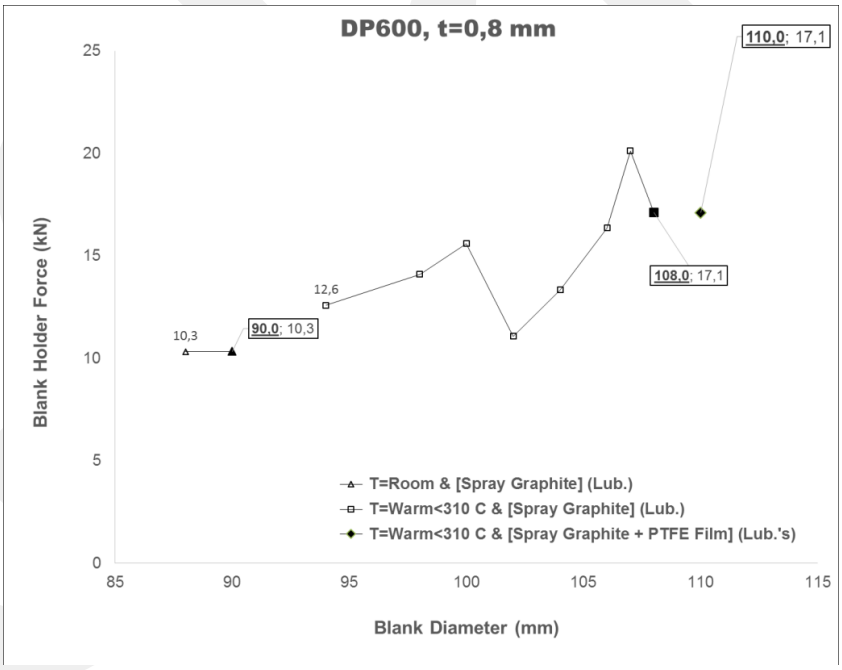

Figure 6.18 BHF vs blank diameter (mm) graph with the application of various temperatures and lubricants, for DP600 and t = 0,8 mm.

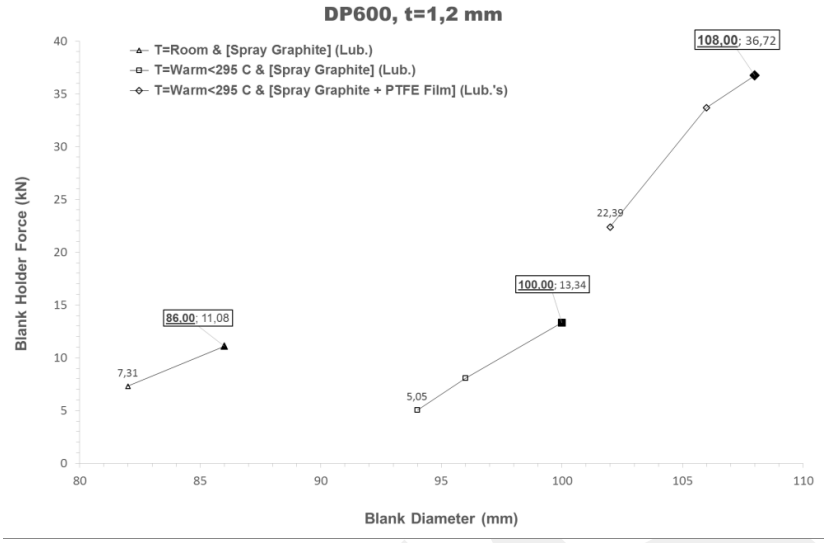

Figure 6.19 BHF vs blank diameter (mm) graph with the application of various temperatures and lubricants, for DP600 and t = 1,2 mm.

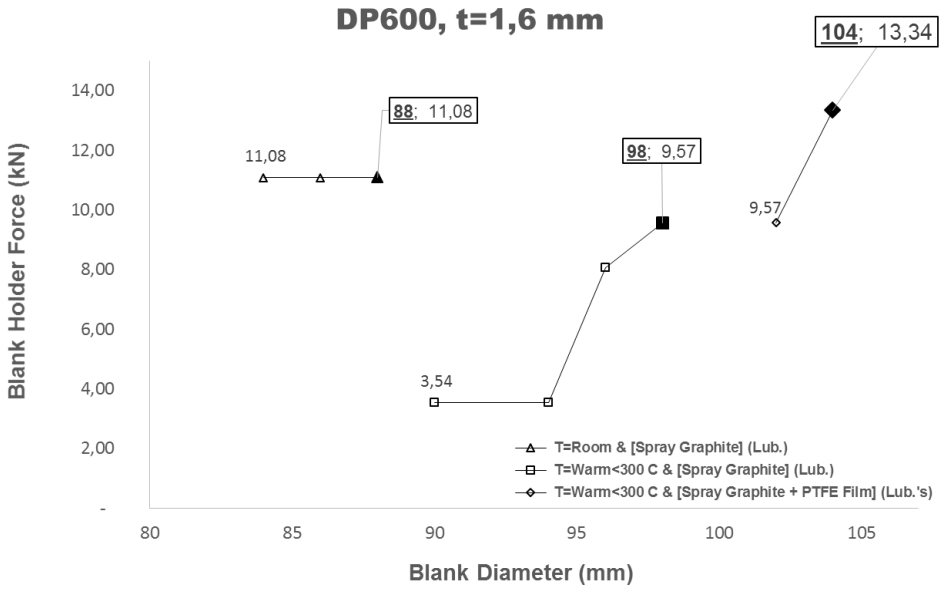

Figure 6.20 The resultant Blank Holder Force (BHF) vs blank diameter (mm) graph with the application of various temperatures and lubricants, for DP600 and t = 1,6 mm

The heating rim of the blank dropped BHF for DP600, t = 1,2 mm and t = 1,6 mm, whereas the slight variations were observed for DP600, t = 0,8 mm.

The similar rate of increase in BHF recorded when the lubricant was changed from spray graphite to the mixed type (Graphite + PTFE) for DP600 sheets having thicknesses, 1,2 and 1,6 mm.

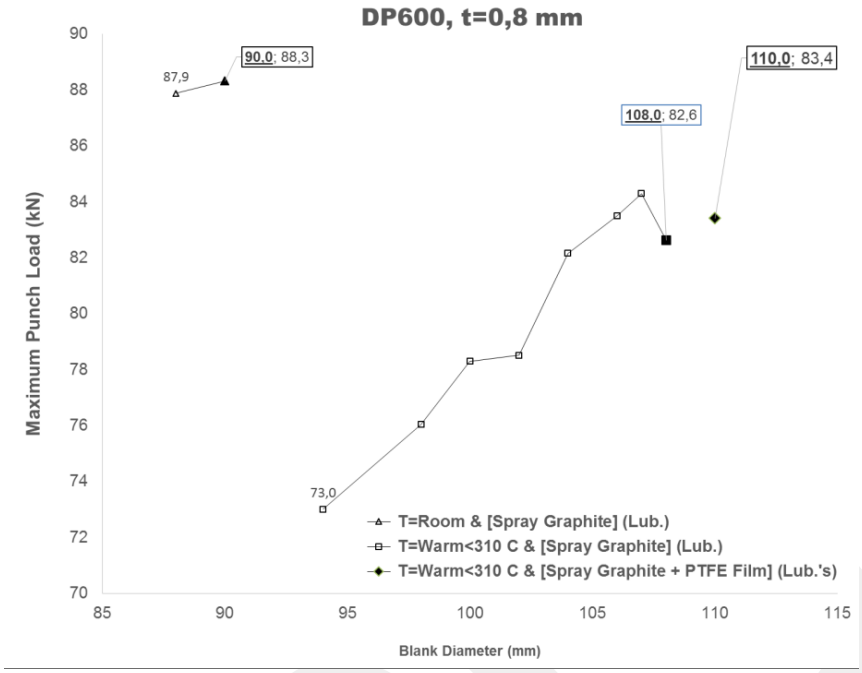

Figure 6.21 The resultant maximum punch load vs blank diameter (mm) graph with the application of various temperatures and lubricants, for DP600 and t = 0,8 mm.

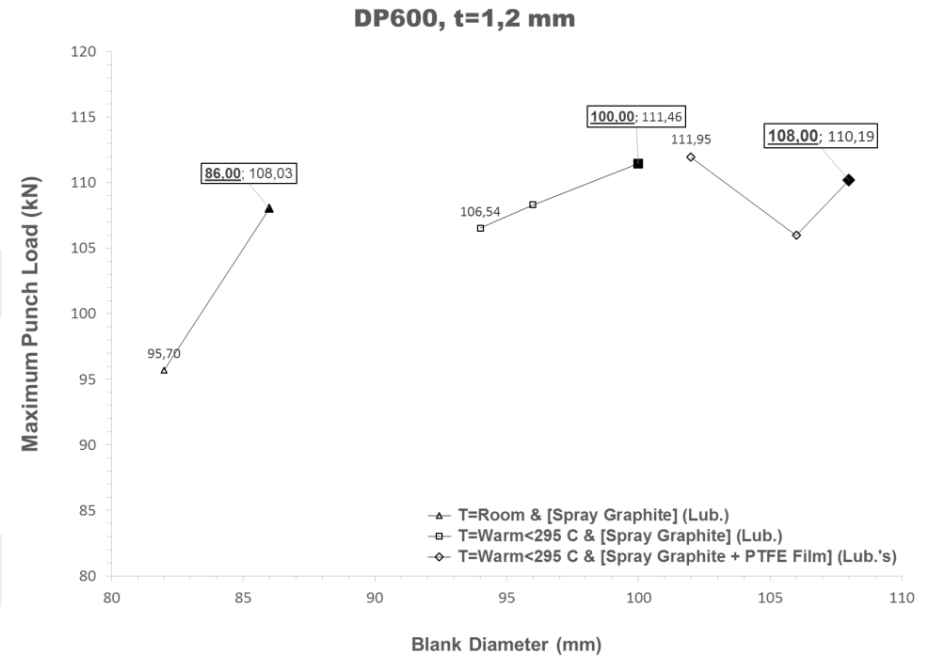

Figure 6.22 The resultant maximum punch load vs blank diameter (mm) graph with the application of various temperatures and lubricants, for DP600 and t = 1,2 mm.

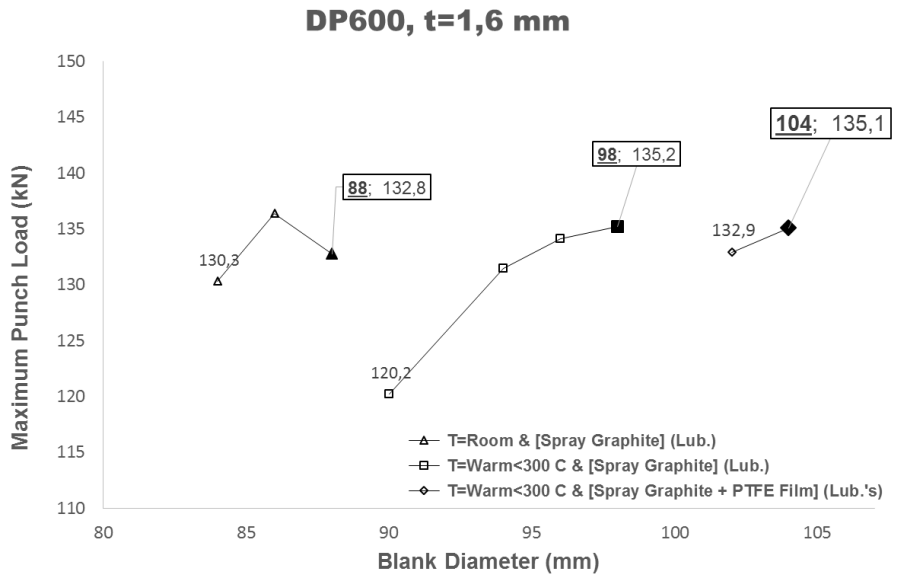

Figure 6.23 The resultant maximum punch load vs blank diameter (mm) graph with the application of various temperatures and lubricants, for DP600 and t = 1,6 mm.

Figures 6.23 shows the effect of temperature and lubricant used which means that the diameter of blanks in other words LDR is improved by the applying same amount of punch load.

By heating of flange area of blank, 26% increase in the diameter of blank is recorded for DP600, t = 1,2 mm which can be seen in Figure 6.22. In addition to this, the maximum load applied by punch is decreased from 88,3 kN at room condition to 83,4 kN at warm temperature by the use of mixed type of lubrications (Spray graphite + PTFE) as shown in Figure 6.21.

6.1.4 The spring back measurements and the concept of the residual stress

In deep drawing operation, an important parameter about the geometry of drawn part is the spring back value. Due to the plastic-elastic forming of a workpiece, there is a spring back at the end of a deep drawing process. The spring back has to be compensated to achieve an accurate result. In the case of complex tools the spring back has to be already considered in the construction phase. Therefore complex software simulations are used. Frequently this is not enough to deliver the desired results. In such cases practical experiments are done, using the trial-and-error plus experience method to correct the tool. However the results (work pieces) are only stable, if all influencing factors are the same.

The application method developed in this dissertation is investigated for the spring back affect. Due to the warm processing conditions in deep drawing operation it is expected to have positive effects on the spring back. The results are given below,

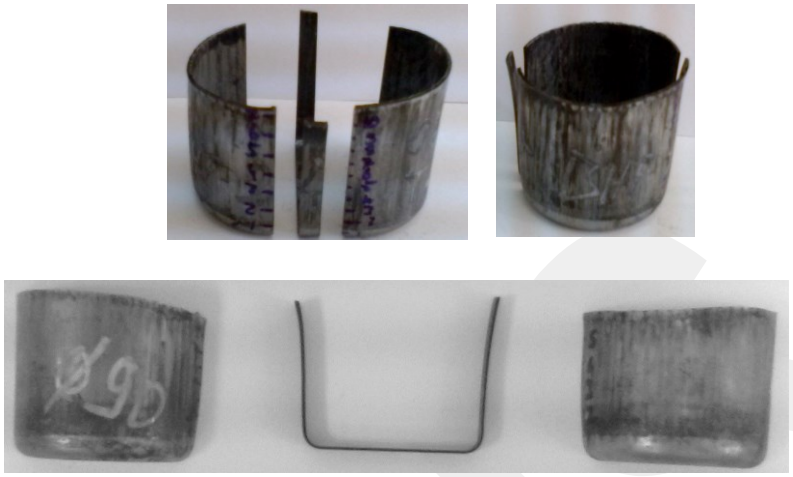

(a) (b) (c)

Figure 6.24 Parts of cup cut for spring back measurements; (a & c) the symmetric parts of cylindrical cup cut, (b) the part of cup stripped along its axis.

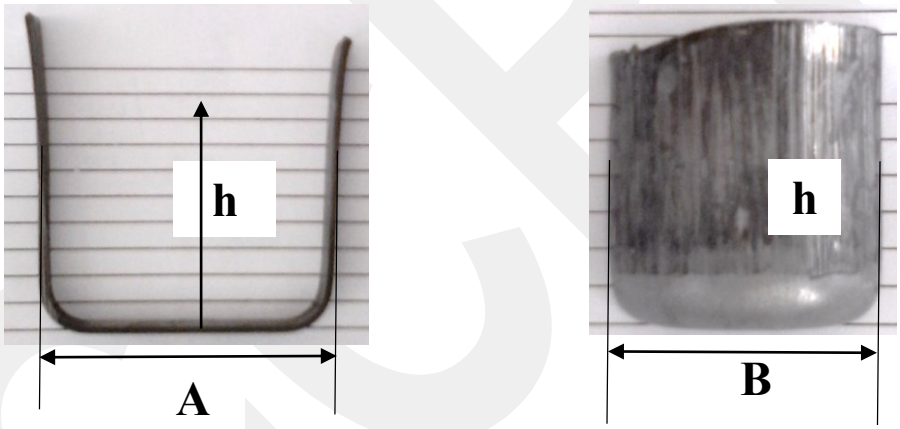

A : Distance between outter edges of the part of cup stripped along its axis
B : Distance between outter edges of the symmetric parts of cylindrical cup cut
h : Heigth from bottom of cup, (mm)

Figure 6.25 Representation of measurement parameters used to investigate the quantity of spring back for the deep drawn cup.

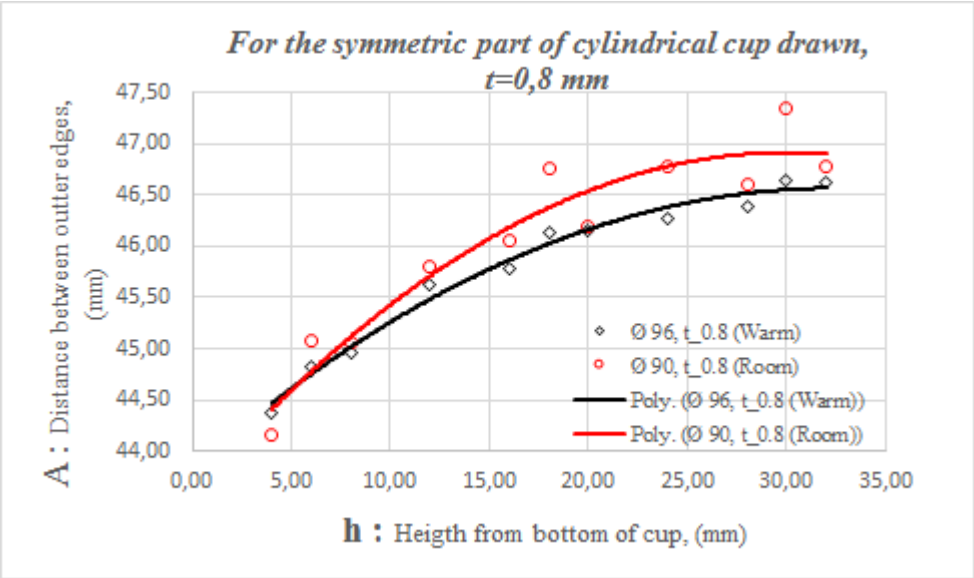

Figure 6.26 Spring back measurements for the symmetric part of cylindrical cup drawn, t = 0,8 mm.

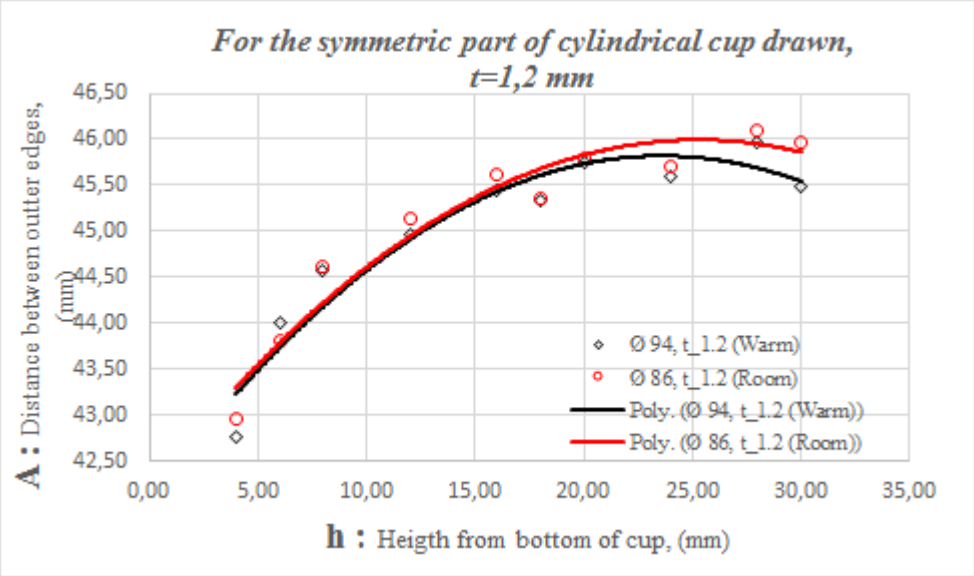

Figure 6.27 Spring back measurements for the symmetric part of cylindrical cup drawn, t = 1,2 mm.

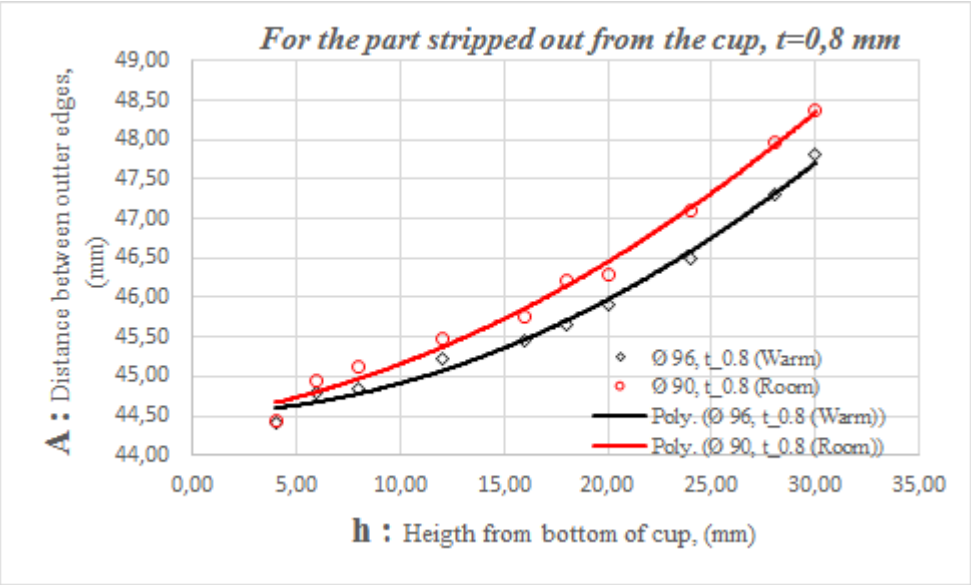

Figure 6.28 Spring back measurements for the part stripped out from the cup, t = 0,8 mm.

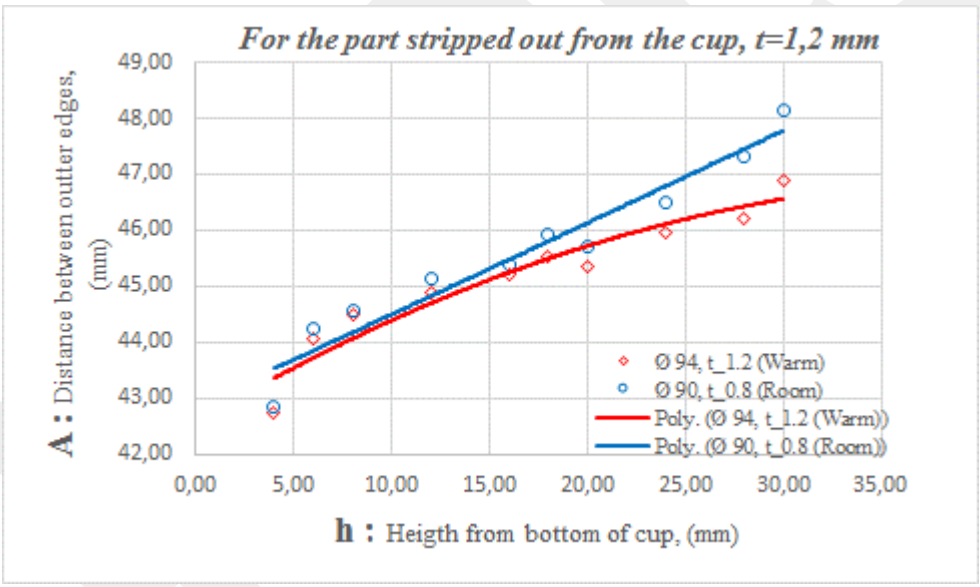

Figure 6.29 Spring back measurements for the part stripped out from the cup, t = 0,8 mm.

Considering the results obtained at room condition and at elevated temperatures, it can be concluded that the spring back magnitude is reduced by the application method developed in this study. The magnitude of spring back value is the indicator of the residual stresses developed as a result of forming operation; due to this, it can easily be realized that with the reduction of the spring back, the residual stresses formed in the material is also reduced.

6.2 DISCUSSION ABOUT THE RESULT OF EXPERIMENTS

The results of the deep drawing tests are shown in Table 6.4 for DP600, HSLA and IF steels. Limiting Drawing Ratios (LDR) are shown for all thicknesses, temperatures and lubricating conditions. Graphite lubrication is used at room temperature. For the warm region, where the temperature of the flange during deep drawing changes between 275 – 180ºC, graphite lubrication is also used. However, a second lubrication consisting of graphite and PTFE is also applied. As seen in the results, graphite + PTFE lubrication is more effective in increasing the LDR. This partly is due to the fact that PTFE sheet provides a layer of insulation for the elevated temperature in warm forming so that lower yield stress becomes decisive, thereby reducing the resistance of the flange region. Similar trends are also seen in the HSLA and IF steels. Highest increase in LDR is seen as 25,58 % in DP600.

Table 6.6 LDR in cold and warm deep drawing for DP600, HSLA and IF steels.

MATERIAL		**AHSS (DP600)**		**HSLA (Erd 7128)**		**HSLA (Erd 7140)**		**IF Steel (DC04)**	
Lubricant	Temp.	D_b	LDR	D_b	LDR	D_b	LDR	D_b	LDR
		t_0=0,8 D_p=43,00		t_0=1,2 D_p=43,00		t_0=1,2 D_p=43,00		t_0=0,8	D_p=43,00
Graphite	Room	90	2,09	90	2,14	90	2,14	102	2,37
Graphite	Warm	107	2,49	102	2,42	96	2,28	112	2,60
Graphite + PTFE	Warm	110	2,56	110	2,61	104	2,47	114	2,65
Graphite + PTFE	Warm Fail	112	2,60	112	2,66	106	2,52	116	2,70
Percent Increase		22,22%		22,22%		15,56%		11,76%	
		t_0=1,2 D_p=42,10		t_0=1,5 D_p=40,89		t_0=1,5 D_p=40,89		t_0=1,2	D_p=42,10
Graphite	Room	86	2,04	88	2,15	88	2,15	97	2,30
Graphite	Warm	100	2,38	94	2,30	92	2,25	108	2,57
Graphite + PTFE	Warm	108	2,57	106	2,59	106	2,59	116	2,76
Graphite + PTFE	Warm Fail	110	2,61	108	2,64	108	2,64		
Percent Increase		25,58%		20,45%		20,45%		19,59%	
		t_0=1,6 D_p=40,89		All dimensions are in millimeters				t_0=1,57	D_p=40,89
Graphite	Room	88	2,09					95	2,32
Graphite	Warm	98	2,33					97	2,37
Graphite + PTFE	Warm	104	2,47					116	2,84
Graphite + PTFE	Warm Fail	106	2,52						
Percent Increase		18,18%						22,11%	

AHSS steel with 1,2 mm thickness. Generally, better increases in LDR are obtained in DP600 steel compared to HSLA and IF steels.

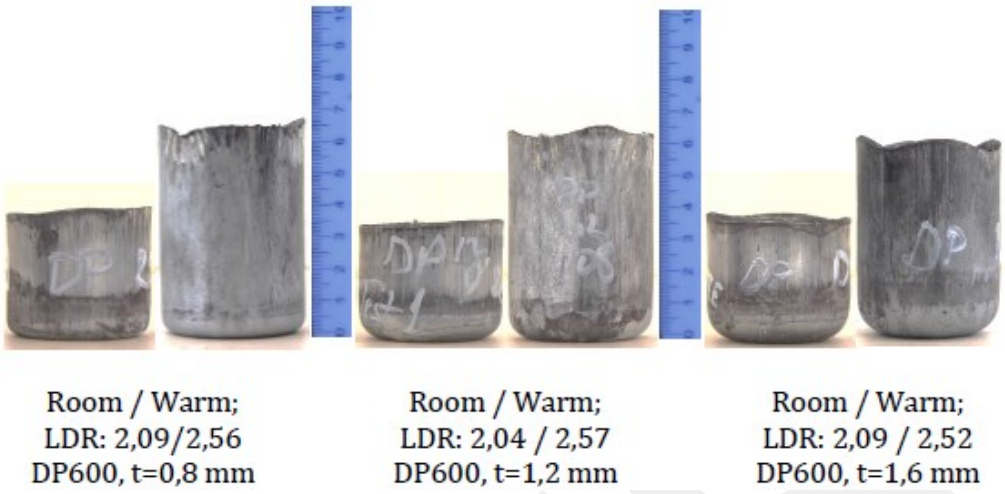

Figure 6.30 Heights of deep drawn cups at room and warm temperatures.

Figure 6.30 shows the heights of deep drawn cups at room temperature and nonisothermal warm condition for DP600 steel in three thicknesses. It is seen that significant increases in cup heights are obtained. For industrial applications, this means a reduction in the number of stages in deep drawing.

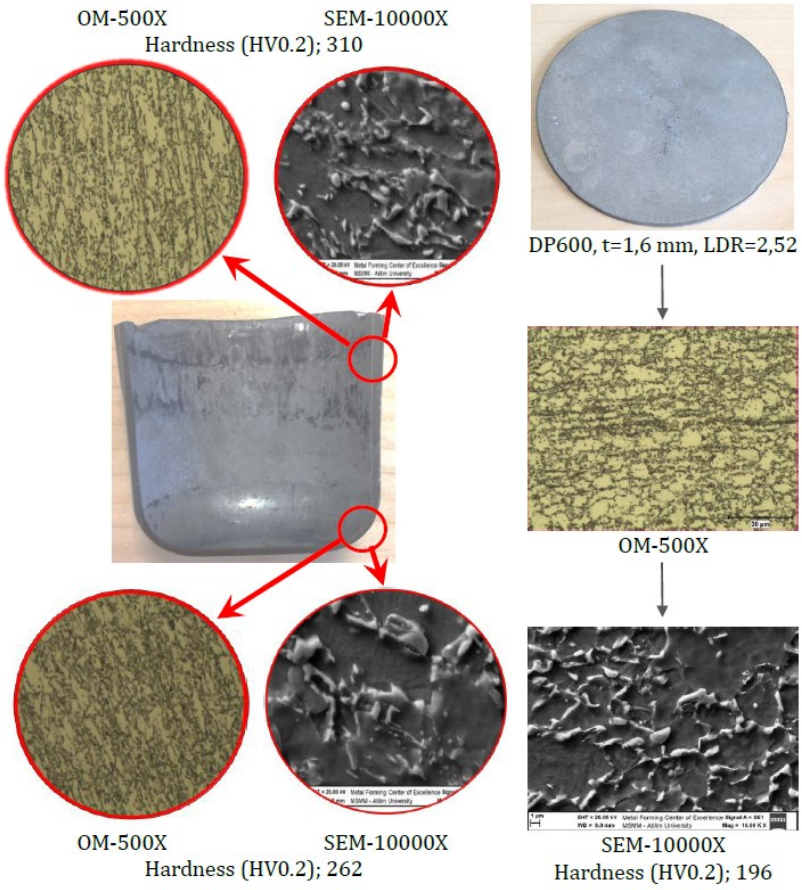

Figure 6.31 Microstructure of a cup in cold and warm conditions.

Figure 6.31 shows microstructure of DP600 with 1,6 mm thickness. Two locations are investigated. Corner of the cup, a transition point between cold and warm region, and a point initially in the flange of the blank which is totally in the warm region. Micrographs are taken by an optical microscope (OM) with 500 magnification and also by a scanning electron microscope (SEM) with 10000 magnification. When the microstructure in these two points are compared to the microstructure of the original material, it is seen that no significant change has taken place. In the original material, there is % 26 martensite and % 74 ferrite. After deformation, these ratios are affected by ±%2,3 which is within experimental error. Small changes are also due to plastic deformation and not due to temperature effect on microstructure. Microhardness measurements in Vickers show that, compared to the virgin material, hardness values have increased around the punch radius and more in the flange region showing work hardening. Table 6.5 gives the thickness distribution in the cup, showing that there is a thickening in the flange region and a thinning in the rest of the cup. However, in nonisothermal warm deep drawing, there is more thickening at the rim of the blank due to high LDR, whereas, thinning level is nearly the same for cold and warm deep drawing over the punch profile.

Table 6.7 Thickness distribution in a DP600 deep drawn cup.

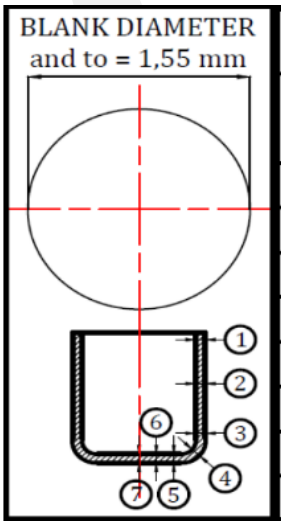

D_b	88,0	98,0	104,0
Condition Lubricant	Room Graphite	Warm Graphite	Warm Graphite+PTFE
LDR	2,09	2,33	2,47
1	2,03	2,11	1,87
2	1,66	1,54	1,53
3	1,54	1,52	1,49
4	1,26	1,30	1,34
5	1,37	1,34	1,44
6	1,40	1,45	1,37
7	1,43	1,42	1,43

CHAPTER 7

CONCLUSIONS
AND
SUGGESTIONS FOR FUTURE WORK

7.1 CONCLUSIONS

Nonisothermal deep drawing is applied to DP600, HSLA and IF steels in the warm range. The flange part is heated to 275ºC - 180ºC in the warm range by induction heating whereas the central part contacting the punch is cooled by water. To find the material properties in the warm range, tensile tests are conducted by the Bahr forming dilatometer for the temperate range (150ºC - 300ºC). Increases up to 25,58 % on LDR are obtained. There is no significant change in the microstructure of the material due to warm forming. It is therefore concluded that the process developed can increase the LDR in deep drawing without decreasing the strength of the dual phase steel and changing its microstructure.

Considering the results obtained at room condition and at elevated temperatures, it can be concluded that the spring back magnitude is reduced by the application method developed in this study. The magnitude of spring back value is the indicator of the residual stresses developed as a result of forming operation; due to this, it can easily be realized that with the reduction of the spring back, the residual stresses formed in the material is also reduced.

7.2 SUGGESTIONS FOR FUTURE WORK

This chapter is also devoted to give the information about the further developments which can be considered for the improvement of LDR in the warm sheet metal forming. The discussions on the future work categorized mainly in two sections, the

setup enhancements, possible researches, in addition to this, during the experiments, it is noticed that the small circular cavities placed under the blank improved the limiting drawing ratio roughly by 4%. In other words, those cavities act like draw bead used in sheet metal forming industry. But this perceived development in deep drawing are not searched in detail in this current dissertation. It is thought to propose this subject as a future work.

7.3 THE SETUP ENHANCEMENTS

The enhancements which can be thought are given below,

1) The hydraulic power control unit can be enhanced with Hydraulic Rational Power Control unit to improve the controlling of blank holder mechanism actuated by hydraulic power unit.
2) The blank holder set can be improved into one of the new models given in section 7.3.2.
3) The location of temperature sensors can be changed into the places where the temperature of blank can be recorded during the deep drawing operation.
4) The out most important improvement in setup is the change of mechanical to servo press having suitable dimensions.
5) The inductance heater can be improved by changing its input frequency range.
6) A more precise cooling system can be improved.
7) A new mixed lubrication system can be thought to be used in experiments.
8) The coating can be applied to reduce the friction coefficient between the contact surfaces in deep draw operation.
9) Some improvements on the punch and die geometry

7.4 FURTHER POSSIBLE RESEARCHES

The further possible research subject on process variables given in section 7.3.1 and the new proposed models in section 7.3.2

7.4.1 About the process parameters

The process parameters thought to be surveyed is given as

- Application of various strain rates during the process
- Temperature distribution by controlling heating and cooling rate
- The effects of punch and die geometry for tests at elevated temperature

- Various blank holder force application considering the required compressive stress to regulate the flow of blank in flange region.

7.4.2 The new models proposed

The most crucial region in deep drawing is placed somewhere near the formed cup radius on the wall of cup. It is required to cool the part of blank drawn just immediately after it is drawn to change the flow stress characteristic from warm to room which refers to forming of more strengthen material in characteristic. If one can think in incremental point of view, more strengthen part of blank is locally produced, it means that this cooled part of blank can withstand the stresses which will be formed in further increments of drawing, so this procedure prevents tearing of blank around cup corner. Actually the similar method is applied by scientists and it is reported that in their experimental studies they get succeeded to improve LDR, 3,2 for Ti alloys.

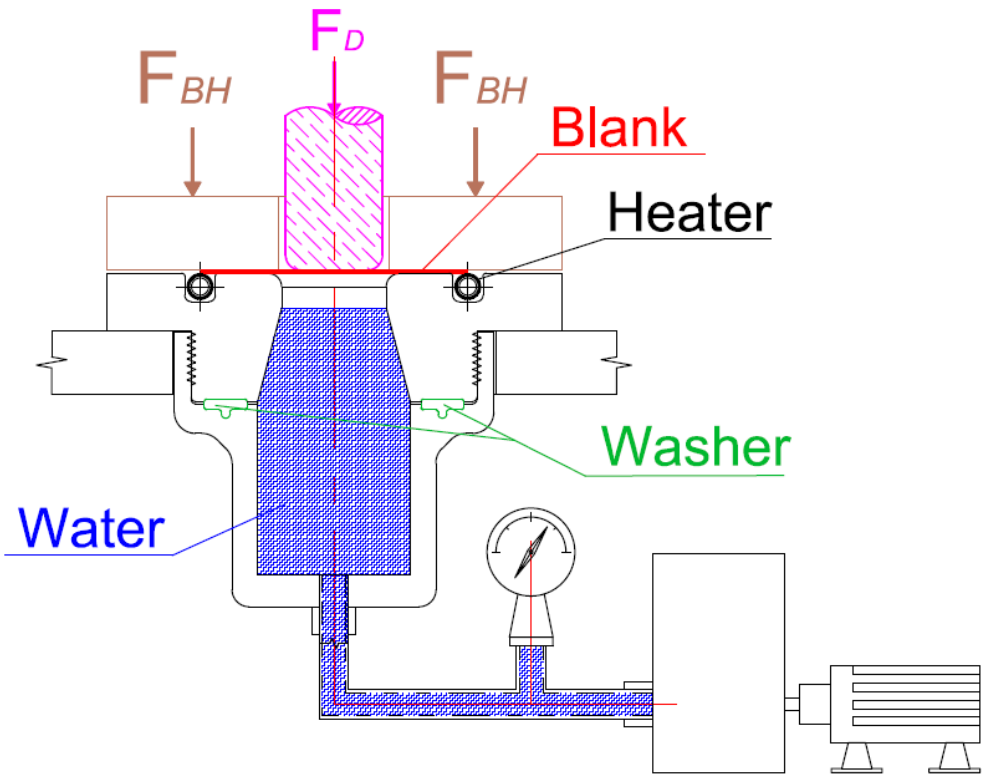

Figure 7.1 Schematic representation of setup for the closed cooling deep drawing.

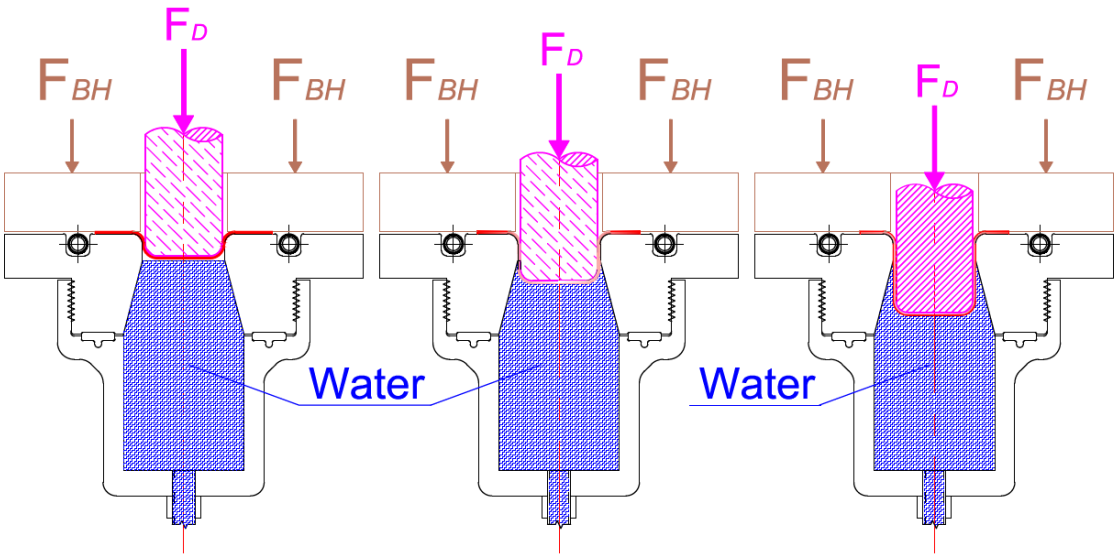

Figure 7.2 Schematic representation of the closed cooling deep drawing.

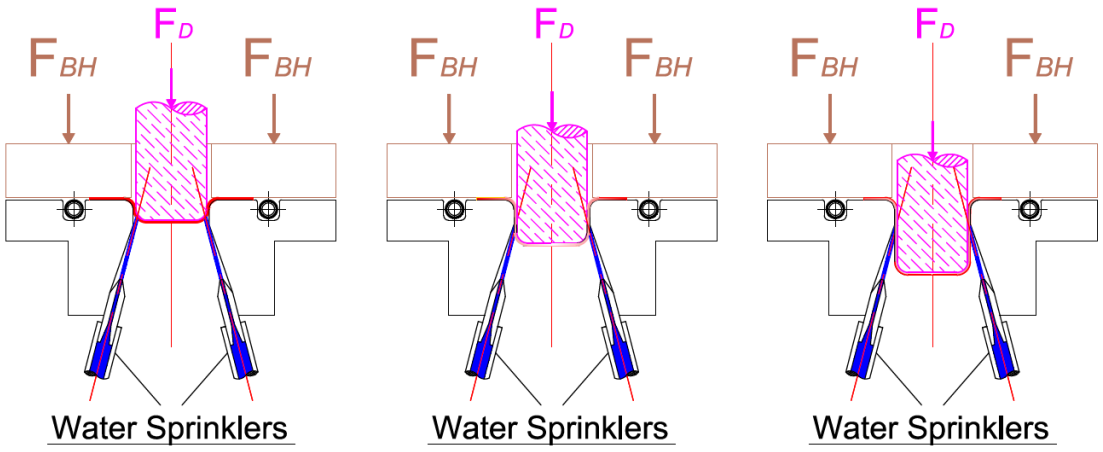

Figure 7.3 Schematic representation of the open cooling deep drawing.

The possible improved methods for blank holder force are schematically given for the experiments at warm temperature.

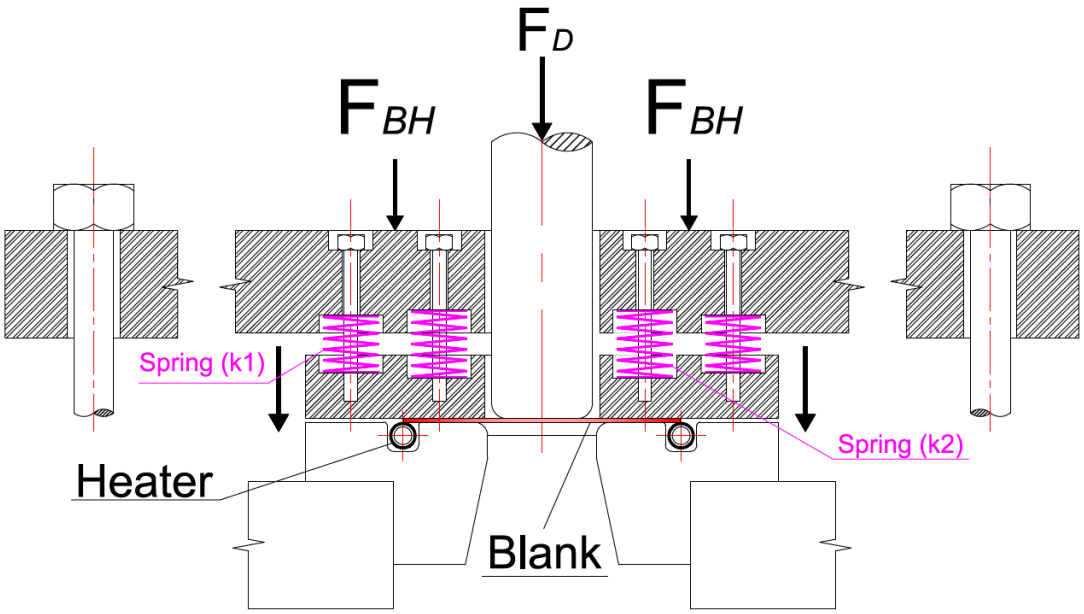

Figure 7.4 Setup for variable blank holder force at warm temperature, spring used system.

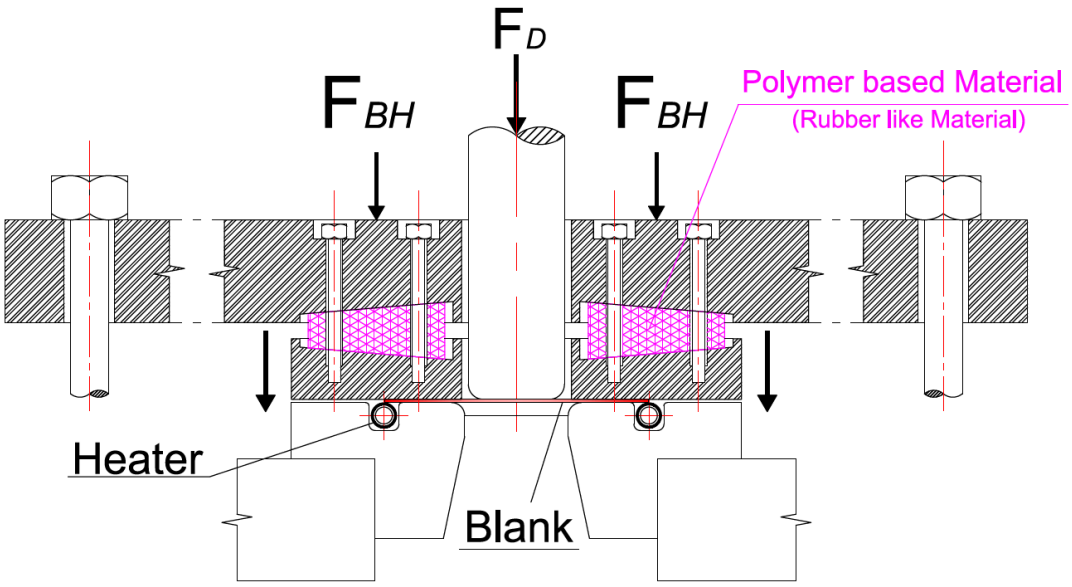

Figure 7.5 Setup for variable blank holder force at warm temperature, Polymer used system.

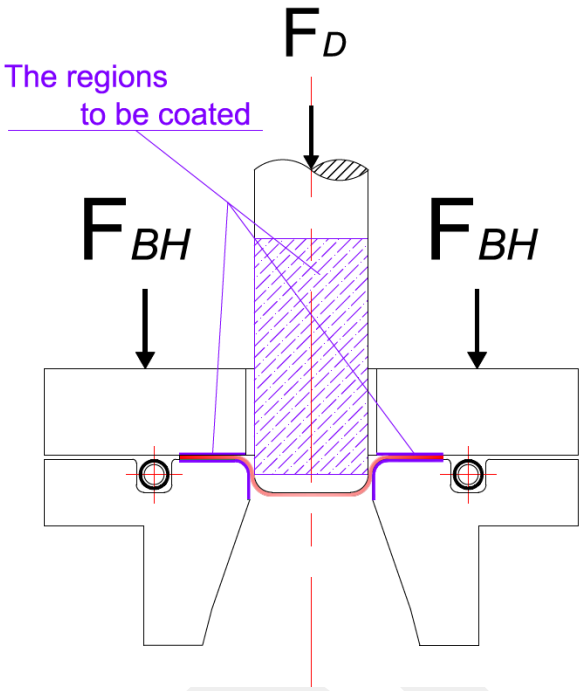

Figure 7.6 The areas required to be coated.

GCRIS

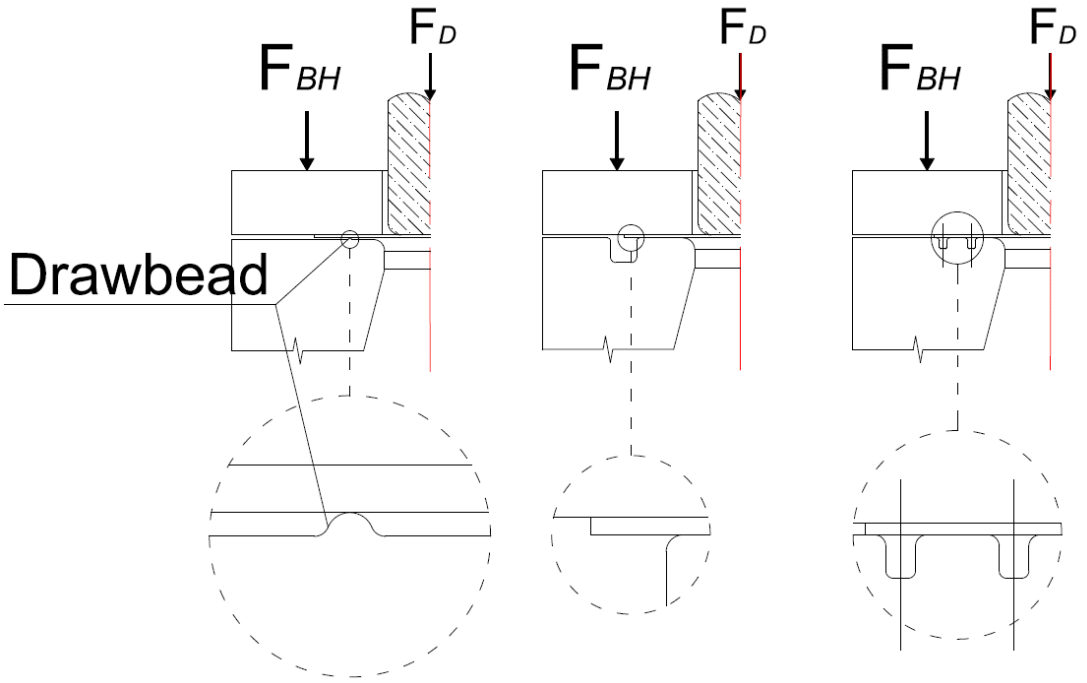

Figure 7.7 Representation of draw cavities acting like draw beads.

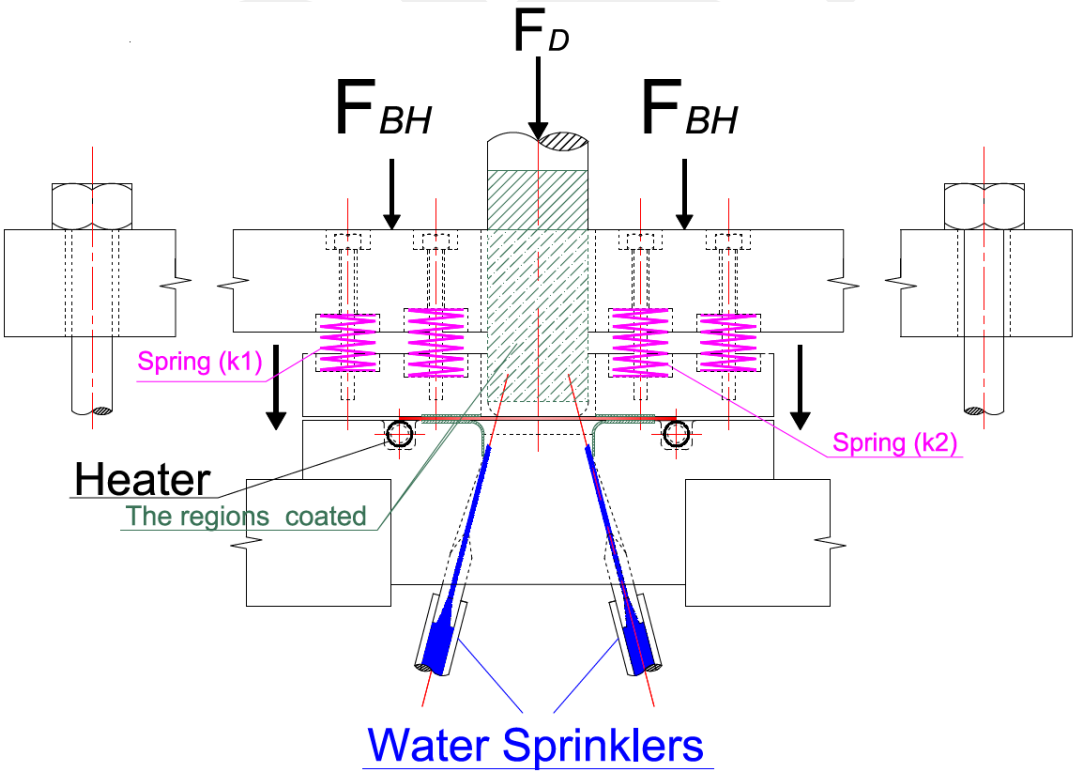

Figure 7.8 New setup combining all required suggestions.

REFERENCES

[1] WorldAutoSteel. (Version 5.0, May 2014) http://www.autosteel.org

[2] WorldAutoSteel. (2011) FutureSteelVehicle – Final engineering report. Retrieved from http://www.autosteel.org/Programs/Future%20Steel%20Vehicle.aspx.

[3] C. Potter, American Iron and Steel Institute, Southfield, MI ref to Global Comparison of Passenger Car and Light Commercial Vehicle Fuel Economy/GHG Emissions Standards; February 2014 Update, International Council for Clean Transportation (ICCT), www.theicct.org

[4] Abraham, A. Ducker Worldwide. (2011, May). Future Growth of AHSS, [PowerPoint presentation at Great Designs in Steel Seminar - 2011]

[5] Geyer, R. (2008, Sept 15). "Parametric Assessment of Climate Change Impacts of Automotive Material Substitution." Environmental Science & Technology, 42 (18), 6973-6979.

[6] By HENRY FOUNTAIN, Material World, Many Faces, and Phases, of Steel in Cars Published: September 14, 2009

[7] Master thesis: High Strain Rate Characterization of Advanced High Strength Steels by Alan C. Thompson A thesis presented to the University of Waterloo, Ontario, Canada, 2006

[8] Courtesy of D. Eriksson, SSAB Tunnplat AB.

[9] Courtesy of C. Walch, voestalpine Stahl GmbH.

[10] R. Neugebauer, T. Altan, M. Geiger, M. Kleiner, A. Sterzing, 2006 “Sheet metal forming at elevated temperatures”, CIRP Annals - Manufacturing Technology, Volume 55, Issue 2, 2006, Pages 793-816

[11] M. Kleiner, M. Geiger, A. Klaus, 2003 “Manufacturing of Lightweight Components by Metal Forming”, CIRP Annals - Manufacturing Technology, Volume 52, Issue 2, 2003, Pages 521-542

[12] K. Mori, S. Maki, Y. Tanaka, 2005, “Warm and Hot Stamping of Ultra High Tensile Strength Steel Sheets Using Resistance Heating”, CIRP Annals - Manufacturing Technology, Volume 54, Issue 1, 2005, Pages 209-212

[13] S. Bruschi, T. Altan, D. Banabic, P.F. Bariani, A. Brosius, J. Cao, A. Ghiotti, M. Khraisheh, M. Merklein, A.E. Tekkaya, 2014, “Testing and modelling of material behaviour and formability in sheet metal forming”; CIRP Annals - Manufacturing Technology Volume 63, Issue 2, 2014, Pages 727–749

[14] Serhat Kaya, Giovanni Spampinato, Taylan Altan, 2008, “An Experimental Study on Nonisothermal Deep Drawing Process Using Aluminum and Magnesium Alloys”, Journal of Manufacturing Science and Engineering DECEMBER 2008, Vol. 130 / 061001-1, Copyright © 2008 by ASME

[15] Shoichiro Yoshihara, Hisashi Nishimura, Hirokuni Yamamoto, Ken-ichi Manabe, (2003), “Formability enhancement in magnesium alloy stamping using a local heating and cooling technique: circular cup deep drawing process”, Journal of Materials Processing Technology 142 609–613

[16] A.W. Hudgins, D.K. Matlock, J.G. Speer, C.J. Van Tyne, 2010, "Predicting instability at die radii in advanced high strength steels", Journal of Materials Processing Technology Volume 210, Issue 5, 19 March 2010, Pages 741–750

[17] S. Rajagopal, 1981, "A Deep Drawing Test for Determining the Punch Coefficient of Friction", Journal of Engineering for Industry MAY 1981, VOL 103 / 197 Copyright © 1981 by ASME

[18] M. H. Pope, J. T. Berry, 1973, "The Prediction of Press Loads in Deep Drawing With Various Conditions of Lubrication at Elevated Temperatures", Journal of Engineering for Industry August 1973 / 895, Copyright © 1973 by ASME

[19] Shrinidhi Chandrasekharan, Hariharasudhan Palaniswamy, Nitin Jain, Gracious Ngaile, Taylan Altan, 2005, "Evaluation of stamping lubricants at various temperature levels using the ironing test" by International Journal of Machine Tools & Manufacture 45 (2005) 379–388

[20] Wenfeng Zhang, Rajiv Shivpuri, 2008, "Investigating Reliability of Variable Blank Holder Force Control in Sheet Drawing Under Process Uncertainties", Journal of Manufacturing Science and Engineering August 2008, Vol. 130 / 041001-1 Copyright © 2008 by ASME

[21] S. Thiruvarudchelvan, W. G. Lewis, 1990, "Deep Drawing With Blank Holder Force Approximately Proportional to the Punch Force", 278/Vol. 112, August 1990 Transactions of the ASME, Copyright © 1990 by ASME

[22] Y. Abe, T. Ohmi, K. Mori, T. Masuda, 2014 "Improvement of formability in deep drawing of ultra-high strength steel sheets by coating of die", Journal of Materials Processing Technology Volume 214, Issue 9, September 2014, Pages 1838–1843

[23] Li Sun, R.H. Wagoner, 2013, “Proportional and non-proportional hardening behavior of dual-phase steels”, International Journal of Plasticity, Volume 45, June 2013, Pages 174-187,

[24] J.C. Gelin, A. Moisan, 1986 “Application of a Thermo-Viscoplastic Model to the Analysis of Defects in Warm Forming Conditions”, CIRP Annals - Manufacturing Technology, Volume 35, Issue 1, 1986, Pages 157-160

[25] Haidong Yu, Yongjin Guo, Xinmin Lai; 2008 “Rate-dependent behaviour and constitutive model of DP600 steel at strain rate from 10^{-4} to 103 s^{-1}”, Materials and Design Crown Copyright 2008 Published by Elsevier Ltd.

[26] S. Curtze, V.-T. Kuokkala, M. Hokka, P. Peura, 2009, “Deformation behavior of TRIP and DP steels in tension at different temperatures over a wide range of strain rates”, Materials Science and Engineering: A Volume 507, Issues 1–2, 15 May 2009, Pages 124–131

[27] Jeehyang Huh, Hoon Huh, Chang Soo Lee, 2013 “Effect of strain rate on plastic anisotropy of advanced high strength steel sheets”, International Journal of Plasticity Volume 44, May 2013, Pages 23–46

[28] T. Sirinakorn, S. Wongwises, V. Uthaisangsuk, 2008 “A study of local deformation and damage of dual phase steel”, Materials & Design, Volume 64, December 2014, Pages 729-742 Journal of Manufacturing Science and Engineering December 2008, Vol. 130 / 061001-1, Copyright © 2008 by ASME

[29] F Ozturk, A Polat, S Toros, R C Picu; “Strain Hardening and Strain Rate Sensitivity Behaviors of Advanced High Strength Steels, Journal of Iron and Steel Research”, International, Volume 20, Issue 6, June 2013, Pages 68-74 F Ozturk, A Polat, S Toros, R C Picu

[30] M. Ghosh, A. Miroux, R.J. Werkhoven, P.J. Bolt, L.A.I. Kestens; 2014 "Warm deep-drawing and post drawing analysis of two Al–Mg–Si alloys", Journal of Materials Processing Technology, Volume 214, Issue 4, April 2014, Pages 756–766

[31] A.K. Gupta, Swadesh Kumar Singh, Lade Jayahari, P.V. Sasidhar, P. Prudvi Reddy, B. BaluNaik, 2014, "Formability studies of ASS 304 and evaluation of friction for Al in deep drawing setup at elevated temperatures using LS-DYNA", Journal of King Saud University - Engineering Sciences, Volume 26, Issue 1, January 2014, Pages 21–31

[32] A. Alaie, J. Kadkhodapour, S. Ziaei Rad, M. Asadi Asadabad, S. Schmauder, 2015, "Formation and coalescence of strain localized regions in ferrite phase of DP600 steels under uniaxial tensile deformation", Materials Science and Engineering: A Volume 623, 19 January 2015, Pages 133–144

[33] Hong Seok Kim, Muammer Koc¸ Jun Ni; 2008, "Development of an analytical model for warm deep drawing of aluminum alloys", journal of materials processing technology 197 (2008) 393–407

[34] R.A. Lingbeek, T. Meinders and S. Ohnimus, 2005 "Compensation of deep drawing tools for springback and tool deformation, unregistered copy. The Netherlands Institute for Metals Research, Mekelweg 2, P.O. Box 5008, 2600GA Delft, Netherlands e-mail: roald.lingbeek@inpro.de, web page: http://www.nimr.nl; INPRO GmbH Hallerstrasse 1, D-10587, Berlin, Germany e-mail: stephan.ohnimus@inpro.de, web page: http://www.inpro.de; University of Twente Faculty of Engineering Technology P.O. Box 217, 7500AE Enschede, Netherlands e-mail: V.T.Meinders@ctw.utwente.nl, Web page: http://www.ctw.utwente.nl

[35] Springer Handbook of Mechanical Engineering, 2008, Manufacturing Engineering,7.2 Metal Forming Fig. 7.107 Page, 595

[36] Handbook of Metallurgical Process Design, editor: George E. Totten, Kiyoshi Funatani,Lin Xie, page 17, CRC Press; 1 edition (May 25 2004)

[37] W. Johnson, T.X. Yu, An outline of engineering dynamics elasticity and plasticity, Plasticity and Modern Metal Forming Technology; 1989, page 113-117, editor : T.Z.BLAZYNSKI

[38] Van Vliet, Krystyn J. (2006); "Mechanical Behavior of Materials"

[39] Finite-element plasticity and metal forming analysis, by G.W. ROWE, C.E.N. STURGESS, P. HARTLEY and I. PILLINGER; CAMBRIDGE UNIVERSITY PRESS, july 7, 2005.

[40] Lange K., 1985, "Deep Drawing", Handbook of Metal Forming, Editors K. Lange, et al., McGraw-Hill, NY

[41] R. Sowerby, J. L. Duncan and E. Chu, The modeling of sheet metal stamping, Journal of Mechanical Sciences, 28 (7) (1986), 415-430.

[42] Ahmetoglu, M.A., 1990, Kinzel, G.L., and Altan, T., "Sheet Metal Forming Process; State of the Technology and Analysis", Report No. ERC/NSM-590- 46, The Ohio State University, Columbus, OHIO.

[43] http://www.noguchi-ss.com, Address 202 Higashiwaki, Nishimiyuki, Toyohashi, Aichi 441-8113 JAPAN Tel +81-532-45-1151, by the date 06.01.2015

[44] Schuler Metal Forming Handbook, 1998 Metal Forming Handbook /Schuler (c) Springer-Verlag Berlin Heidelberg 1998, page 157

[45] Hosford et al., 1962 Hosford, W., 1962, Backofen, W., and Burke, J., "Texture Hardening", Transactions of ASM, no. 55, pp. 264-267.

[46] Banabic D., Bunge H.-J., Pöhlandt K. & Tekkaya A.E., 2000, Formability of Metallic Materials, Springer, page 190

[47] Kobayashi, S., OH, S.I:, Altan, T., “Metal forming and the finite element method”, New York Oxford, Oxford University Press, 1989, 73-88

[48] Deep Drawing of Round Cups Using Variable Blank Holder Pressure, By: Arjan L. P. Coremans, Visiting Student Eindhoven University of Technology, The Netherlands, NSF Engineering Research Center for Net Shape Manufacturing The Ohio State University 1971 Neil Avenue Columbus, Ohio 43210 June 1992

[49] Zünkler, X., 1973, "Workhardening Influence on Drawing Force and Limit. Drawing Ratio During Deep Drawing" (in German), Blech Rohre Profile, no. 20, 1973, pp. 343-346.

[50] http://www.ntnu.edu/simlab/testing/bup, Ref date; 22.02.2015

[51] http://thermophysical.tainstruments.com/instruments/dilatometers/dil-805ad-quenching-and-deformation-dilatometer/, Ref Date, 15.01.2015

[52] Metal Forming Center of Excellence, Atılım University – Ankara, 2015

[53] www.celesco.com/_datasheets/clwg.pdf ; Ref date, 26.02.2015.

[54] http://www.tml.jp/e/product/transducers/civil_eng/loadcell/ ; Ref date, 27.02.2015

[55] www.optris.com/optris-ct-xl-3m/ ; Ref date, 28.02.2015

APPENDICES

A. MATERIAL DATA

A.1 Chemical Composition of the materials studied

A.2 Flow Curves at Room Temp

A.2.1 DP600 (Dual Phase)

A.2.2 Erdemir 7128 (HSLA)

A.2.3 Erdemir 7140 (HSLA)

A.2.4 Erdemir DC04 (IF Steel)

A.3 Flow Curves at 200^{o}C

A.3.1 DP600 (Dual Phase)

A.3.2 Erdemir 7128 (HSLA)

A.3.3 Erdemir 7140 (HSLA)

A.3.4 Erdemir DC04 (IF Steel)

A.4 Flow Curves at 300^{o}C

A.4.1 DP600 (Dual Phase)

A.4.2 Erdemir 7128 (HSLA)

A.4.3 Erdemir 7140 (HSLA)

A.4.4 Erdemir DC04 (IF Steel)

A.5Forming Limit Curves

A.5.1 DP600 (Dual Phase), t = 1,6 mm

A.5.2 Erdemir 7128 (HSLA), t = 1,5 mm

A.6 SEM Data

A.7 Properties of Drawn Parts

B. THE TEMPERATURE GRAPHS

B.1.1 DP600 (Dual Phase)

B.1.2 Erdemir 7128 (HSLA)

B.1.3 Erdemir 7140 (HSLA)

B.1.4 Erdemir DC04 (IF Steel)

C. THE RESULT OF EXPERIMENTS

C.1 The Changes in the Blank Holder Pressure (BHP) vs blank diameter

C.1.1 DP600 (Dual Phase)

C.1.2 Erdemir 7128 (HSLA)

C.1.3 Erdemir 7140 (HSLA)

C.1.4 Erdemir DC04 (IF Steel)

C.2 The Punch Load vs Displacement

C.2.1 DP600 (Dual Phase)

C.2.2 Erdemir 7128 (HSLA)

C.2.3 Erdemir 7140 (HSLA)

C.2.4 Erdemir DC04 (IF Steel)

C.3 The Changes in the Limiting Drawing Ratio and blank diameters accordingly

C.3.1 DP600 (Dual Phase)

C.3.2 Erdemir 7128 (HSLA)

C.3.3 Erdemir 7140 (HSLA)

C.3.4 Erdemir DC04 (IF Steel)

C.4 The Changes in the Maximum Punch Load with respect to blank diameters

C.4.1 DP600 (Dual Phase)

C.4.2 Erdemir 7128 (HSLA)

C.4.3 Erdemir 7140 (HSLA)

C.4.4 Erdemir DC04 (IF Steel)

C.5 The Changes in the Blank Force (BHF) vs blank diameter

C.5.1 DP600 (Dual Phase)

C.5.2 Erdemir 7128 (HSLA)

C.5.3 Erdemir 7140 (HSLA)

C.5.4 Erdemir DC04 (IF Steel)

APPENDIX A

A. MATERIAL DATA

A.1 Chemical Composition of the materials studied

Chemical Composition (%) of the materials studied

	DP600	DC04	7128	7140		DP600	DC04	7128	7140
C	0,0833	0,0234	0,0354	0,0785	Pb	<0,002	<0,002	<0,002	<0,002
Mn	1,47	0,165	0,251	1,24	Sn	0,00395	0,0023	0,0021	0,0034
Si	0,366	0,0322	0,0053	0,0180	Mg	<0,001	<0,001	<0,001	<0,001
P	0,027	0,0005	<0,0005	0,028	As	<0,0015	0,0034	0,0061	0,0042
S	<0,0005	<0,0005	0,0043	0,0044	Zr	<,0015	<0,0015	<0,0015	<0,0015
Cr	0,808	0,0229	0,0241	0,0424	Bi	<0,002	<0,002	<0,002	<0,002
Al	0,0468	0,0551	0,0529	0,0657	Ca	0,00318	0,0011	0,00098	0,00016
Cu	0,0291	0,0591	0,0396	0,0299	Ce	<0,0015	<0,0015	<0,0015	<0,0015
Ni	0,0477	0,0332	0,0315	0,0545	Se	<0,0015	<0,0015	<0,0015	0,0016
Co	0,0123	0,075	0,0094	0,0118	La	<0,0005	<0,0005	<0,0005	<0,0005
Ti	<0,001	<0,001	<0,001	0,0153	Sb	0,0032	<0,002	0,0035	0,0056
V	0,00961	0,0023	0,0046	0,0786	Ta	0,02	<0,02	<0,02	<0,02
Nb	<0,004	<0,004	0,0235	0,0442	N	0,0197	0,0128	0,0116	0,0152
Mo	<0,001	<0,001	<0,001	<0,001	B	0,00044	<0,0002	<0,0002	0,0002
W	<0,007	<0,007	<0,007	<0,007	Zn	0,00291	<0,001	<0,001	<0,001
Fe	97	99,5	99,5	98,2	Te	0,00247	0,0011	0,0014	0,0027

DP600 (DP, Dual Phase Steel)
ERDEMİR DC04 (Interstitial-free Grade, IF; Steel)
ERDEMİR 7128 (HSLA, High Strength Low Alloy)
ERDEMİR 7140 (HSLA, High Strength Low Alloy)

Figure A.1 The chemical composition of steels searched in this study, DP600 (Dual Phase), Erdemir DC04 (IF) and 7128 & 7140 (HSLA)

A.2 Flow Curves at Room Temp

A.2.1 DP600 (Dual Phase)

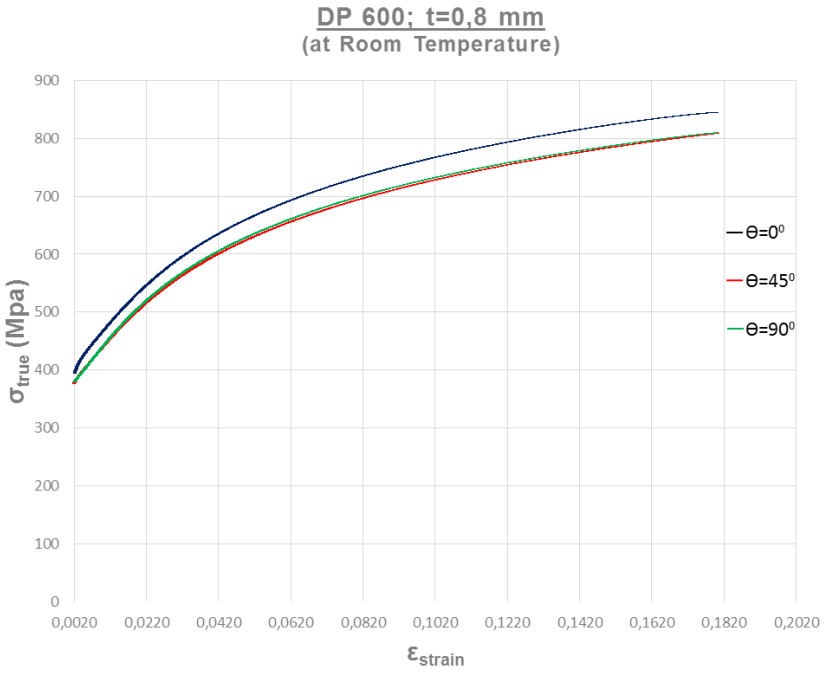

Figure A.2 The flow curves of DP600 at the angles,0º,45º and 90º due to the rolling direction, t = 0,8 mm at room temperature

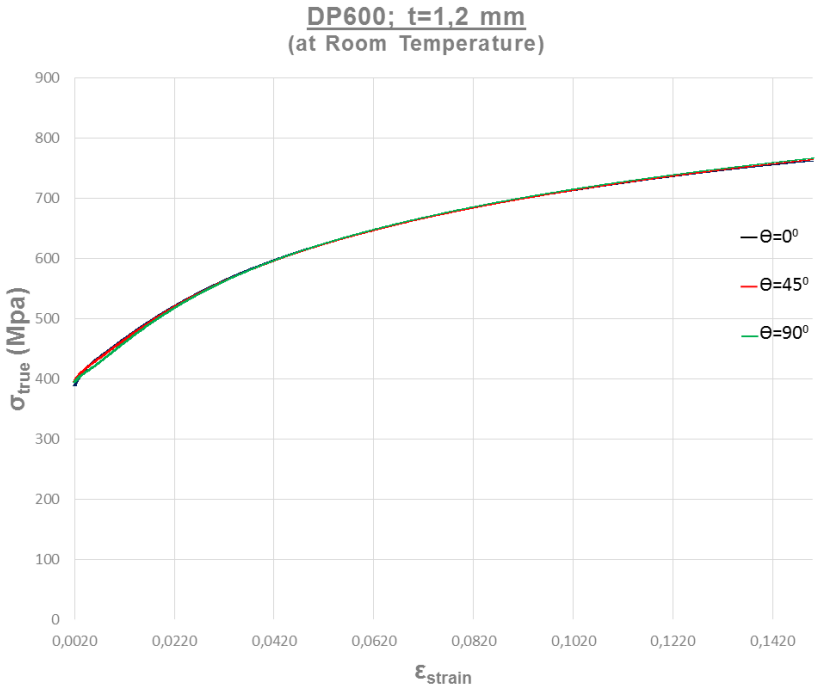

Figure A.3 The flow curves of DP600, 0º,45º and 90º due to the rolling direction, t = 1,2 mm at room temperature

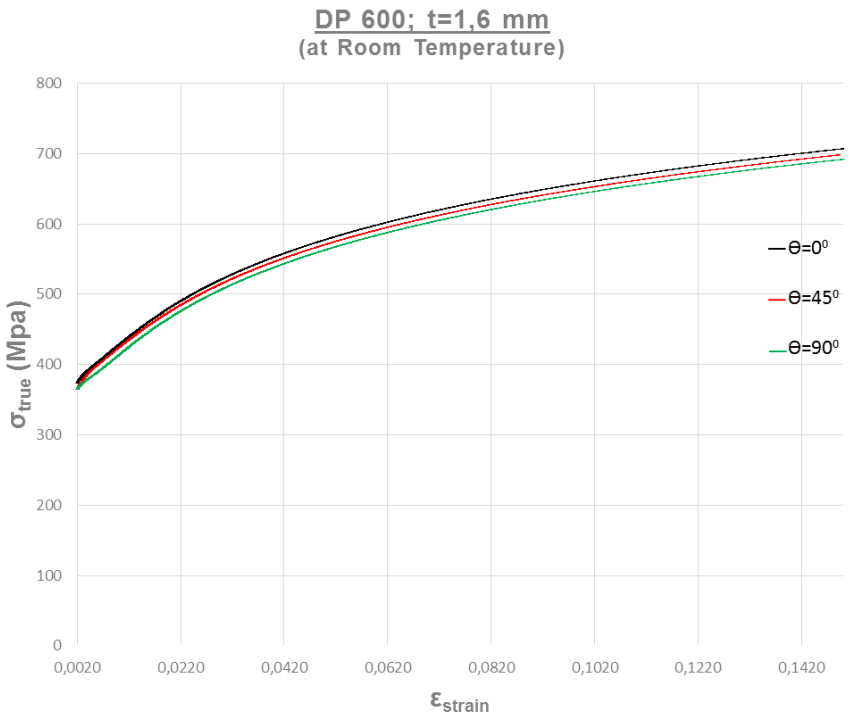

Figure A.4 The flow curves of DP600, 0º,45º and 90º due to the rolling direction, t = 1,2 mm at room temperature

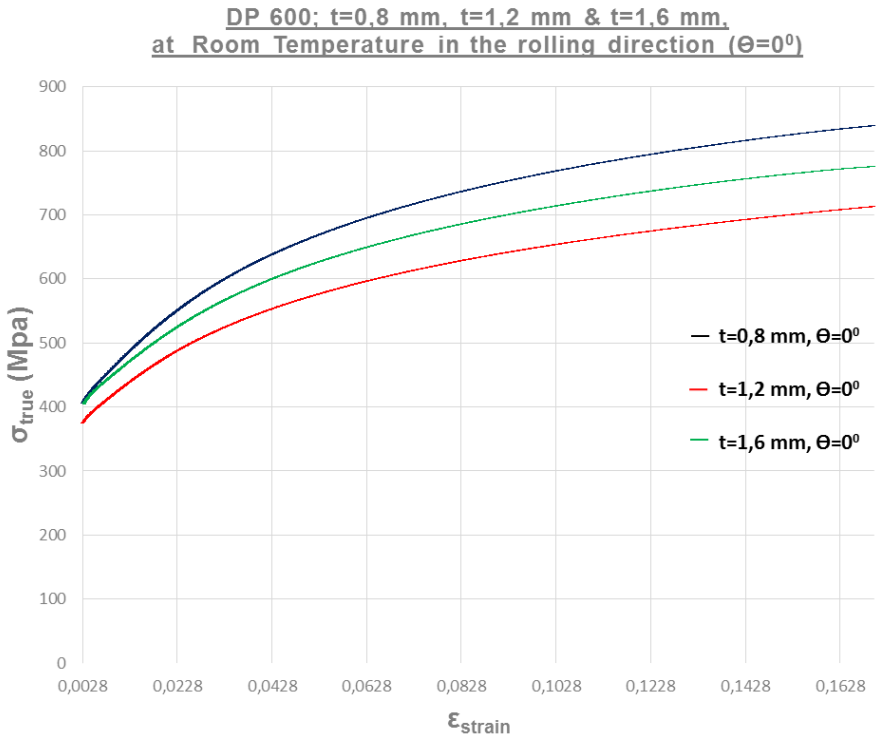

Figure A.5 The comparison of the flow curves of DP600, t = 0,8, 1,2 and 1,6 mm at room temperature in the rolling direction.

A.2.2 Erdemir 7128 (HSLA)

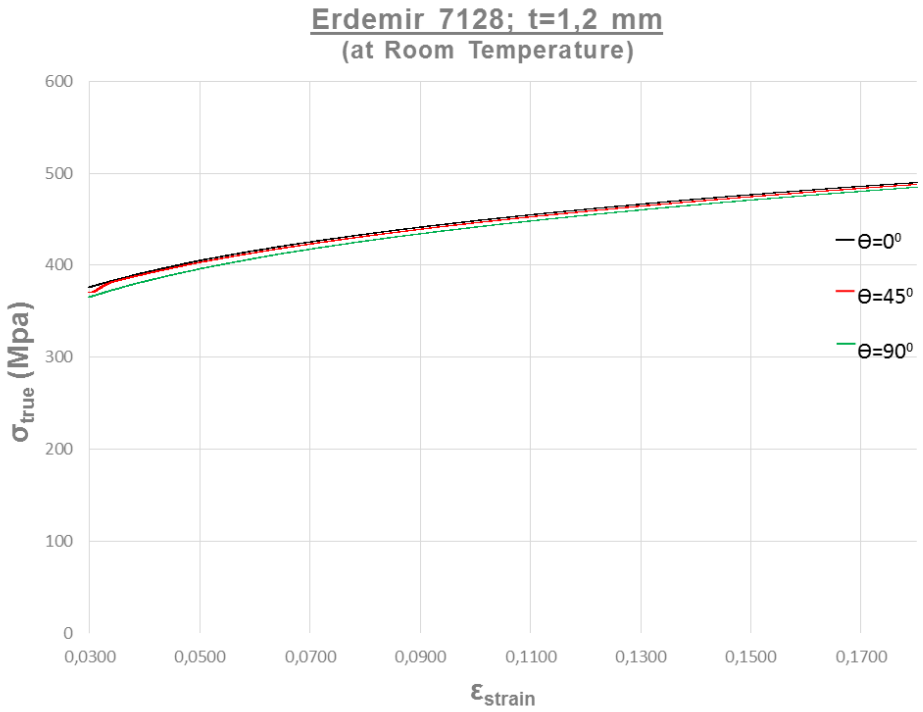

Figure A.6 The flow curves of Erdemir 7128 (HSLA), 0º,45º and 90º due to the rolling direction, t = 1,2 mm at room temperature

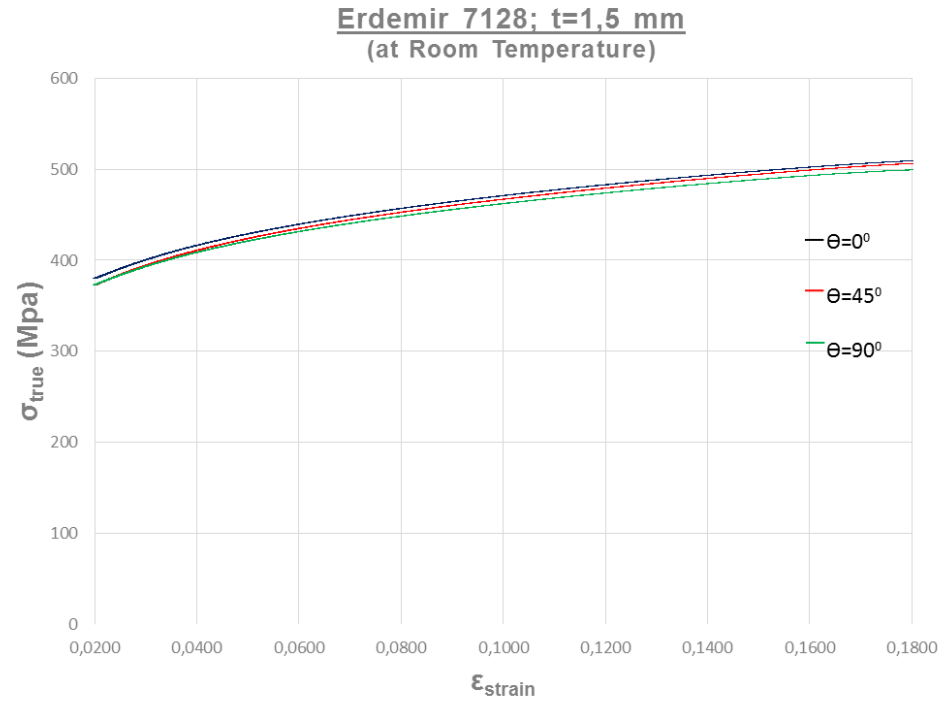

Figure A.7 The flow curves of Erdemir 7128 (HSLA), 0º,45º and 90º due to the rolling direction, t = 1,5 mm at room temperature

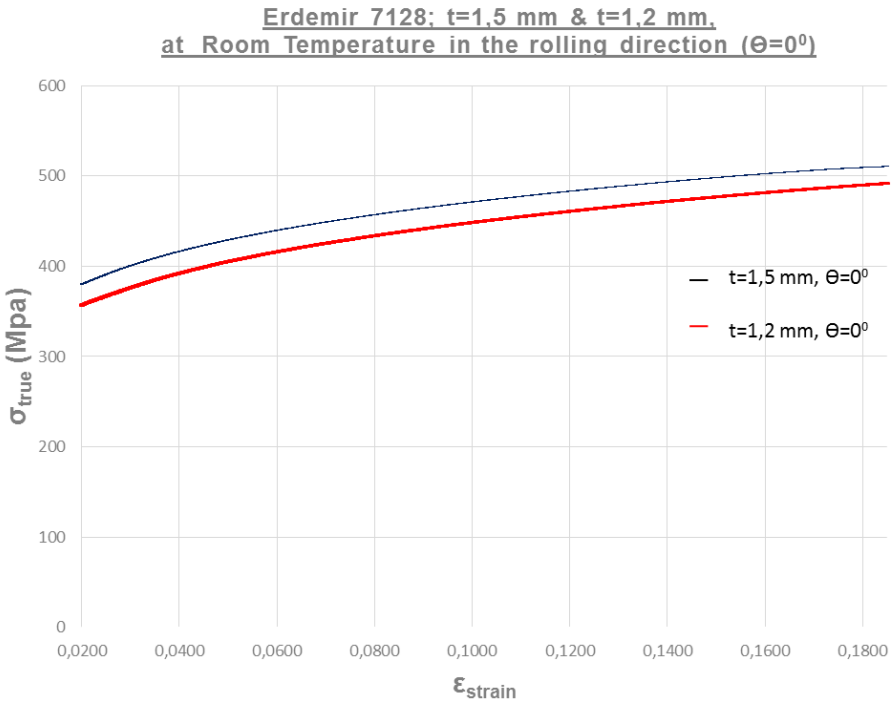

Figure A.8 The comparison of the flow curves of Erdemir 7128 (HSLA), t = 1,2 and 1,5 mm at room temperature in the rolling direction.

A.2.3 Erdemir 7140 (HSLA)

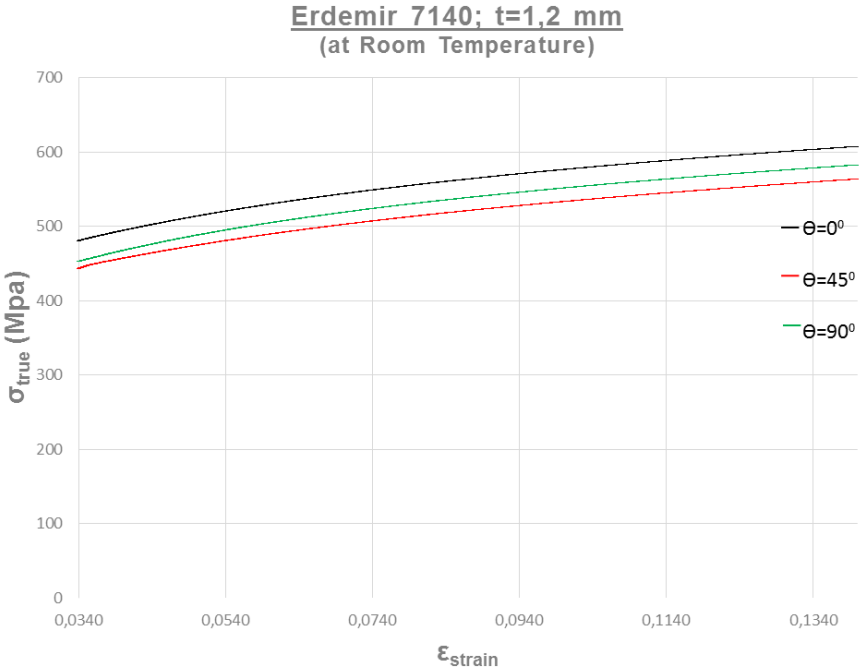

Figure A.9 The flow curves of Erdemir 7140 (HSLA), 0º,45º and 90º due to the rolling direction, t = 1,2 mm at room temperature

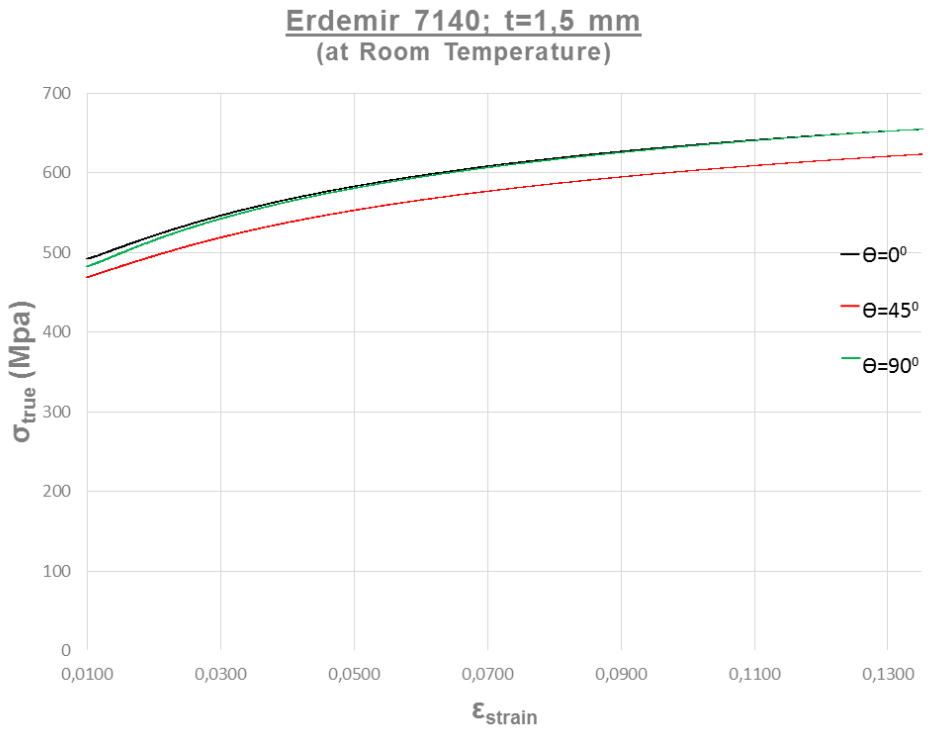

Figure A.10 The flow curves of Erdemir 7140 (HSLA), 0º,45º and 90º due to the rolling direction, t = 1,5 mm at room temperature

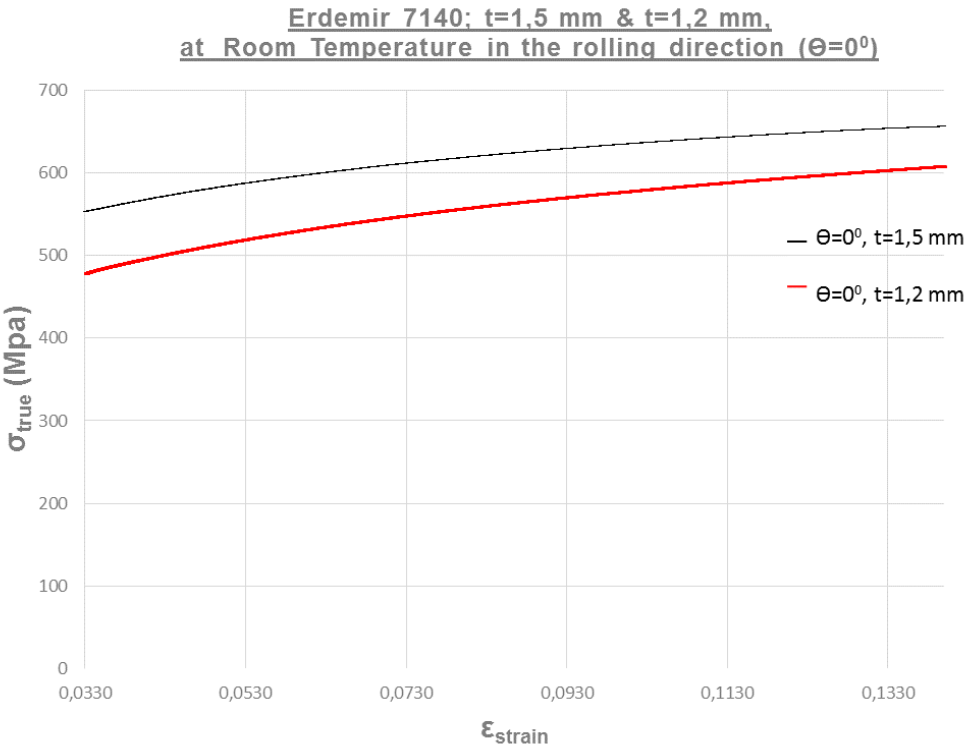

Figure A.11 The comparison of the flow curves of Erdemir 7140 (HSLA), t = 1,2 and 1,5 mm at room temperature in the rolling direction.

A.2.4 Erdemir DC04 (IF Steel)

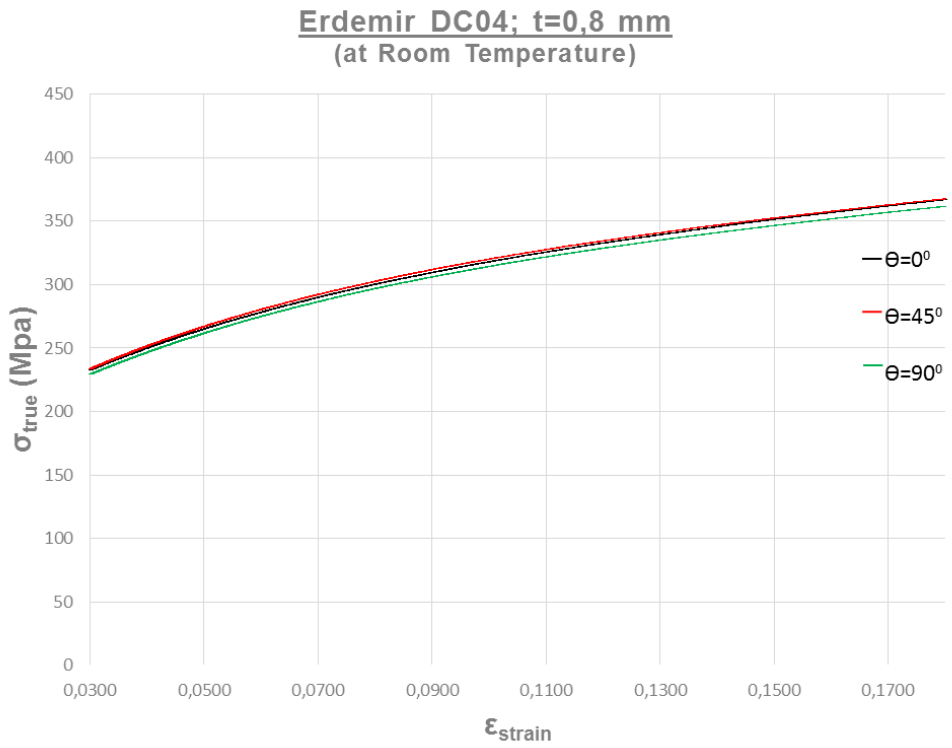

Figure A.12 The flow curves of Erdemir DC04 (IF Steel), 0º,45º and 90º due to the rolling direction, t = 0,8 mm at room temperature

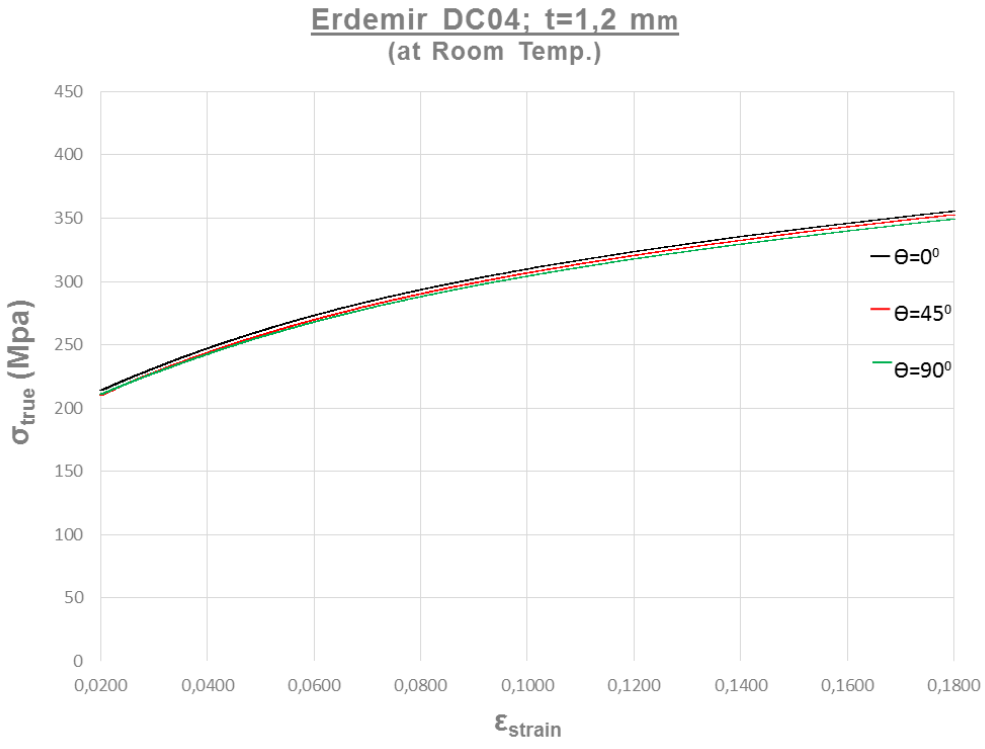

Figure A.13 The flow curves of Erdemir DC04 (IF Steel), 0º,45º and 90º due to the rolling direction, t = 1,2 mm at room temperature

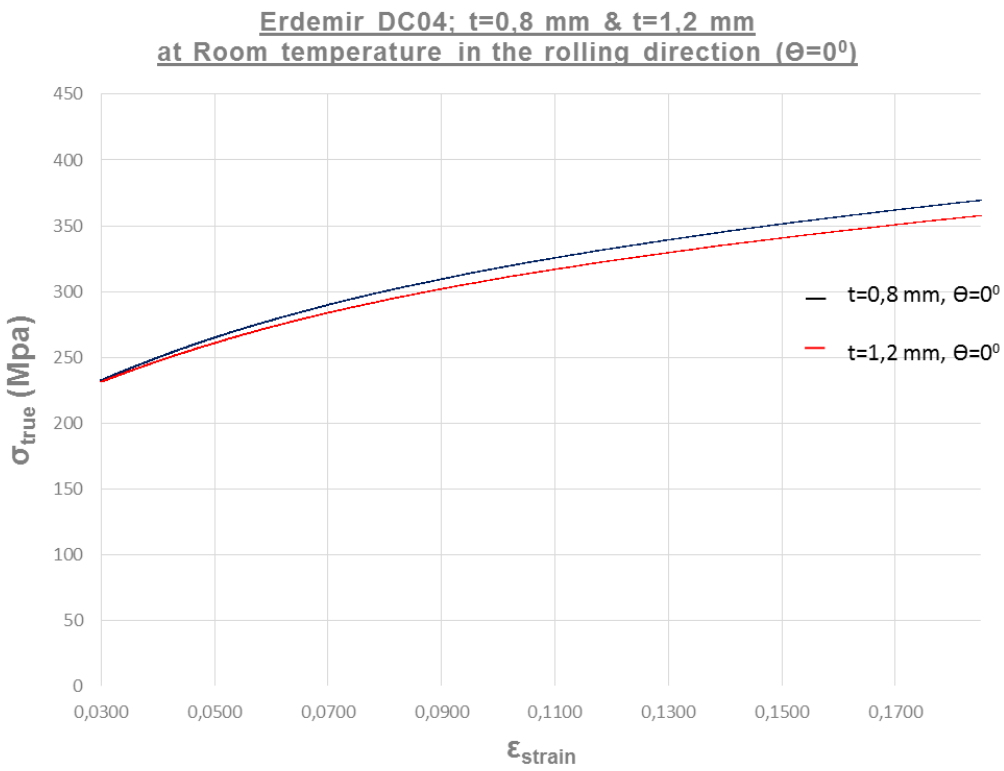

Figure A.14 The comparison of the flow curves of Erdemir DC04 (IF Steel), t = 0,8 and 1,2 mm at room temperature in the rolling direction.

A.5 Forming Limit Curves

A.5.1 DP600 (Dual Phase), t = 1,6 mm

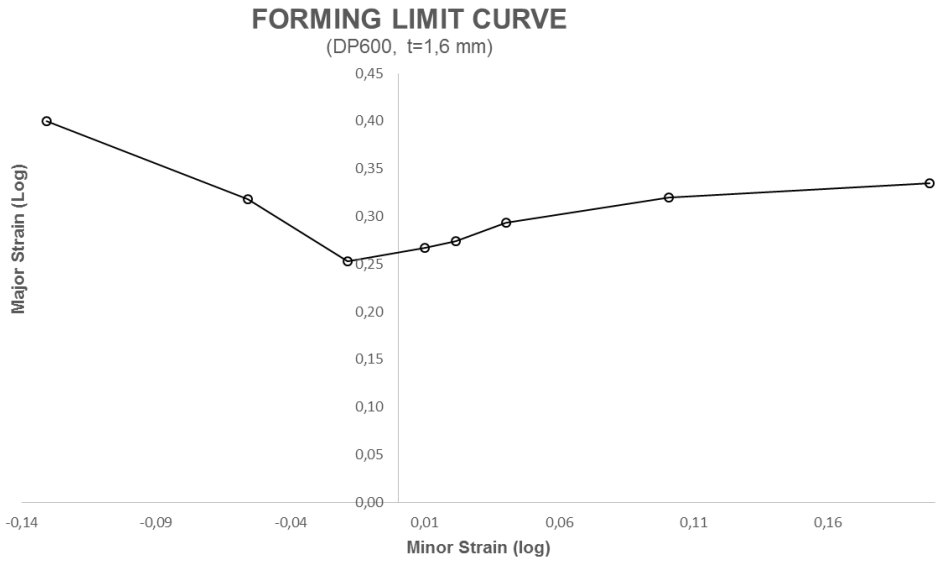

Figure A.15 The forming limit curve of DP600, t = 1,6 mm at room temperature

A.5.2 Erdemir 7128 (HSLA), t = 1,5 mm

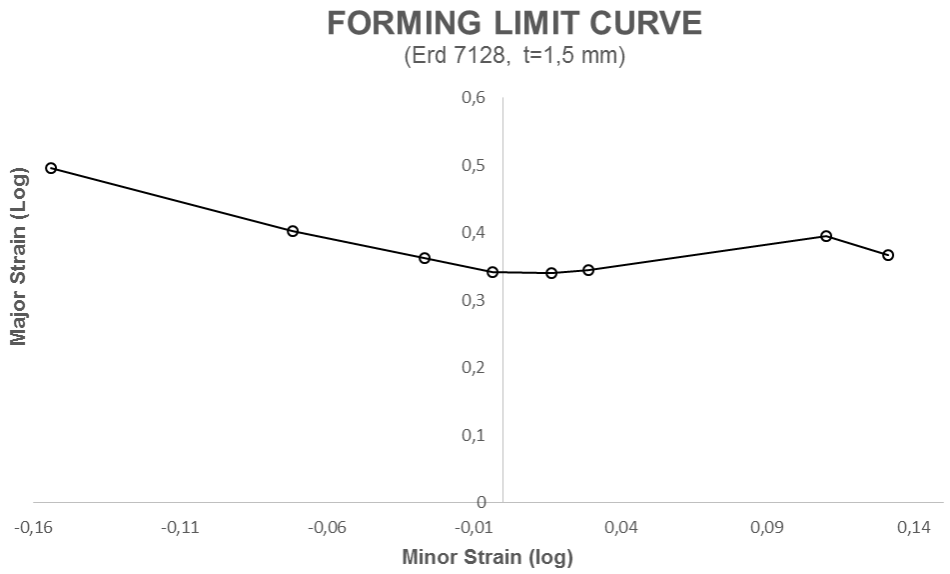

Figure A.16 The forming limit curve of Erdemir 7128 (HSLA), t = 1,5 mm at room temperature

GCRIS

APPENDIX B

THE TEMPERATURE GRAPHS

B.1.1 DP600 (Dual Phase)

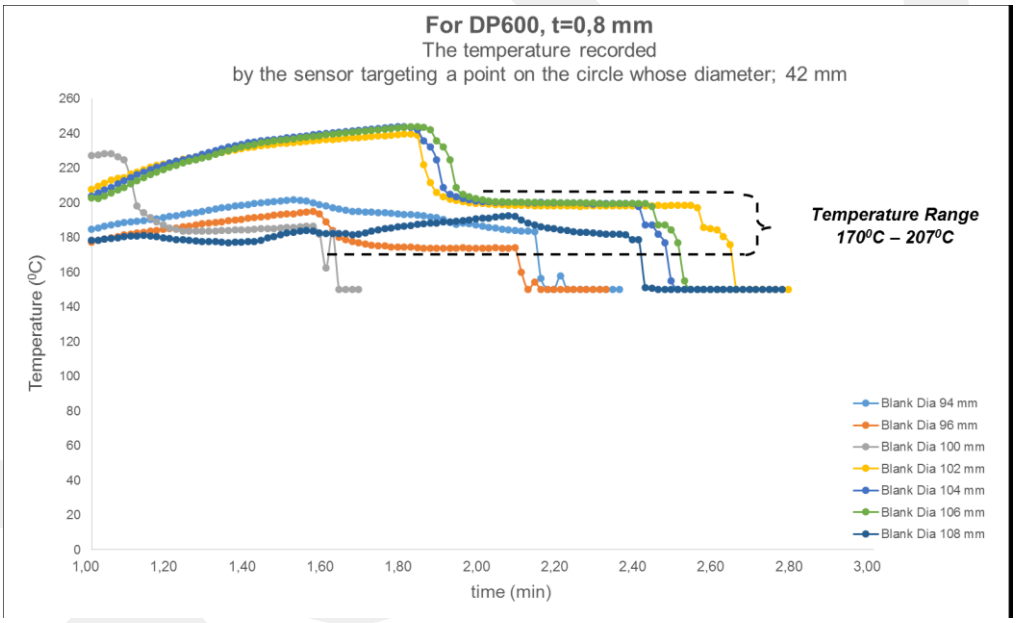

Figure B.1 For DP600 (Dual Phase), t = 0,8 mm, The temperature recorded by the sensor targeting a point on the circle whose (blank) Diameter; 42 mm

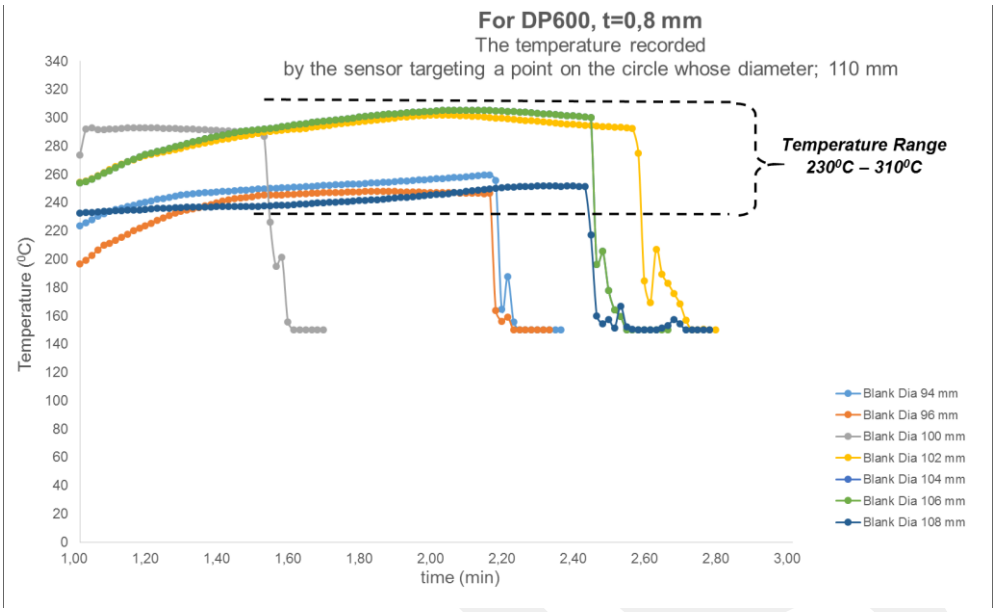

Figure B.2 For DP600 (Dual Phase), t = 0,8 mm, The temperature recorded by the sensor targeting a point on the circle whose (blank) Diameter; 110 mm

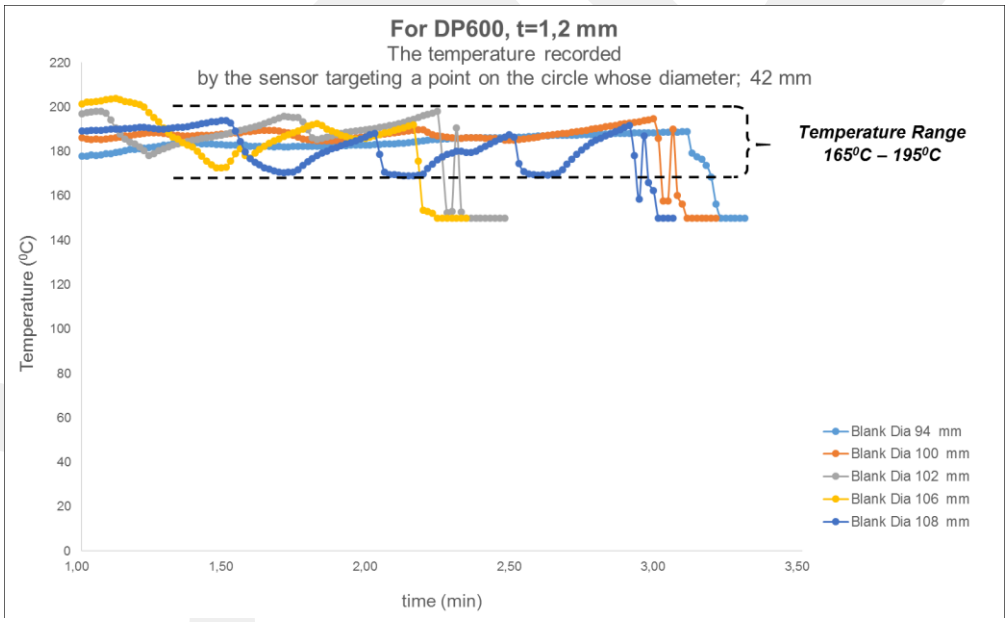

Figure B.3 For DP600 (Dual Phase), t = 1,2 mm, The temperature recorded by the sensor targeting a point on the circle whose (blank) Diameter; 42 mm

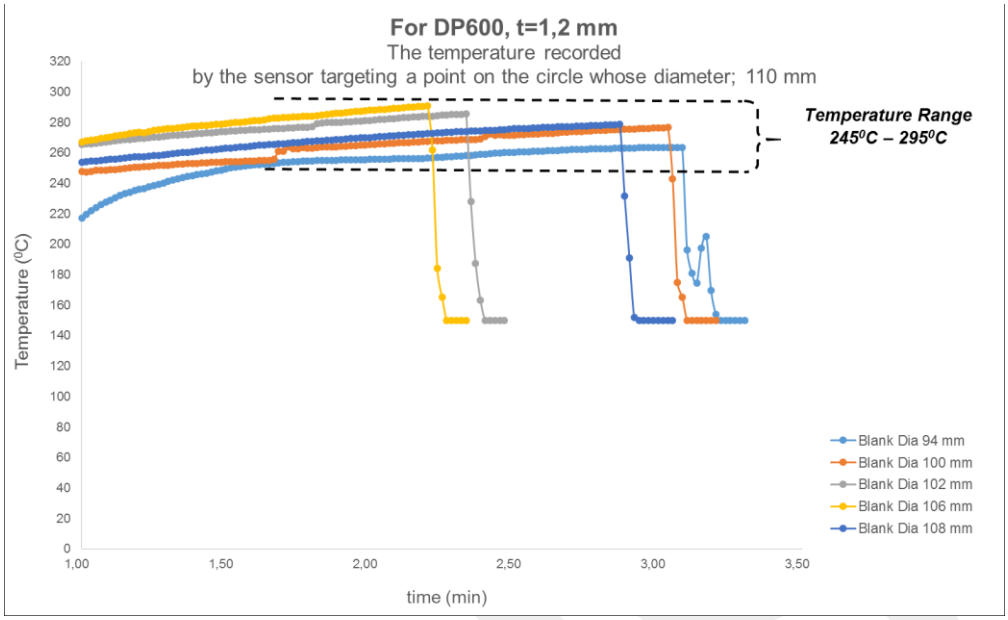

Figure B.4 For DP600 (Dual Phase), t = 1,2 mm, The temperature recorded by the sensor targeting a point on the circle whose (blank) Diameter; 110 mm

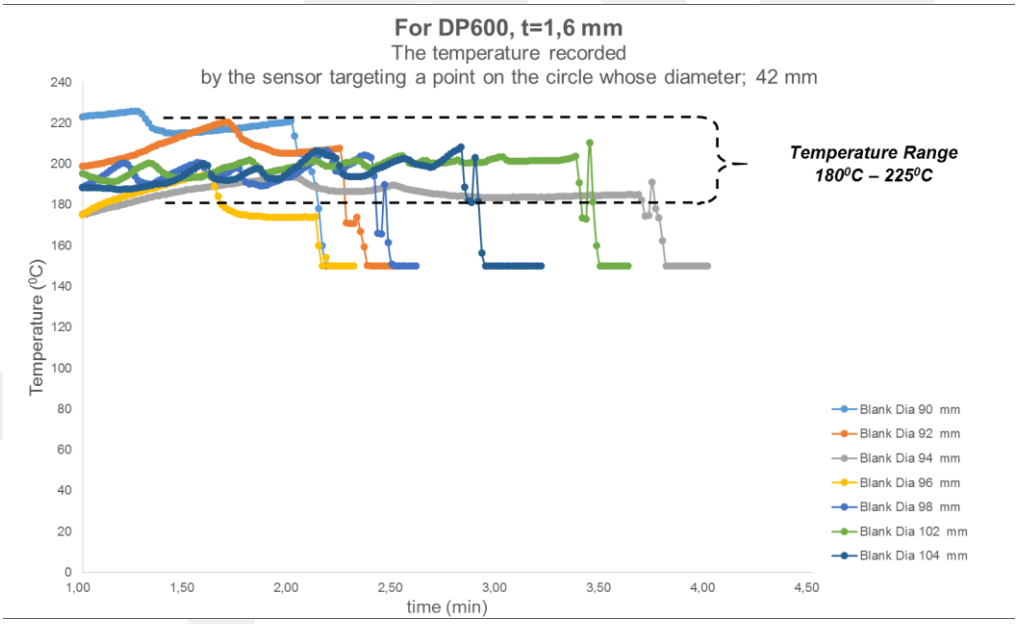

Figure B.5 For DP600 (Dual Phase), t = 1,6 mm, The temperature recorded by the sensor targeting a point on the circle whose (blank) Diameter; 42 mm

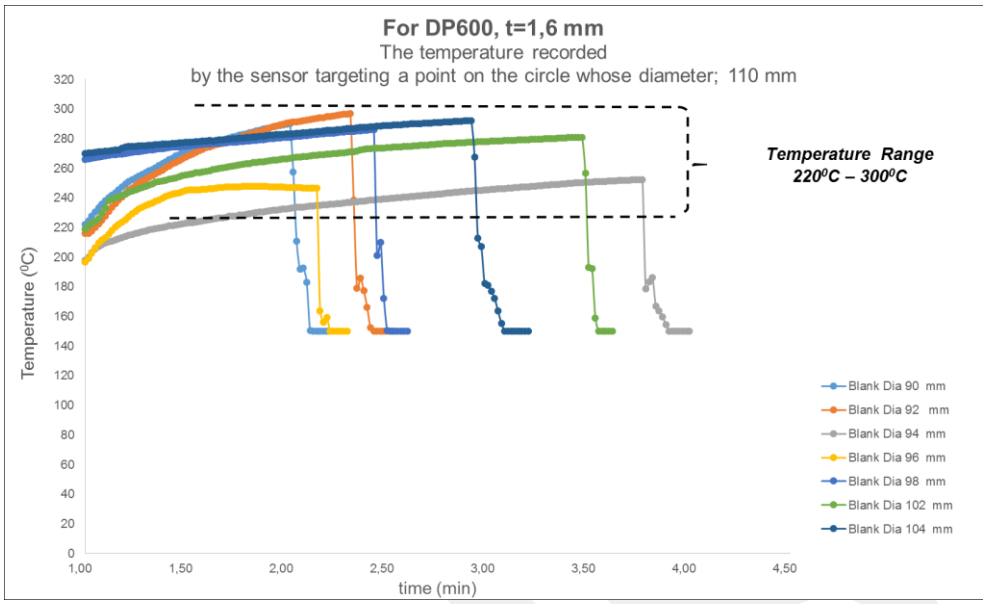

Figure B.6 For Erdemir DP600 (Dual Phase), t = 1,6 mm, The temperature recorded by the sensor targeting a point on the circle whose (blank) Diameter; 110 mm

B.1.2 Erdemir 7128 (HSLA)

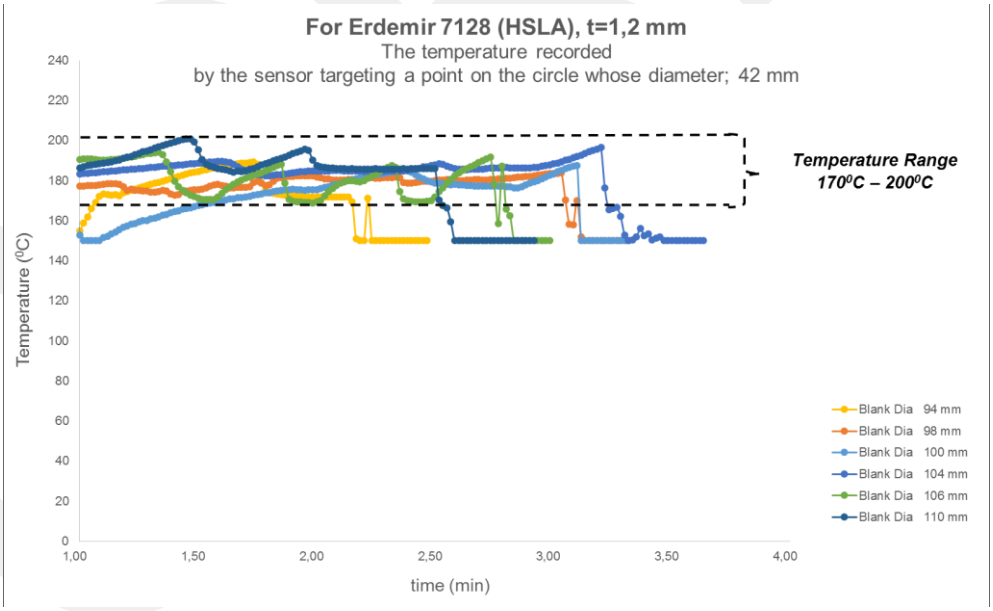

Figure B.7 For Erdemir 7128 (HSLA), t = 1,2 mm, The temperature recorded by the sensor targeting a point on the circle whose (blank) Diameter; 42 mm

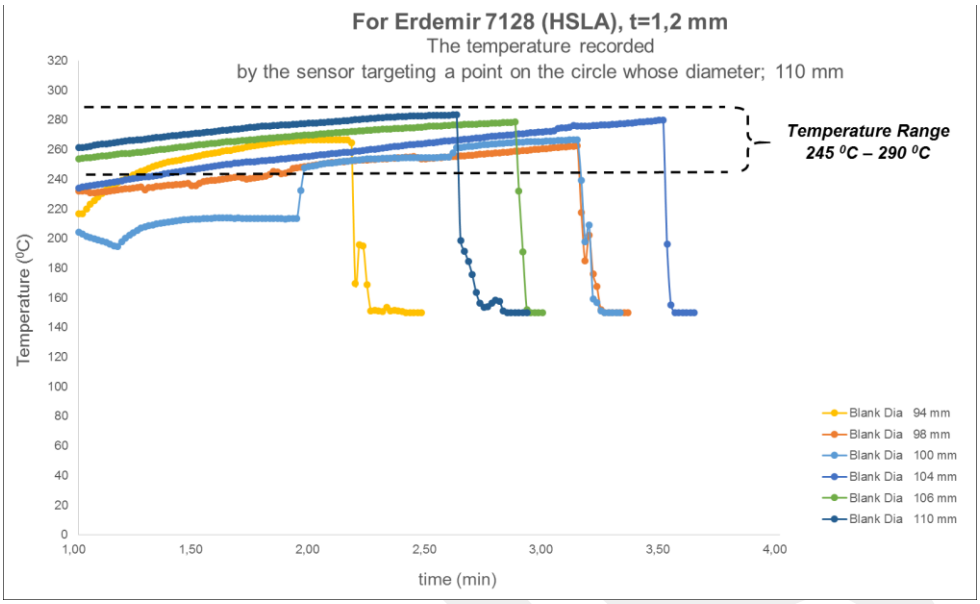

Figure B.8 For Erdemir 7128 (HSLA), t = 1,2 mm, The temperature recorded by the sensor targeting a point on the circle whose (blank) Diameter; 110 mm

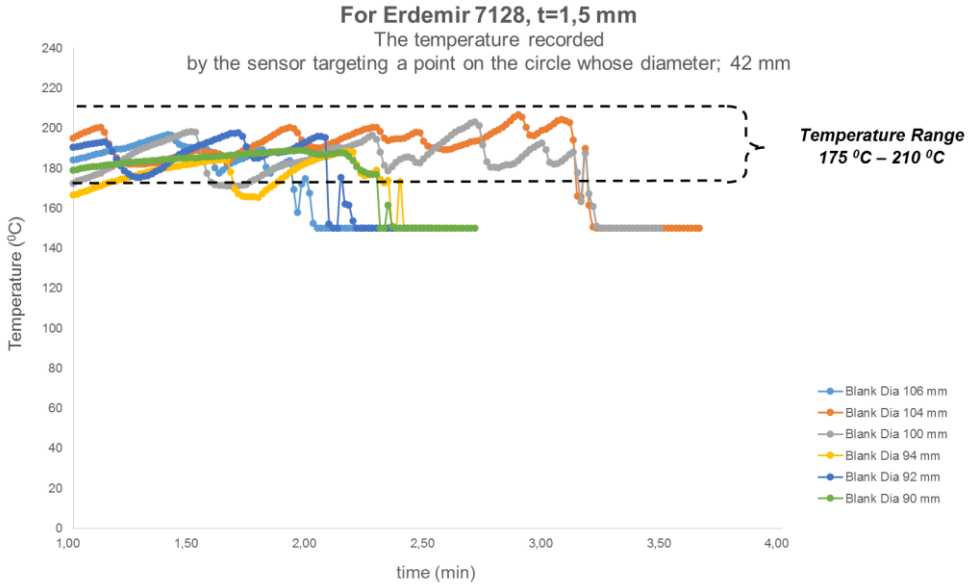

Figure B.9 For Erdemir 7128 (HSLA), t = 1,5 mm, The temperature recorded by the sensor targeting a point on the circle whose (blank) Diameter; 42 mm

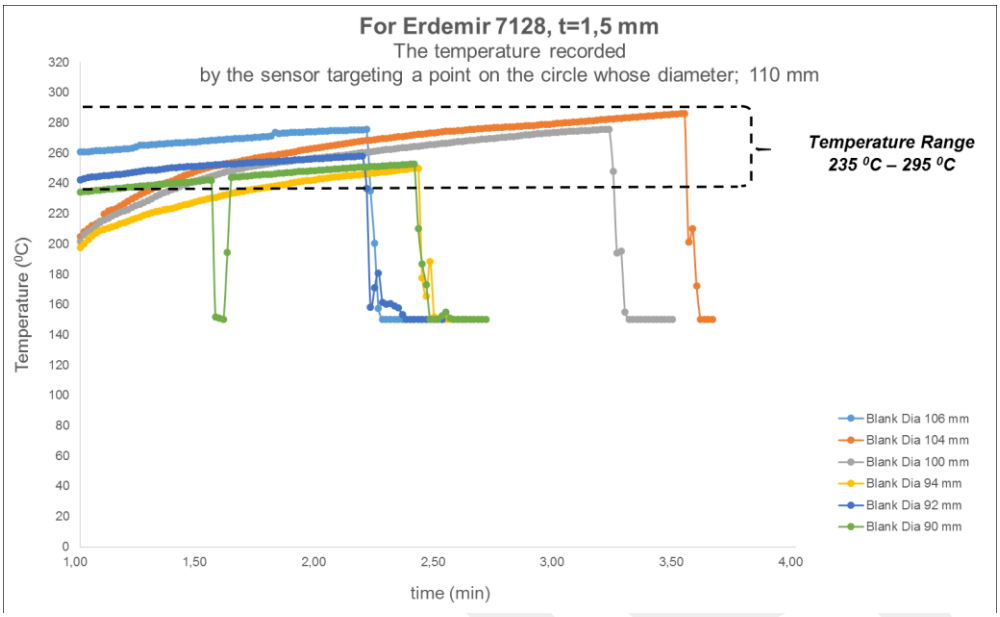

Figure B.10 For Erdemir 7128 (HSLA), t = 1,5 mm, The temperature recorded by the sensor targeting a point on the circle whose (blank) Diameter; 110 mm

B.1.3 Erdemir 7140 (HSLA)

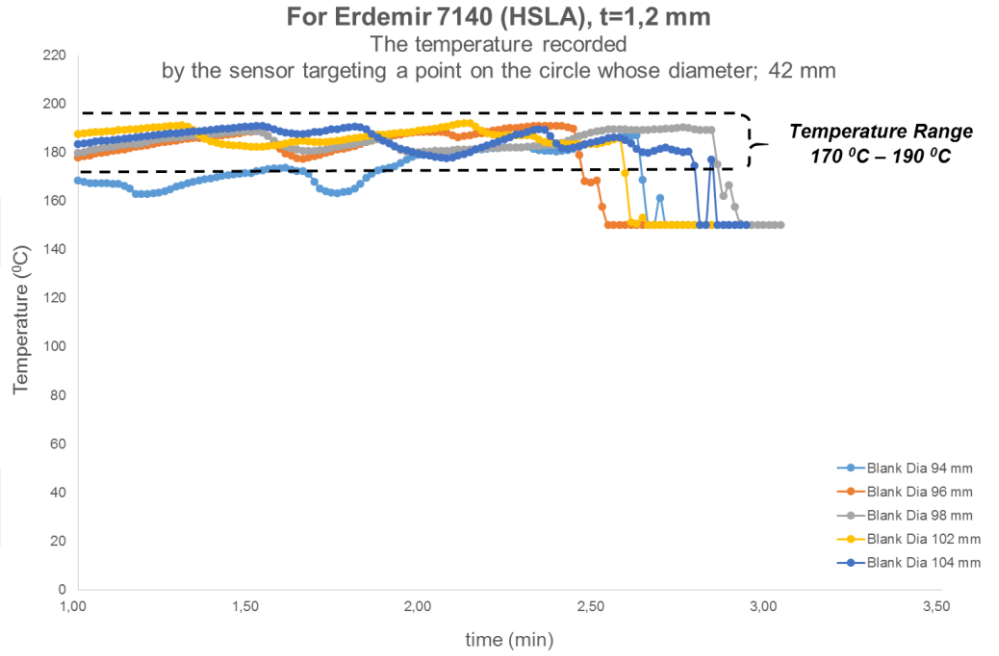

Figure B.11 For Erdemir 7140 (HSLA), t = 1,2 mm, The temperature recorded by the sensor targeting a point on the circle whose (blank) Diameter; 42 mm

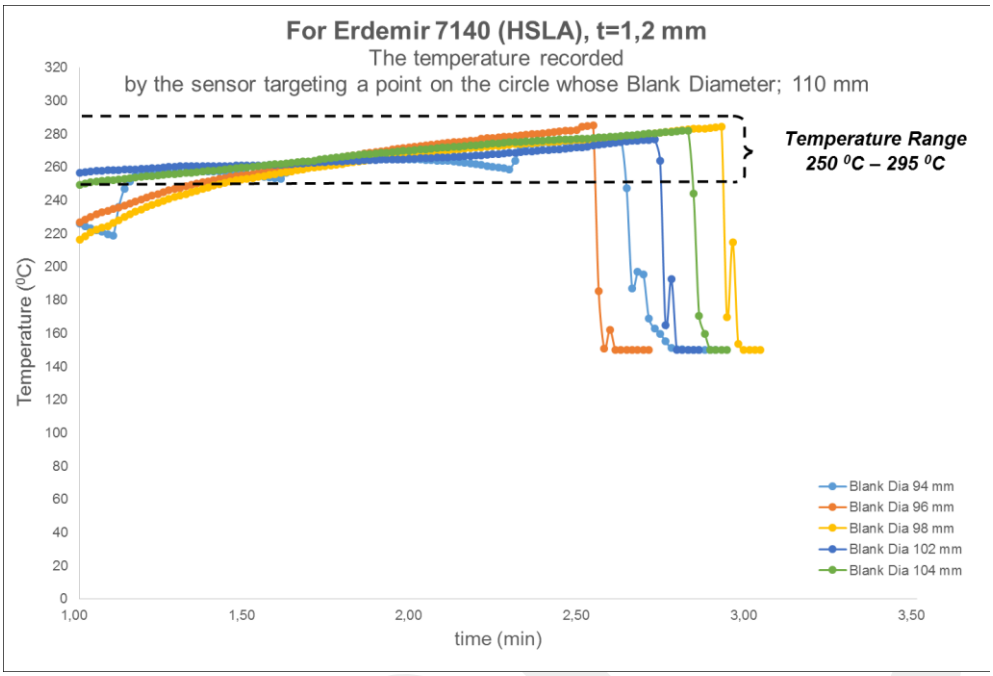

Figure B.12 For Erdemir 7140 (HSLA), t = 1,2 mm, The temperature recorded by the sensor targeting a point on the circle whose (blank) Diameter; 110 mm

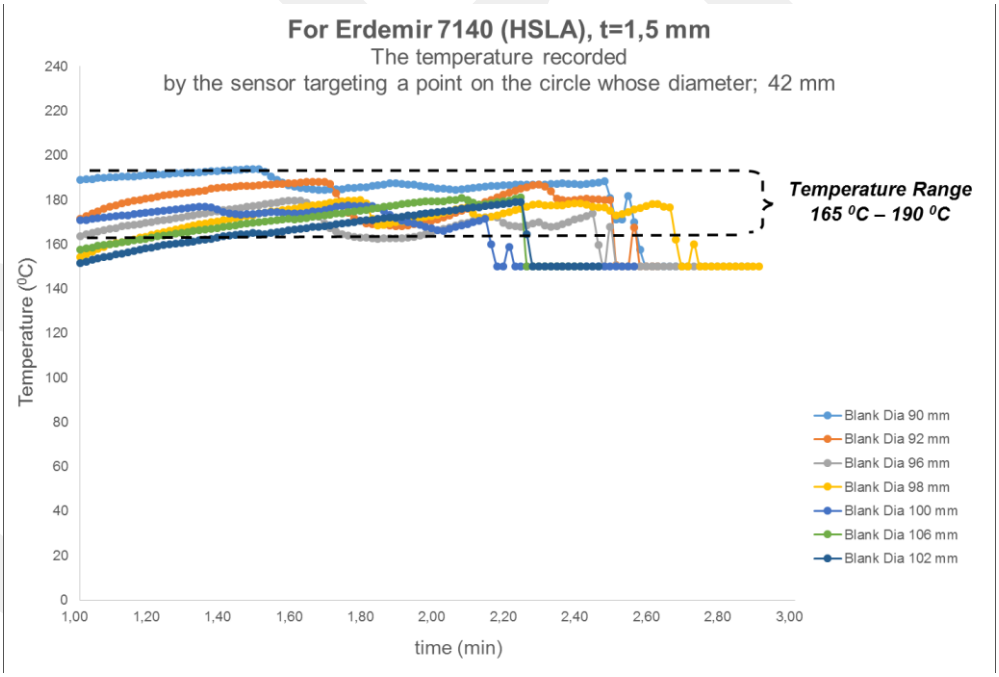

Figure B.13 For Erdemir 7128 (HSLA), t = 1,5 mm, The temperature recorded by the sensor targeting a point on the circle whose (blank) Diameter; 42 mm

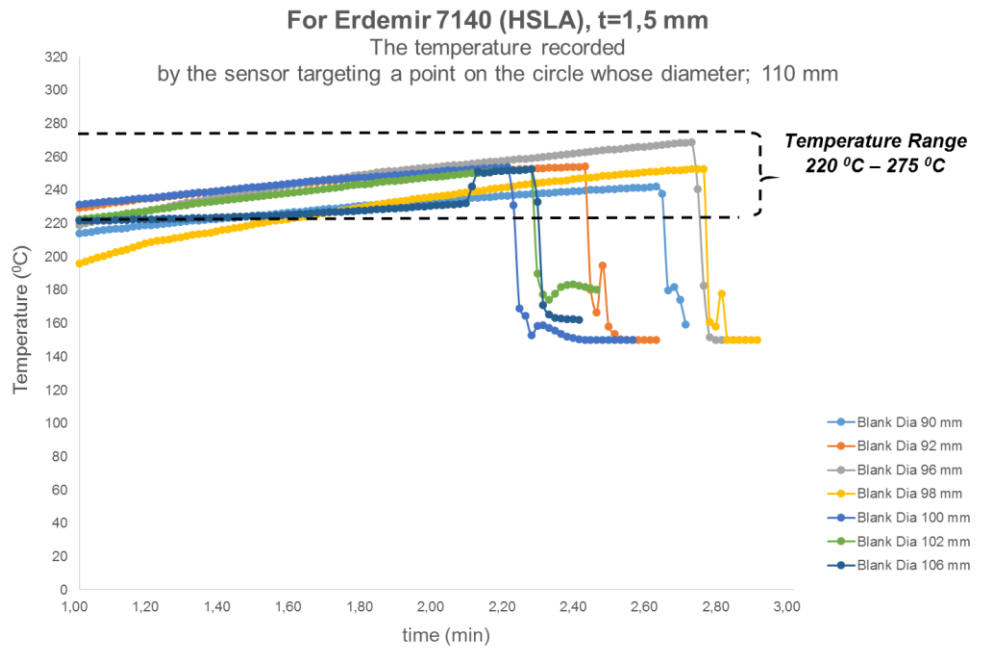

Figure B.14 For Erdemir 7140 (HSLA), t = 1,5 mm, The temperature recorded by the sensor targeting a point on the circle whose (blank) Diameter; 110 mm

B.1.4 Erdemir DC04 (IF Steel)

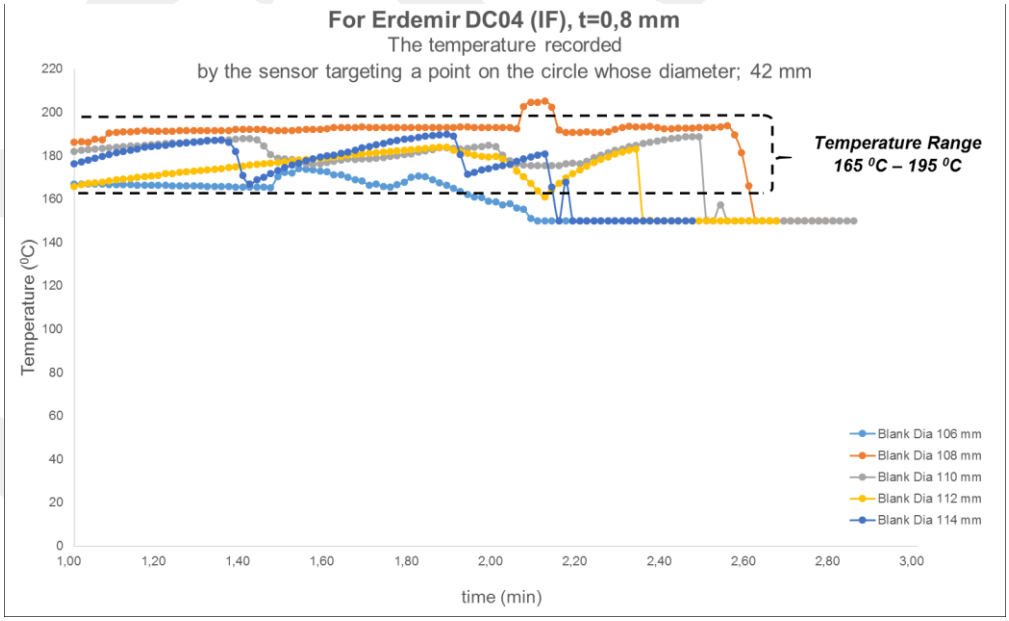

Figure B.15 For DC04 (IF Steel), t = 0,8 mm, The temperature recorded by the sensor targeting a point on the circle whose (blank) Diameter; 42 mm

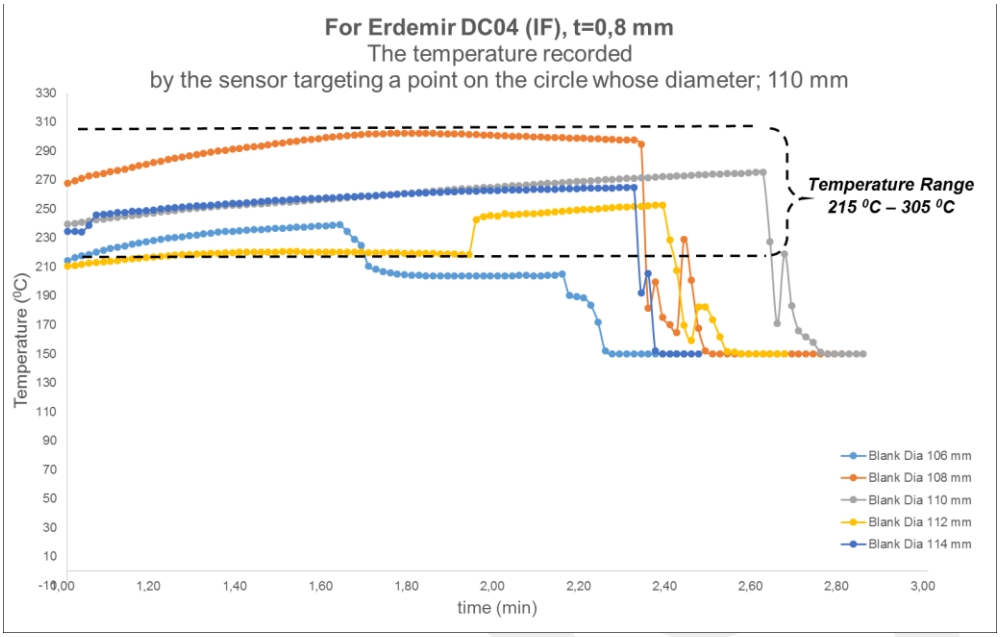

Figure B.16 For DC04 (IF Steel), t = 0,8 mm, The temperature recorded by the sensor targeting a point on the circle whose (blank) Diameter; 110 mm

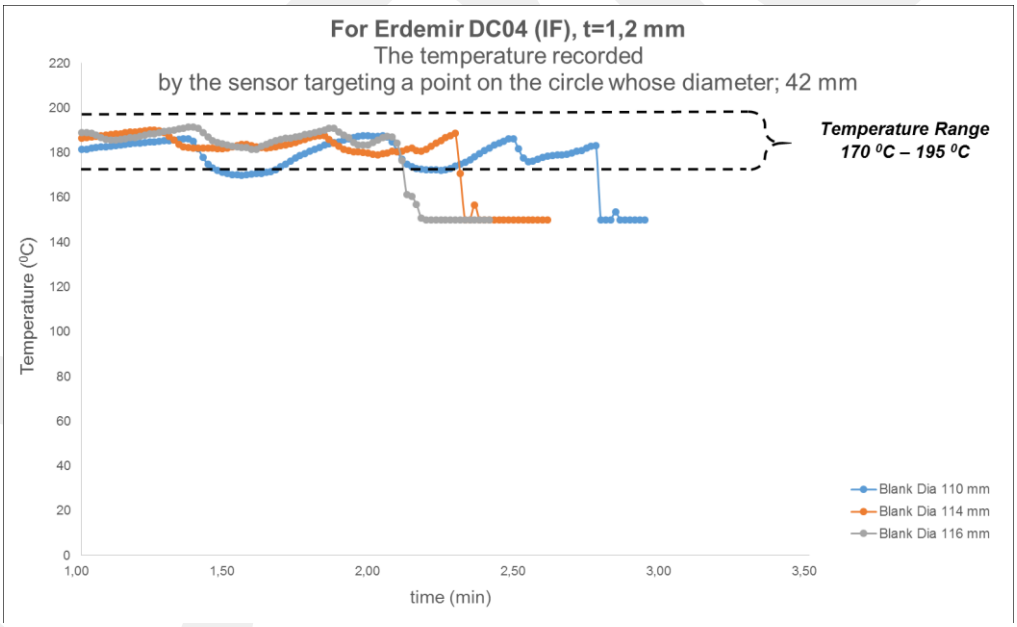

Figure B.17 For DC04 (IF Steel), t = 1,2 mm, The temperature recorded by the sensor targeting a point on the circle whose (blank) Diameter; 42 mm

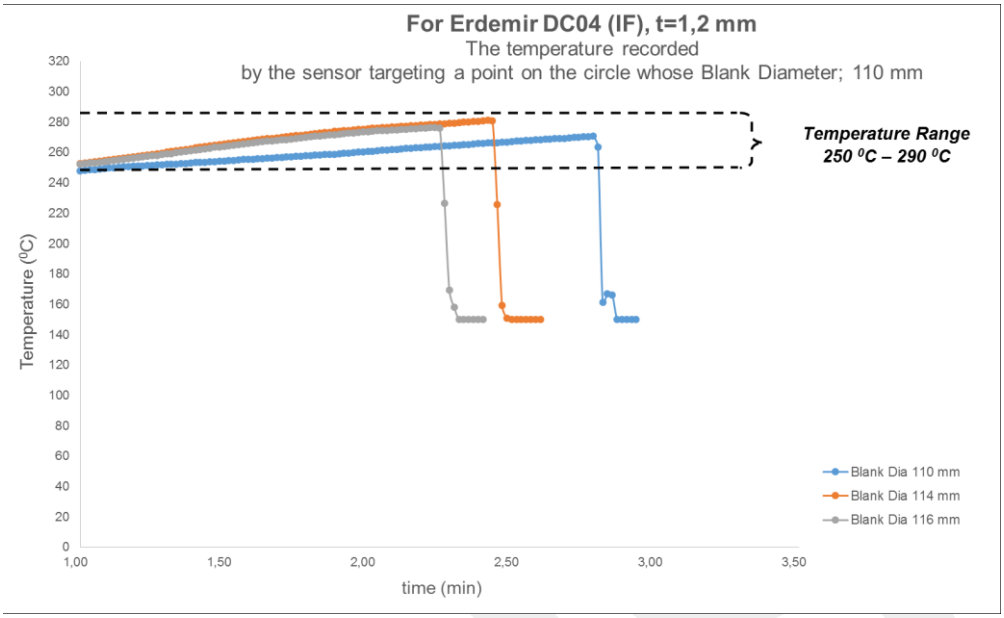

Figure B.18 For DC04 (IF Steel), t = 1,2 mm, The temperature recorded by the sensor targeting a point on the circle whose (blank) Diameter; 110 mm

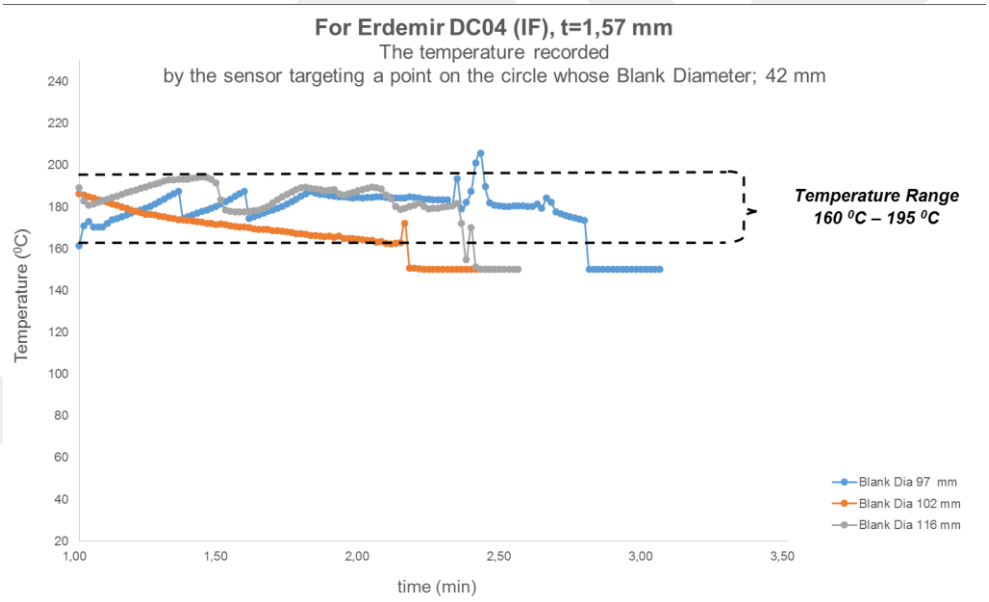

Figure B.19 For DC04 (IF Steel), t = 1,57 mm, The temperature recorded by the sensor targeting a point on the circle whose (blank) Diameter; 42 mm

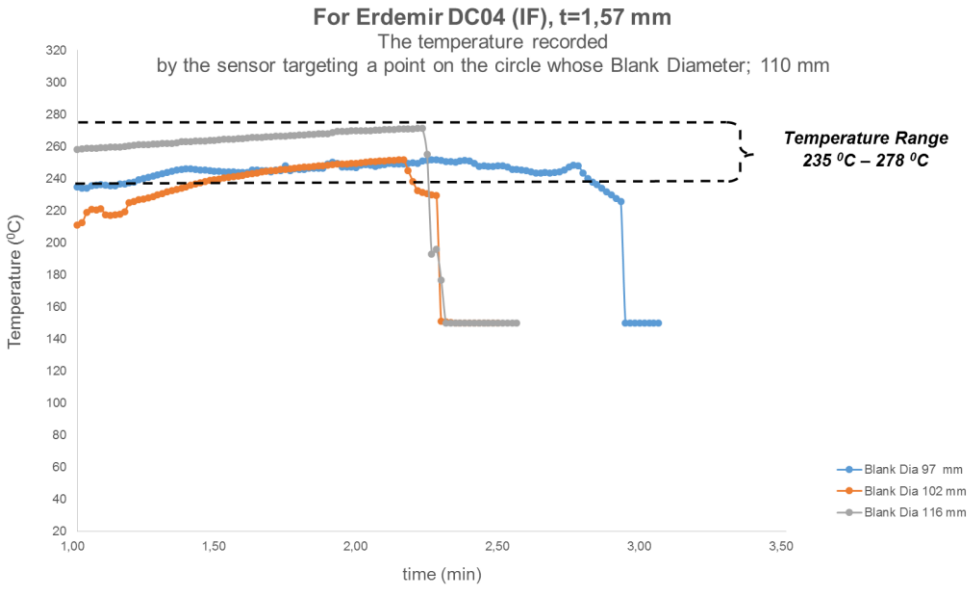

Figure B.20 For DC04 (IF Steel), t = 1,57 mm, The temperature recorded by the sensor targeting a point on the circle whose (blank) Diameter; 110 mm

GCRIS

APPENDIX C

THE RESULT OF EXPERIMENTS

C.1 The Changes in the Blank Holder Pressure (BHP) vs Blank Diameter

C.1.1 DP600 (Dual Phase)

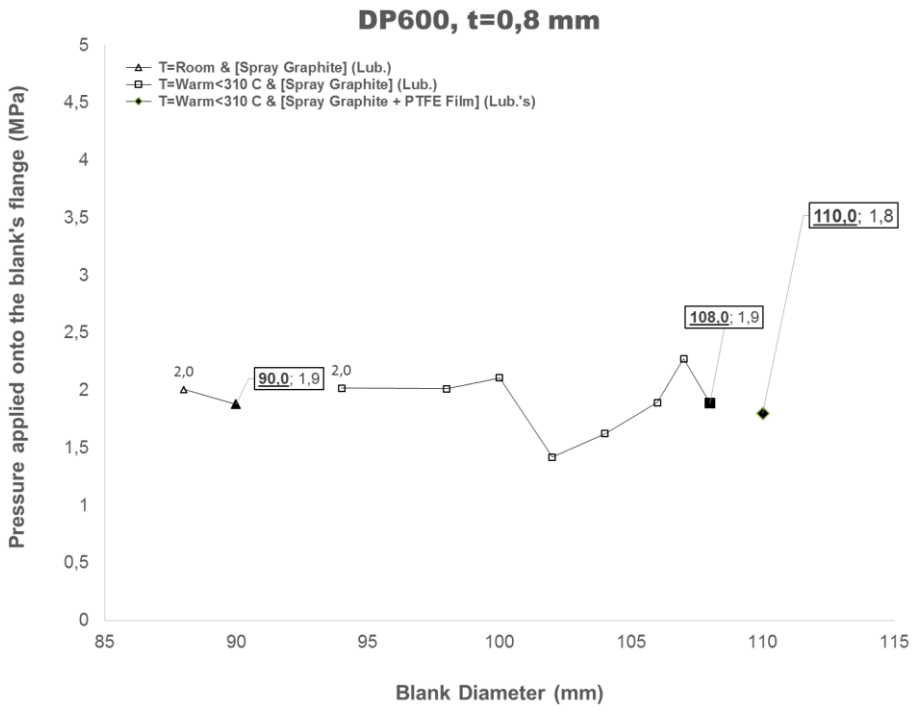

Figure C.1 The graph of the Blank Holder Pressure (MPa) applied to the blank's flange region vs its diameter (mm) for DP600 (Dual Phase), t = 0,8 mm.

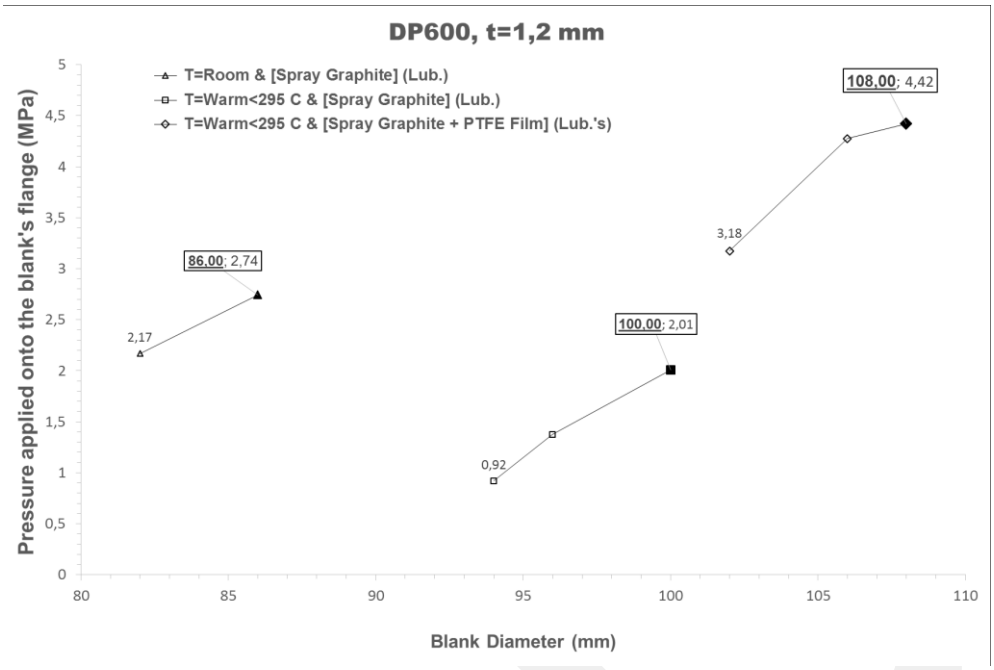

Figure C.2 The graph of the Blank Holder Pressure (MPa) applied to the blank's flange region vs its diameter (mm) for DP600 (Dual Phase), t = 1,2 mm.

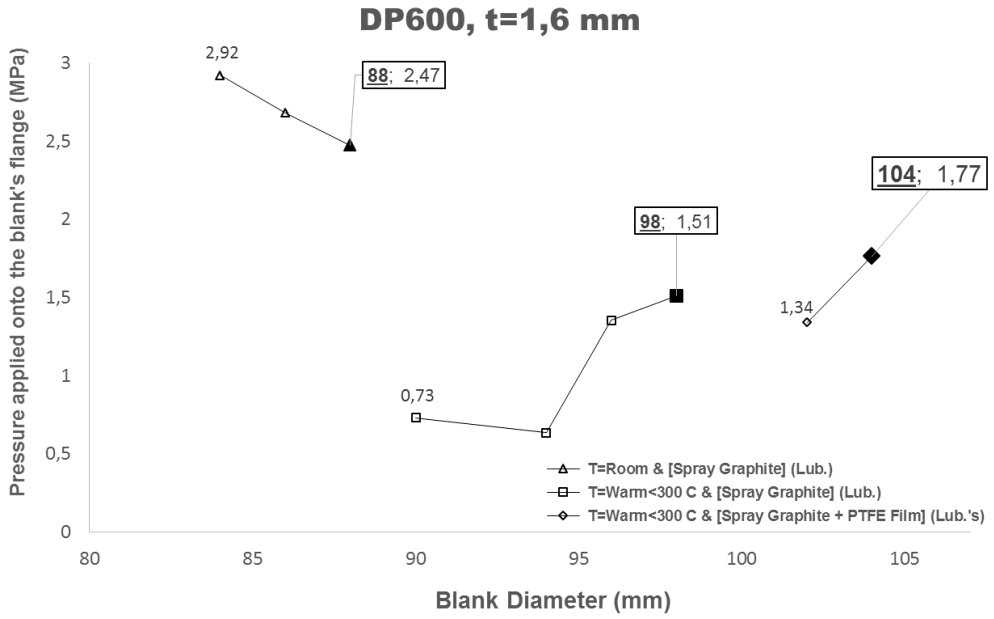

Figure C.3 The graph of the Blank Holder Pressure (MPa) applied to the blank's flange region vs its diameter (mm) for DP600 (Dual Phase), t = 1,6 mm.

C.1.2 Erdemir 7128 (HSLA)

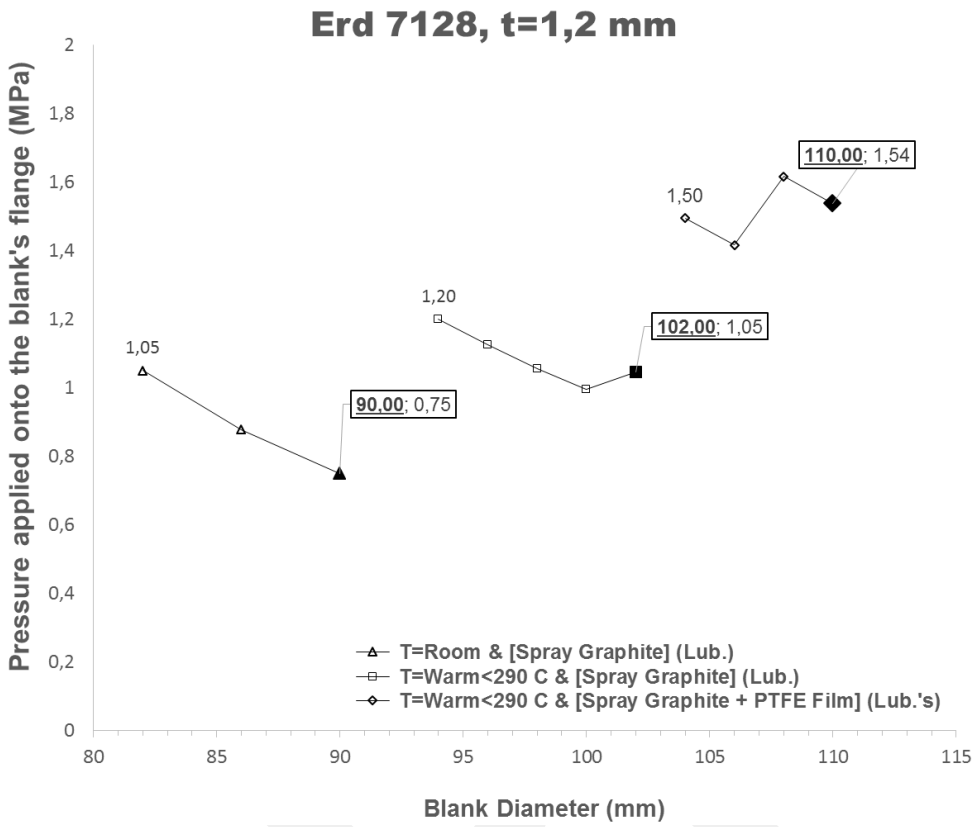

Figure C.4 The graph of the Blank Holder Pressure (MPa) applied to the blank's flange region vs its diameter (mm) for Erdemir 7128 (HSLA), t = 1,2 mm.

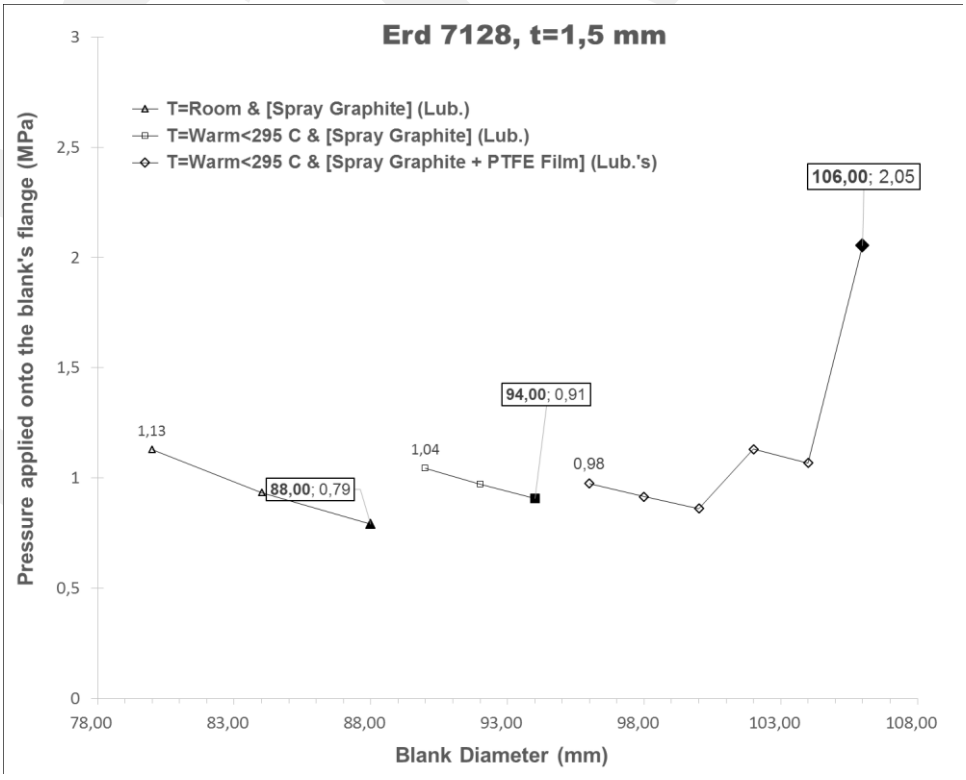

Figure C.5 The graph of the Blank Holder Pressure (MPa) applied to the blank's flange region vs its diameter (mm) for Erdemir 7128 (HSLA), t = 1,5 mm.

C.1.3 Erdemir 7140 (HSLA)

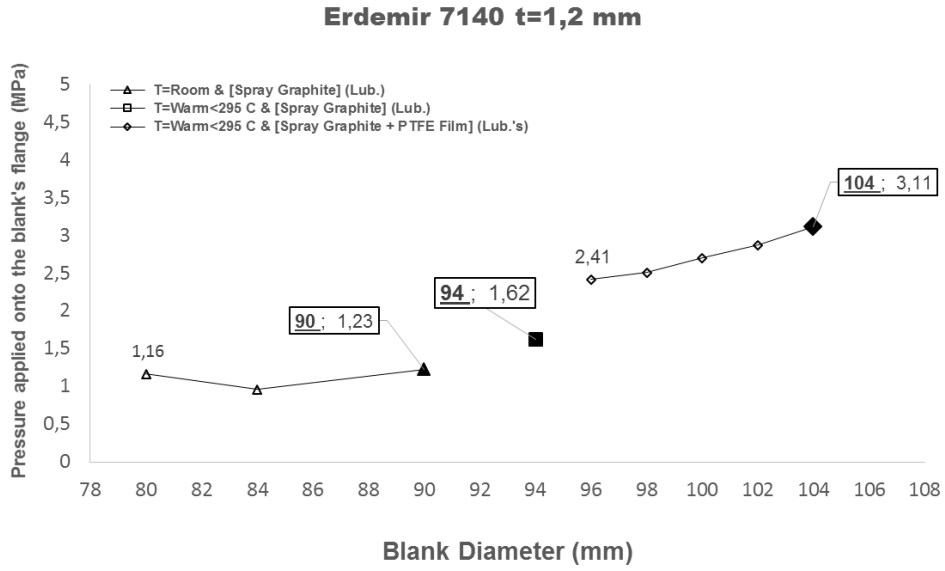

Figure C.6 The graph of the Blank Holder Pressure (MPa) applied to the blank's flange region vs its diameter (mm) for Erdemir 7140 (HSLA), t = 1,2 mm.

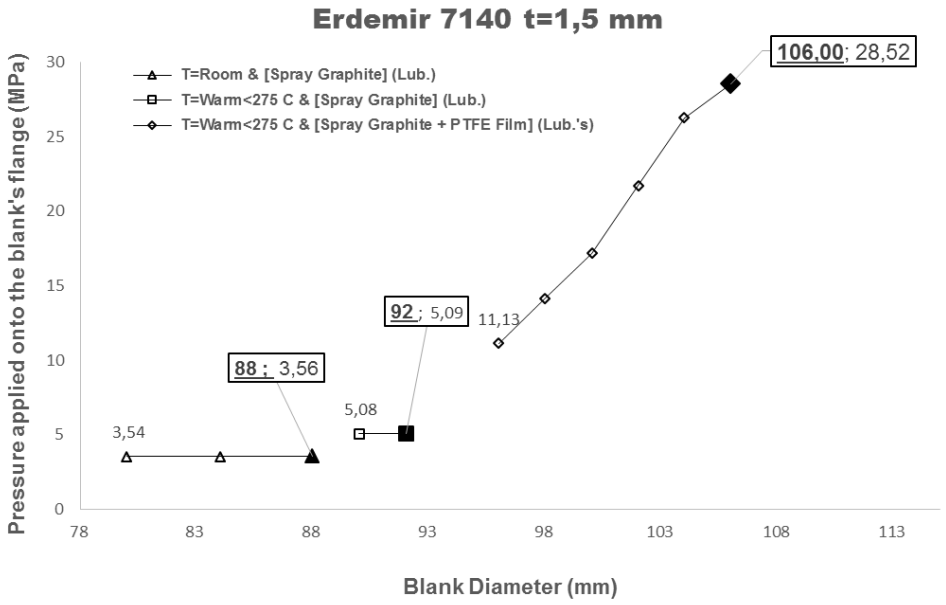

Figure C.7 The graph of the Blank Holder Pressure (MPa) applied to the blank's flange region vs its diameter (mm) for Erdemir 7140 (HSLA), t = 1,5 mm.

C.1.4 Erdemir DC04 (IF Steel)

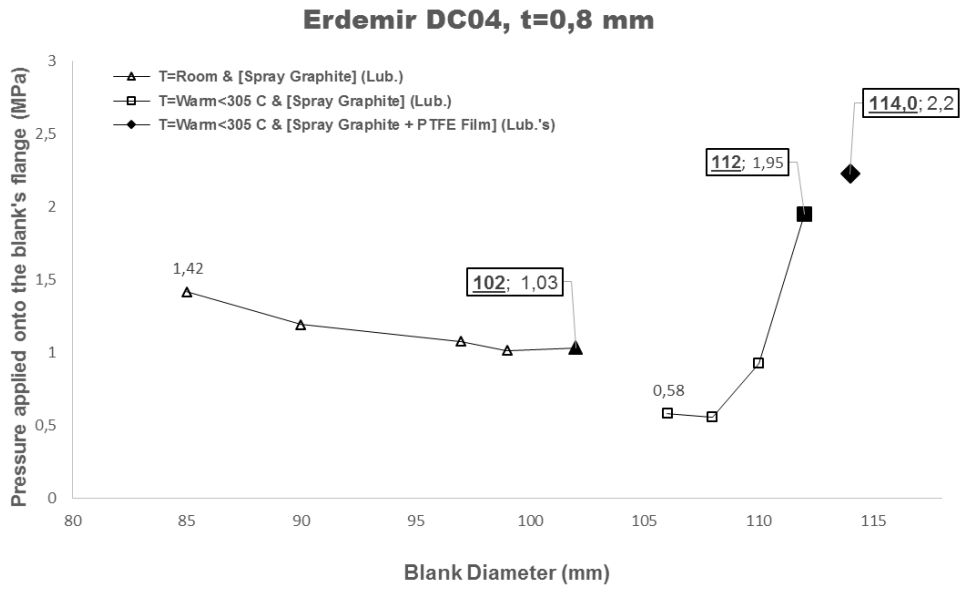

Figure C.8 The graph of the Blank Holder Pressure (MPa) applied to the blank's flange region vs its diameter (mm) for Erdemir DC04 (IF Steel), t = 0,8 mm.

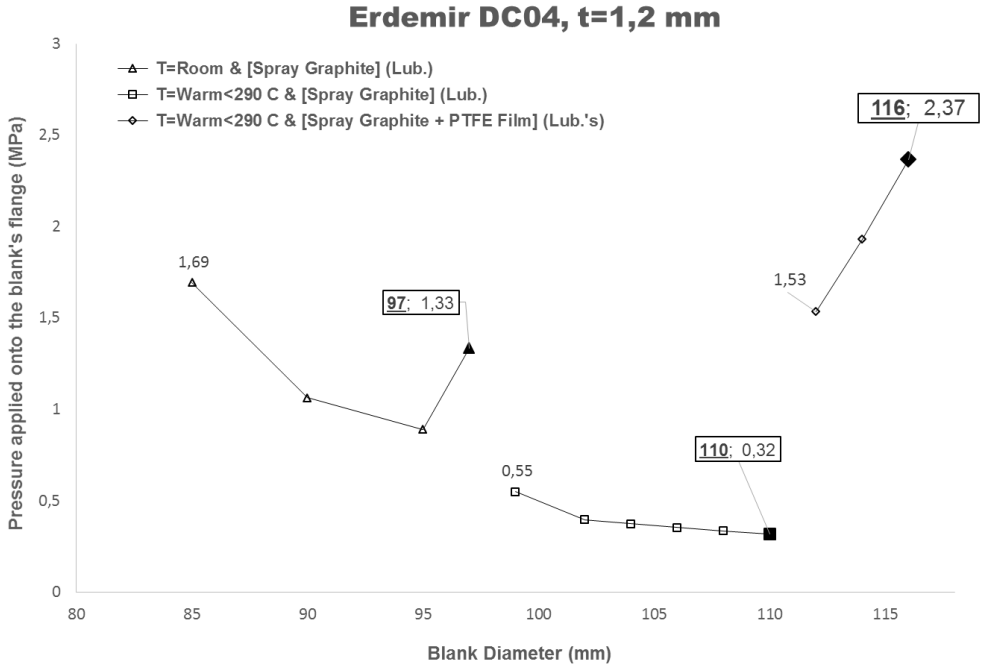

Figure C.9 The graph of the Blank Holder Pressure (MPa) applied to the blank's flange region vs its diameter (mm) for Erdemir DC04 (IF Steel), t = 1,2 mm.

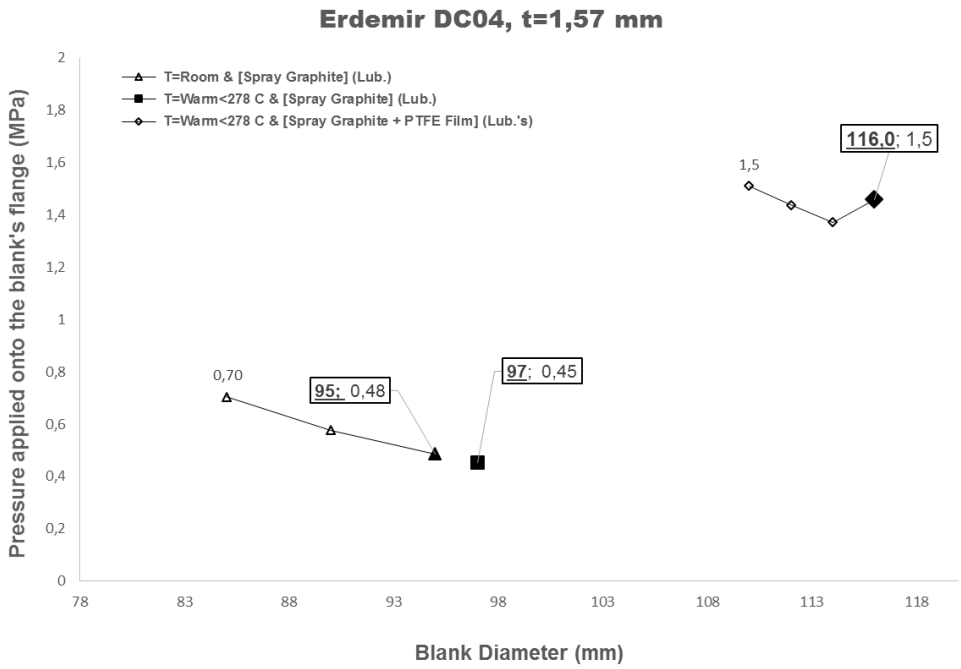

Figure C.10 The graph of the Blank Holder Pressure (MPa) applied to the blank's flange region vs its diameter (mm) for Erdemir DC04 (IF Steel), t = 1,57 mm.

C.2 The Punch Load vs Displacement

C.2.1 DP600 (Dual Phase)

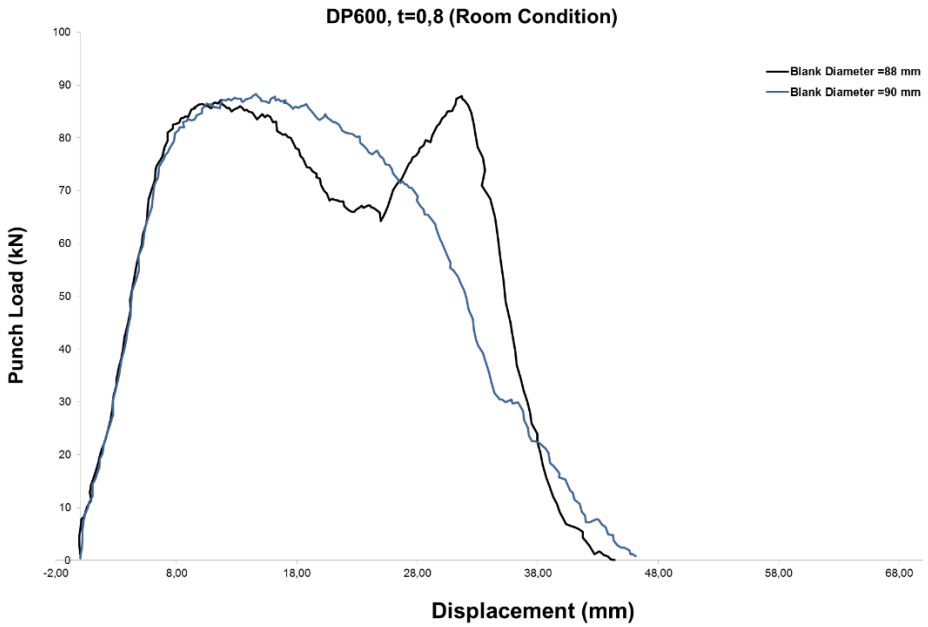

Figure C.11 For DP600 (Dual Phase), t = 0,8 mm, The Punch Load vs Displacement at Room Temperature.

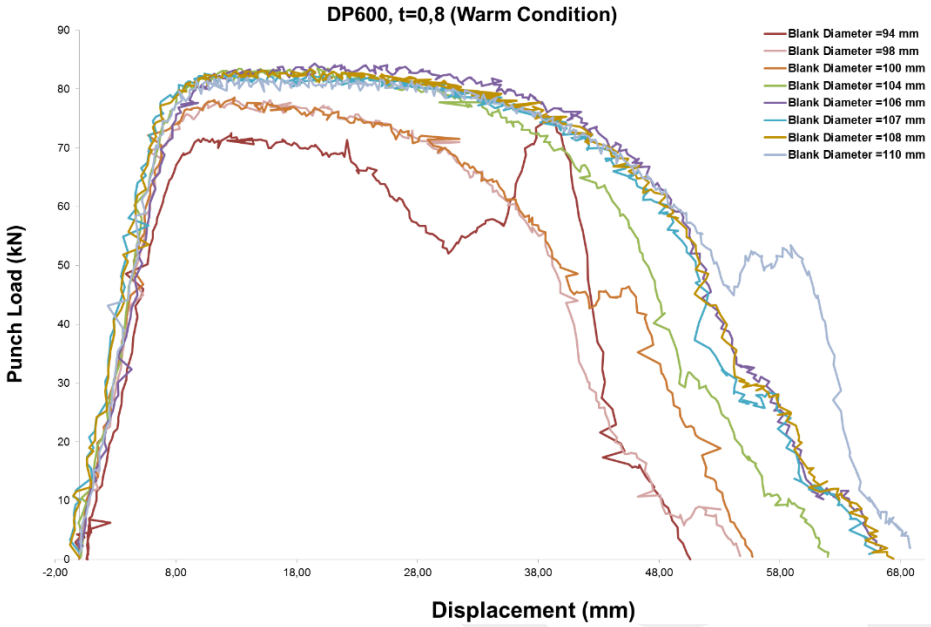

Figure C.12 For DP600 (Dual Phase), t = 0,8 mm, The Punch Load vs Displacement at the Warm Temperatures; T_{110mm}<310°C and T_{42mm}<210°C.

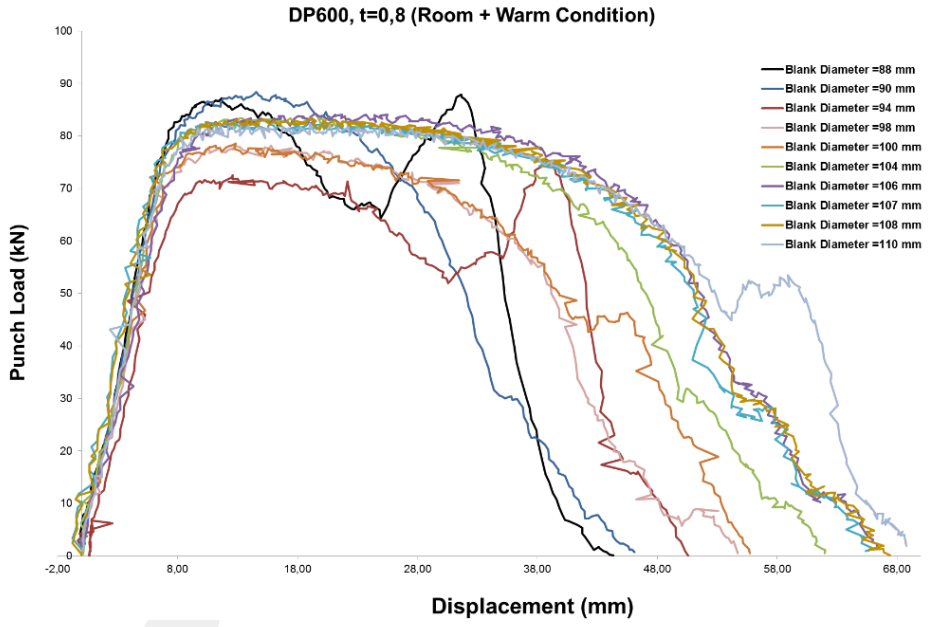

Figure C.13 For DP600 (Dual Phase), t = 0,8 mm, The graph of Punch Load vs Displacement at Room and Warm Conditions.

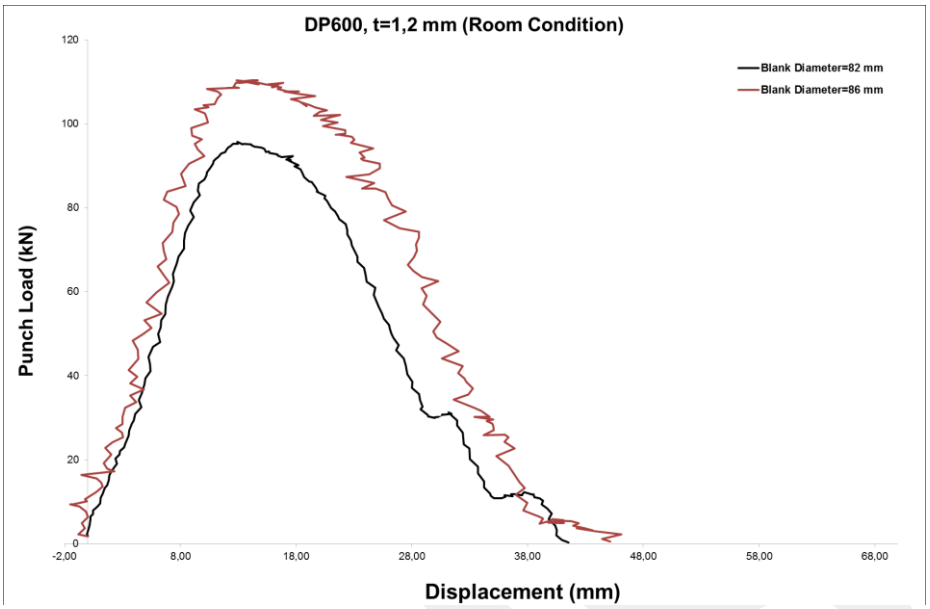

Figure C.14 For DP600 (Dual Phase), t = 1,2 mm, The Punch Load vs Displacement at Room Temperature.

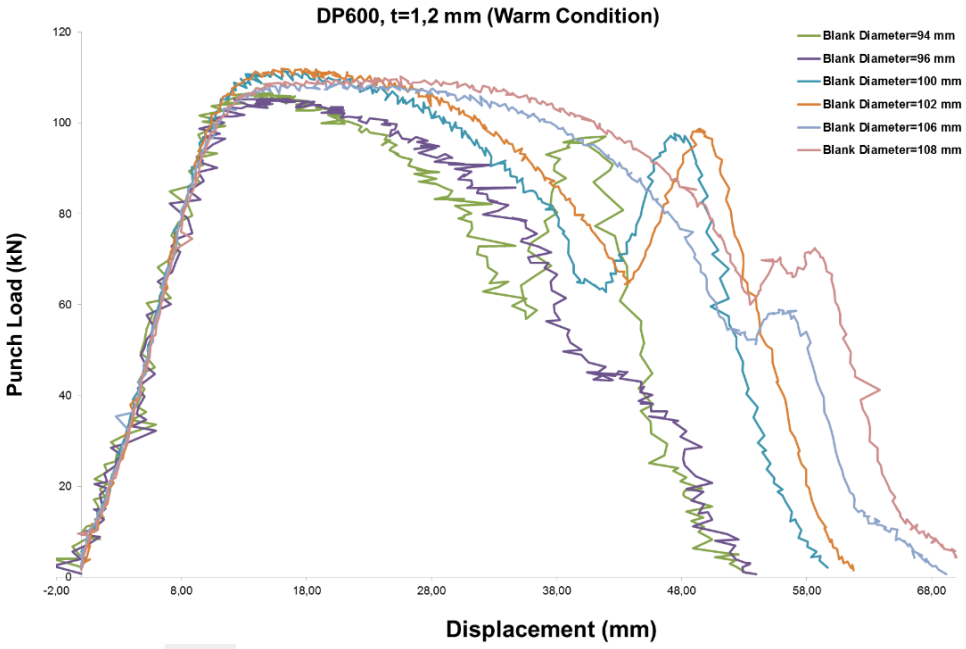

Figure C.15 For DP600 (Dual Phase), t = 1,2 mm, The Punch Load vs Displacement at the Warm Temperatures; T_{110mm}<295°C and T_{42mm}<195°C.

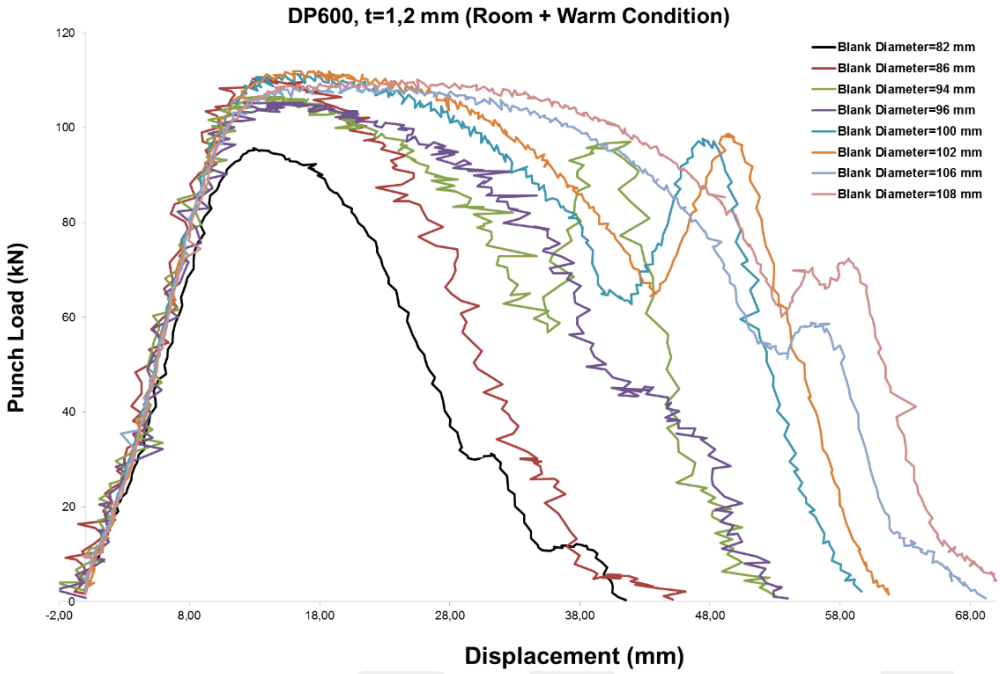

Figure C.16 For DP600 (Dual Phase), t = 1,2 mm, The graph of Punch Load vs Displacement at Room and Warm Conditions.

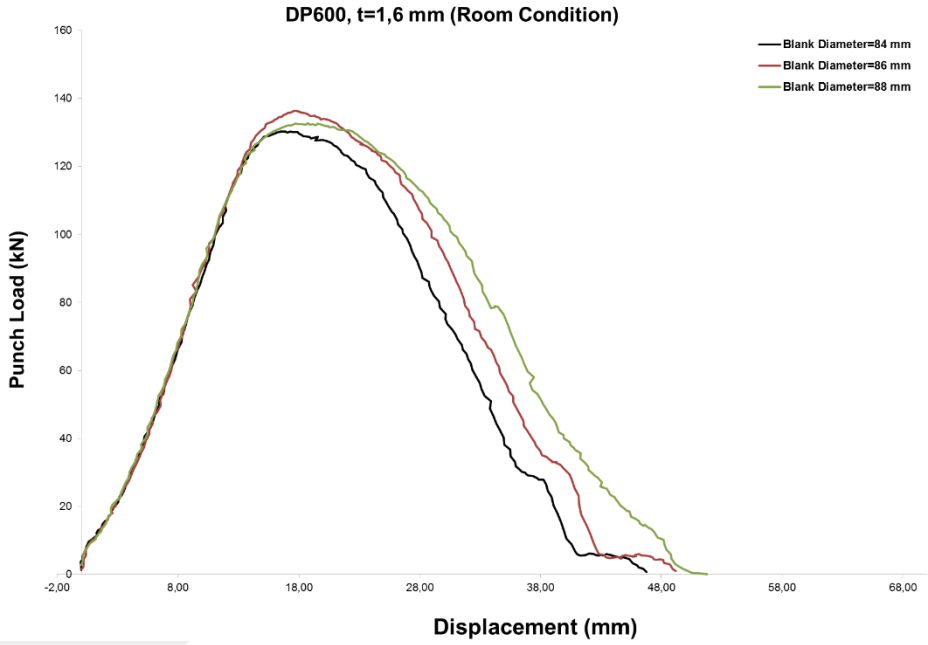

Figure C.17 For DP600 (Dual Phase), t = 1,6 mm, The Punch Load vs Displacement at Room Temperature.

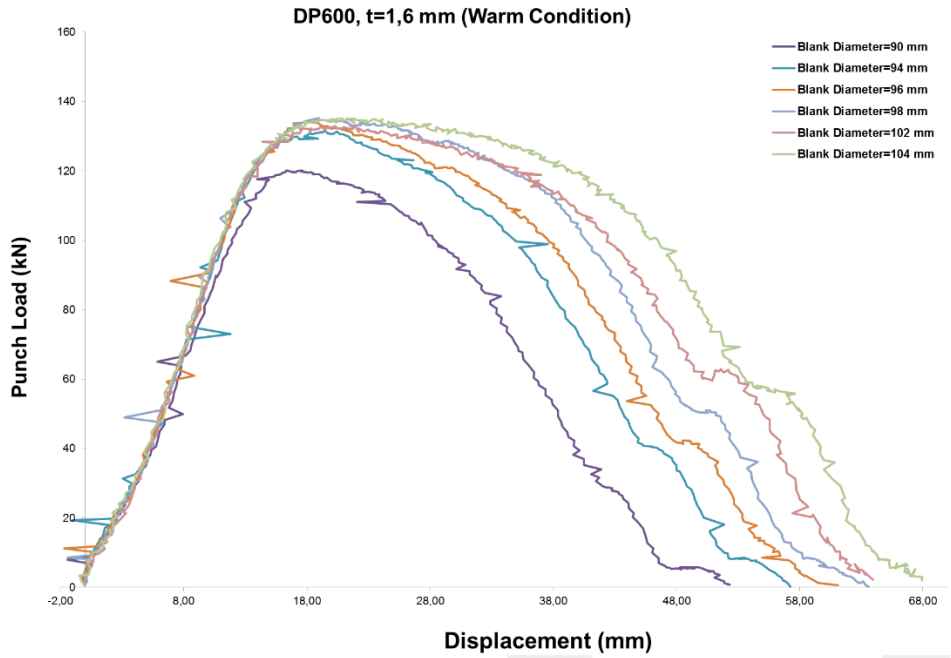

Figure C.18 For DP600 (Dual Phase), t = 1,6 mm, The Punch Load vs Displacement at the Warm Temperatures; T_{110mm}<300°C and T_{42mm}<225°C.

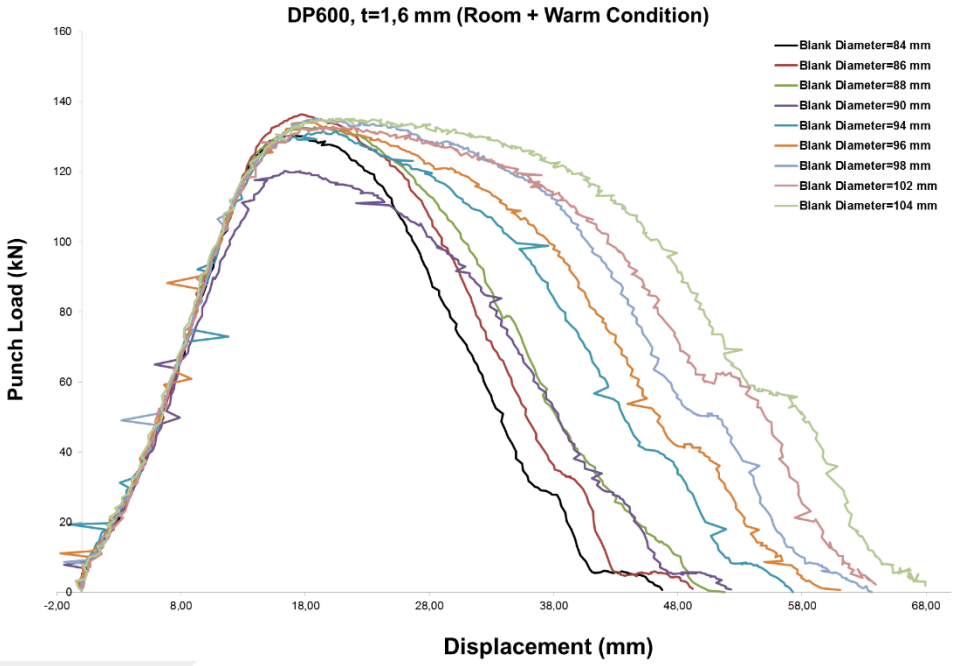

Figure C.19 For DP600 (Dual Phase), t = 1,6 mm, The graph of Punch Load vs Displacement at Room and Warm Conditions.

C.2.2 Erdemir 7128 (HSLA)

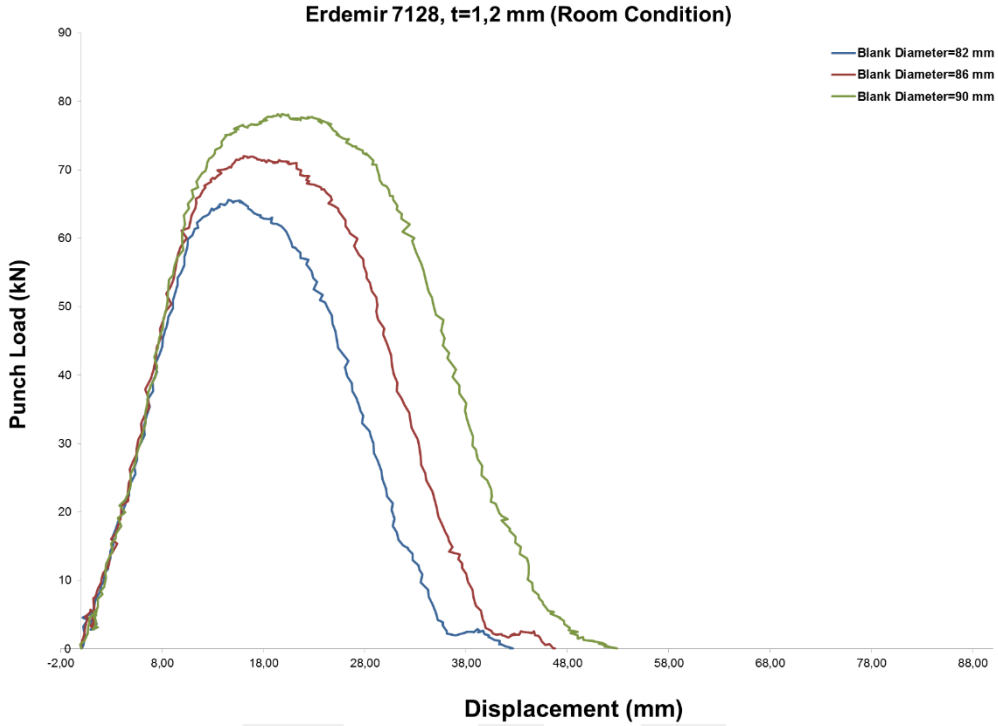

Figure C.20 For Erdemir 7128 (HSLA), t = 1,2 mm, The Punch Load vs Displacement at Room Temperature.

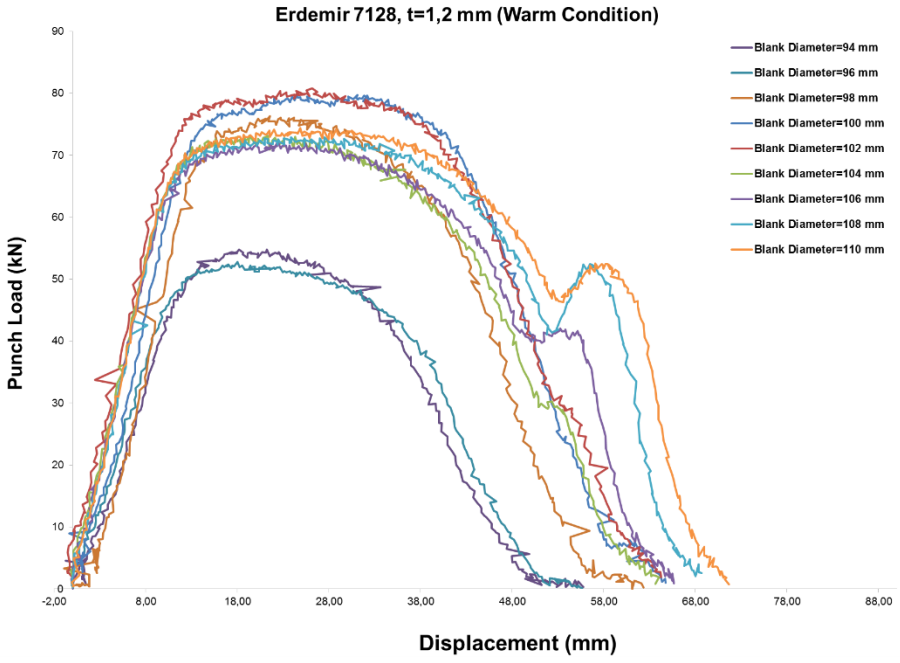

Figure C.21 For Erdemir 7128 (HSLA), t = 1,2 mm, The Punch Load vs Displacement at the Warm Temperatures; T_{110mm}<290°C and T_{42mm}<200°C.

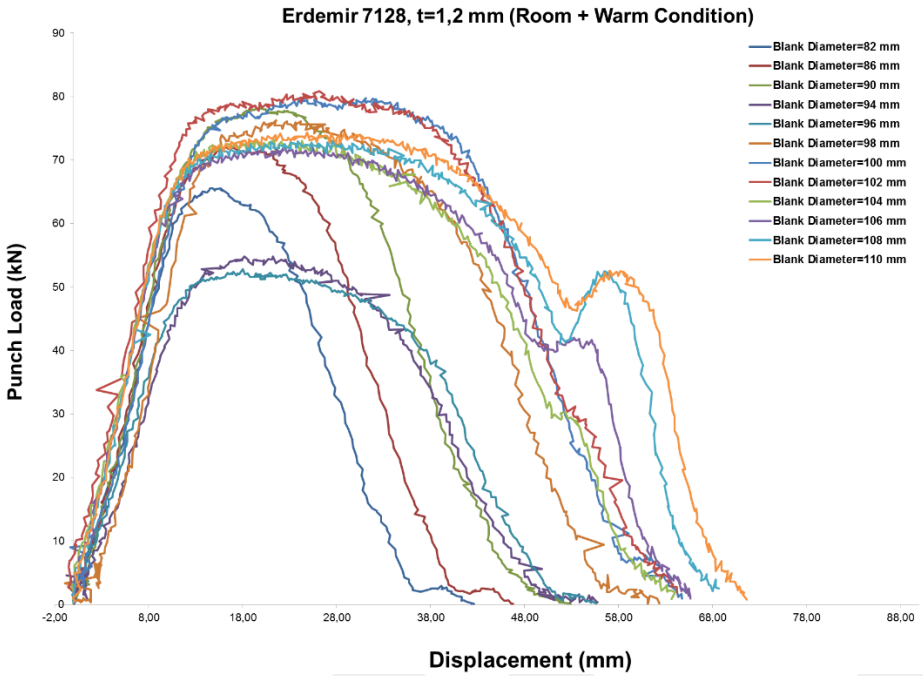

Figure C.22 For Erdemir 7128 (HSLA), t = 1,2 mm, The graph of Punch Load vs Displacement at Room and Warm Conditions.

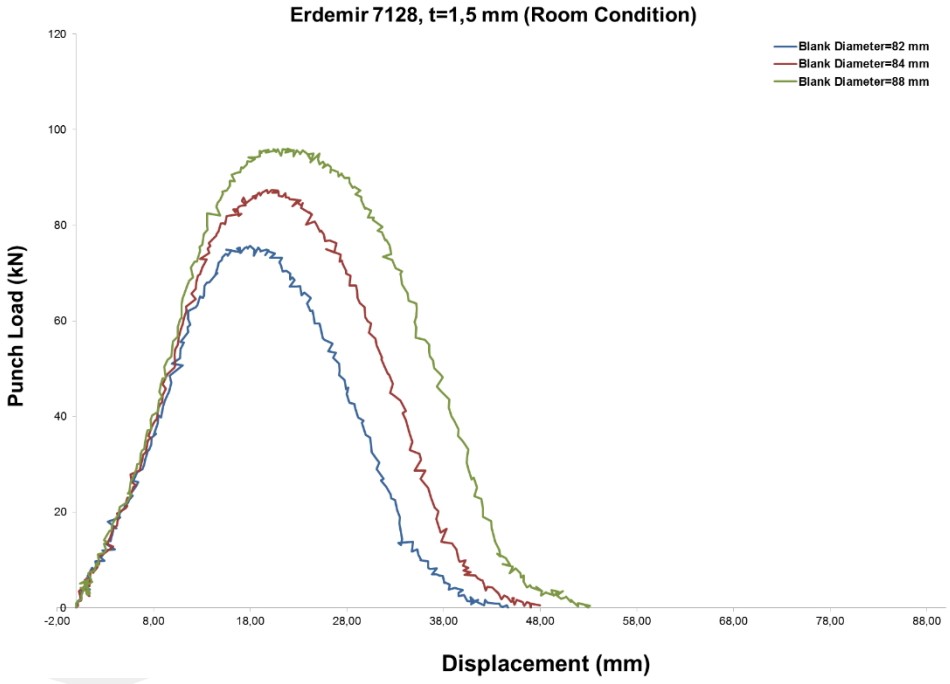

Figure C.23 For Erdemir 7128 (HSLA), t = 1,5 mm, The Punch Load vs Displacement at Room Temperature.

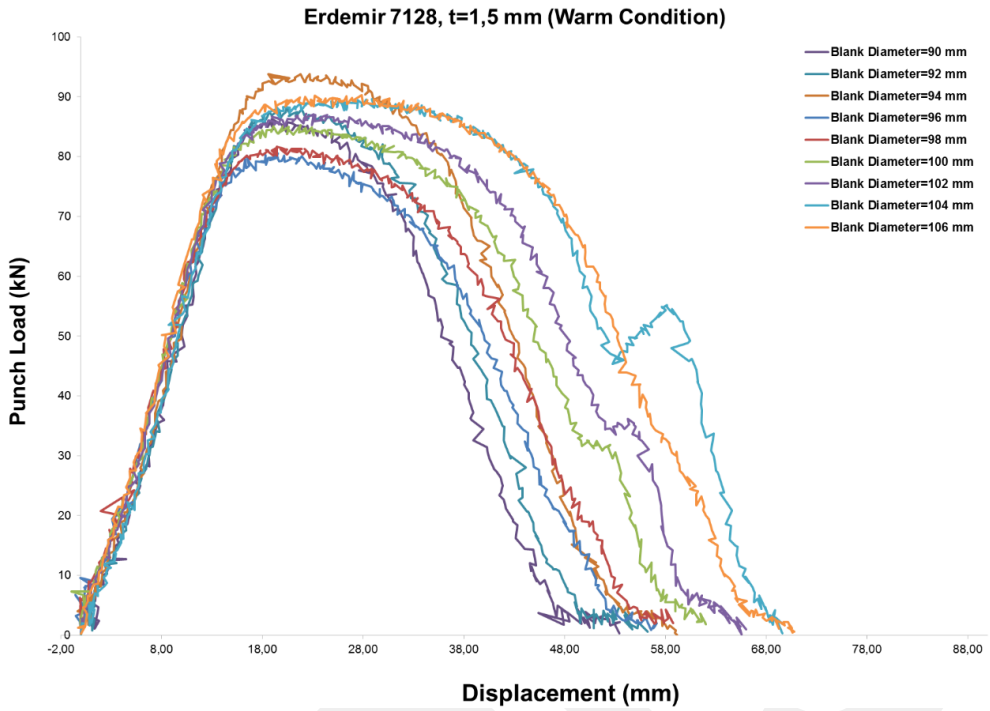

Figure C.24 For Erdemir 7128 (HSLA), t = 1,5 mm, The Punch Load vs Displacement at the Warm Temperatures; T_{110mm}<295°C and T_{42mm}<210°C.

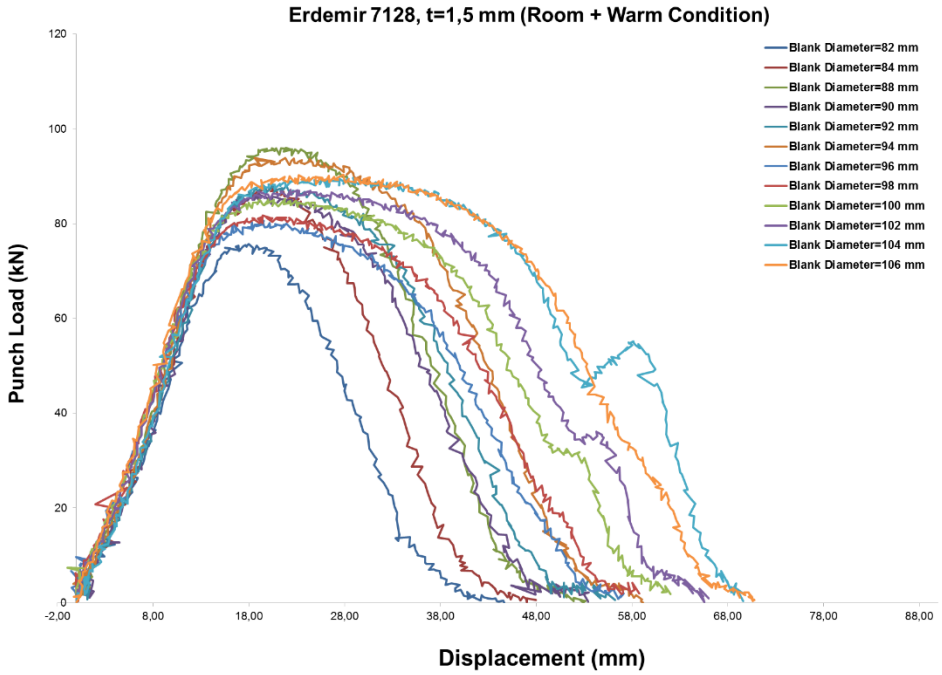

Figure C.25 For Erdemir 7128 (HSLA), t = 1,5 mm, The graph of Punch Load vs Displacement at Room and Warm conditions.

C.2.3 Erdemir 7140 (HSLA)

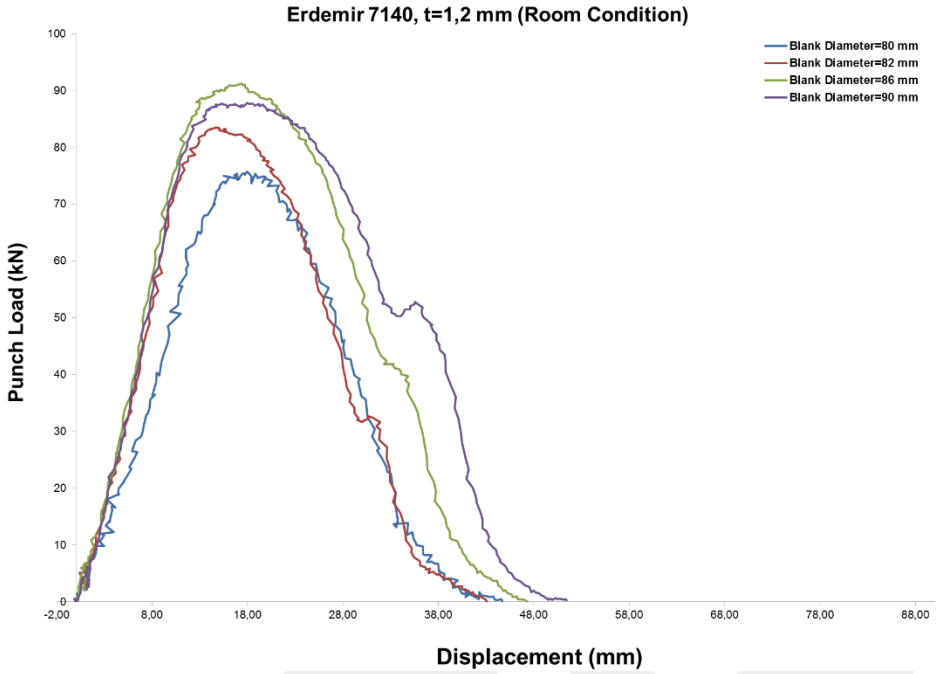

Figure C.26 For Erdemir 7140 (HSLA), t = 1,2 mm, The Punch Load vs Displacement at Room Temperature.

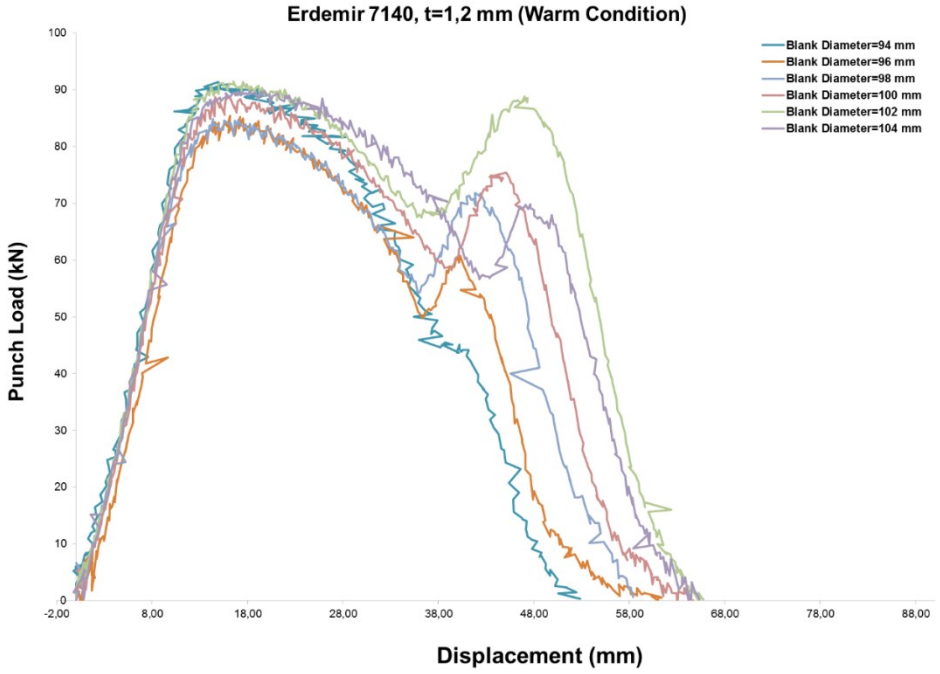

Figure C.27 For Erdemir 7140 (HSLA), t = 1,2 mm, The Punch Load vs Displacement at the Warm Temperatures; T_{110mm}<295°C and T_{42mm}<190°C.

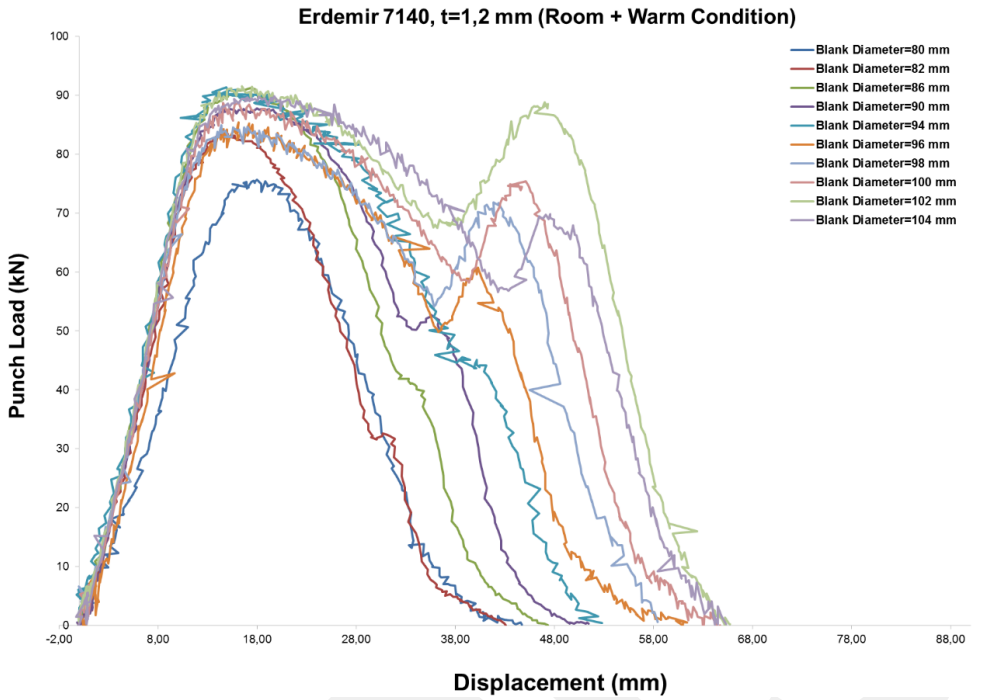

Figure C.28 For Erdemir 7140 (HSLA), t = 1,2 mm, The graph of Punch Load vs Displacement at Room and Warm Conditions.

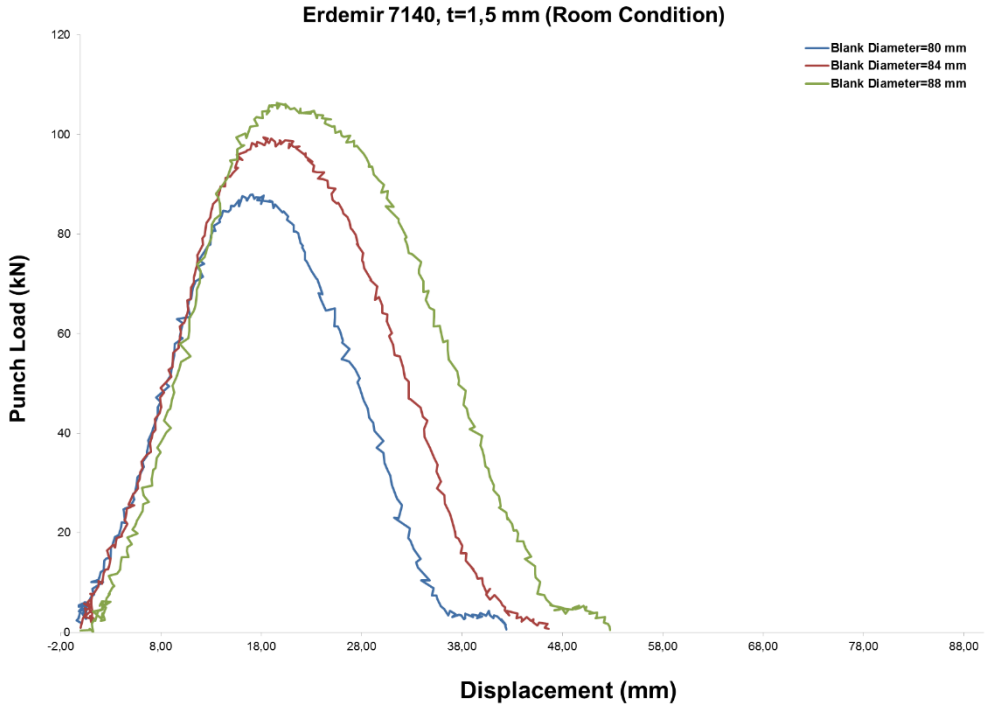

Figure C.29 For Erdemir 7140 (HSLA), t = 1,5 mm, The Punch Load vs Displacement at Room Temperature.

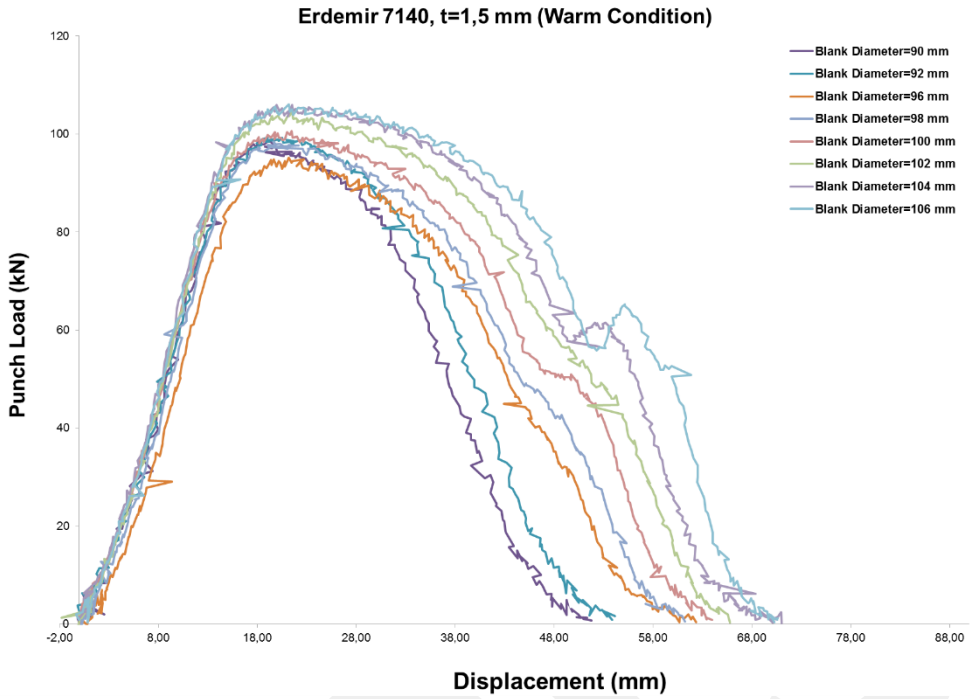

Figure C.30 For Erdemir 7140 (HSLA), t = 1,5 mm, The Punch Load vs Displacement at the Warm Temperatures; T_{110mm}<275°C and T_{42mm}<190°C.

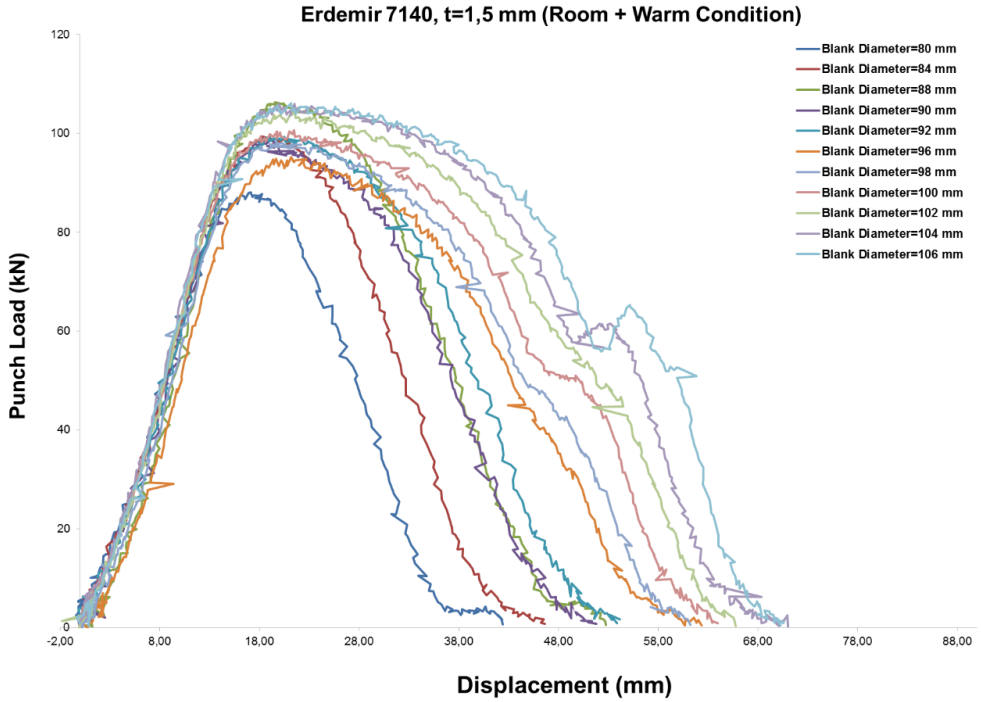

Figure C.31 For Erdemir 7140 (HSLA), t = 1,5 mm, The graph of Punch Load vs Displacement at Room and Warm conditions.

C.2.4 Erdemir DC04 (IF Steel)

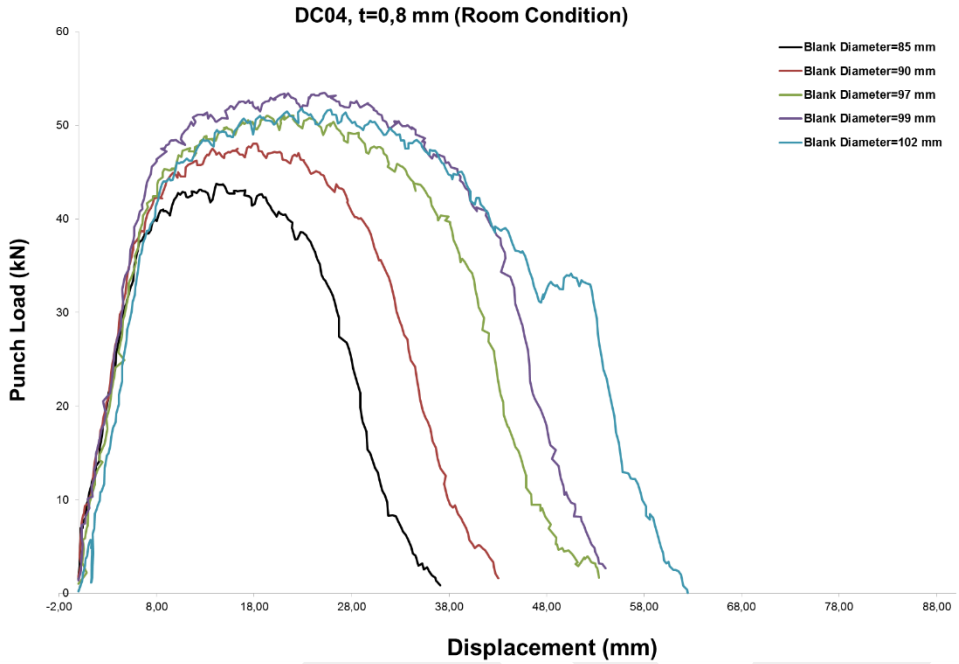

Figure C.32 For Erdemir DC04 (IF Steel), t = 0,8 mm, The Punch Load vs Displacement at Room Temperature.

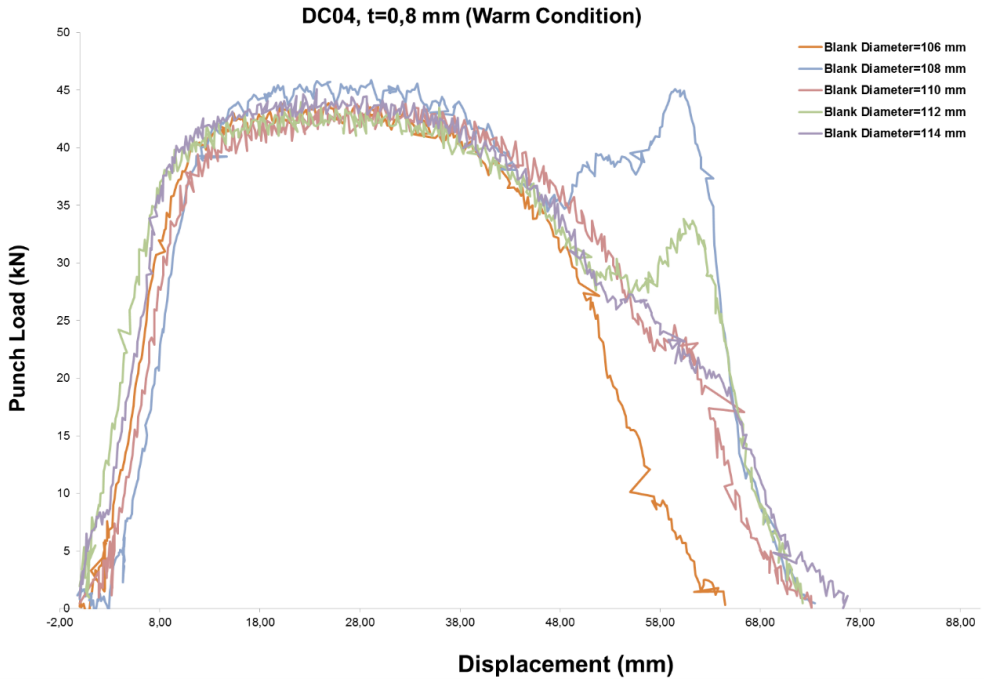

Figure C.33 For Erdemir DC04 (IF Steel), t = 0,8 mm, The Punch Load vs Displacement at the Warm Temperatures; T_{110mm}<305°C and T_{42mm}<210°C.

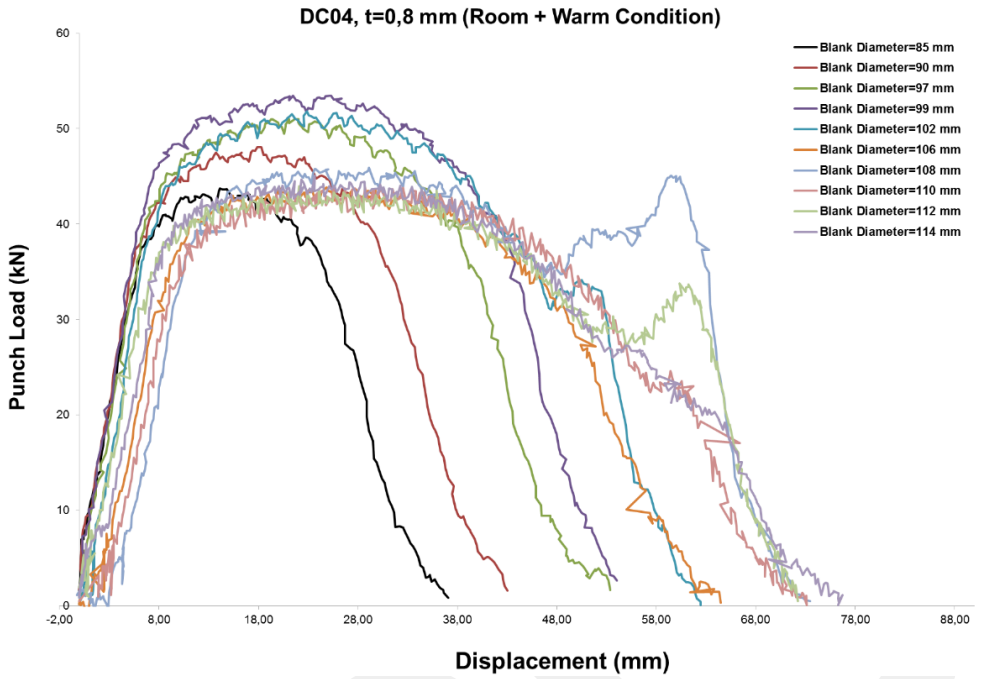

Figure C.34 For Erdemir DC04 (IF Steel), t = 0,8 mm, The graph of Punch Load vs Displacement at Room and Warm Conditions.

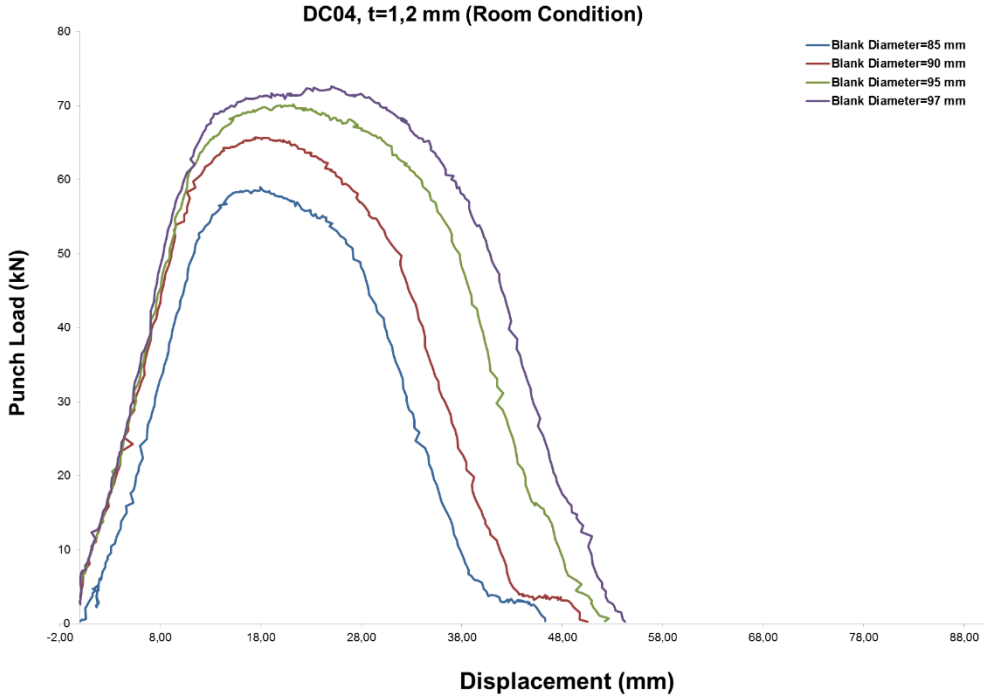

Figure C.35 For Erdemir DC04 (IF Steel), t = 1,2 mm, The Punch Load vs Displacement at Room Temperature.

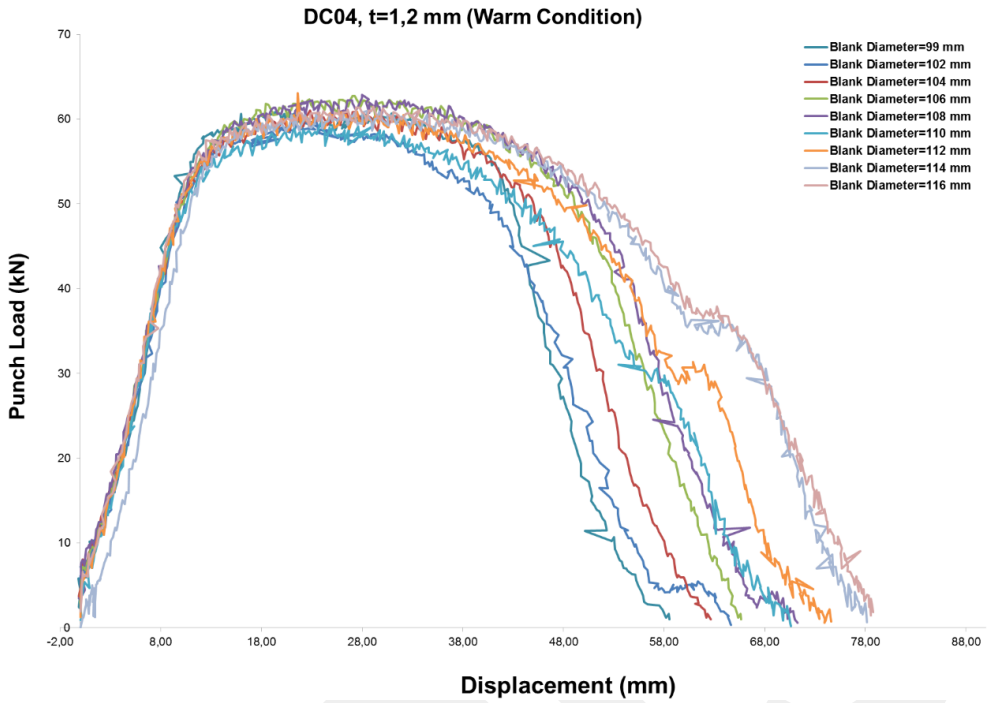

Figure C.36 For Erdemir DC04 (IF Steel), t = 1,2 mm, The Punch Load vs Displacement at the Warm Temperatures; T_{110mm}<290°C and T_{42mm}<195°C.

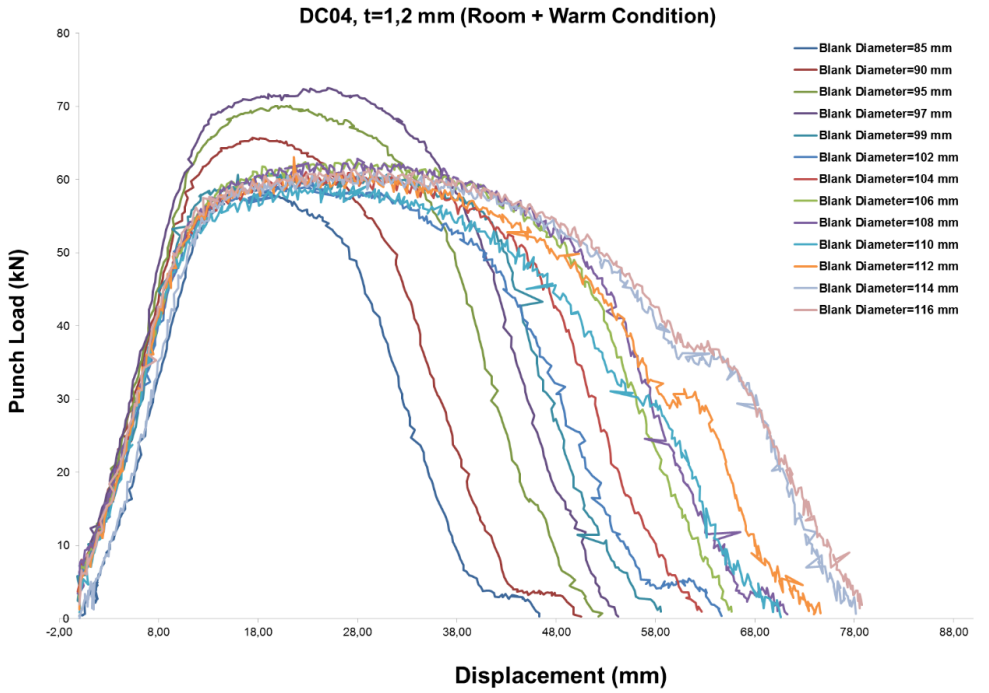

Figure C.37 For Erdemir DC04 (IF Steel), t = 1,2 mm, The graph of Punch Load vs Displacement at Room and Warm Conditions.

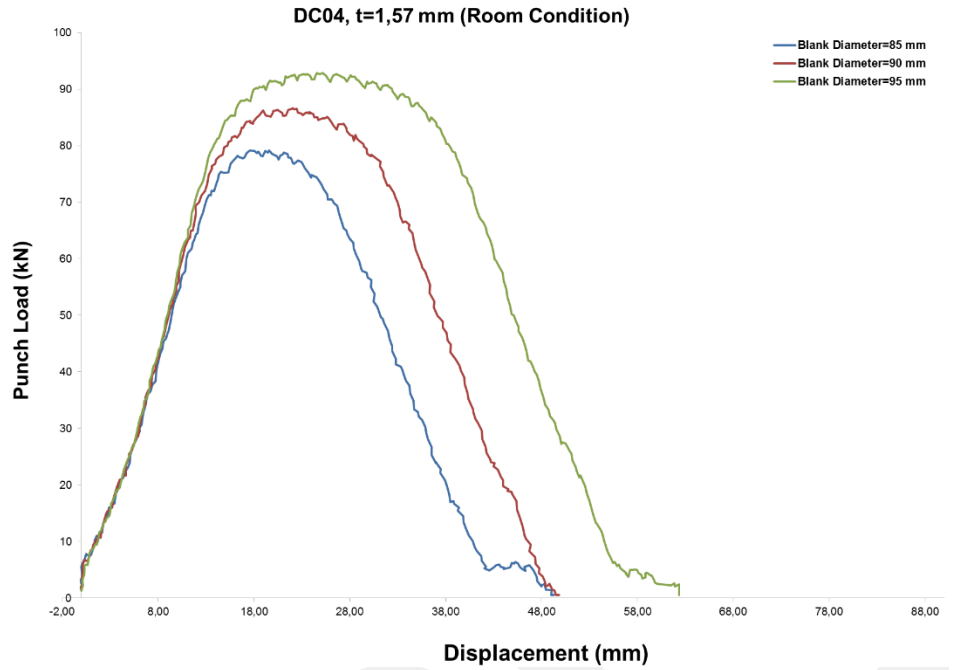

Figure C.38 For Erdemir DC04 (IF Steel), t = 1,57 mm, The Punch Load vs Displacement at Room Temperature.

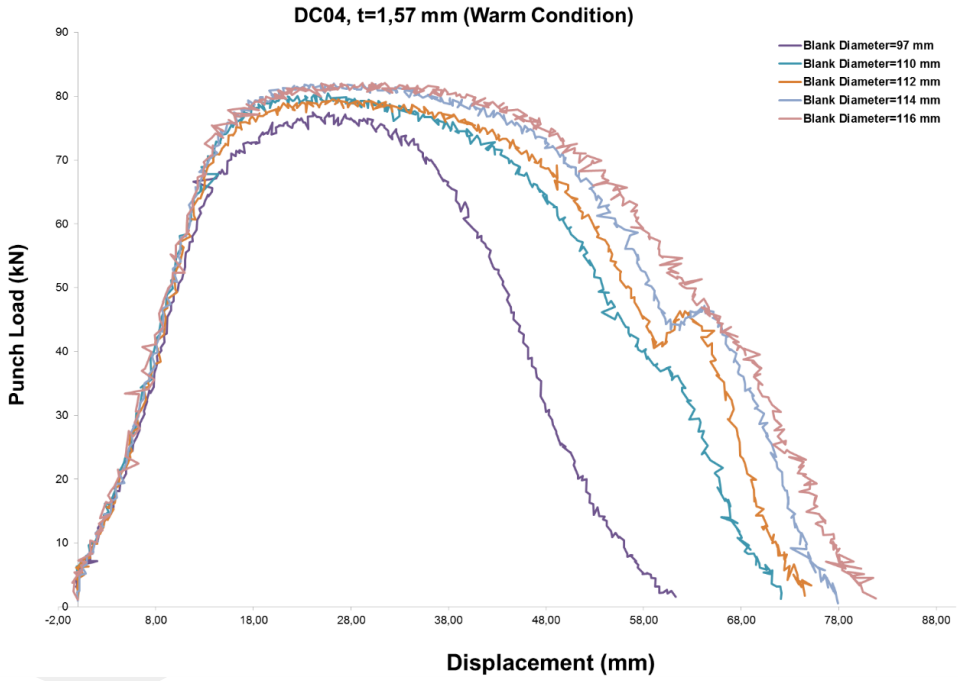

Figure C.39 For Erdemir DC04 (IF Steel), t = 1,57 mm, The Punch Load vs Displacement at the Warm Temperatures; T_{110mm}<278°C and T_{42mm}<195°C.

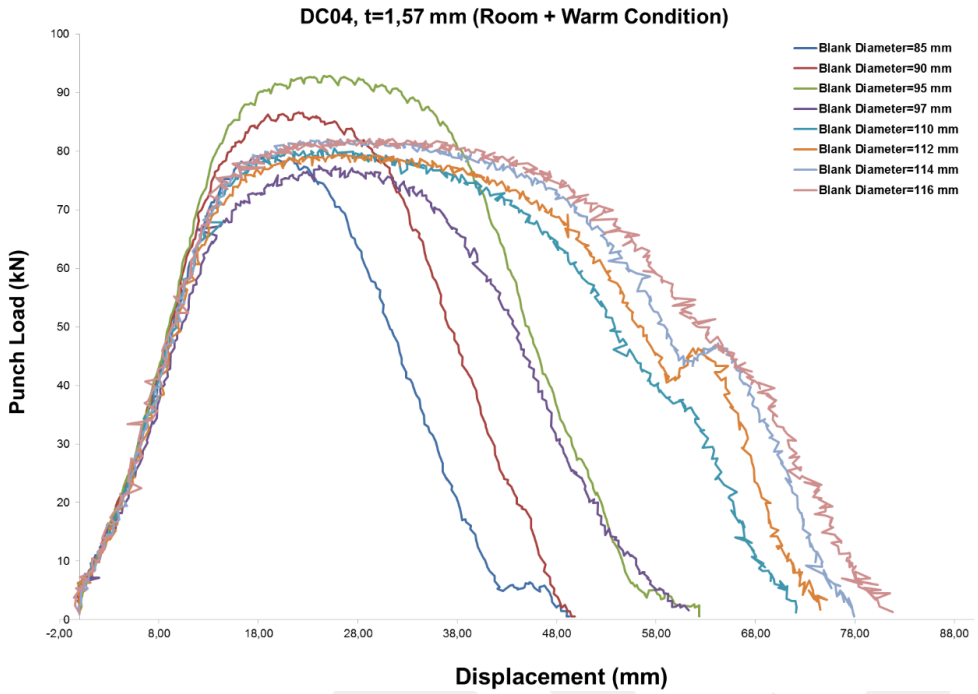

Figure C.40 For Erdemir DC04 (IF Steel), t = 1,57 mm, The graph of Punch Load vs Displacement at Room and Warm Conditions.

C.3 The Changes in the Limiting Drawing Ratio and blank diameters accordingly

C.3.1 DP600 (Dual Phase)

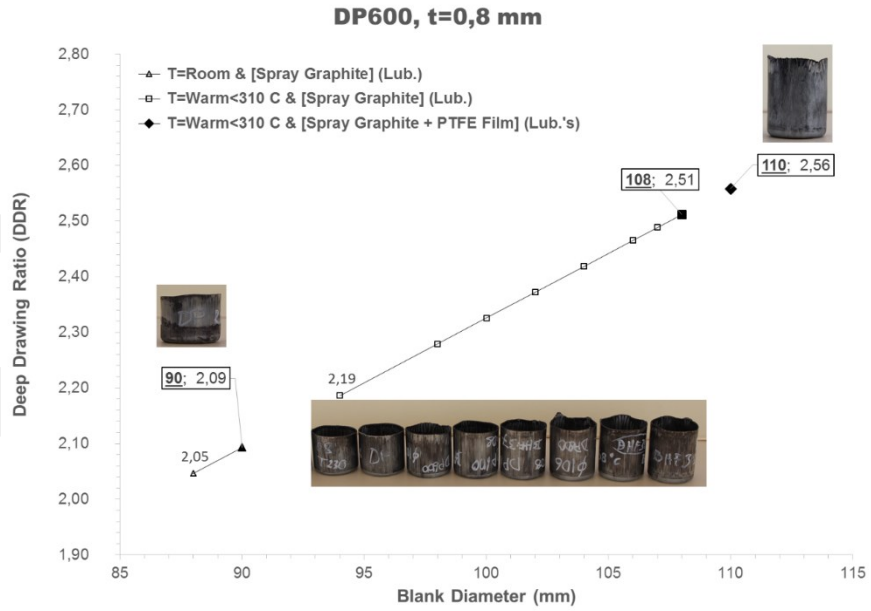

Figure C.41 For DP600 (Dual Phase), t = 0,8 mm; The graph showing the Deep Drawing Ratio (DDR) vs Blank Diameter (mm) at Room and Warm Conditions by using various lubricants (Spray Graphite and PTFE Film)

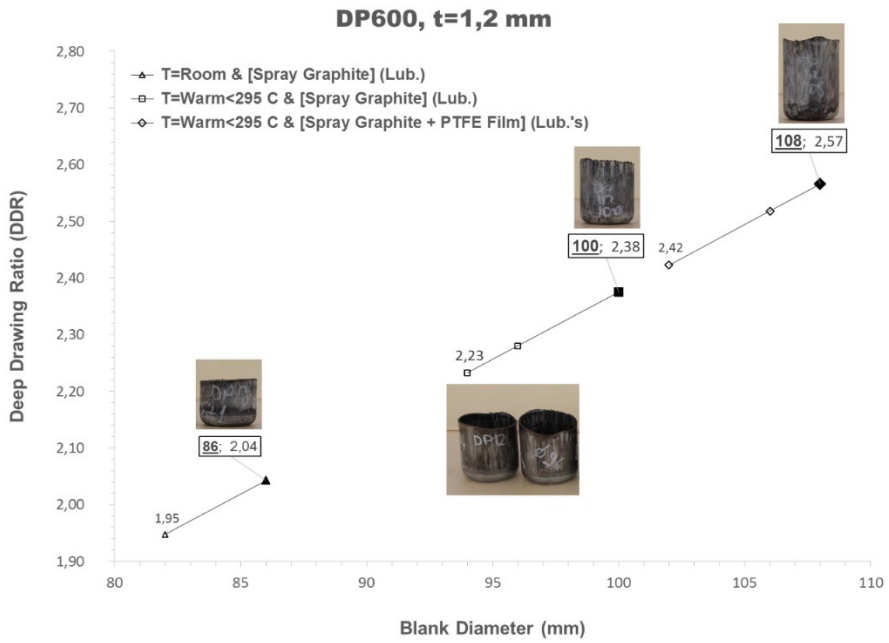

Figure C.42 For DP600 (Dual Phase), t = 1,2 mm; The graph showing the Deep Drawing Ratio (DDR) vs Blank Diameter (mm) at Room and Warm Conditions by using various lubricants (Spray Graphite and PTFE Film).

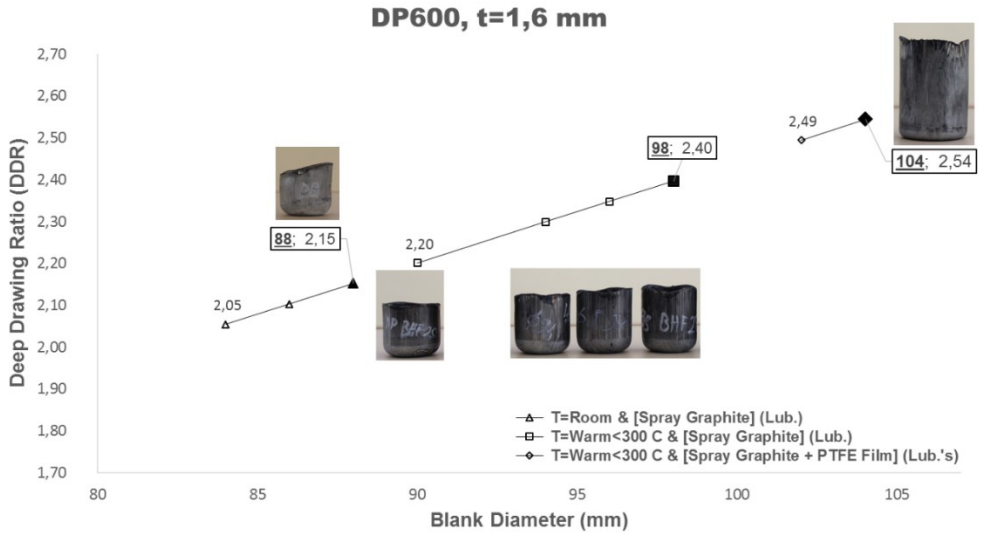

Figure C.43 For DP600 (Dual Phase), t = 1,6 mm; The graph showing the Deep Drawing Ratio (DDR) vs Blank Diameter (mm) at Room and Warm Conditions by using various lubricants (Spray Graphite and PTFE Film)

C.3.2 Erdemir 7128 (HSLA)

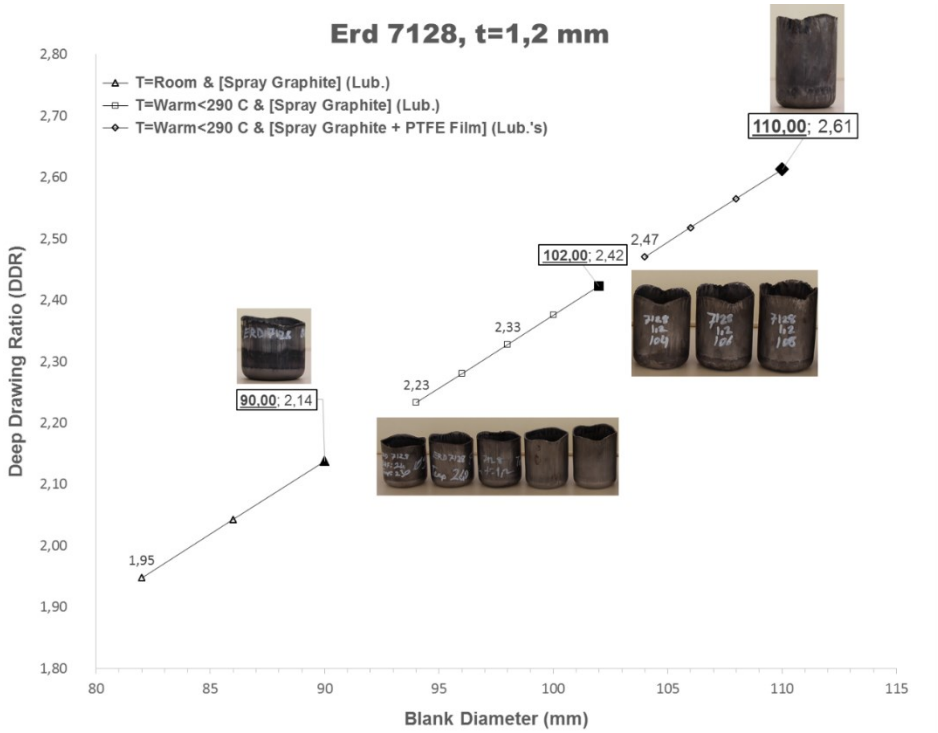

Figure C.44 For Erdemir 7128 (HSLA), t = 1,2 mm; The graph showing the Deep Drawing Ratio (DDR) vs Blank Diameter (mm) at Room and Warm Conditions by using various lubricants (Spray Graphite and PTFE Film)

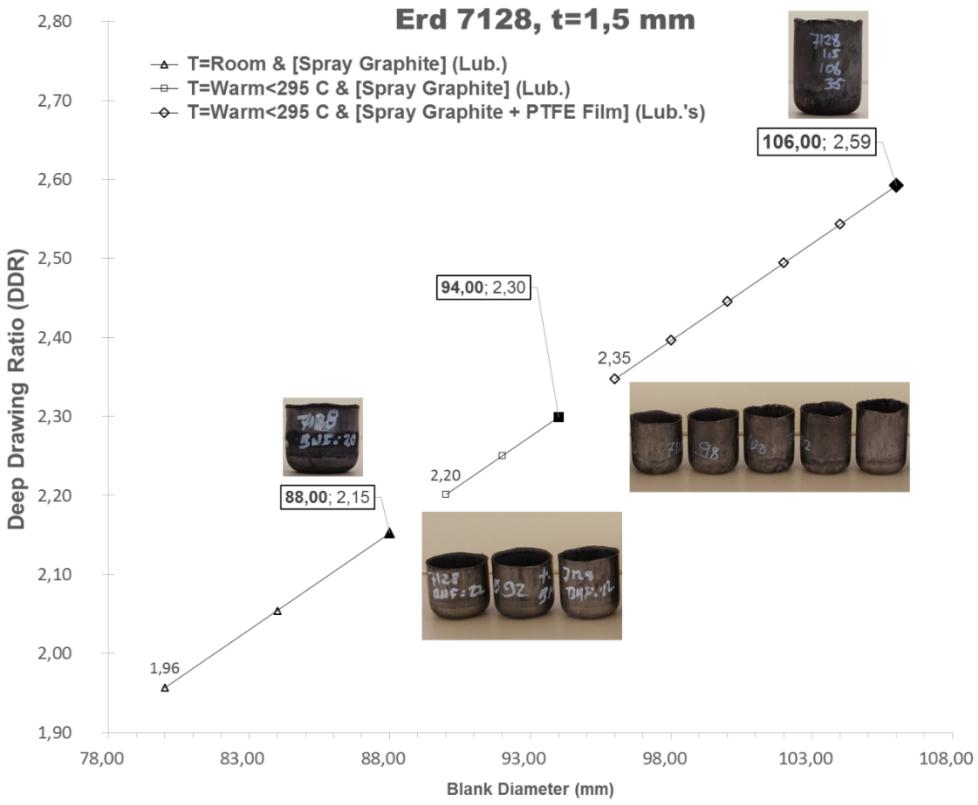

Figure C.45 For Erdemir 7128 (HSLA), t = 1,5 mm; The graph showing the Deep Drawing Ratio (DDR) vs Blank Diameter (mm) at Room and Warm Conditions by using various lubricants (Spray Graphite and PTFE Film)

C.3.3 Erdemir 7140 (HSLA)

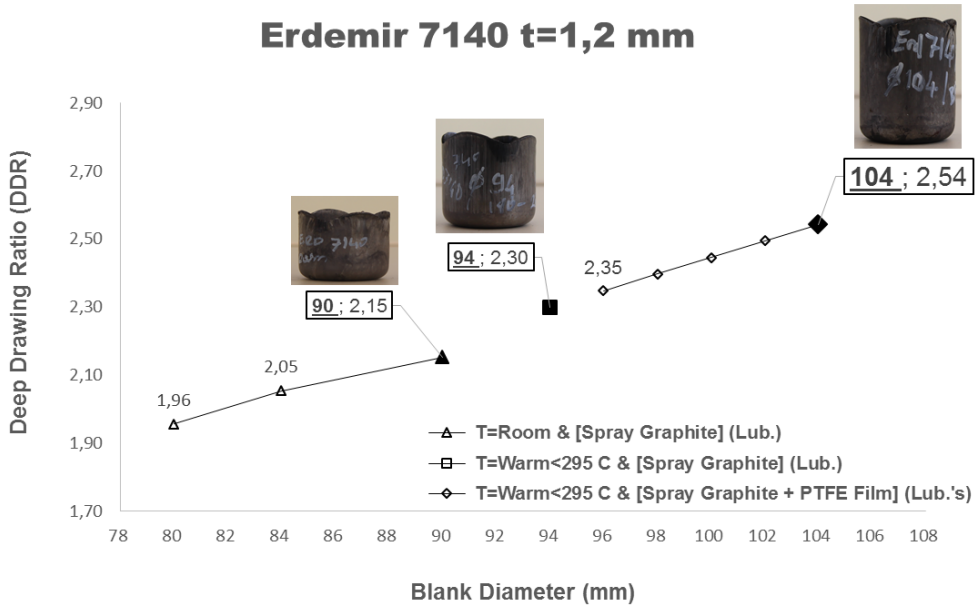

Figure C.46 For Erdemir 7140 (HSLA), t = 1,2 mm; The graph showing the Deep Drawing Ratio (DDR) vs Blank Diameter (mm) at Room and Warm Conditions by using various lubricants (Spray Graphite and PTFE Film)

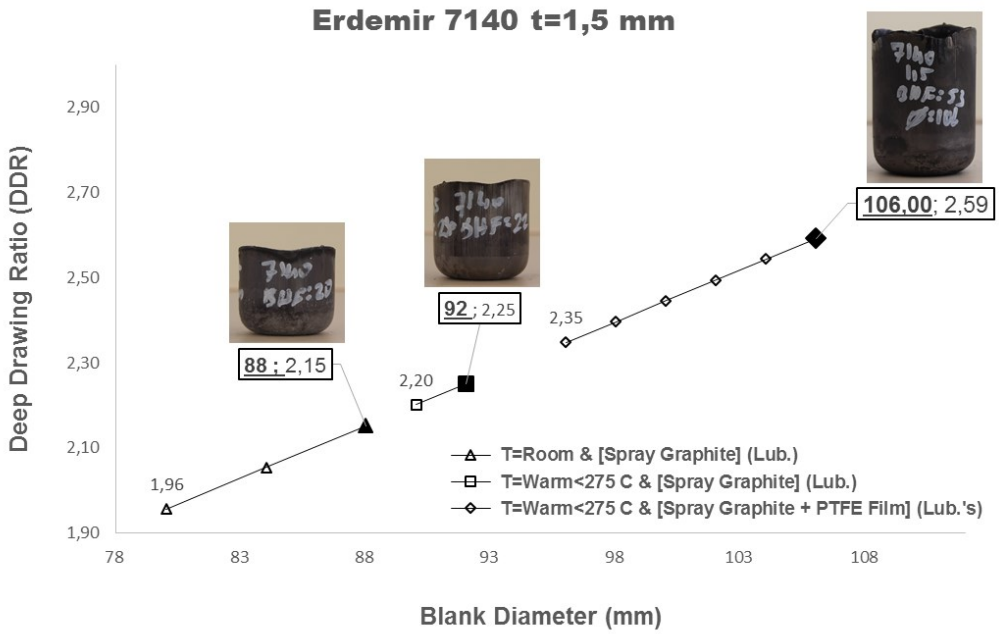

Figure C.47 For Erdemir 7140 (HSLA), t = 1,5 mm; The graph showing the Deep Drawing Ratio (DDR) vs Blank Diameter (mm) at Room and Warm Conditions by using various lubricants (Spray Graphite and PTFE Film)

C.3.4 Erdemir DC04 (IF Steel)

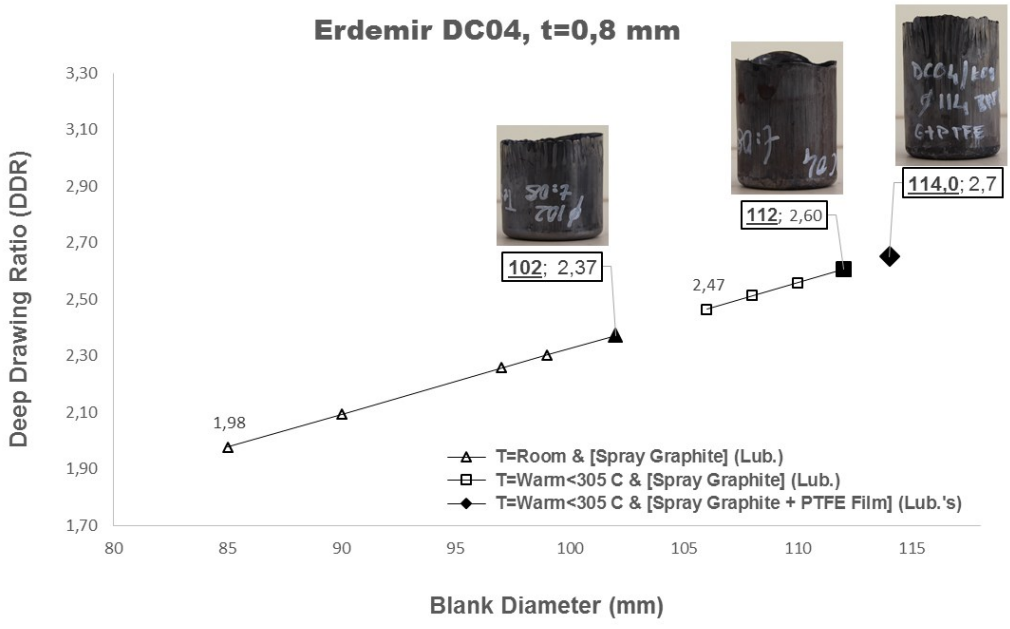

Figure C.48 For Erdemir DC04 (IF Steel), t = 0,8 mm; The graph showing the Deep Drawing Ratio (DDR) vs Blank Diameter (mm) at Room and Warm Conditions by using various lubricants (Spray Graphite and PTFE Film)

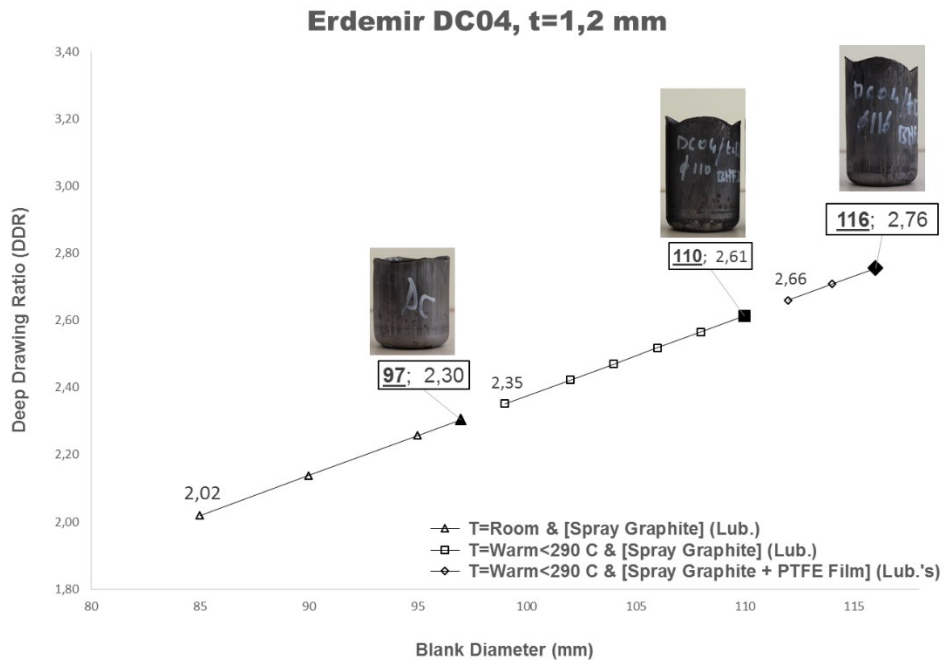

Figure C.49 For Erdemir DC04 (IF Steel), t = 1,2 mm; The graph showing the Deep Drawing Ratio (DDR) vs Blank Diameter (mm) at Room and Warm Conditions by using various lubricants (Spray Graphite and PTFE Film)

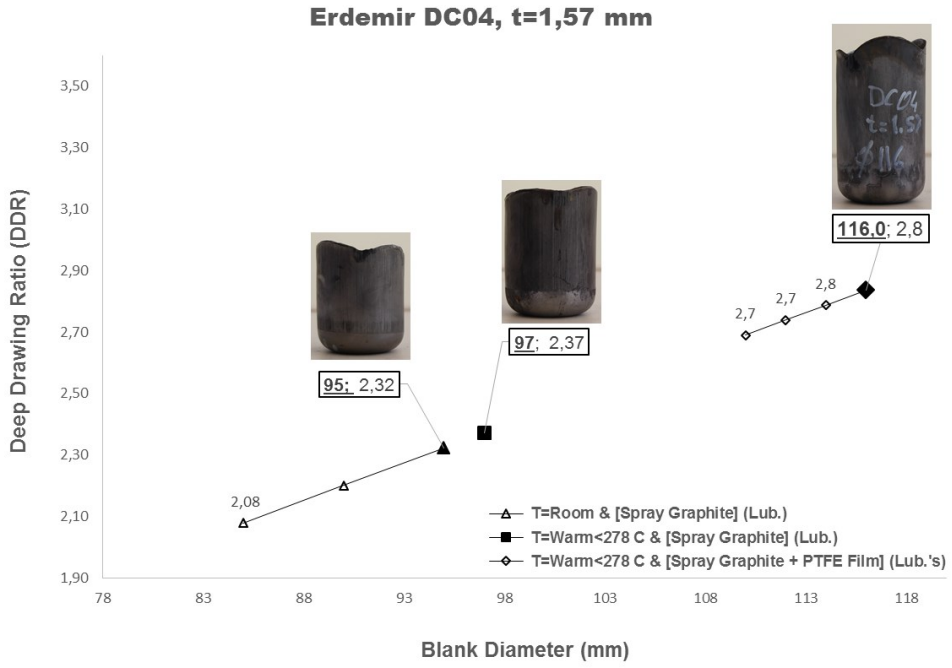

Figure C.50 For Erdemir DC04 (IF Steel), t = 1,57 mm; The graph showing the Deep Drawing Ratio (DDR) vs Blank Diameter (mm) at Room and Warm Conditions by using various lubricants (Spray Graphite and PTFE Film)

C.4 The Changes in the Maximum Punch Load with respect to blank diameters

C.4.1 DP600 (Dual Phase)

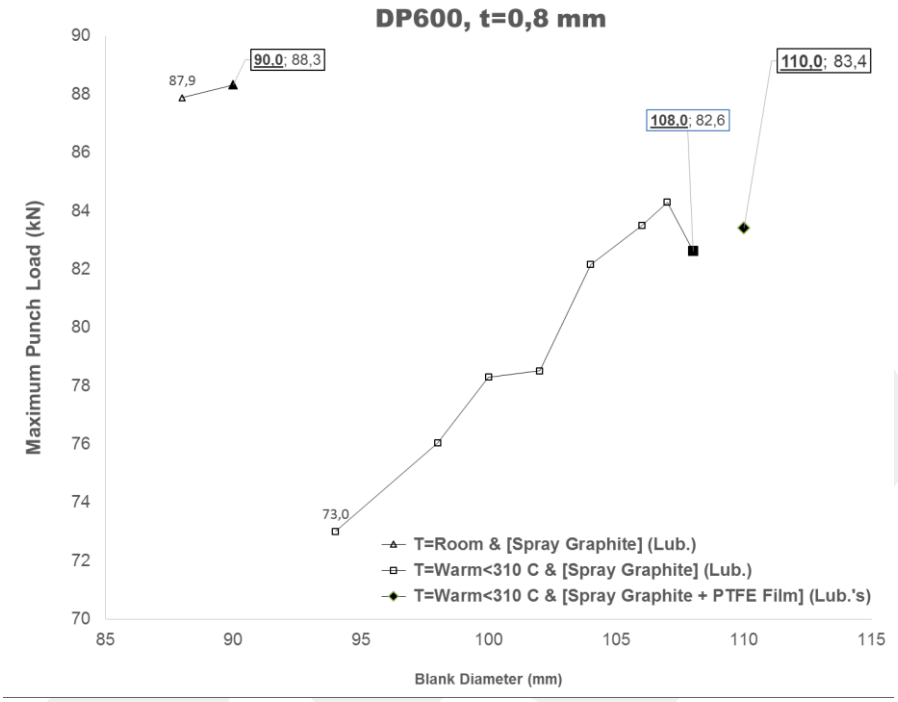

Figure C.51 The resultant Blank Holder Force (BHF) vs blank Diameter (mm) graph with the application of various temperatures and lubricants, for DP600 and t = 0,8 mm.

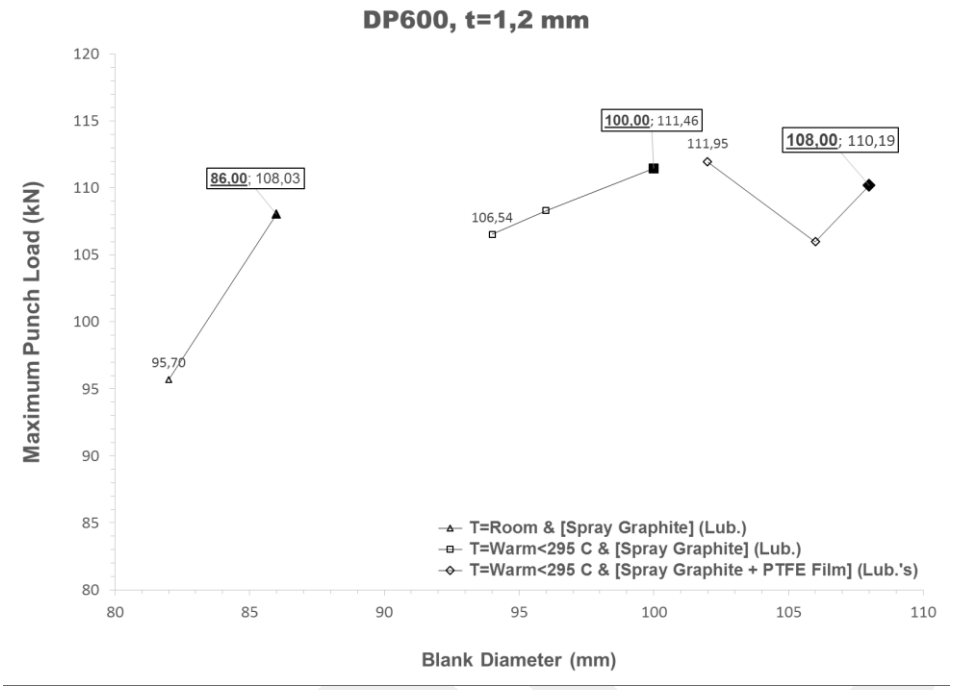

Figure C.52 The resultant Blank Holder Force (BHF) vs blank Diameter (mm) graph with the application of various temperatures and lubricants, for DP600 and t = 1,2 mm.

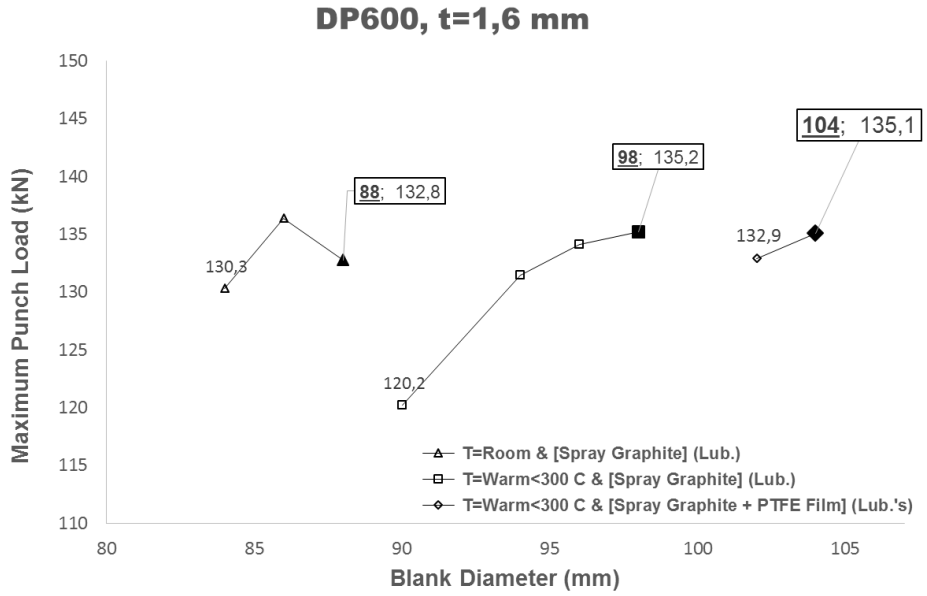

Figure C.53 The resultant Blank Holder Force (BHF) vs blank Diameter (mm) graph with the application of various temperatures and lubricants, for DP600 and t = 1,6 mm.

C.4.2 Erdemir 7128 (HSLA)

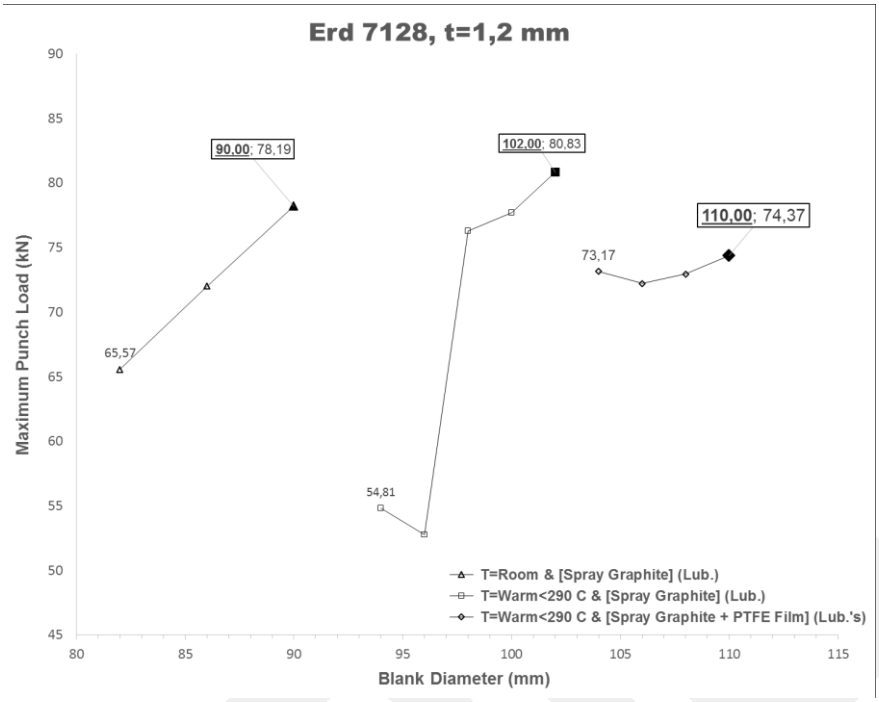

Figure C.54 The resultant Blank Holder Force (BHF) vs blank Diameter (mm) graph with the application of various temperatures and lubricants, for Erd7128 and t = 1,2 mm.

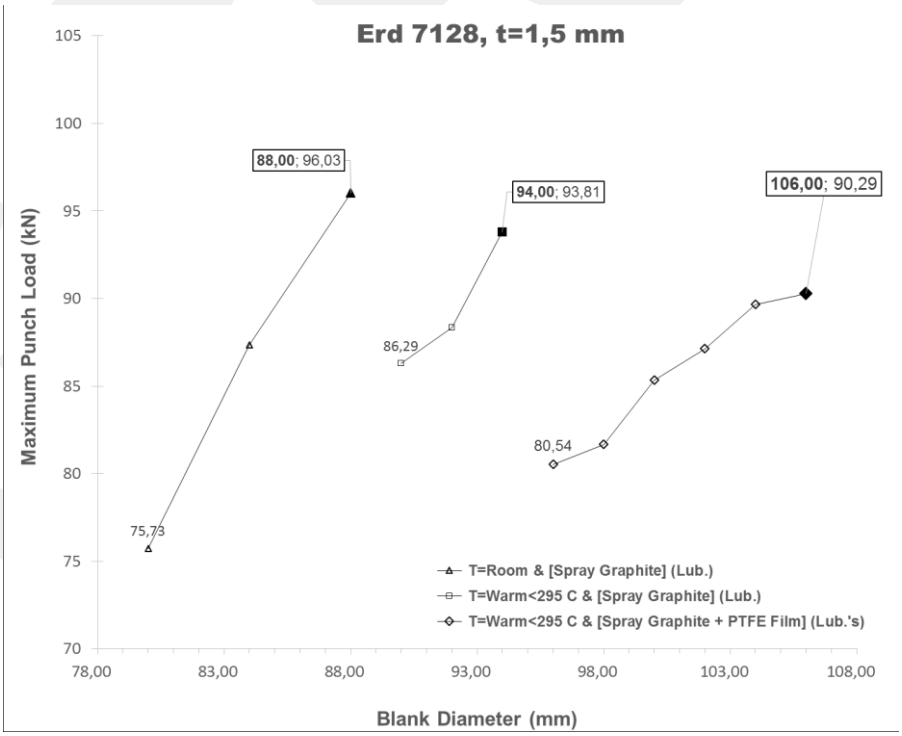

Figure C.55 The resultant Blank Holder Force (BHF) vs blank Diameter (mm) graph with the application of various temperatures and lubricants, for Erd7128 and t = 1,5 mm.

C.4.3 Erdemir 7140 (HSLA)

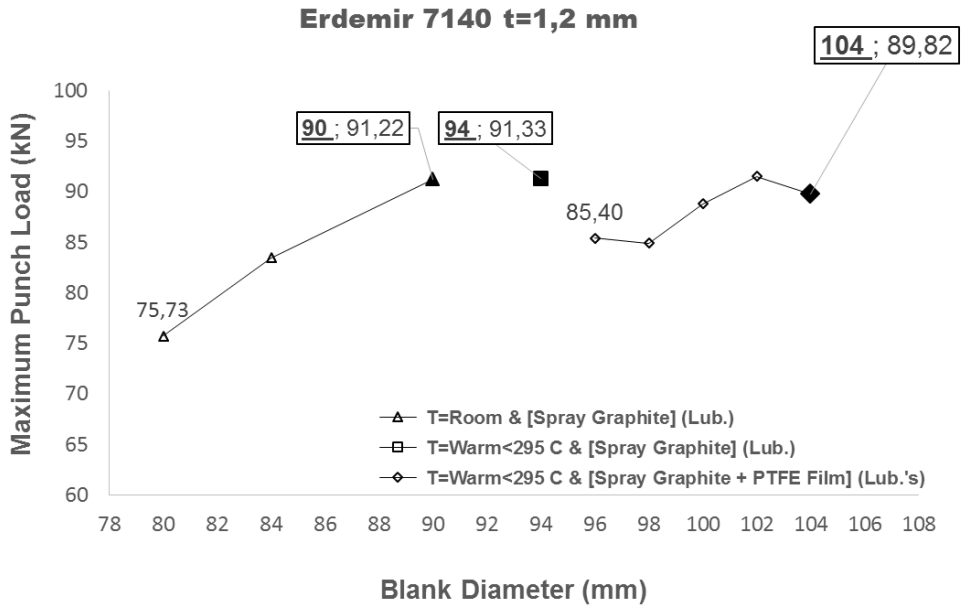

Figure C.56 The resultant Blank Holder Force (BHF) vs blank Diameter (mm) graph with the application of various temperatures and lubricants, for Erd7140 and t = 1,2 mm.

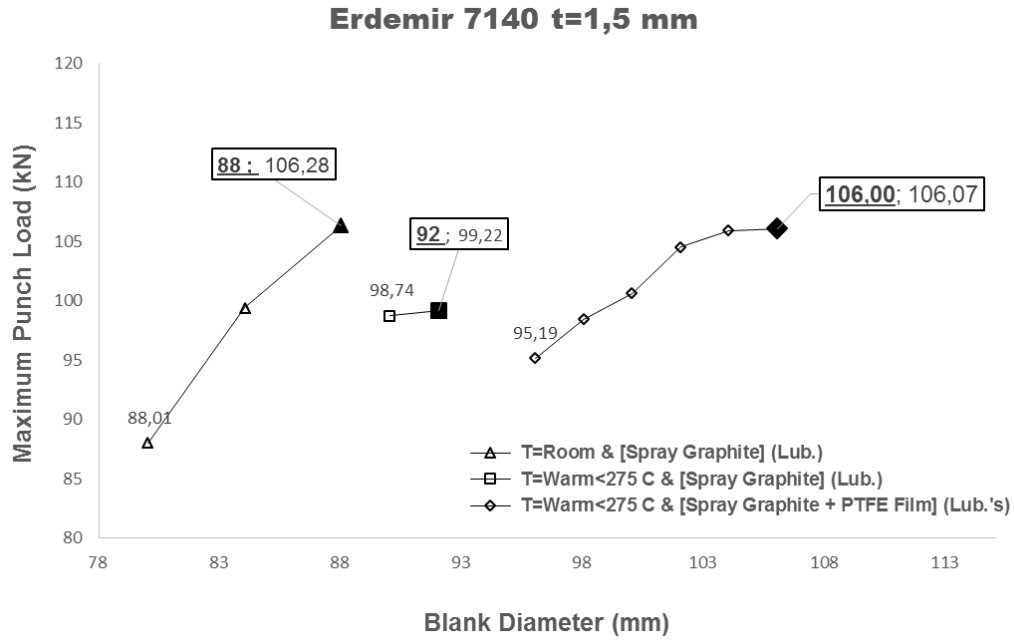

Figure C.57 The resultant Blank Holder Force (BHF) vs blank Diameter (mm) graph with the application of various temperatures and lubricants, for Erd7140 and t = 1,5 mm.

C.4.4 Erdemir DC04 (IF Steel)

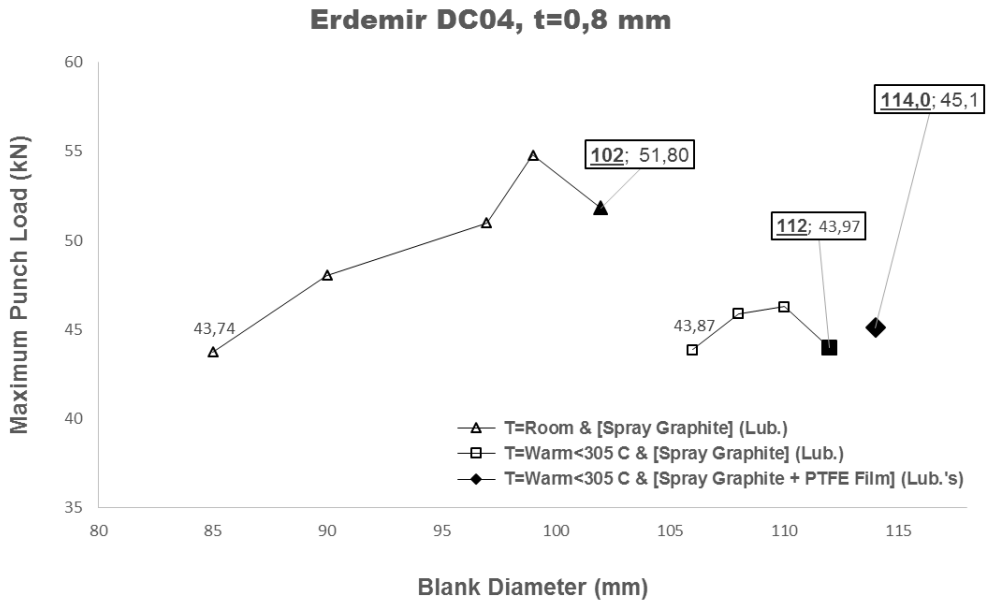

Figure C.58 The resultant Blank Holder Force (BHF) vs blank Diameter (mm) graph with the application of various temperatures and lubricants, for DC04 and t = 0,8 mm.

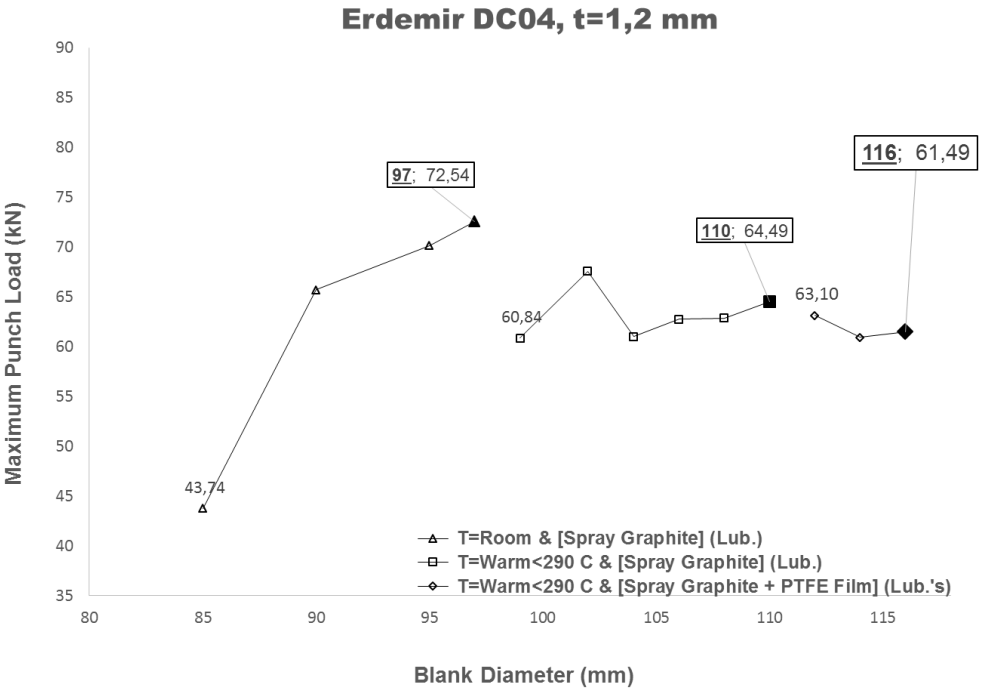

Figure C.59 The resultant Blank Holder Force (BHF) vs blank Diameter (mm) graph with the application of various temperatures and lubricants, for DC04 and t = 1,2 mm.

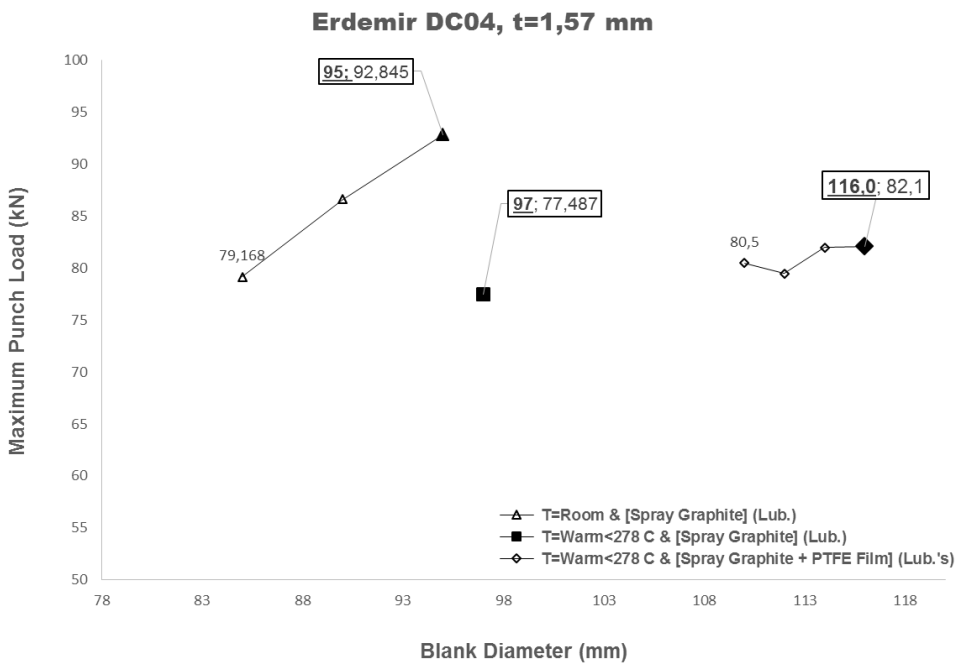

Figure C.60 The resultant Blank Holder Force (BHF) vs blank Diameter (mm) graph with the application of various temperatures and lubricants, for DC04 and t = 1,57 mm.

C.5 The Changes in the Blank Holder Force (BHF) vs blank diameter

C.5.1 DP600 (Dual Phase)

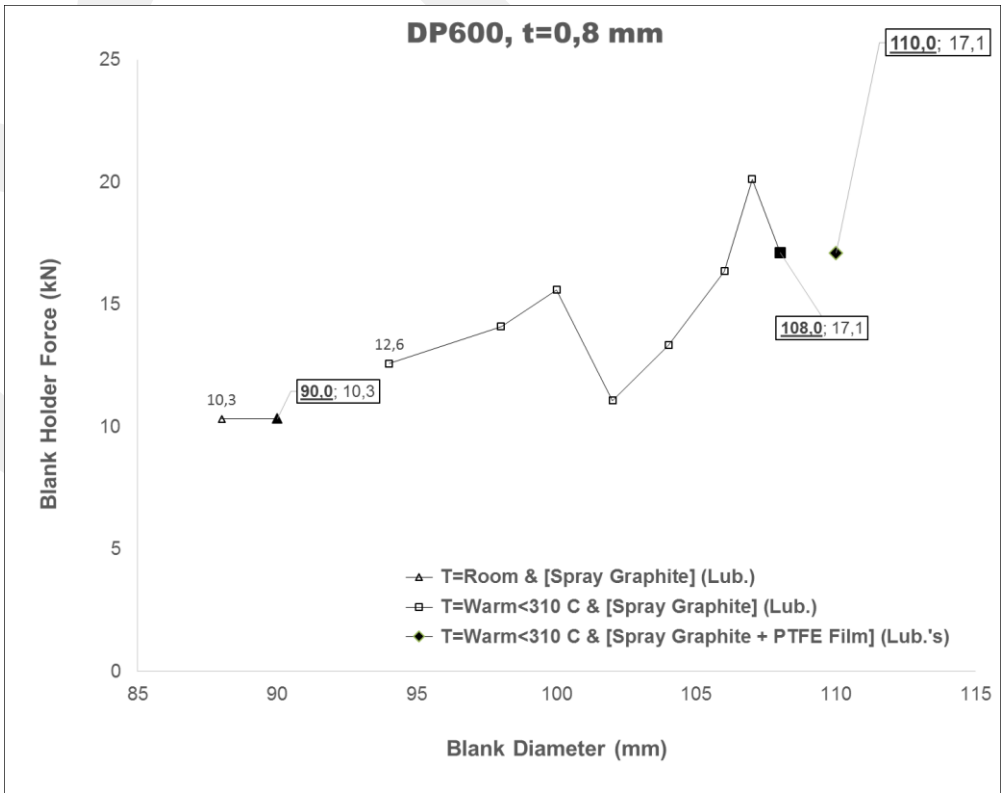

Figure C.61 The graph of the Blank Holder Force (kN) vs its diameter (mm) for DP600 (Dual Phase), t = 0,8 mm.

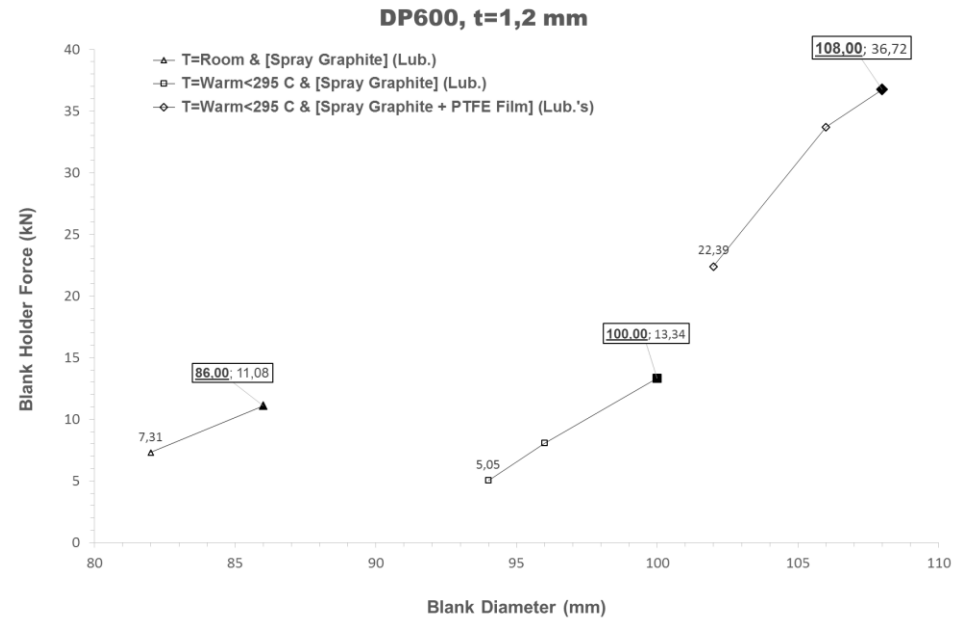

Figure C.62 The graph of the Blank Holder Force (kN) vs its diameter (mm) for DP600 (Dual Phase), t = 1,2 mm.

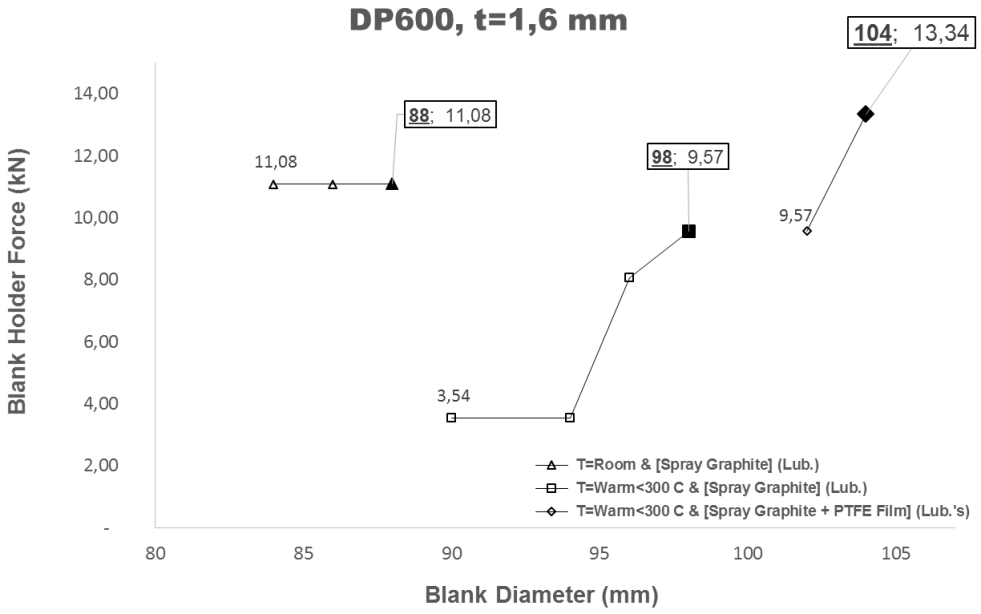

Figure C.63 The graph of the Blank Holder Force (kN) vs its diameter (mm) for DP600 (Dual Phase), t = 1,6 mm.

C.5.2 Erdemir 7128 (HSLA)

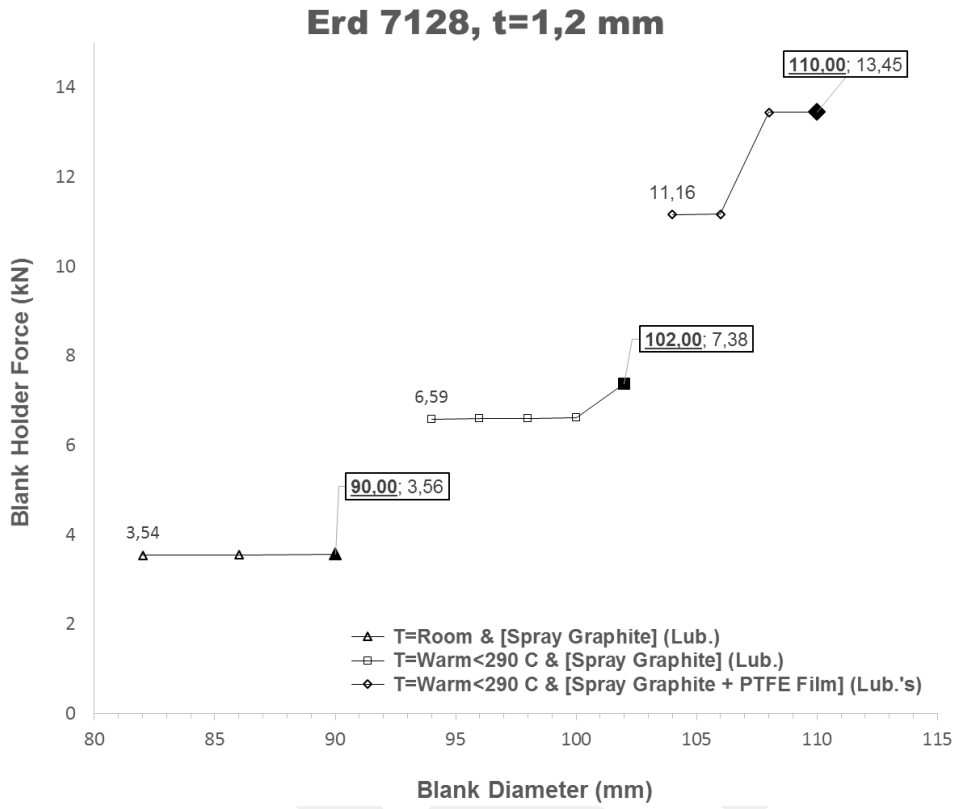

Figure C.64 The graph of the Blank Holder Force (kN) vs its diameter (mm) for Erdemir 7128 (HSLA), t = 1,2 mm.

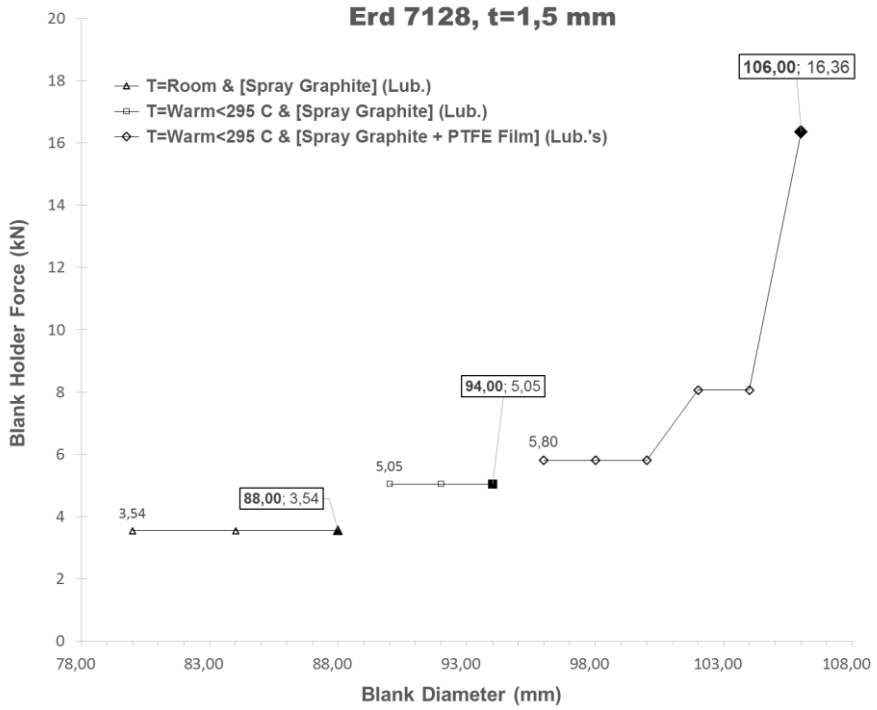

Figure C.65 The graph of the Blank Holder Force (kN) vs its diameter (mm) for Erdemir 7128 (HSLA), t = 1,5 mm.

C.5.3 Erdemir 7140 (HSLA)

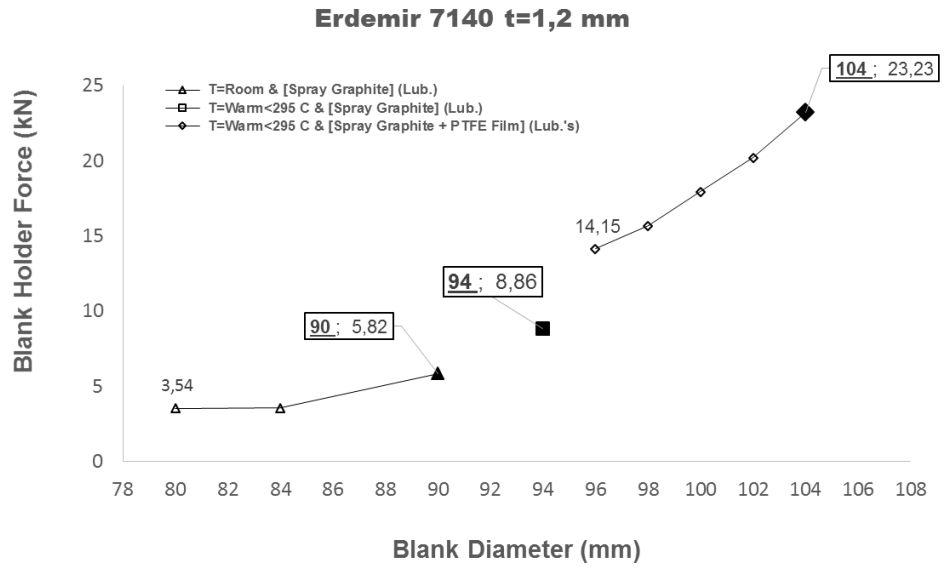

Figure C.66 The graph of the Blank Holder Force (kN) vs its diameter (mm) for Erdemir 7140 (HSLA), t = 1,2 mm.

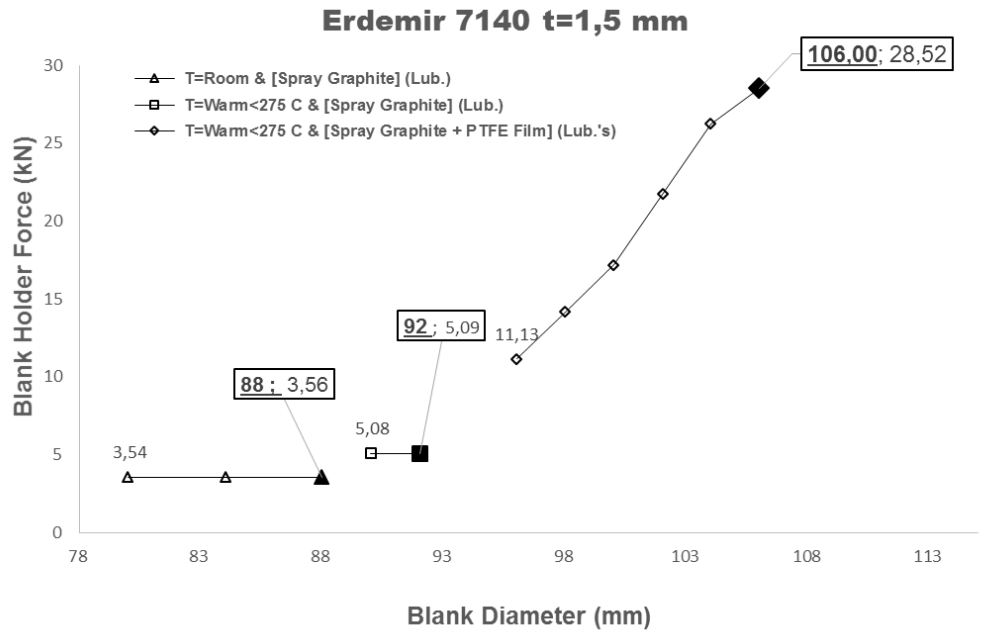

Figure C.67 The graph of the Blank Holder Force (kN) vs its diameter (mm) for Erdemir 7140 (HSLA), t = 1,5 mm.

C.5.4 Erdemir DC04 (IF Steel)

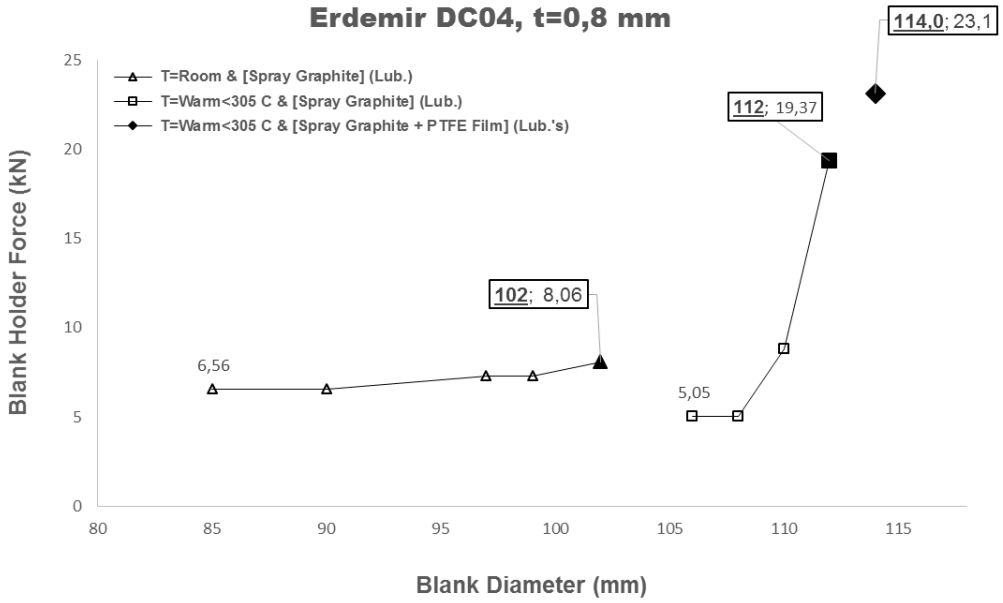

Figure C.68 The graph of the Blank Holder Force (kN) vs its diameter (mm) for Erdemir DC04 (IF Steel), t = 0,8 mm.

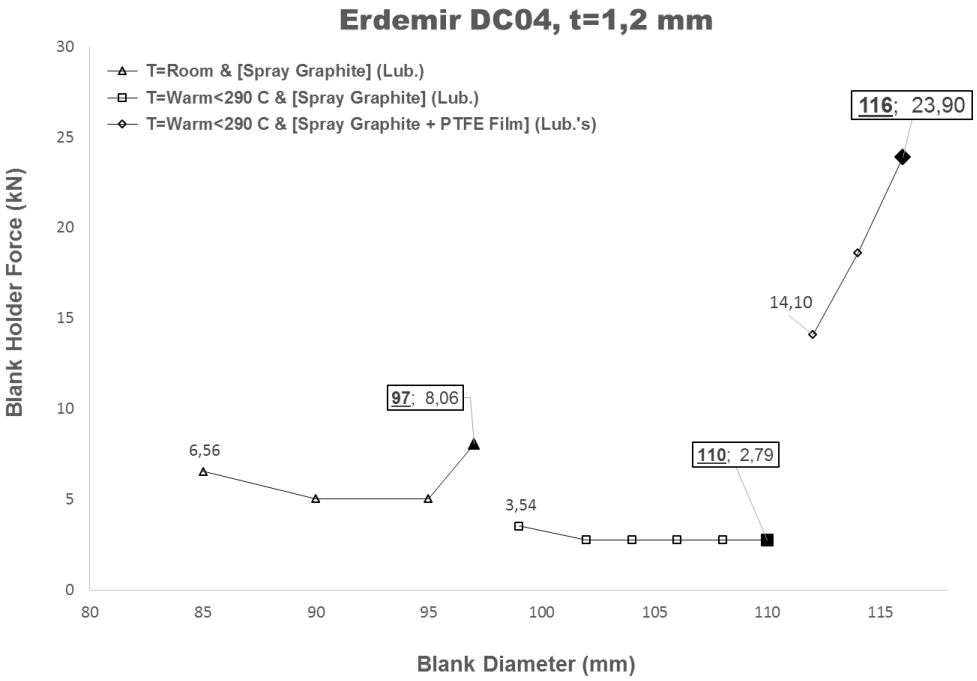

Figure C.69 The graph of the Blank Holder Force (kN) vs its diameter (mm) for Erdemir DC04 (IF Steel), t = 1,2 mm

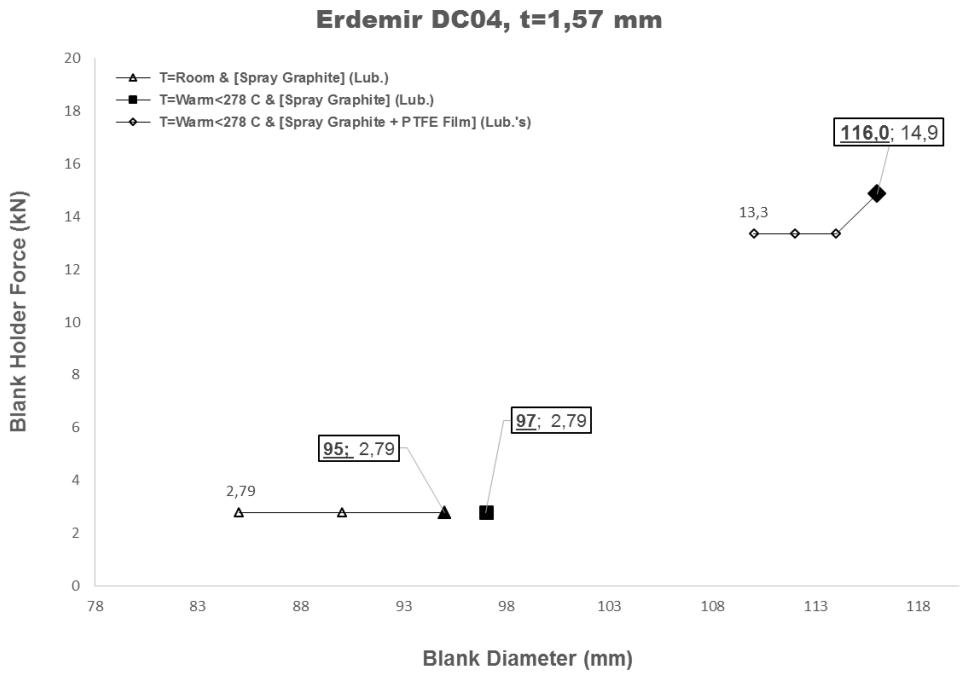

Figure C.70 The graph of the Blank Holder Force (kN) vs its diameter (mm) for Erdemir DC04 (IF Steel), t = 1,57 mm.

GCRIS